P-ISSN 2525-2461 • E-ISSN 2615-9937

Vietnam Journal of Science, Technology and Engineering

DECEMBER 2021 • VOLUME 63 NUMBER 4

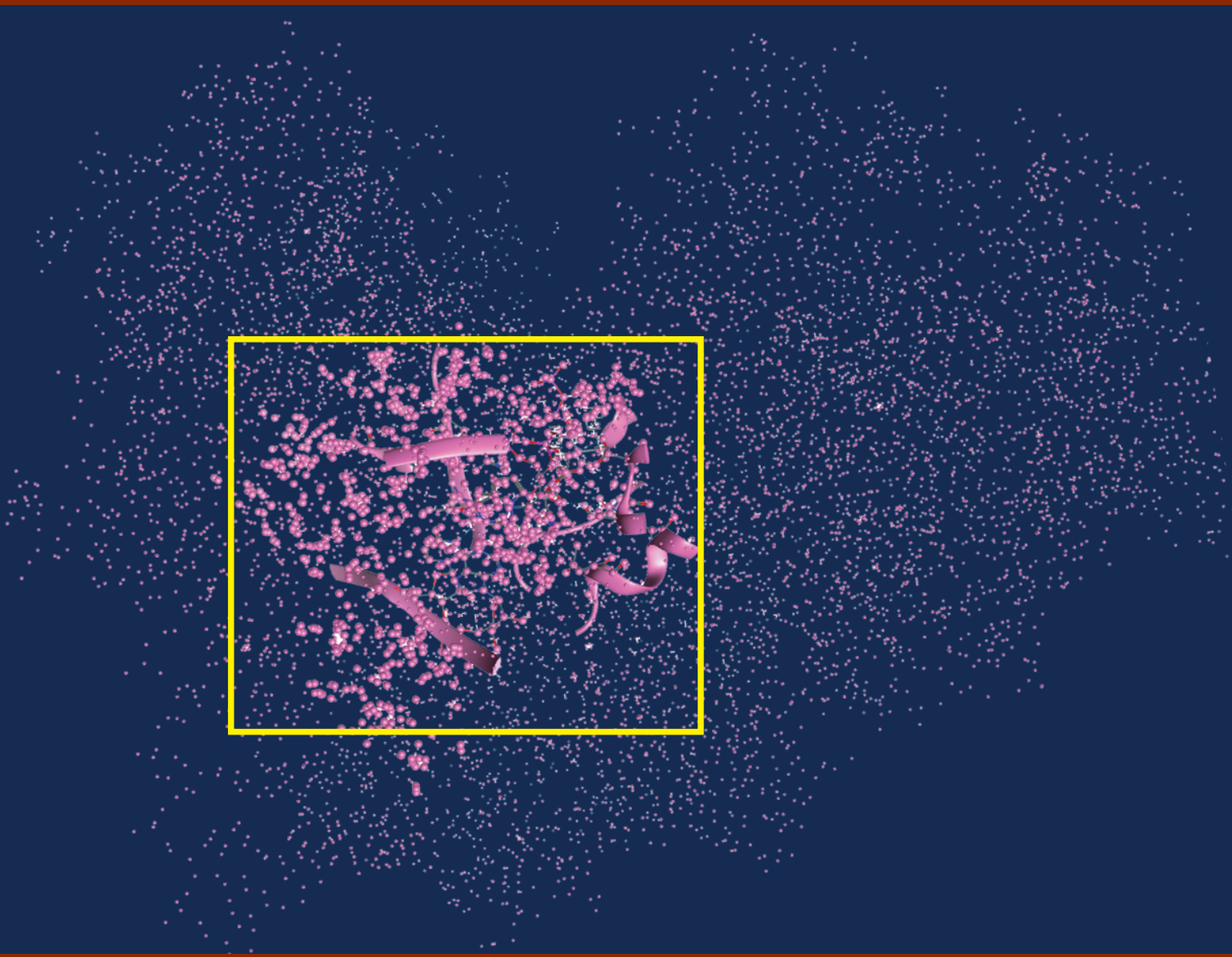

In silico screening of drug inhibitors of SARS-CoV-2 RNA-dependent RNA polymerase target

VIETNAM JOURNAL OF SCIENCE, TECHNOLOGY AND ENGINEERING * DECEMBER 2021 * VOLUME 63 NUMBER 4
vietnamscience.vn or vietnamscience.vjst.vn

Vietnam Journal of Science, Technology and Engineering (VJSTE) **is a quarterly double-blind peer-reviewed academic journal. VJSTE publishes research articles and review articles in all areas of science, technology and engineering with the focus on the physical sciences, life sciences and environmental sciences including the following topics:**

- **Physical Sciences**
- **Agriculture**
- **Medicine**
- **Pharmacology**
- **Biology**
- **Biotechnology**
- **Biomedical Applications**
- **Ecology**
- **Climatology**
- **Environmental Science.**

CLASSIFICATION SCHEME

1. **Mathematics and Computer Science**
   - **1.1. Mathematics**
   - **1.2. Computer Science**
   - **1.3. Computational Science**
2. **Physical Sciences**
   - **2.1. Physics**
   - **2.2. Chemistry**
   - **2.3. Engineering**
3. **Life Sciences**
   - **3.1. Agriculture**
   - **3.2. Medicine**
   - **3.3. Pharmacology**
   - **3.4. Biology**
   - **3.5. Biotechnology**
   - **3.6. Biomedical Applications**
4. **Earth Sciences**
   - **4.1. Geography**
   - **4.2. Geology**
   - **4.3. Geophysics**
   - **4.4. Oceanography**
5. **Environmental Sciences**
   - **5.1. Ecology**
   - **5.2. Climatology**
   - **5.3. Environmental Science**

CONTENTS

DECEMBER 2021 • VOLUME 63 NUMBER 4

6

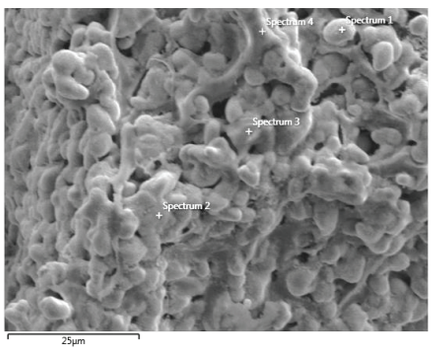

(A)

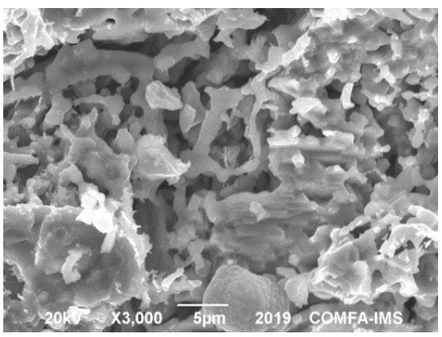

(B)

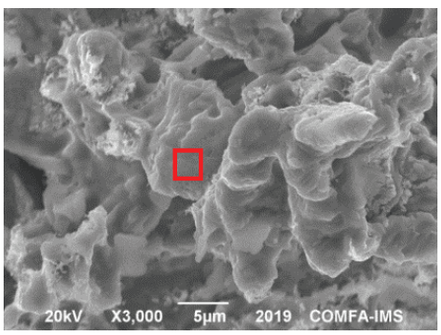

(C)

PHYSICAL SCIENCES

3 Study on the reducibility of iron ore pellets at high temperature.
Cao-Son Nguyen, Thanh-Hoan Nguyen, Son-Lam Nguyen, Anh-Hoa Bui

8 Synthesis of a new furan-bearing triazine dichloride compound.
Thi Thuy Dung Phung, Thu Thuy Truong, Thanh Luan Nguyen, Tran Ha Nguyen

11 Induction and evaluation of secondary metabolite and antioxidant activity in adventitious root of *Codonopsis javanica*.
Thi Huong Trinh, Quoc Tuan Nguyen, Thi Huyen Trang Nguyen, Dang Giap Do, Trong Tuan Tran

17 Physicochemical parameters and mineral components in Vietnam honey as a promising tool for classifying biological origin of honeys.
Thu Huong Nguyen, Thanh Long Ngo, Huu Quang Nguyen

23 Adsorptive removal of methyl orange and methylene blue from aqueous solutions with *Acacia crassicarpa* activated carbon.
Tue Ngoc Nguyen, Khanh Quoc Dang, Duc Trung Nguyen

28 Effects of compressing parameters and $Mg(OH)_2$ content on mechanical properties and flame retardancy of rice straw-fibre reinforced composites.
Doan Van Hong Thien, Thao Phuong Nguyen, Mong Linh Nguyen Thi, Ngoc Tuyet Tran, Thanh Nhan Le, Trung Nam Nguyen, Manh Can Le, Chanh-Nghiem Nguyen, Dan-Thuy Van-Pham

LIFE SCIENCES

36 Clinical and subclinical characteristics of brain-dead donors for liver transplantation in Viet Duc University Hospital.
Thanh Khiem Nguyen, Hong Son Trinh, Gia Anh Pham, Ham Hoi Nguyen, Trung Nghia Bui, Manh Thau Cao, Quang Nghia Nguyen, Viet Khai Ninh, Tuan Hiep Luong, Tien Quyet Nguyen

42 Study on α-glucosidase inhibitory activity of 40 kinds of vegetables, tubers, and fruits in An Giang.
Thi-My-Linh Lam, Minh-Tuan Le, Manh-Ha Bui

CONTENTS

DECEMBER 2021 • VOLUME 63 NUMBER 4

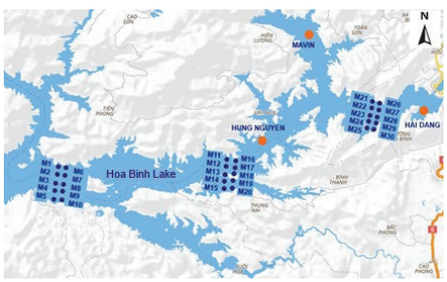

67

47 ***In silico*** **screening of drug inhibitors of SARS-CoV-2 RNA-dependent RNA polymerase target.**

Thanh Tung Bui, Bao Kim Nguyen, Minh Ngoc Le, The Toan Nguyen, The Hai Pham

55 The antidepressant-like effects of an n-butanol fraction of *Ocimum sanctum* Linn. extract in unpredictable chronic mild stress-induced depression in mice.

Thu Hien Nguyen, Thi Xoan Le, Van Tai Nguyen, Thi Nguyet Hang Pham, Minh Khoi Nguyen, Matsumoto Kinzo

62 Effects of different shrimp extracts on *Vibrio parahaemolyticus* growth and virulence.

Nguyen Thuan Thien Truong, The Hao Nguyen, Cong Chinh Bui, Thi Thu Hoai Nguyen

ENVIRONMENTAL SCIENCES

66 Evaluating the potential of aquaculture in the Hoa Binh reservoir with carrying capacity and water quality indices.

Diep Thi Ngoc Phan, Binh Duc Nguyen, Paul Liew, Ha Thi Thu Pham, Tung Thanh Nguyen, Hieu Trung Nguyen

72 An empirical relationship between $PM_{2.5}$ and aerosol optical depth from MODIS satellite images for spatial simulation over Ho Chi Minh city.

Vo Quoc Bao, Tran Thi Van

79 Rice straw open burning: Emissions, effects and multiple benefits of non-burning alternatives.

Nguyen Thi Kim Oanh

86 Establishing 3D hydrogeological solid model and database for sustainable groundwater management in the Vietnam Mekong delta.

Vu Thanh Tam, Nguyen Ngoc Ha, Ho Van Thuy

95 Table of contents in 2021.

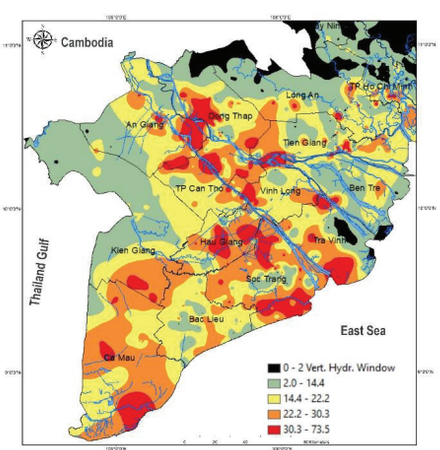

(A)

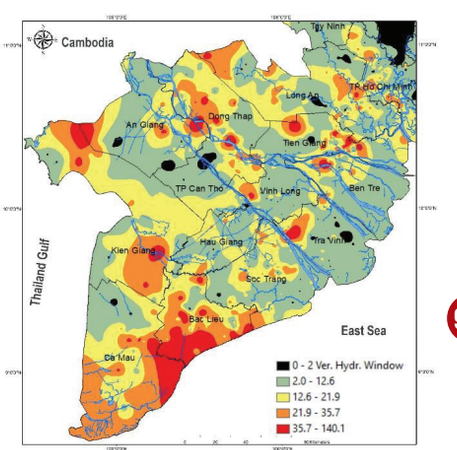

(B)

DOI: 10.31276/VJSTE.63(4).03-07

Study on the reducibility of iron ore pellets at high temperature

Cao-Son Nguyen, Thanh-Hoan Nguyen, Son-Lam Nguyen, Anh-Hoa Bui*

School of Materials Science and Engineering, Hanoi University of Science and Technology, 1 Dai Co Viet Street, Bach Khoa Ward, Hai Ba Trung District, Hanoi, Vietnam

Received 4 August 2020; revised 10 September 2021; accepted 8 October 2021

Abstract:

The behaviour of iron ore pellets in a blast furnace must be considered to improve ironmaking operations, especially when a large amount of the pellets is used. This study presents the reduction degree, mineralogical composition, and morphology of the pellet reduced in a gas mixture of 60% CO and 40% Ar at temperatures between 900 and 1,100°C. The pellet was prepared from iron ore from the Cao Bang province, Vietnam, by rotary drum. The obtained results showed that the reduction degree of the pellet increased with increasing reduction time and temperature. The activation energy of the reducing reaction was calculated to be 63.2 kJ/mol, which indicated that reduction occurred more easily in the present condition. X-ray diffraction (XRD) results revealed mineralogical phases such as hematite (Fe_2O_3), magnetite (Fe_3O_4), wüstite (FeO), metallic iron (Fe), and fayalite (Fe_2SiO_4) existing in the pellets when reduced for different times and temperatures. Fe and Fe_2SiO_4 were found to be the majority in the pellet that was reduced for 90 min at 1,100°C. Scanning electron microscopy (SEM) observations suggested the formation of a liquid phase, e.g., Fe_2SiO_4, which retarded the reducing reaction because it hindered the diffusion of gas flow inside the pellet. This phenomenon is essential to blast furnace ironmaking because pellets must be completely reduced before they move down to the liquid zone.

Keywords: **blast furnace, iron ore pellet, mineralogy, morphology, reduction degree.**

Classification numbers: **2.1, 2.3**

1. Introduction

Because fine iron ore cannot be used in a blast furnace, sintering or pelleting processes need to be applied to make lump ore. Among those methods, pelleting is considered to be superior to sintering in the aspect of environmental performance [1]. The rich and fine (smaller than 40 µm grain size) iron ores cannot be used for sintering, however they are efficient for fabricating pellets [2]. As a raw material, iron ore pellets have contributed to the improvement of operating efficiencies and stability during ironmaking in a blast furnace [3-5]. Therefore, it is important to increase the ratio of pellets used in the furnace for both improved environmental friendliness and to promote the healthy operation of blast furnace ironmaking.

The behaviour of the pellet in a blast furnace at high temperature has been of great interest to those wanting to increase the amount of pellets in a blast furnace. However, increasing the pellet ratio faces some challenges due to the formation of a liquid phase in the pellet at increased temperature [6, 7]. The temperature of the pellet increases when they move down to the lower part of the blast furnace and make contact with the high temperature gas ascending from the tuyeres. The appearance of a liquid phase would have a negative effect on the reducibility of the pellets due to the prevention of reduction gas flowing into the pellet. It has been acknowledged that the reducibility of the pellet is an important factor for the evaluation of pellet utilization in a blast furnace. In turn, the reducibility is largely influenced by changing pellet morphology at high temperature. Despite the fact that there are some research works focusing on this issue, there is a lack of information on the morphology and reduction kinetics of the Vietnamese pellet at high temperatures. This study investigates the reduction kinetics and morphology of the pellet, which was made of iron ore from the Cao Bang province of Vietnam. Also, the mineralogical composition of the pellet in the reduced atmosphere was clarified and discussed.

*Corresponding author: Email: hoa.buianh@hust.edu.vn

2. Experimental method

Iron ore was taken from the Cao Bang province of Vietnam. Iron ores and bentonite powders, which both had grain sizes below 25 µm, were completely mixed in a rotating machine for 10 min. The ratio of bentonite and iron ore was 2:98 in mass. The chemical and mineralogical compositions of the iron ore and the bentonite were analysed and is given in Table 1.

Table 1. The compositions of the used iron ore and bentonite (% mass).

The iron ore							
Fe_3O_4	Fe_2O_3		SiO_2	$Fe_2O_3.H_2O$	$CaCO_3$+$CaSO_4.2H_2O$		
59.53	21.05		8.36	7.76	3.30		
The bentonite							
Al_2O_3	CaO	Fe_2O_3	MgO	SiO_2	TiO_2	Na_2O_3	LOI
14.13	1.84	13.29	2.15	55.59	2.00	2.85	8.15

Green pellets were prepared from the ore using a rotary drum, as shown in Fig. 1. When the mixture was charged into the rotary drum, some small pellets were initially formed. The mixture was continuously added together with sprayed water, which caused the formed pellets to gradually grow. The total moisture content was controlled to be about 10% of the mass of the mixture during the pelleting process. Finally, green pellets were obtained with suitable grain size varied from 10 to 16 mm. For the purpose of increasing strength, the green pellets were heated at 1,200°C in a resistance furnace for 120 min and then cooled down to room temperature together with the furnace.

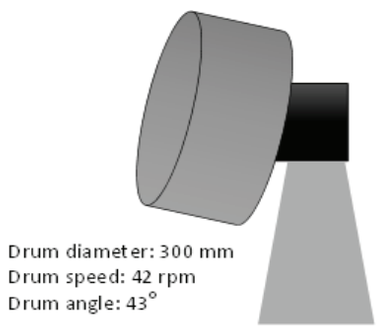

Fig. 1. Rotary drum machine.

Reducibility of the pellet was examined in the system shown in Fig. 2. The reduction gas (60% CO + 40% Ar) was controlled at a flow rate of 80 ml/s and introduced into a vertical alumina tube of the resistant furnace. The pellet was put inside a crucible that was connected with a balance on the top of the system. The weight of the pellet was lost due to oxygen removal from iron oxides during the reduction process so the reduction degree (f) was calculated using Eq. 1:

$$f = \frac{m_0 - m_t}{m_0} \times 100 \quad (1)$$

where m_0 and m_t are the weight of the pellet before and after the reduction, respectively.

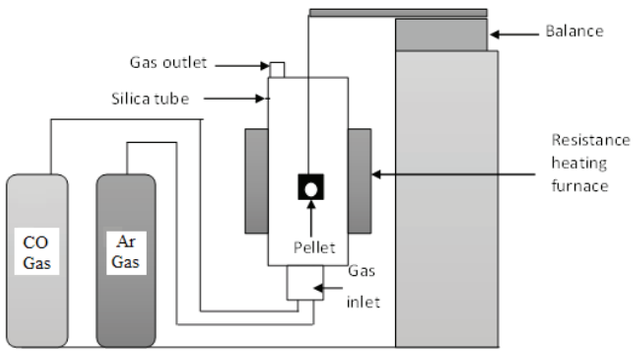

Fig. 2. Schematic diagram of the experimental setup for reducibility test.

The reduction degree of the heated pellets was examined at 900, 1,000, and 1,100°C. After cooling in the furnace, the mineralogical characteristics of the pellet were investigated using X-ray diffraction (XRD, Bruker) and the microstructure was observed using a scanning electron microscope (SEM, Jeol).

3. Results and discussion

3.1. Reduction process of pellets at high temperature

Figure 3 shows the XRD pattern of the pellets reduced at different reaction times. The peaks of magnetite (Fe_3O_4) and wüstite (FeO) were observed in the pellet after 20 min, i.e., an indirect reduction of hematite (Fe_2O_3) to Fe_3O_4 was confirmed following reaction 1. When the pellet was reduced for 30 min, the peak of Fe_3O_4 significantly weakened and FeO was observed as shown in Fig. 3B. It was confirmed that FeO was obtained due to the partial reduction of Fe_3O_4 in accordance with reaction 2. Careful examination of XRD results showed that there was fayalite (Fe_2SiO_4 or $2FeO.SiO_2$) existing in the pellet. This is attributed to the contact of SiO_2 and reduced FeO, which then resulted in the formation of Fe_2SiO_4 (reaction 3). In addition, the reduction of Fe_2O_3 was found to

increase with reduction time. No peak from Fe_3O_4 was observed in the pellets that were reduced for 40 or 60 min (see Figs. 3C and 3D), but the peaks of FeO and metallic iron (Fe) were obtained with high intensity. When the reduction time was 90 min, the Fe peak strengthened and those of Fe_2SiO_4 weakened significantly (Fig. 3E). The intensities of the FeO and Fe peaks increased as the pellets were kept longer in the reduced atmosphere and the reduction of FeO was present after 60 min reduction time at 1,100°C. This result has proved the transformation of Fe_2O_3 to FeO, which subsequently was reduced to Fe in reaction 4.

$$3Fe_2O_3 + CO = 2Fe_3O_4 + CO_2 \quad \text{(Reaction 1)}$$

$$Fe_3O_4 + CO = FeO + CO_2 \quad \text{(Reaction 2)}$$

$$2FeO + SiO_2 = Fe_2SiO_4 \quad \text{(Reaction 3)}$$

$$FeO + CO = Fe + CO_2 \quad \text{(Reaction 4)}$$

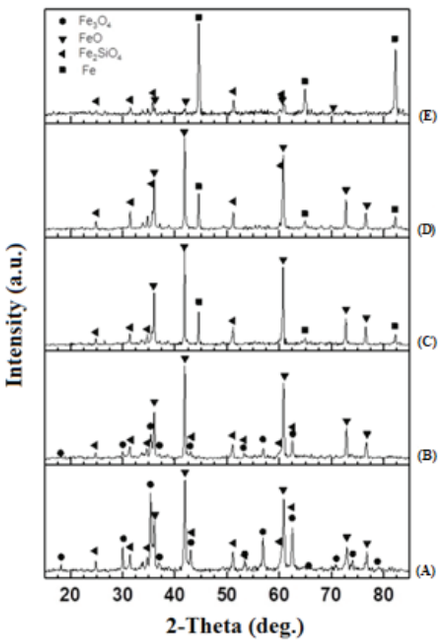

Fig. 3. XRD pattern of the pellets reduced at 1,100°C for (A) 20 min, (B) 30 min, (C) 40 min, (D) 60 min, and (E) 90 min.

3.2. Reduction kinetic of the pellet

Figure 4 shows an increase of the reduction degree with increasing reduction temperature. The reduction degree reached 89% at a temperature of 1,100°C after a reduction time of 90 min. Meanwhile, it was 80% for the case of 900°C after the same reduction time. This result is in agreement with the research of H. Chen, et al. (2015) [8].

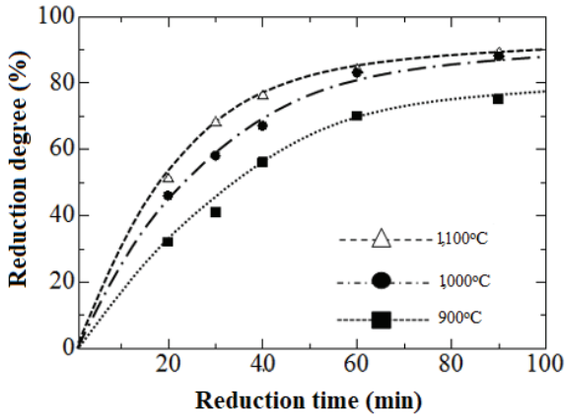

Fig. 4. Variation of the reduction degree with reduction time and temperature.

In order to correctly understand the reducibility of the pellet at high temperatures, the activation energy (E_a) was estimated. In this study, the values of the E_a (kJ/mol) were calculated using the Arrhenius equation:

$$\ln K = \ln A - \frac{E_a}{RT} \quad (2)$$

where A is the Arrhenius factor or the frequency factor, K is kinetics constant, R ($JK^{-1}mol^{-1}$) is gas constant, and T (K) is temperature. The value of the constant K was calculated from the diffusion model of R. Zhong, et al. (2020) who proposed the reduction through a layer as in the following [9, 10]:

$$Kt = [1-(1-f)^{1/3}]^2 \quad (3)$$

where f is the reduction degree, K is coefficient constant, and t (min) is time. From the reduction results, a linear relationship between $[1-(1-f)^{1/3}]^2$ and time was plotted in Fig. 5, which shows the calculated K values as the slope of the straight line.

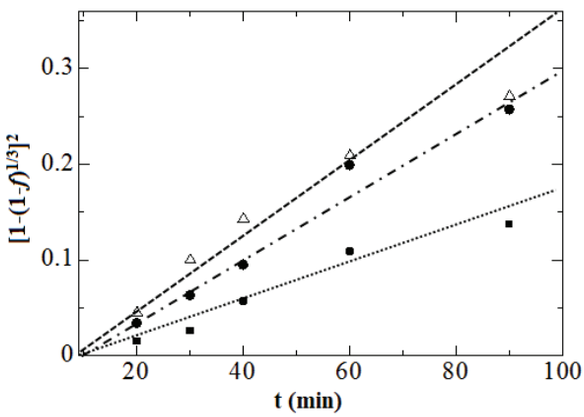

Fig. 5. Relationship between $[1-(1-f)^{1/3}]^2$ and time.

After calculation of the K value, the relationship between ln$K$ and (1/T) was plotted in Fig. 6, where the value of E_a was calculated from the slope of the straight line. The calculated E_a was about 63.2 kJ/mol for the reduction of the iron ore in the present condition. It is known that the initial reactant could be Fe_2O_3 or Fe_3O_4 in the reduction process of iron oxides. According to S.P. Trushenski, et al. (1974) and W.K. Jozwiak, et al. (2007) [11, 12], the values of E_a were reported as 118 and 115 kJ/mol for Fe_2O_3 and Fe_3O_4, respectively. The fact that E_a in this study is smaller than expected from the literature indicates that the reduction reaction of Cao Bang iron ore occurs more easily under the conditions of using 60% CO and a high temperature of 1,100°C.

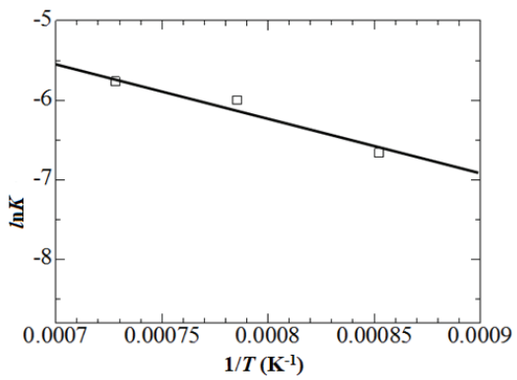

Fig. 6. Arrhenius plot for the reduction of the pellets.

3.3. Morphology variation with time affecting the reduction of the pellet

Figure 6 shows that the reduction degree significantly increased in the first 40 min of reduction time and remained slowly increasing until the end. The formation of the fayalite liquid phase would be the main factor diminishing the reducibility of the pellets. Clear evidence for this is given in Fig. 7, in which a liquid phase was seen in the pellet reduced for more than 20 min (Figs. 7B and 7C). Table 2 shows the typical compositions of the liquid phase in the 40-min-reduced pellet using EDS analysis. The results suggested that the liquid phase contained fayalite (Fe_2SiO_4), which had a negative effect on the reducibility of the pellet. When the liquid phase occurs, it connects and creates larger liquid clusters, which were seen as the large blocks in the cooled pellets (Fig. 7C). The amount of the liquid phase in the pellet with 40 min reduction time was confirmed to be much more than that of the 20 min reduction. This finding was consistent with the results of L.Y. Yi, et al. (2015) [13] who concluded that the amount of liquid phase increased with increasing time at high temperatures and retarded the reduction rate of the iron oxide. Increasing the reduction time caused an increase of the liquid phase, which filled the pores of the pellet and finally shrank after the pellet cooled. The pores in the pellet are preferential for diffusion of the reduction gas, so the reduction degree must decreased with the porosity of the pellet [14]. This is similar to the other results, that is, that slag formation like fayalite retarded diffusion of the reducing gas flow within the pellet through the liquid layer and lead to a decrease in the reducibility of the pellet [15]. Therefore, it can be concluded that formation of a liquid phase is one of the main factors that decrease the reducibility of the pellet in a reduced atmosphere. This phenomenon plays a very important role in the operation of the blast furnace in which the pellets must be completely reduced before they move down to the liquid zone.

Table 2. The compositions of the liquid phase in the 40 min reduction (% mass).

O	Fe	Si	Al	Ca	Others
53.94	32.16	7.70	3.61	1.26	1.33

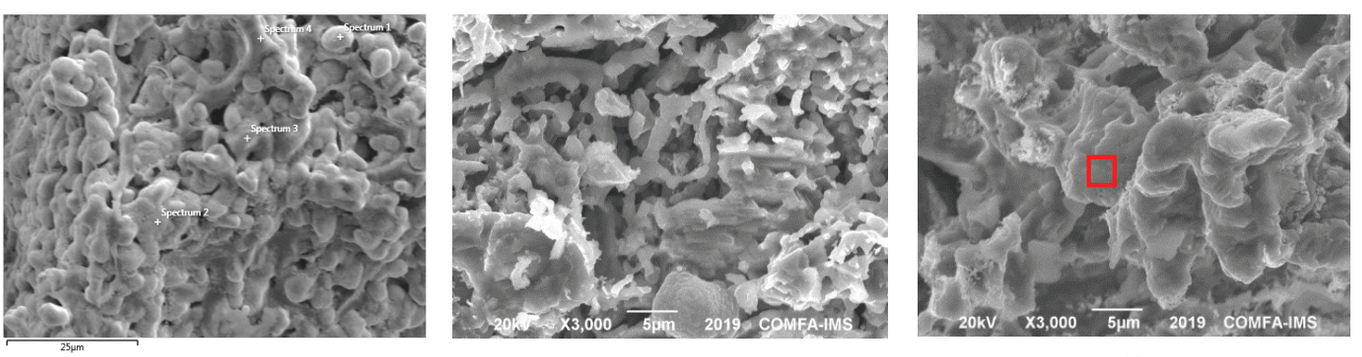

(A) (B) (C)

Fig. 7. SEM images of the pellets reduced at 1100°C for (A) 0 min; (B) 20 min; (C) 40 min.

4. Conclusions

The reduction degree, activation energy, and morphology of the pellets prepared from iron oxide of the Cao Bang province, Vietnam have been investigated in a gas mixture of 60% CO and 40% Ar at temperatures between 900-1,100°C. The main results are as follows:

1. The mineralogical composition of the pellet was identified by XRD, which validated the sequence of the reduction reactions proposed by the theory. Metallic Fe was confirmed to be prominent in the pellet reduced for 90 min.

2. A reduction degree of 90% after 40 min reduction time at 1,100°C was calculated based on the loss of pellet weight during the reduction. The reducibility of the pellet was found to increase with increased temperature.

3. The value of activation energy was calculated to be 63.2 kJ/mol for the reduced reaction of the Cao Bang iron ore. Reducibility was considered to be good in condition with a reduced atmosphere containing 60% CO gas and high temperatures.

4. SEM images of the pellets showed evidence of liquid formation - one of the main factors that decrease the reducibility of the pellet in the reduced atmosphere at high temperature. The amount of the liquid phase that negatively affected the reduction degree was confirmed to increase with increasing reduction time at 1,100°C.

CRedit author statements

Cao-Son Nguyen, Thanh-Hoan Nguyen: Conceptualization, Methodology, Data curation, Formal analysis, Writing - Review & Editing; Son-Lam Nguyen, Anh-Hoa Bui: Conceptualization, Methodology, Writing - Original draft preparation, Writing - Review & Editing.

COMPETING INTERESTS

The authors declare that there is no conflict of interest regarding the publication of this article.

REFERENCES

[1] J.M. Mourao, M. Huerta, U.V.D. Medeiros, et al. (2012), "Guidelines for selecting pellet plant technology", *6th International Congress on The Science and Technology of Ironmaking-ICSTI*, Brazil, pp.2162-2175.

[2] A. Babich, D. Senk, H.W. Gudenau, et al. (2008), *Ironmaking*, Verlagshaus Mainz GmbH, 402pp.

[3] S. Dwarapudi, T.K. Ghosh, V. Tathavadkar, et al. (2012), "Effect of MgO in the form of magnesite on the quality and microstructure of hematite pellets", *International Journal of Minerals Process*, **112-113**, pp.55-62, DOI: 10.1016/j.minpro.2012.06.006.

[4] M. Geerdes, R. Chaigneau, I. Kurunov, et al. (2015), *Modern Blast Furnace Ironmaking*, IOS Press, 228pp.

[5] T. Umadevi, P. Kumar, N.F. Lobo, et al. (2011), "Influence of pellet basicity (CaO/SiO_2) on iron ore pellet properties and microstructure", *ISIJ International*, **51(1)**, pp.14-20, DOI: 10.2355/isijinternational.51.14.

[6] S.H. Lee (2009), *Reduction and Softening/Melting Behavior of Olivine Pellet in The Experimental Blast Furnace*, Doctoral Thesis, The University of New South Wales, 185pp.

[7] M. Iljana (2017), *Iron Ore Pellet Properties under Simulated Blast Furnace Condition*, Doctoral Thesis, Lulea University of Technology, 29pp.

[8] H. Chen, Z. Zheng, W. Shi (2015), "Investigation on the kinetics of iron ore fines reduction by CO in a micro-fluidized bed", *Procedia Engineering*, **102(3)**, pp.1726-1735, DOI: 10.1016/j.proeng.2015.01.308.

[9] R. Zhong, L. Yi, Z. Huang, et al. (2020), "Reduction mechanism and kinetics of a low grade iron ore-coal composite pellets improved by sodium salt", *ISIJ International*, **60(4)**, pp.649-655, DOI: 10.2355/isijinternational.ISIJINT-2019-381.

[10] D. Guo, M. Hu, C. Pu, et al. (2015), "Kinetics and mechanisms of direct reduction of iron ore-biomass composite pellets with hydrogen gas", *International Journal of Hydrogen Energy*, **40(14)**, pp.4733-4740, DOI: 10.1016/j.ijhydene.2015.02.065.

[11] S.P. Trushenski, K. Li, W.O. Philbrook (1974), "Nontopochemical reduction of iron oxides", *Metallurgical Transactions*, **5**, pp.1149-1158, DOI: 10.1007/BF02644326.

[12] W.K. Jozwiak, E. Kaczmarek, T.P. Maniecki, et al. (2007), "Reduction behaviour of iron oxides in hydrogen and carbon monoxide atmospheres", *Applied Catalysis A: General*, **326(1)**, pp.17-27, DOI: 10.1016/j.apcata.2007.03.021.

[13] L.Y Yi, Z.C. Huang, T. Jiang, et al. (2015), "Swelling behavior of iron ore pellet reduced by H_2-CO mixtures", *Powder Technology*, **269**, pp.290-295, DOI: 10.1016/j.powtec.2014.09.018.

[14] F.O. Boechat, L.T. Rocha, R.M. Carvalho, et al. (2018), "Amenability of reduced iron ore pellets to mechanical degradation", *ISIJ International,* **58(6)**, pp.1028-1033, DOI: 10.2355/isijinternational.ISIJINT-2017-734.

[15] D. Wagner, O. Devisme, F. Patisson, et al. (2006), "A laboratory study of the reduction of iron oxides by hydrogen", *The Sohn International Symposium on Advanced Processing of Metals and Materials*, **2**, pp.111-120.

DOI: 10.31276/VJSTE.63(4).08-10

Synthesis of a new furan-bearing triazine dichloride compound

Thi Thuy Dung Phung[1], Thu Thuy Truong[2], Thanh Luan Nguyen[1], Tran Ha Nguyen[1, 2*]

[1]National Key Laboratory of Polymer and Composite Materials, Vietnam National University - Ho Chi Minh City, Linh Trung Ward, Thu Duc City, Ho Chi Minh City, Vietnam
[2]Faculty of Materials Technology, University of Technology, Vietnam National University - Ho Chi Minh City, 268 Ly Thuong Kiet Street, Ward 14, District 10, Ho Chi Minh City, Vietnam

Received 27 October 2020; revised 18 December 2020; accepted 24 December 2020

Abstract:

Due to their strong electron affinity and symmetrical structure, triazine and its derivatives are widely recognized as electron-deficient units with good electrical and optical characteristics. When triazine-based molecular acceptor units are used in organic solar cell architectures, various positive impacts on device performance result, including increased crystallinity, increased charge transport mobility, and increased absorption. Good mechanical and thermostable qualities are only a couple of the special benefits that organic materials with an s-triazine ring in their backbone also enjoy. According to additional study, triazine-based polymers are used as a starting point for dyes, crosslinking agents, and flame-retardant compounds. Additionally, it has been demonstrated that polymers containing conjugated triazine rings offer outstanding optoelectronic characteristics for organic light-emitting diodes. Donor-acceptor compounds have been receiving increased attention lately, especially in opto-electronic applications. In this work, a novel compound named triazine-furan, comprised of a triazine acceptor moiety and a furan donor side group, was designed and synthesised for the first time. The influences of temperature and the feeding proportion of cyanuric chloride to furfurylamine were investigated to optimise the reaction yield and purification process. The synthesised compound was characterised using thin-layer chromatography (TLC), Fourier-transform infrared spectroscopy (FTIR), and proton nuclear magnetic resonance (^{1}H-NMR) spectroscopy.

Keywords: **compound, conjugated diene, cyanuric chloride, triazine.**

Classification numbers: **2.1, 2.3**

1. Introduction

Triazine and its derivatives are well known as electron□deficient units that possess excellent electronic and photonic properties owing to their high electron affinity and symmetrical structure [1-3]. The use of triazine-based molecular acceptor units in organic solar cell structures give rise to many beneficial effects on device performance such as higher crystallinity, charge transport mobility, as well as broadened absorption [4]. Organic materials with an s-triazine ring in their backbone also benefit from unique advantages such as good mechanical and thermostable properties [5]. Other research indicates that triazine-based polymers are employed as a precursor to flame-retardant materials, dyes, and crosslinking agents [6, 7]. Besides, polymers containing conjugated triazine rings have been shown to possess excellent optoelectronic properties for organic light-emitting diodes [8].

Indeed, donor-acceptor (D-A) organic materials have attracted substantial interest in opto-electronic applications such as organic solar cells, thin-film transistors, and organic light-emitting diodes [9, 10]. It has been reported in the literature that incorporating donor groups into the triazine moiety results in donor-acceptor systems with interesting characteristics such as a two-photon absorbing cross-section [11]. Several units, including ferrocenyl, phenyl, and thiophene, have been combined with triazine in donor-acceptor systems [12-14].

Therefore, in this work, a novel compound named triazine-furan (TF), comprised of a triazine acceptor moiety and a furan donor side group, was designed and synthesised for the first time.

The authors use cyanuric chloride and furfurylamine as reaction agents with N, N-diisopropylethylamine (DIPEA) as the catalyst to synthesize the compound. Factors including temperature and molar ratio between cyanuric chloride and furfurylamine are controlled over the reaction to optimize the reaction yield and product purity. The authors use chemical analytical techniques such as proton nuclear magnetic (^{1}HNMR), Fourier-transform infrared spectroscopy (FTIR), and thin-layer chromatography (TLC) to identify the purity and reaction yield of the synthesised compounds.

2. Materials and methods

2.1. Materials

The materials used were cyanuric chloride (CyC, Sigma Aldrich, 99%), furfurylamine (FuA, Sigma Aldrich, 99%), and N,N-diisopropylethylamine (DIPEA, Sigma Aldrich, 99%). All the solvents were purchased from Fisher Chemicals.

*Corresponding author: Email: nguyentranha@hcmut.edu.vn

2.2. Instrumentation

Proton nuclear magnetic resonance (^{1}H-NMR) spectra were recorded in a deuterated chloroform solvent ($CDCl_3$), with TMS as an internal reference, on a Bruker Avance 500 MHz spectrometer. FTIR spectra were collected as an average of 524 scans with a resolution of 4 cm^{-1} on an FT-IR Tensor 27 spectrometer. Thin-layer chromatography plates were purchased from Sigma-Aldrich.

2.3. Synthesis of TF compound

The preparation of triazine-furan (TF) was carried out in a round-bottomed flask, the concentration of the reaction solution was 4 M in dried tetrahydrofuran (THF). In a dilute solution of cyanuric chloride in dried THF, a mixture of furfurylamine and DIPEA was dissolved in dried THF and added dropwise at the various temperatures (various values from -20°C to room temperature). The reaction was continuously stirred at the designed temperature for 4 h and then followed by TLC. After the reaction was stopped, the obtained mixture was washed with distilled water, dried over K_2CO_3, then purified by flash chromatography (hexane/ethyl acetate, 5:1 (v/v)) to yield TF.

3. Results and discussion

The synthesis pathway of triazine-furan (TF) from cyanuric chloride (CyC) and furfurylamine (FuA) is shown in Scheme 1. The conversion of FuA (Rf=0) and CyC (Rf =0.85) to TF (Rf=0.7) was followed by TLC (hexane/ethyl acetate=5/1 (v/v)).

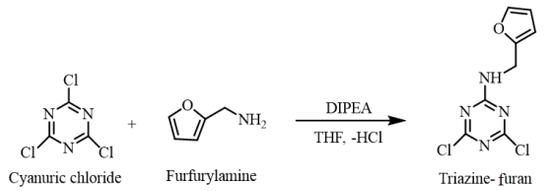

Scheme 1. Synthesis of the TF compound.

After the purification process, the final product was structurally characterised by 1H-NMR and the result is shown in Fig. 1 with δ (ppm): 6.57 (a, 1H, NH), 4.67 (b, 2H, N- CH2), 6.31-6.34 (c, d, 2H, -CH=), and 7.37 (e, 1H, O-CH=). The product was also analysed by FTIR (Fig. 2), which illustrated the characteristic vibration of the triazine ring as evidenced by the absorption bands at 1604.71 and 1591.21 cm^{-1} and the band of 790.78 cm^{-1} that is attributed to the C-Cl stretching vibration. Besides, the bands at 3249.92-3120.70 cm^{-1} and 790.78 cm^{-1} are assigned to the secondary amine and furan groups, respectively. Thus, the resulting spectrum contributes to the confirmation of the intended chemical structure of the title compound.

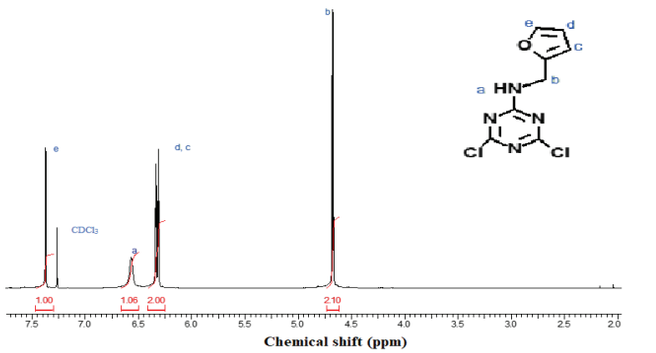

Fig. 1. ^{1}H-NMR spectrum of the TF product.

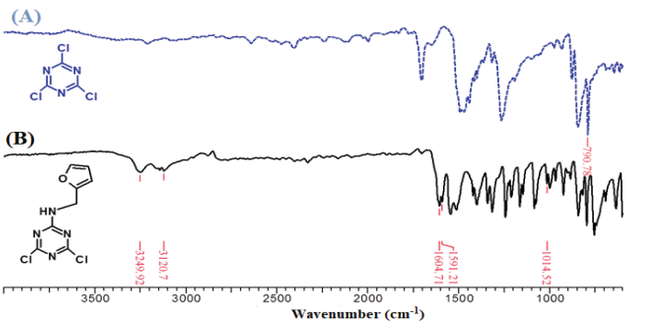

Fig. 2. FTIR spectrum of (A) cyanuric chloride and (B) the triazine-furan product.

3.1. Effect of temperature

Because the reactivity of cyanuric chloride is strongly influenced by temperature, we studied the temperature dependence of the reaction. With the use of equimolar amounts of cyanuric chloride and furfurylamine, the reactions were carried out at various temperatures from -20 to 30°C (room temperature). The reaction was followed by TLC and the yields obtained were compared. The results of the comparison are shown in Fig. 3, which indicates a nearly double increase in yields from 21% at 30°C to 40% at 0°C. When the reaction was carried out at -10°C, the yield increased to 63%, but the yield remained the same value as the temperature was cooled down further to -20°C. Therefore, a temperature of -10°C was chosen to perform this reaction.

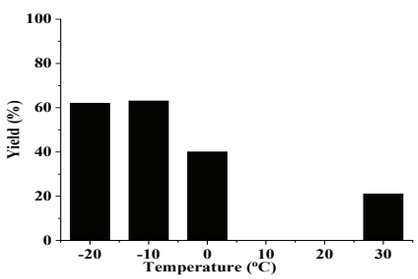

Fig. 3. Synthesis yield of TF at various reaction temperatures.

3.2. Effect of feeding molar ratio of cyanuric chloride/ furfurylamine

For further study, the reaction yield was expected to increase by shifting the reaction quilibrium. The reaction was carried out with various feeding molar ratios of CyC/FuA from 1 to 2. As shown in Table 1, by fixing the temperature at -10°C and increasing the molar ratio of CyC/FuA from 1.00 to 1.25 and 1.5, the yield increased and reached a maximum of 92% at a feeding molar ratio of 1.5.

Table 1. Data summary of triazine furan (TF) preparation.

Entry	$[CyC]_0$:$[FuA]_0$:$[DIPEA]_0$	Temperature (°C)	Yield (%)
1	1.0/1.0/1.0	-20	62
2	1.0/1.0/1.0	-10	63
3	1.0/1.0/1.0	0	40
4	1.0/1.0/1.0	30	21
5	1.0/1.0/1.0	-10	63
6	1.25/1.0/1.25	-10	77
7	1.5/1.0/1.5	-10	92
8	2.0/1.0/2.0	-10	81

However, when a higher molar ratio was examined, the TF product was obtained at a lower yield. The use of a large excess of CyC in the higher molar ratio may cause a product loss during purification, which may explain the low yield with a molar ratio above 1.5. Thus, a feeding molar ratio of 1.5 for CyC/FuA and a temperature of -10°C were chosen as the optimum conditions for synthesis of the compound.

4. Conclusions

The new furan-bearing triazine dichloride compound, so called triazine-furan (TF), was successfully prepared via a direct coupling reaction between cyanuric chloride and furfurylamine in the presence of DIPEA. It was found that the feeding molar ratio of 1.5 for CyC/FuA and temperature of -10°C are the optimum conditions for the preparation of TF, which resulted in a yield of 92%.

CRedit author statements

Thi Thuy Dung Phung, Thu Thuy Truong: Conceptualization, Methodology, Data curation, Formal analysis, Writing - Review & Editing; Thanh Luan Nguyen, Tran Ha Nguyen: Conceptualization, Methodology, Writing - Original draft preparation, Writing - Review & Editing.

ACKNOWLEDGEMENTS

This research is funded by Vietnam National University, Ho Chi Minh city (VNU-HCM) under grant number B2019-20-12.

COMPETING INTERESTS

The authors declare that there is no conflict of interest regarding the publication of this article.

REFERENCES

[1] I. Nenner, G.J. Schulz (1975), "Temporary negative ions and electron affinities of benzene and *N*-heterocyclic molecules: Pyridine, pyridazine, pyrimidine, pyrazine, and *s*-triazine", *J. Chem. Phys.*, **62**, pp.1747-1758, DOI: 10.1063/1.430700.

[2] R. Fink, C. Frenz, M. Thelakkat, et al. (1997), "Synthesis and characterization of aromatic poly(1,3,5-triazine-ether)s for electroluminescent devices", *Macromolecules*, **30**, pp.8177-8181, DOI: 10.1021/ma970528x.

[3] H. Meier, E. Karpuk, H.C. Holst (2006), "Star-shaped pushpull compounds having 1,3,5-triazine cores", *Eur J. Org. Chem*., **2003(21)**, pp.2609-2617, DOI: 10.1002/ejoc.200300132.

[4] Y. Duan, X. Xu, H. Yan, et al. (2017), "Pronounced effects of a triazine core on photovoltaic performance - Efficient organic solar cells enabled by a pdi trimer-based small molecular acceptor", *Adv. Mater.*, **29(7)**, DOI: 10.1002/adma.201605115.

[5] S.M. Osman, S.N. Khattab, E.S.A. Aly, et al. (2017), "1,3,5-triazine-based polymer: Synthesis, characterization and application for immobilization of silver nanoparticles", *J. Polym. Res.*, **24**, DOI: 10.1007/s10965-017-1385-2.

[6] J.X. Jiang, A. Trewin, F. Su, et al. (2009), "Microporous poly(tri(4-ethynylphenyl)amine) networks: Synthesis, properties, and atomistic simulation", *Macromolecules*, **42(7)**, pp.2658-2666, DOI: 10.1021/ma802625d.

[7] J.X. Jiang, F. Su, A. Trewin, et al. (2008) "Synthetic control of the pore dimension and surface area in conjugated microporous polymer and copolymer networks", *J. Am. Chem. Soc.*, **130(24)**, pp.7710-7720, DOI: 10.1021/ja8010176.

[8] N. Chakravarthi, U.K. Aryal, K. Gunasekar, et al. (2017), "Triazine-based polyelectrolyte as an efficient cathode interfacial material for polymer solar cells", *ACS Appl. Mater. Interfaces*, **9(29)**, pp.24753-24762, DOI: 10.1021/acsami.7b03187.

[9] H.A.M. Mullekom, J.A.J.M. Vekemans, E.E. Havinga, et al. (2001), "Developments in the chemistry and band gap engineering of donor-acceptor substituted conjugated polymers", *Materials Science and Engineering: R: Reports,* **32(1)**, pp.1-40, DOI: 10.1016/S0927-796X(00)00029-2.

[10] Z.G. Zhang, J. Wang (2012), "Structures and properties of conjugated donor-acceptor copolymers for solar cell applications", *J. Mater Chem.*, **22(10)**, pp.4178-4187, DOI: 10.1039/C2JM14951F.

[11] C. Y. Zhi, F. Qi, X. Gang, et al. (2005), "Cooperative enhancement of two-photon absorption of multibranched compounds with vinylenes attaching to the s-triazine core", *Chem. Lett.*, **34(5)**, pp.644-645, DOI: 10.1246/cl.2005.644.

[12] R. Maragani, R. Misra (2013), "Donor-acceptor ferrocenyl triazines: Synthesis and properties", *Tetrahedron Lett.*, **54(39)**, pp.5399-5402, DOI: 10.1016/j.tetlet.2013.07.119.

[13] R. Misra, P. Gautam, R. Sharma, et al. (2013), "Donor-π-acceptor-π-donor ferrocenyl benzothiadiazoles: Synthesis, structure, and properties", *Tetrahedron Lett*., **54(5)**, pp.381-383, DOI: 10.1016/j.tetlet.2012.11.016.

[14] R. Maragani, T. Jadhav, S.M. Mobin, et al. (2012), "Synthesis, structure, photophysical, and electrochemical properties of donor-acceptor ferrocenyl derivatives", *Tetrahedron Lett.*, **68(36)**, pp.7302-7308, DOI: 10.1016/j.tet.2012.06.094.

DOI: 10.31276/VJSTE.63(4).11-16

Induction and evaluation of secondary metabolite and antioxidant activity in adventitious root of *Codonopsis javanica*

Thi Huong Trinh[1*], Quoc Tuan Nguyen[2], Thi Huyen Trang Nguyen[2], Dang Giap Do[2], Trong Tuan Tran[2]

[1]*Ho Chi Minh City University of Food Industry, 140 Le Trong Tan Street, Tay Thanh Ward, Tan Phu District, Ho Chi Minh City, Vietnam*
[2]*Institute of Tropical Biology, Vietnam Academy of Science and Technology, 9/621 Hanoi Highway, Linh Trung Ward, Thu Duc City, Ho Chi Minh City, Vietnam*

Received 21 May 2021; revised 24 June 2021; accepted 9 July 2021

Abstract:

In this study, the effects of auxin (IBA, NAA), explants, and culture conditions (light/dark) on adventitious root induction of *Codonopsis javanica* were investigated. The results showed that dark conditions were more suitable for adventitious root induction than light conditions. All three types of explants (internodes, leaves, and nodes) induced adventitious roots, and the appropriate concentration of auxin was 0.5 mg/l IBA. After 4 weeks of incubation under dark conditions, the rooting percentage and number of roots/explant of internode, leaf, and node segments on media supplemented with 0.5 mg/l IBA were 100% and 33.87 roots, 97.78% and 23.48 roots, 100% and 25.20 roots, respectively. These adventitious roots were analysed for the presence of alkaloids, carbohydrates, saponin, fixed oils and fats, phenol, flavonoids, gum, and mucilage. The total polysaccharide content, total phenolic content, and the antioxidant activity (IC_{50}) of *C. javanica* adventitious root biomass were 16.98%, 1.876 (mg GAE/g DW), and 2.44 (mg/ml), respectively. These results indicate that the adventitious roots of *C. javanica* contain bioactive compounds, which can be used as a material source for multiplication in large-scale systems.

Keywords: **adventitious roots, antioxidant activity, auxin, *Codonopsis javanica*, explant, light condition, secondary metabolite.**

Classification number: **2.2**

1. Introduction

Genus *Codonopsis* belongs to the family *Campanulaceae*, which has 42 species distributed around the world but mainly in central, east, and south Asia [1]. Several *Codonopsis* species have been widely used in traditional medicine. According to J.Y. He, et al. (2015) [2], the root of the *Codonopsis* species contains main compounds such as pyrrolidine alkaloid (Codonopyrrolidiums A, B), phenylpropanoid (Tangshenoside I), and polyacetylene (Lobetyol, lobetyolin, lobetyolinin, and cordifolioidyne B). *Codonopsis javanica* is found in Vietnam. *C. javanica* is distributed quite widely from the northern region to the southern central provinces of Vietnam such as Kon Tum, Lam Dong, Lao Cai, Lang Son, Lai Chau... *C. javanica* and other *Codonopsis* species have been used to treat diabetes and other diseases. The extracts of *C. javanica* possess insecticidal action against *Aedes albopictus* [3]. K.N. Chen, et al. (2013) [4] studied the reduction of blood insulin and the antioxidant capacity of *C. javanica* root extract in an insulin-resistant mouse model. According to a survey by P.H. Nguyen, et al. (2014) [5], *C. javanica* is a traditional medicine plant used by the K'Ho people in the buffer zone of Chu Sang Sin, the national park in Vietnam. Nowadays, *C. javanica* has been used in high demand not only as medicine but also as a daily food supplement. Due to overexploitation and deforestation, the reserves of medicinal plants are decreasing. For many years, *C. javanica* has been included in Vietnam's Red Data Book and recognised as a priority target for conservation actions [6].

Nowadays, *Codonopsis* genus has not only been studied in terms of medicinal materials but also in terms of micropropagation and preservation. For example, J.H. Peng, et al. (2010) [7] succeeded in regenerating *C. lanceolata* plants. S. Wojciech, et al. (2011) [8] carried out the project of micropropagation of *C. pilosula* (Franch.) Nannf. from axillary buds. Besides, the compounds of *C. javanica* have mainly been found in the roots. Therefore, the adventitious root culture of *C. javanica* is a suitable solution for large-scale root production that is independent of natural conditions and an alternative to traditional methods. The formation and development of adventitious roots of *C. lanceolata* were studied by P.R. Krishna, et al. (2007) [9] and C.H. Ahn, et al. (2008) [10]. In 2012, J.A. Kim, et al. [11] studied adventitious

[*]*Corresponding author: Email: trinhthihuongcsdl@gmail.com*

rooting of *Codonopsis* species such as *C. lanceolata*, *C. pilosula,* and *C. ussuriensis*.

In this study, the roles of several auxins such as IBA and NAA in the induction of adventitious root from different explants of *C. javanica* was studied. This adventitious root is then used to quantify several important groups of compounds such as polysaccharides, phenolic compounds, and antioxidant activity.

2. Materials and methods

2.1. Materials

Codonopsis javanica (Blume) Hook.f. & Thomson originating in Kon Tum were used as the subject of this study.

C. javanica plantlets (4 cm of height) cultured on the MS [12] medium without plant growth regulator for 4 weeks were used material for experiments in this study.

2.2. Methods

Effect of auxin and light condition and explants on the adventitious root induction: The explants (internode/node/leaf) were placed on the MS medium containing 8 g/l agar (Ha Long, Vietnam), 30 g/l sucrose, and IBA (Duchefa, Netherland) or NAA (Duchefa, Netherland) with different concentrations of 0.5; 1.0; 1.5; 2.0; 2.5; 3.0 mg/l and without auxin supplementation treatment was the control.

The internode and node explants were cut to 1.0 cm in length, and the leaf explants were cut to 0.5x0.5 cm in size.

All cultures were placed under white fluorescence (Philips, Vietnam) with a light intensity of 40±2 µmol m^{-2} s^{-1}, 12 h/day at 22±2°C and 60% relative humidity (RH), or dark condition. The treatments were repeated 3 times with 3 bottles/time and 5 explants/bottle.

The observation targets such as rate of adventitious root formation explants (%) and the average number of roots/explant were collected after 4 weeks of culture.

Evaluation quality of C. javanica adventitious root biomass: The quantification of total phenolic and polysaccharide contents and the antioxidant activity of *C. javanica* adventitious root biomass cultured in the optimal medium is given below.

Preparation of ethanol extracts of C. javanica adventitious root biomass: The dried samples of *C. javanica* adventitious roots were weighted, then separately macerated with 30 ml ethanol (4×30 ml for 24 h at room temperature). After filtration, the solvent was evaporated in vacuum at 50°C to obtain crude ethanol extract.

Quantification of total polysaccharide content of C. javanica adventitious root biomass: Soluble sugar content was determined by the method of phenol - sulfuric acid. To calculate the content in the original sample, Eq. (1) is used [13]:

$$\text{Sugar content } (\%) = \frac{\text{Sugar concentration in PS powder (µg/ml)}}{\text{sample concentration PS (µg/ml)}} * \text{PS extract performance} \quad (1)$$

Quantification of total phenolic content of C. javanica adventitious root biomass: The total phenolic content was determined according to the Folin-Ciocalteu method [14]. Briefly, 1 mg of the crude extract is dissolved in 1 ml of distilled water and 0.1 ml of the diluted sample solution is placed into an Eppendorf tube. Then, 0.5 ml of 10% Folin-Ciocalteu solution is added and the solution is mixed well. Next, the mixture is incubated to react for 5 min, and then 0.4 ml 7.5% Na_2CO_3 solution was added and mix well. The solution was incubated at room temperature for 1 h, then the optical absorbance was measured at 765 nm.

Evaluation antioxidant activity and bioactive compound of C. javanica adventitious root biomass:

Qualitative chemical components: the explant powder was extract by ethanol. The ethanol and extracts were analysed for the presence of phytochemicals by using standard qualitative chemical procedures [15, 16]. The colour reaction was used to test the presence of common metabolite classes such as alkaloid, carbohydrate, glycosides, protein, saponin, phenolic compound, flavonoid, fixed oils, gum, and mucilage.

Antioxidant activity: 2,2-Diphenyl-1-picrylhydrazyl (DPPH) radical-scavenging capacity assays were used to determine the total antioxidant activity of the explant crude extract. The extract was initially diluted to concentrations varying from 0.0625 mg/ml to 1 mg/ml and assays were performed in a 96-well microplate. The reaction mixture in each well of the 96-well microplate consisted of 100 µl of DPPH solution (300 µM) and 100 µl of the sample. Ethanol and ascorbic acid (2 mg/ml) were used as negative and positive control, respectively. The plate was kept for 30 min at 37°C, and the absorbance was immediately recorded at 517 nm on a Bio-Rad Benchmark Plus Microplate Spectrophotometer (USA). The scavenging activity percentage was determined according to L.L. Mensor, et al. (2001) [17]:

$$AA\% = 100 - \left[\frac{(Abs_{sample} - Abs_{control}) \times 100}{Abs_{control}}\right] \quad (2)$$

The radical scavenging activity of the extract was expressed in form of the IC_{50} values defined as the concentration of the sample required to decrease the absorbance at 517 nm by 50%.

3.3. Data analysis

Experiments were a completely randomized design and each treatment was repeated at least three times. All collected data were analysed by Minitab. All diagrams were drawn by Microsoft Excel® 2010.

3. Results and discussion

3.1. Results

3.1.1. Effect of auxin and light condition on the adventitious root induction from internode explant

The results showed that in both light and dark conditions, IBA and NAA showed differential effects on adventitious root induction from internode explants of *C. javanica*. The data in Table 1 shows that the rooting percentage and number of roots per explants in the dark condition were higher than in the light condition. The rate of adventitious root induction was the highest on the medium supplemented with 0.5 mg/l IBA; the rooting percentage was 100% and the number of roots per explant was 33.87 roots. The formation of adventitious roots were totally absent in the culture containing higher concentration of NAA (3.0 mg/l) and the control in both light and dark conditions (Fig. 1).

Table 1. The effect of IBA, NAA and light condition on the adventitious root induction from internode explants after 4 weeks of incubation.

Auxin	Concentration (mg/l)	Light		Dark	
		No. of roots/ explant	*Rooting percentage (%)*	*No. of roots/ explant*	*Rooting percentage (%)*
IBA	0.0	0.00^{d}	0.00^{e}	0.00^{h}	0.00^{g}
	0.5	0.00^{d}	0.00^{e}	**33.87^{a}**	**100.00^{a}**
	1.0	11.99^{a}	60.00^{a}	19.59^{b}	75.56^{b}
	1.5	9.97^{ab}	51.11^{ab}	14.79^{c}	66.67^{bc}
	2.0	8.37^{b}	46.67^{ab}	11.70^{cde}	57.78^{cd}
	2.5	4.22^{c}	22.22^{cd}	11.42^{de}	57.78^{cd}
	3.0	2.00^{cd}	15.56^{de}	8.59^{ef}	31.11^{ef}
NAA	0.0	0.00^{d}	0.00^{e}	0.00^{h}	0.00^{g}
	0.5	0.00^{d}	0.00^{e}	12.06^{cd}	46.67^{de}
	1.0	8.03^{b}	35.56^{bc}	10.33^{de}	37.78^{ef}
	1.5	4.22^{c}	11.11^{de}	9.00^{def}	28.89^{f}
	2.0	0.00^{d}	0.00^{e}	6.11^{fg}	28.89^{f}
	2.5	0.00^{d}	0.00^{e}	3.17^{g}	28.89^{f}
	3.0	0.00^{d}	0.00^{e}	0.00^{h}	0.00^{g}

Means in the same column that are followed by different letters are significantly different (p≤0.05) using Duncan's Multiple Range Test.

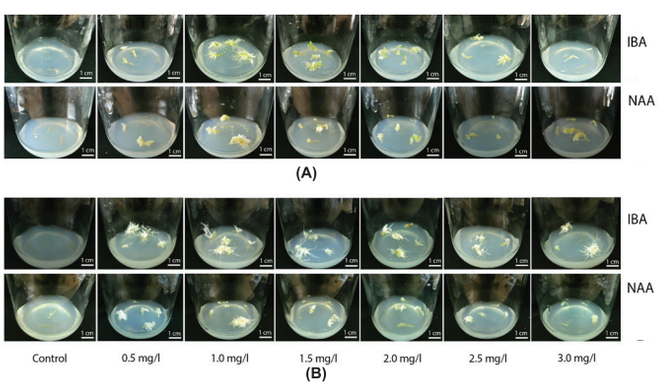

Fig. 1. Effect of IBA, NAA and light condition on the adventitious root induction from internode explants after 4 weeks of incubation. (A) Light condition; **(B)** Dark condition.

3.1.2. Effect of auxin and light condition on the adventitious root induction from leaf explant

In this experiment, NAA affected root induction more effectively than IBA in light conditions. The rooting percentage and number of roots per explant in NAA-added medium (the rate ranged from 37.78-80% and 3.89-17.90 roots/explant, respectively) were higher than IBA-added medium (the rate ranged from 17.78-60% and 1.37-6.81 roots/explant, respectively). After 4 weeks of incubation in the light condition, the highest rooting percentage and number of adventitious roots per explant were 80% and 17.90, respectively, on the medium supplemented with 0.5 mg/l NAA.

Table 2 shows that the dark condition also enhanced root formation better than the light condition. In the dark condition, the rate of adventitious root induction was the highest on the medium supplemented with 0.5 mg/l IBA (the rooting percentage and the number of roots per explant were 97.78% and 23.48 roots, respectively) after 4 weeks of culture. The adventitious root induction decreased with increasing IBA concentrations from 1 to 3 mg/l. Fig. 2 shows that the leaf explants produced adventitious roots from the cut ends, and the roots formed directly from the leaf sample and not through the callus. The leaf explants did not produce adventitious root on the control under both incubation conditions.

Table 2. The effect of IBA, NAA and light condition on the adventitious root induction from leaf explants after 4 weeks of incubation.

Auxin	Concentration of auxin (mg/l)	Light		Dark	
		No. of roots/ explant	*Rooting percentage (%)*	*No. of roots/ explant*	*Rooting percentage (%)*
IBA	0.0	0.00^{g}	0.00^{g}	0.00^{g}	0.00^{e}
	0.5	0.00^{g}	0.00^{g}	**23.48^{a}**	**97.78^{a}**
	1.0	2.33^{fg}	17.78^{fg}	17.28^{b}	80.00^{ab}
	1.5	6.81^{cde}	60.00^{abc}	11.50^{c}	71.11^{bc}
	2.0	4.61^{def}	42.22^{bcde}	8.73^{de}	60.00^{bcd}
	2.5	3.67^{efg}	31.11^{def}	7.77^{def}	46.67^{cd}
	3.0	1.37^{fg}	20.00^{efg}	6.72^{ef}	37.78^{d}
NAA	0.0	0.00^{g}	0.00^{g}	0.00^{g}	0.00^{e}
	0.5	17.90^{a}	80.00^{a}	12.62^{c}	80.00^{ab}
	1.0	13.52^{b}	64.44^{ab}	9.98^{cd}	75.56^{ab}
	1.5	9.07^{c}	60.00^{abc}	8.17^{def}	71.11^{bc}
	2.0	7.66^{cd}	51.11^{bcd}	7.54^{def}	64.44^{bc}
	2.5	6.13^{cde}	42.22^{bcde}	6.90^{ef}	62.22^{bcd}
	3.0	3.89^{ef}	37.78^{cdef}	5.43^{f}	48.89^{cd}

Means in the same column that are followed by different letters are significantly different (p≤0.05) using Duncan's Multiple Range Test.

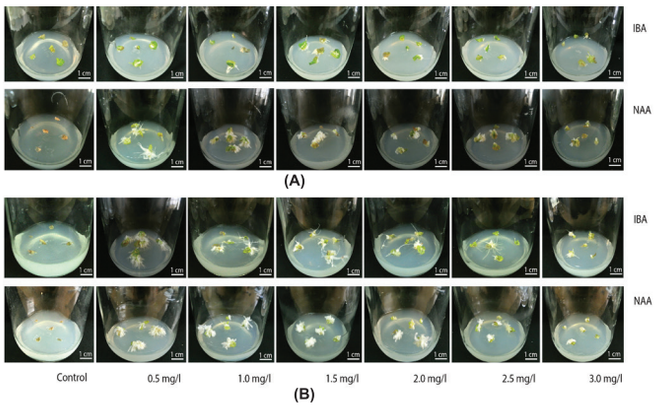

Fig. 2. Effect of IBA, NAA and light condition on the adventitious root induction from leaf explants. (A) Light condition; **(B)** Dark condition.

3.1.3. Effect of auxin and light condition on the adventitious root induction from node explant

The rate of adventitious root induction, as well as the average number of roots/explant on the medium containing IBA and NAA with levels from 0.5 to 3.0 mg/l, were significantly different after 4 weeks of incubation under both light and dark conditions. IBA was more effective than NAA for adventitious root induction from node explants of *C. javanica* in dark conditions, but NAA was quite more effective than IBA in light condition. Table 3 shows that the root induction decreased with the increasing IBA and NAA concentrations (from 1 to 3 mg/l) in both conditions. The root induction was the highest on the medium supplemented with 0.5 mg/l IBA in the dark condition (the rate and the number of roots per explant were 100% and 25.20 roots, respectively). The number of adventitious roots per explant under dark conditions were higher than light conditions.

In the control, the node segments did not induce adventitious root, but instead formed shoots. This was because the node segment contained auxiliary buds that were not inhibited in the medium without auxin supplementation, and shoots regenerated (Fig. 3).

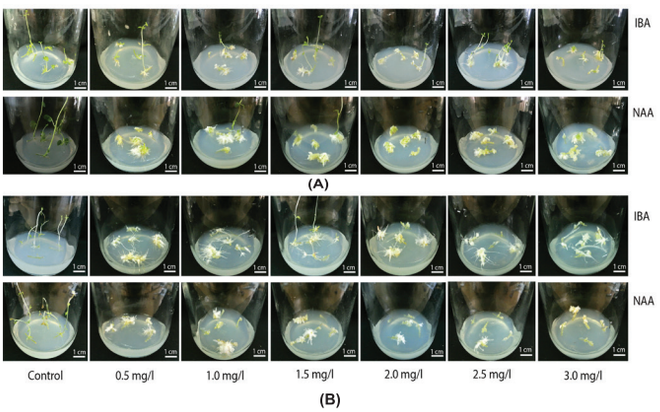

Fig. 3. The effect of IBA, NAA and light condition on the adventitious root induction from node explants. (A): light condition; **(B):** dark condition.

3.1.4. Preliminary phytochemical screening

After induction of roots from different explant sources, the adventitious roots of *C. javanica* were initially cultured to proliferate on liquid media and incubated under shaking conditions at 120 rpm. The results showed that the roots proliferated 3.87 times in the MS medium supplemented with 0.5 mg/l IBA, 30 g/l sucrose (data not shown). After 4 weeks of incubation in the liquid medium, adventitious root samples

Table 3. The effect of IBA, NAA and light condition on the adventitious root induction from node explants after 4 weeks of incubation.

Auxin	Concentration (mg/l)	Light		Dark	
		No. of roots/ explant	*Rooting percentage(%)*	*No. of roots/ explant*	*Rooting percentage (%)*
IBA	0.0	0.00^{g}	0.00^{e}	0.00^{h}	0.00^{j}
	0.5	4.44^{f}	24.44^{d}	**25.20^{a}**	**100.00^{a}**
	1.0	10.60^{bc}	57.78^{ab}	$18,87^{b}$	88.89^{ab}
	1.5	8.01^{cde}	51.11^{bc}	13.50^{cd}	82.22^{abc}
	2.0	6.27^{def}	51.11^{bc}	9.98^{def}	75.56^{bcd}
	2.5	4.66^{ef}	46.67^{bc}	8.94^{def}	62.22^{cdef}
	3.0	3.87^{f}	35.56^{cd}	6.47^{fg}	57.78^{defg}
NAA	0.0	0.00^{g}	0.00^{e}	0.00^{h}	0.00^{j}
	0.5	15.83^{a}	73.33^{a}	17.61^{bc}	71.11^{bcde}
	1.0	12.90^{ab}	60.00^{ab}	12.18^{de}	51.11^{efgh}
	1.5	11.06^{bc}	53.33^{abc}	10.28^{def}	46.67^{fghi}
	2.0	9.91^{bc}	51.11^{bc}	8.44^{ef}	37.78^{ghi}
	2.5	8.30^{cd}	46.67^{bc}	5.86^{fg}	28.89^{hi}
	3.0	6.47^{def}	33.33^{cd}	2.44^{gh}	26.67^{i}

Means in the same column that are followed by different letters are significantly different (p≤0.05) using Duncan's Multiple Range Test.

Table 4. Results of qualitative test for phytochemicals.

Test/reagents		*C. javanica* adventitious root biomass
Alkaloid	Mayer's	-
	Wagner's	+
Carbohydrate	Mollish's	+
	Fehling's	+
Saponin	Foam test	+
Fixed oils and fats	Spot test	+
	Saponification test	+
Tanin	$FeCl_3$	-
Phenolic compounds	Ferric chloride test	+
Flavonoid	Alkaline	+
Gum and mucilage	Absolute alcohol	+

were used to quantify some important compounds. Some specific reactions and colour change reactions were used to screen phytochemicals from the ethanol extract of sample powders. The result showed that *C. javanica* adventitious root biomass contains alkaloid, carbohydrate, saponin, phenolic compounds, flavonoid, fixed oil and fats, gum, and mucilage (Table 4).

3.1.5. Total phenolic, polysaccharide content and the antioxidant activity of C. javanica adventitious root biomass

After screening some important bioactive compounds of the adventitious roots, the explant was also used to quantify two important bioactive compounds such as polysaccharide and polyphenol content. Results showed that the adventitious root biomass presented polysaccharides (16.98%), polyphenol (1.876 mg GAE/g DW), and the half-maximal inhibitory concentration (IC_{50}) value determined by the 2,2-diphenyl-1-picrylhydrazyl was 2.44 mg/ml (Table 5).

Table 5. Total polysaccharide and polyphenol contents, and the antioxidant activity of the adventitious root biomass.

***C. javanica* of adventitious root biomass**	
Polysaccharide content (%)	16.98
Polyphenol content (mg GAE/g DW)	1.876
IC_{50} (mg/ml)	2.44

3.2. Discussion

Auxin is one factor that plays an important role in organogenesis and especially in adventitious root induction. The responses of each species to the type and concentration of auxin were different. Therefore, the determination of the appropriate auxin type and concentration is essential. In this study, IBA and NAA were used to investigate the induction of adventitious root and the result showed that IBA and NAA significantly affected the process of adventitious root induction of *C. javanica*. According to A.S. Basra (2004) [18], IBA and NAA were more effective than IAA in other research. The optimal concentration of IBA or NAA for the adventitious root induction of *C. javanica* was relatively low as the concentration varied in the range of 0.5 mg/l to 1.0 mg/l. This result is also consistent with the conclusions of J.A. Kim, et al. (2012) [11] when studying adventitious root induction in species of the genus *Codonopsis*. The authors demonstrated that culture media supplemented with 0.5 mg/l NAA were suitable for root induction from the root segment of *C. lanceolata* and leaves of *C. ussuriensis*. Meanwhile, in the medium supplemented with higher auxin concentration, the adventitious root formation was less effective [11]. Explants did not induce adventitious root on both IBA and NAA-free medium, which reaffirmed the important role of auxin in the process of adventitious root induction. The results in Tables 1, 2, and 3 showed that IBA was the most suitable auxin to induce adventitious root induction of *C. javanica* in vitro. According to P.R. Krishna, et al (2007) [9], the rate of *C. lanceolata* adventitious root formation on the medium containing IBA was highest with a rate of 100%.

As mentioned above, the adventitious root formation of *C. javanica* results directly from the explant without callus induction phase. N. Praveen, et al (2009) [19] showed that adventitious root of *Andrographis paniculata* was formed directly from leaf explants without the callus induction phase. In the study of M.A. Baque, et al. (2010) [20], 1.0 mg/l IBA was proven as the best auxin source for adventitious root induction of *M. citrifolia* without the callus phase. However, in some case, adventitious roots dedifferentiated to form calli [20]. According to X. Gao, et al. (2005) [21], *Panax notoginseng* adventitious root were formed from callus on the IBA-supplemented medium.

In this study, all three types of explants (internode, nodes, and leaf) induced adventitious root (Fig. 4). Depending on the type of auxin as well as the culture conditions, the root formation rate, and the number of roots per explant were different. Evaluating the possibility of generating adventitious roots from three different types of explants such as node, internode, and leaf, it was found that the number of adventitious roots per internode explant of *C. javanica* was higher than node and leaf explant. C.H. Ahn, et al. (2008) [10] studied the induction of adventitious root of *C. lanceolata* and indicated that the number of adventitious roots per stem explant was higher than leaf and root explant. In the process of *C. javanica* adventitious root induction, most internode explants induced adventitious root under dark control. This could be explained that dark incubation enhanced the accumulation of endogenous IAA in the internode explant during adventitious root induction [22]. However, the result in this study was contrary to that of M.A. Baque, et al. (2010) [20] as fluorescent light was suitable for adventitious root induction of *M. citrifolia*. This showed that adventitious root formation was not only dependent on genotype, species, and growth regulator concentration, but also type of tissue, organ, age, and stage of plant development [23].

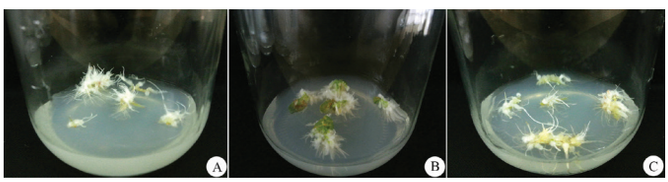

Fig. 4. Three types of explants [internode (A), leaf (B), and node (C)] produced adventitious root on the MS medium supplemented with 0.5 mg/l IBA under dark conditions.

The adventitious root biomass presented polysaccharides (16.98%). This result is similar to some species of the genus *Codonopsis* such as *C. pilosula* and *C. lanceolata* [1]. The content of a polyphenol in the *C. javanica* root was 1.876 mg GAE/g DW, and the IC_{50} value was 2.44 mg/ml. Compared to the results of N.P. Tri, et al. (2020) [24], the content of polyphenol and the antioxidant activity of adventitious root were less than the natural plant-derived root. According to [20], the total phenolic content of *C. javanica* extract derived from this root was 2.9 mg GAE/g DW, and IC_{50} values determined by DPPH tests of the *C. javanica* root extract were 1042.3 µg/ml [24]. This can be explained by the short adventitious root culture

period resulting in low accumulation of secondary compounds. Besides, under *in vitro* conditions, we can control the medium culture as well as use some elicitors to stimulate the increase in the content of bioactive compounds. In this study, the adventitious root contained an alkaloid, saponin, flavonoid, fixed oil and fats, gum, and mucilage in the *in vitro* condition. According to T.K. Lim (2015) [25], *C. javanica* natural root also contained glucose, essential oil, fatty substances, and alkaloids. The presence of these important compounds in the *in vitro* explants suggested that these explants could be used as a potential material source in traditional treatment against various diseases affecting humans and animals. More research about bioactivities needs to be done to analyse this potential.

4. Conclusions

All three types of explant (internode, nodes, and leaf) initiated adventitious root induction. The optimal concentration of IBA or NAA for the adventitious root induction of *C. javanica* was relatively low with the concentration varying in the range of 0.5 mg/l to 1.0 mg/l. The number of adventitious roots per internode explant of *C. javanica* was higher than node and leaf explant.

C. javanica adventitious root biomass contains alkaloid, carbohydrate, saponin, phenolic compounds, flavonoid, fixed oil, fats, gum, and mucilage. The adventitious root biomass presented polysaccharides (16.98%), polyphenol (1.876 mg GAE/g DW), and the IC_{50} value was 2.44 mg/ml.

CRedit author statements

Thi Huong Trinh, Quoc Tuan Nguyen, Thi Huyen Trang Nguyen: Conceptualization, Methodology, Data curation, Formal analysis, Writing - Review & Editing; Dang Giap Do, Trong Tuan Tran: Conceptualization, Methodology, Writing - Original draft preparation, Writing - Review & Editing.

ACKNOWLEDGEMENTS

The authors would like to thank the HCM-Fosted, Department of Science and Technology for supporting this study under number 13/2019/HD-QPTKHCN.

COMPETING INTERESTS

The authors declare that there is no conflict of interest regarding the publication of this article.

REFERENCES

[1] J.Y. He, Z. Shu, K. Katsuko (2014), "HPLC/UV analysis of polyacetylenes, phenylpropanoid and pyrrolidine alkaloids in medicinally used *Codonopsis* species", *Phytochemical Analysis*, **25(3)**, pp.213-219, DOI: 10.1002/pca.2494.

[2] J.Y. He, M. Na, Z. Shu, et al. (2015), "The genus *Codonopsis* (Campanulaceae): A review of phytochemistry, bioactivity and quality control", *Journal Nat. Med.,* **69**, pp.1-21, DOI: 10.1007/s11418-014-0861-9.

[3] F. Macchioni, S. Carugini, F. Cecchi, et al. (2004), "Aqueous extract of *Codonopsis javanica* against larval and pupal stages of *Aedes albopictus* [tiger mosquito]", *Ann. Fac. Medic. Veter. Pisa. (Italy)*, **57**, pp.215-220.

[4] K.N. Chen, W.H. Peng, C.W. Hou, et al. (2013), "*Codonopsis javanica* root extracts attenuate hyperinsulinemia and lipid peroxidation in fructose-fed insulin resistant rats", *Journal of Food and Drug Analysis*, **21(4)**, pp.347-355, DOI: 10.1016/j.jfda.2013.08.001.

[5] P.H. Nguyen, D.C. Luu, Q.B. Nguyen (2014), "A survey of traditional medicinal plants used by K'ho people in the buffer zone of Chu Yang Sin national park, Vietnam", *Journal of Vietnamese Environment*, **6(3)**, pp.276-280.

[6] Ministry of Science and Technology, Vietnam Academy of Science and Technology (2007), *Vietnam Red Data Book Part II. Plants*, Publishing House for Science and Technology, 611pp (in Vietnamese).

[7] J.H. Peng, Y.J. Yu, M.Z. Zhang (2010), "Study on tissue culture and plantlet regeneration of *Codonopsis lanceolata*", *Acta Botanica Boreali-Occidentalia Sinica,* **30(1)**, pp.184-189.

[8] S. Wojciech, T. Bogna, M. Adam (2011), "Micropropagation of *Codonopsis pilosula* (Franch.) Nannf. by axillary shoot multiplication", *Acta Biologica CracoviensiaSeries Botanica*, **53(2)**, pp.87-93, DOI: 10.2478/v10182-011-0031-2.

[9] P.R. Krishna, M.A. Chari, M.K. Kim, et al. (2007), "Induction of adventitious roots and extraction of *Codonoposide* from *Codonopsis lanceolata*", *Natural Products: An Indian Journal*, **3(3)**, pp.129-131.

[10] C.H. Ahn, K.H. Bae, J.S. Yi, et al. (2008), "Induction and growth of adventitious roots and bioreactor culture in *Codonopsis lanceolata*", *Journal of Plant Biotechnology*, **35(2)**, pp.155-161.

[11] J.A. Kim, E.J. Park, Y.E. Choi (2012), "Induction and proliferation of ddventitious roots in *Codonopsis* spp.", *Korean Journal of Medicinal Crop Science*, **20(6)**, pp.493-499, DOI: 10.7783/KJMCS.2012.20.6.493.

[12] T. Murashige, F. Skoog (1962), "A revised medium for rapid growth and bioassays with tobacco tissue cultures", *Physiologia Plantarum*, **15(3)**, pp.473-497, DOI: 10.1111/j.1399-3054.1962.tb08052.x.

[13] T. Masuko, A. Minami, N. Iwasaki, et al. (2005), "Carbohydrate analysis by a phenol-sulfuric acid method in microplate format", *Anal. Biochem.*, **339(1)**, pp.69-72, DOI: 10.1016/j.ab.2004.12.001.

[14] O. Folin, V. Ciocalteu (1927), "On tyrosine and tryptophane determinations in proteins", *Journal of Biological Chemistry*, **73(2)**, pp.627-650.

[15] I. Culei (1982), "Methodology for the analysis of vegetable drugs", *Practical Manual on The Industrial Utilization of Medicinal and Aromatic Plants*, Bucharest Office of Joint UHIDO, Bucharest, Romania, pp.67-81.

[16] J.B. Harbone (1984), *Phytochemical Methods*, 2nd Champion and Hall Publishers, London, 288pp.

[17] L.L. Mensor, F. Boylan, G. Leitao, et al. (2001), "Screening of Brazilian plant extracts for antioxidant activity by the use of DPPH free radical method", *Phytotherapy Research*, **15(2)**, pp.127-130, DOI: 10.1002/ptr.687.

[18] A.S. Basra (2004), *Plant Growth Regulators in Agriculture and Horticulture*, The Haworth Press, New York, 255pp.

[19] N. Praveen, S.H. Manohar, P.M. Naik, et al. (2009), "Production of andrographolide from adventitious root cultures of *Andrographis paniculata*", *Current Science*, **96(5)**, pp.694-697.

[20] M.A. Baque, E.J. Hahn, K.Y. Paek (2010), "Induction mechanism of adventitious root from leaf explants of *Morinda citrifolia* as affected by auxin and light quality", *In vitro Cellular & Developmental Biology-Plant*, **46**, pp.71-80, DOI: 10.1007/s11627-009-9261-3.

[21] X. Gao, C. Zhu, W. Jia, et al. (2005), "Induction and characterization of adventitious roots directly from leaf explants of *Panax notoginseng*", *Biotechnoly Letters*, **27(22)**, pp.1771-1775, DOI: 10.1007/s10529-005-3553-4.

[22] H. Yang, Y. Klopotek, M.R. Hajirezaei, et al. (2019), "Role of auxin homeostasis and response in nitrogen limitation and dark stimulation of adventitious root formation in petunia cuttings", *Annals of Botany*, **124(6)**, pp.1053-1066, DOI: 10.1093/aob/mcz095.

[23] P.D. Tiberiapop, B. Catherine (2011), "Auxin control in the formation of adventitious roots", *Notulae Botanicae Horti Agrobotanici Cluj-Napoca*, **39(1)**, pp.307-316, DOI: 10.15835/nbha3916101.

[24] N.P. Tri, T.N. Van, Q.T. Tran, et al. (2020), "Effects of various processing parameters on polyphenols, flavonoids, and antioxidant activities of *Codonopsis javanica* root extract", *Nat. Prod. Commun.*, **15(9)**, pp.1-12, DOI: 10.1177/1934578X20953276.

[25] T.K. Lim (2015), "Codonopsis javanica", *Edible Medicinal and Non- Medicinal Plants*, Springer, **9**, pp. 870-873, DOI: 10.1007/978-94-017-9511-1_32.

DOI: 10.31276/VJSTE.63(4).17-22

Physicochemical parameters and mineral components in Vietnam honey as a promising tool for classifying biological origin of honeys

Thu Huong Nguyen[1*], Thanh Long Ngo[1], Huu Quang Nguyen[2]

[1]*Department of Analytical Chemistry, University of Science, Vietnam National University - Ho Chi Minh City, 227 Nguyen Van Cu Street, Ward 4, District 5, Ho Chi Minh City, Vietnam*

[2]*Department of Chemistry, Chungnam National University, 99 Daehak-ro Street, Yuseong-gu District, Daejeon City, Korea*

Received 21 February 2020; revised 23 April 2020; accepted 8 May 2020

Abstract:

For many years honey is known as a natural sweetener agent with high nutritional value and brings many health benefits, the desirable flavor and medicinal properties of premium honey make it highly desirable. Because of this perticular reason, honey has been a target of adulteration through the mixing of low-quality honey and mislabelling of the honey's origin. Vietnam was ranked the sixth largest in the world and the second largest in Asia in the amount of honey exported in 2018. The aim of this research considers the potential of using mineral and physicochemical data to authenticate the origin of honey. To this end, 40 samples of 8 botanica collected from 18 different regions of Vietnam were analysed for its metal contents (Na, K, Mg, Ca, Al, Cu, Fe, Mn, Zn, Pb, Cd, Ni, Cr, Co, As, Hg) and physicochemical parameters (pH and electrical conductivity). The data were processed by multivariate analysis, which allowed the classification of honey according to its botanical origin.

Keywords: **authenticity, honey, mineral, multivariate analysis, physicochemical parameters.**

Classification number: **2.2**

1. Introduction

Vietnam was ranked the sixth largest in the world and the second largest in Asia in the amount of honey exported in 2018. However, honey export has recently suffered a dramatic decrease in terms of production, quality, and value. A statistic reported that Vietnam exported honey at a comparative price with India in 2013, but in 2017, prices became 10% cheaper than India. In 2018 the export value of the natural honey of Vietnam was approximately 67.7 million US dollars, which was down 49.2% from 2014 when it fell into the twelfth position on the world market [1]. The highest priced honey products come from New Zealand at 23.25 €/kg, while the honey price in Vietnam only reached 1.22 €/kg, which is the lowest price for honey products for export [2]. Vietnamese honey is also facing the risk of losing of both import and export markets. In the domestic market, Vietnamese honey either lacks or is underqualified for specific compositions or is mixed with illegal products to increase commercial profits. For those reasons, potential customers are now showing suspicion and hesitancy thus limiting their purchasing power. While the average honey consumption level in the world is about 700 g per person per year, the figure is just 30-40 g per person per year in Vietnam. This is due to the lack of a good policy to control the quality of honey, especially to detect fake or artificially produced honey. The sale of unidentified honey is also unregulated, which makes consumers hesitant to purchase honey products. Therefore, a simple and effective quality control method, as well as one that improves the traceability of honey, is essential. Methods assessing the authenticity of foodstuffs and honey in particular has become an indispensable issue in quality control and food safety. Honey's properties and compositions, both wild and farmed, depend not only on the nectar but also on other factors such as bee strains, geographic areas, seasons, storage methods, and even cultivation technology and harvesting conditions. Therefore, it is not trivial to correctly identify the source of honey. In previous works, different parameters such as moisture, electrical conductivity, carbohydrate, pH, and mineral content in honey were discriminated by multivariate data analysis, and the results exhibited high classification power [3-5]. M. Oroian, et al. (2017) [6] reported the coupled use of honey parameters and chemometric analysis is a powerful method to determine the origin of honey as well as other food products.

[*]*Corresponding author: Email: ngthuong@hcmus.edu.vn*

The main objective of this study is to measure some common physicochemical parameters and elements of honey samples cultivated in various known botanical origins. The results were to evaluate the quality of honey from several provinces in Vietnam and to perform multivariate statistical analysis to find the relation of these parameters with the botanical origins of the honeybee.

2. Methodologies

2.1. Sampling and sample storage

In this study, 40 samples of eight botanical origins of honey (acacia, coffee flower, jungle flower, longan flower, lychee flower, rambutan flower, rubber, and mutifloral) were taken from 18 different regions of Vietnam. The samples were provided by the individual beekeepers and natural honey hunters from 2016 to 2019. Their botanical and geographic origins are shown in Table 1. After delivery to the laboratory, the samples were kept at room temperature in plastic or glass bottles until analysis. To reduce the viscosity and ensure representability of the sample, the honey container was sonicated and later a mass of honey was digested or diluted prior to the measurement [7].

Table 1. Botanical and geographical origin of the 40 honey samples analysed.

Sample No.	Geographic origin	Biographic origin	No. of sample
BG	Bac Giang	Lychee flower	2
BP	Binh Phuoc	Rubber	1
BT	Ben Tre	Mutifloral	1
BT2	Ben Tre	Rubber	1
BT3	Ben Tre	Longan flower	1
CG	Can Gio	Jungle	1
CM	Ca Mau	Jungle	1
CM2	Ca Mau	Acacia	1
DB	Dien Bien	Jungle	2
DL	Dak Lak	Coffee flower	1
DN	Dong Nai	Rambutan flower	1
GL	Gia Lai	Jungle	1
GL2	Gia Lai	Rubber	1
KT	Kon Tum	Jungle	1
KT2	Kon Tum	Coffee flower	1
LD	Lam Dong	Coffee flower	14
NA	Nghe An	Jungle	1
PQ	Phu Quoc	Acacia	1
QN	Quang Ngai	Acacia	1
ST	Soc Trang	Longan flower	2
TG	Tien Giang	Longan flower	1
TN	Tay Ninh	Longan flower	1
T	Blended honey	Longan+Lychee flower	2

2.2. Sample analysis

2.1.1. Electrical conductivity and pH determination

The electrical conductivity of the honey was measured using an InLab 731-ISM conductivity electrode connected to a Mettler Toledo SevenExcellence meter (USA). According to the method proposed by the International Honey Commission (IHC) [8], the electrical conductivity measurement was performed on a 20% (w/v) diluted honey solution at 20°C. To achieve this, first 20 g dry honey was dissolved in milli-Q water. This solution was transferred quantitatively to a 100-ml volumetric flask and milli-Q water was added. Afterward, 40 ml of the sample solution was transferred to a 100-ml beaker, which was temperature controlled at 20±0.5°C. The conductivity electrode was then immersed in the sample solution and the electrical conductivity of this solution was measured in units of $\mu S.cm^{-1}$ after equilibrium was reached. All samples were measured in triplicate.

The pH values of the honey samples were determined according to the method proposed by the IHC [8] using an Inlab Expert Pro-ISM pH electrode (Mettler Toledo, USA). First, 10 g of the honey sample was dissolved in 75 ml of milli-Q water in a 250-ml beaker to obtain a 10% (w/v) honey solution. The solution was vortexed for 2 min and the pH value was obtained. Each sample was measured twice and the results were given as mean values.

2.1.2. Elemental analysis

Digestion procedures for determining minerals: because the majority of the organic matrix could interfere with the precision of analytical results, it is necessary to pre-treat the samples prior to analysis. There are a range of methods to remove the predominance of sugar in the honey such as solid-phase extraction, wet digestion, dry ash, and microwave digestion.

High temperature dry ashing was used to digest the organic substances and release the metals into the solution before determining the metal ion content using flame atomic absorption spectroscopy (F-AAS) and inductively coupled plasma mass spectrometry (ICP-MS). The sample was initially homogenized by vortexing. Five grams of the sample was placed in a porcelain crucible, then 1 ml NH_4HPO_4 (200 $mg.l^{-1}$) and 1.0 ml concentrated H_2SO_4 (Merck) were added as matrix modifiers. This mixture must be heated for 4 h to remove water by using the medium setting of a hot plate. Next, the dried sample was transferred to a furnace and the temperature of the furnace was slowly increased from 250 to 500°C at a heating rate of 2°C/min and kept at its

final temperature for 12 h to ensure the organic matter was fully destroyed. The residuals left were diluted by adding 5 ml HNO_3 (25% solution) and was made up to a volume of 10 ml by using HNO_3 (1% solution). This solution was measured for its metal ion contents via AAS and ICP-MS techniques.

Determination of total metal concentration: an Agilent 7700x inductively coupled plasma mass spectrometer was used to measure the concentrations of zinc (Zn), copper (Cu), aluminium (Al), iron (Fe), manganese (Mn), chromium (Cr), nickel (Ni), cobalt (Co), lead (Pb), cadmium (Cd), arsenic (As), and mercury (Hg) with ^{103}Ru and ^{197}Au as internal standards, while a Shimadzu AA-6650 flame atomic absorption spectrophotometer was used to determine the concentrations of sodium (Na), potassium (K), magnesium (Mg), and calcium (Ca).

FAAS was chosen to determine Na, K, Mg, and Ca contents because this method provides high accuracy and sensitivity to alkaline and earth-alkaline metals. Samples were diluted to ensure the measured results were the most accurate. In addition, FAAS utilizes an air/acetylene flame with a relatively low atomic temperature that could limit ionization interference for K and Na.

A certified reference material is not commercially available due to the practical problem representative of this kind of sample. In this study, a spike recovery was done to assess the accuracy of the digestion procedure. The results of the recovery study are presented in Table 2. The recovery percentages ranged between 81 and 102%, which fall within the normal acceptable range of a good recovery. Therefore, the methods used in this study achieved the required accuracy and reliability levels of all the metal contents in this study.

Table 2. Recovery of the metal elements in this study.

Elements	Concentration	C_{sample}	C_{spike}	C_{found} (mean±SD)	Recovery (%)
Na	mg.kg^{-1}	71.32	70	66.0±2.9	94.3±7.5
K	mg.kg^{-1}	577.4	600	152±22	86±7.5
Mg	mg.kg^{-1}	1.93	2.3	2.20±0.02	97.3±1.4
Ca	mg.kg^{-1}	21.3	27.5	48.1±0.4	97.5±2.8
Mn	mg.kg^{-1}	1.20	1.00	0.99±0.05	98.7±2.9
Fe	mg.kg^{-1}	2.73	3.00	2.55±0.09	84.9±6.1
Cu	mg.kg^{-1}	0.66	0.60	1.15±0.01	81.1±1.2
Zn	mg.kg^{-1}	0.51	1.00	0.86±0.03	86.3±5.9
Al	mg.kg^{-1}	2.84	5.00	5.10±0.12	102.1±4.0
Cr	µg.kg^{-1}	23.47	25.04	23.4±1.1	93.6±8.5
Cd	µg.kg^{-1}	0.68	2.05	1.6±5.9	82±13
Pb	µg.kg^{-1}	12.74	15.03	12.2±0.6	81.7±8.5

2.3. Data processing

The analysed data combined with multivariate statistical analysis including principal component analysis (PCA) and partial least square discriminant analysis (PLS-DA) were applied to the characterization of the botanical and geographical origins of the studied honeys. In this study, all PCA and PLS models and data pre-treatments were done by SIMCA-P software (Umetrics, Sweden).

3. Results and discussion

3.1. Physicochemical properties

According to international regulations (CODEX and EU standards), the determination of the conductivity of honey is carried out at a 20% (w/v) concentration of honey. Conductivity is closely related to the concentration of mineral and organic acids and shows high variability both internally and externally between honey groups. The electrical conductivity of honey is limited by the CODEX standard for honey, which states that the conductivity should be no more than 800 µS.cm^{-1} [9]. The conductivity of the honey samples can range from 96.50 to 630.05 µS.cm^{-1} and are described in Fig. 1. The data indicated the lowest conductivity was found in jungle flower honey from Dien Bien (96.50 µS.cm^{-1}), while the highest conductivity was found in samples from the forest regions, namely QN, NA, and BT3, which exceeded the maximum value of 800 µS.cm^{-1} stipulated by CODEX. High electrical conductivity often indicates an increased content of mineral compounds. It is possible that the environment surrounding honeycombs or the beekeeping process could have changed the honey's composition through the nectar, which is the main food source of honeybees. Therefore, in order to more precisely explain this issue, it is necessary to find out more information from the beekeepers about the nest position as well as the bees' food composition. For the Quang Ngai (QN) and Nghe An (NA) samples, due to their limited number, no conclusion can be given until the number of analysed samples is increased.

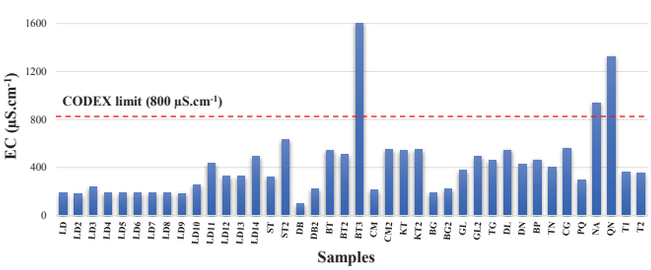

Fig. 1. Electrical conductivity of 40 collected samples performed at 10% (w/v) dilution ratio of honey.

Other studies have recently shown that the pH of honey depends on the free acid and total acid parameters, which could significantly contribute toward locating the biological origin of honey. Honey contains a number of acidic compounds including various amino acids (0.05-0.1% by weight) and organic acids (0.17 to 1.17%, averaged at 0.57% by weight). The average pH value of honey is 3.9 and usually varies between 3.4 to 4.35 [9]. As apparent from Fig. 2, the honeys have relatively low pH values, which limit the growth of microorganisms. All of 40 analysed honeys met permissible pH values set by the CODEX 2001 [10] and EU standards (pH 3.2-5.5). The pH values obtained in this study (3.44 to 4.35) were equivalent to those previously reported in Algeria, Poland, and Portugal honeys, which vary between pH 3.50 and 4.58 [11-13].

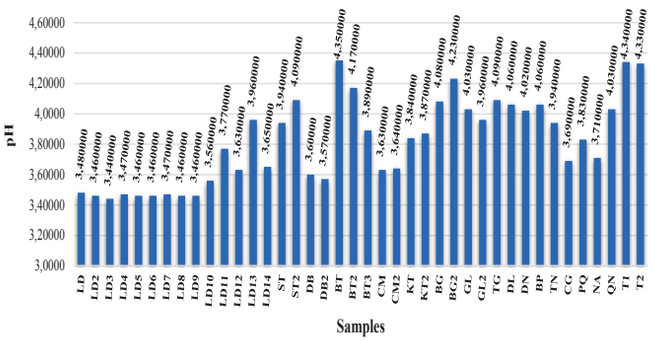

Fig. 2. pH values of 40 collected samples performed at 20% (w/v) dilution ratio of honey.

3.2. Mineral components in Vietnam honey

The mineral components of the 40 Vietnamese honeys are shown in Table 3. As depicted in the table, potassium is the predominate element, which ranged between 200 and 2851 mg.kg^{-1}, which agrees with previous works [14]. The highest K content was found in the Ben Tre (BT) sample, followed by the Phu Quoc sample with 1544 mg.kg^{-1}. Along with K, some other minerals such as Na, Ca, and Mg could be considered as major metal components, which ranged from 3.18 to 535.5 mg.kg^{-1}, 3.63 to 115.0 mg.kg^{-1}, and 2.21 to 114.7 mg.kg^{-1}, in the honey samples, respectively.

Other essential elements including Al, Fe, Cu, Zn, and Mn were found at minor content levels. In particular, Al and Fe contents ranged from 1 to 30 mg.kg^{-1} in all honey samples. It was also found that Cu, Zn, and Mn had mean values lower than 8 mg.kg^{-1}.

Table 3. The concentration of major metals (K, Na, Ca, Mg), minor metals (Zn, Cu, Al, Fe, Mn), and trace metals in honey from different countries.

Elements		Vietnam[a]	Turkey	Spain	New Zealand
K (mg.kg^{-1})	C_{min}	200.3	143	670	200
	C_{max}	2851.9	6029		3640
Na (mg.kg^{-1})	C_{min}	3.18	9.3	47.3	1.1
	C_{max}	535.5	172		110
Ca (mg.kg^{-1})	C_{min}	3.63	3.3	34.2	7.21
	C_{max}	115.0	900		94.3
Mg (mg.kg^{-1})	C_{min}	2.21	2	73.2	7.52
	C_{max}	114.7	111		86.3
Zn (mg.kg^{-1})	C_{min}	0.17	<1	-	0.2
	C_{max}	3.39	20.2	-	2.46
Cu (mg.kg^{-1})	C_{min}	0.11	<1	0.393	0.09
	C_{max}	0.86	3.5		0.7
Al (mg.kg^{-1})	C_{min}	0.92	<1	-	0.23
	C_{max}	29.0	0.96	-	21.3
Fe (mg.kg^{-1})	C_{min}	0.70	0.04	3.62	0.67
	C_{max}	18.9	19.7		3.39
Mn (mg.kg^{-1})	C_{min}	0.17	<1	2.514	0.18
	C_{max}	7.76	74.2		4.75
Pb (µg.kg^{-1})	C_{min}	5.86	<1	-	3.01
	C_{max}	145.47	<1	-	40
Cd (µg.kg^{-1})	C_{min}	0.50	<1	-	<1
	C_{max}	34.09	<1	-	149
Cr (µg.kg^{-1})	C_{min}	1.46	-	-	<1
	C_{max}	170.02	-	-	370
As (µg.kg^{-1})	C_{min}	0.14	-	-	<1
	C_{max}	11.28	-	-	80
Ni (µg.kg^{-1})	C_{min}	18.41	-	-	-
	C_{max}	618.1	-	-	-
Co (µg.kg^{-1})	C_{min}	1.24	-	-	-
	C_{max}	29.76	-	-	-
Hg (ng.kg^{-1})	C_{min}	10.75	-	-	-
	C_{max}	268.8	-	-	-

[a]: results of this study; -: either not detected or not provided by the studies.

The mean and range of the concentrations of each trace element in the honey samples are shown in Table 4. The order of the mean trace element content from low to high is Hg, As, Cd, Co, Cr, Pb, Ni. The amount of trace element concentrations varied widely in the honey samples but were all below the minimum limit allowed in honey set by the Standards of the Vietnam Health Ministry for food products (QCVN 8-2011-BYT) and CODEX Alimentarius Commission (As<1.0 mg.kg^{-1}, Pb<1.0 mg.kg^{-1}, Cd<2.0 mg.kg^{-1}, Hg<0.05 mg.kg^{-1}) [10, 15].

It is noticeable that some heavy trace metal elements, including lead, cadmium, and mercury, were found at a relatively high level, which is associated more with soil and environment contamination.

Table 4. Concentration of trace metals in honey of different regions of Vietnam. All results in µg.kg $^{-1}$ except Hg in ng.kg $^{-1}$.

	Cr (µg.kg^{-1})	Ni (µg.kg^{-1})	Co (µg.kg^{-1})	Pb (µg.kg^{-1})	Cd (µg.kg^{-1})	As (µg.kg^{-1})	Hg (ng.kg^{-1})
Mean	24.4	120	10.6	66	5.04	2.39	81.9
Range	1.46-170	18.4-618	1.24-29.8	5.86-91.8	0.5-34.1	0.14-11.3	10.8-269

Overall, the concentrations of the 16 metal elements in this study varied significantly with the geographical and botanical origins of the honey samples. Also noticeable are variations within samples with the same origin. Therefore, multivariate data analysis is required to evaluate the relationship between the metal contents and other parameters of the honey, as well as to develop a classification model based on the physicochemical and mineral contents according to the origin of the honey samples.

3.3. Characterisation of the honeybee

In an attempt to establish the classification between 6 botanical origins and 18 graphical origins of honey, the PCA model was applied to the analysis data. PCA was able to evaluate the element composition of honey types. Fig. 3 shows the score plot of PCA corresponding to the data matrix. The two principal components (PCs) explained 85% of the variables of data set. The two PCs, PC1 and PC2, explained 65% and 20% of the variability, respectively. As seen in Fig. 3, the honey samples belonging to the following provinces tend to be separate from the rest: Lam Dong, Bac Giang, Gia Lai, and Kon Tum, although there was some overlapping of honey groups.

The model was slightly improved (R^2=0.861) after excluding 13 out of 18 analysis criteria, however, low classification ability was still observed (Q^2<0.5). This could be explained by the totally unsupervised nature of the PCA method, which might fail to achieve good separation in models that contain too many individual variables or classes. Therefore, the more supervised PLS-DA model should be considered to improve classification and explanation ability, in addition to supplying a prediction ability to the model.

To assess the PLS-DA model, a VIP (variable importance plot) was carried out to evaluate the level of contribution from each variable (VIP>0.7). Variables that did not distribute to the model were rejected to try for a better model. In the PLS model t[1] vs t[2], the R^2 and Q^2 were 0.858 and 0.812, respectively, after application of the stepwise PLS-DA to the data. The selected variables include pH, EC, K, Mg, Fe, Ni, Pb, and Cd.

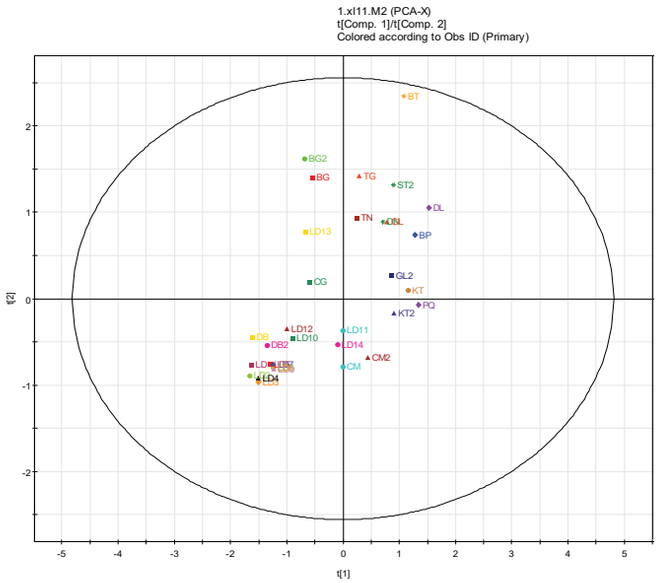

Fig. 3. Principal component analysis of the multielement scores of graphical origin of honeys. BG: Bac Giang, LD: Lam Dong, DB: Dien Bien, CM: Ca Mau, KT: Kon Tum, PQ: Phu Quoc, CG: Can Gio, TG: Tien Giang, ST: Soc Trang, DN: Dong Nai, GL: Gia Lai, BP: Binh Phuoc, DL: Dak Lak, TN: Tay Ninh.

Figure 4 presents the classification of honey in its corresponding botanical source with five separated groups (coffee, jungle, lychee, acacia, longan). There were some coffee honey samples that overlapped with the sample belonging to the jungle honey group. This can be explained by the fact that jungle honey is normally multifloral.

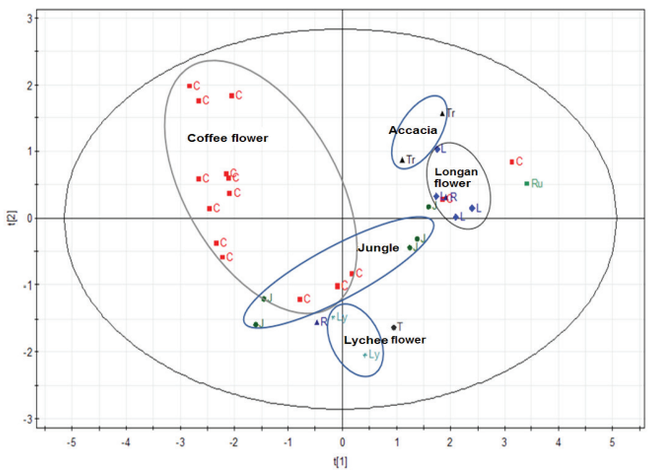

Fig. 4. Score plot of PLS-DA analysis used to distinguish all honey samples (n=40). C - coffee flower; J - jungle; Ly - lychee flower; L - longan flower; Ru - rubber; Tr - acacia; R - rambutan flower; T - blended honey.

The trueness of the model was checked by using two commercial blend samples from a beekeeper. Based on market demand, customers like to use honey products that are light in colour, dense, and scented. For example, unifloral honey, such as longan flower honey, has a fragrant scent but is less dense. Lychee honey is scented and is easily crystallized, while rubber honey is dark, not fragrant, and has a high density. Therefore, suppliers tend to mix these types of honey together but still want to ensure the quality of the honey. The two samples of honey used to evaluate the interpretation and prediction of the analytical model were mixes between the longan flower honey and the lychee flower honey. The score plot of the PLS-DA indicated that this blended honey (T) was located between the lychee group and the longan group and had characterizations of both groups. Therefore, it can be said that PLS-DA is a suitable tool for the differentiation and classification of studied honeys.

4. Conclusions

In this work, all the studied Vietnamese honey samples met the regulations of the Codex Alimentarius Commission and the Ministry of Public Health of Vietnam in terms of pH, electrical conductivity, and concentrations of toxic heavy metals. The use of elemental and common physicochemical profiles of 8 plants from 18 different areas in Vietnam was coupled with multivariate analysis for classification purposes. Although the present results do not display a clear separation of honey types from a variety of geographic origins, the final PLS model had values of R^2=0.858 and Q^2=0.812 (R^2>0.7 and Q^2>0.5), which exhibited a potential approach for discriminating Vietnamese honeys from different botanical origins. From a market manager perspective, these results establish a fast tool for classifying of Vietnamese honey, which contribute to the formulation of food safety policies, ensure the success of national brands, create customer trust, and boost the sustainable development of beekeeping activities.

CRedit author statements

Thu Huong Nguyen, Thanh Long Ngo, Huu Quang Nguyen: Conceptualization, Methodology, Data curation, Formal analysis, Conceptualization, Methodology, Writing - Original draft preparation, Writing - Review & Editing.

ACKNOWLEDGEMENTS

This research is funded by the University of Science, Vietnam National University - Ho Chi Minh city, under grant number T2018-13. The authors are grateful for the financial support of the University of Science. The authors also would like to thank Dr. Le Minh Hoang for helping to collect samples from the various provinces of Vietnam.

COMPETING INTERESTS

The authors declare that there is no conflict of interest regarding the publication of this article.

REFERENCES

[1] Statista (2020), *Food and Beverage*, https://www.statista.com/markets/423/topic/451/food-beverage/#statistic1, accessed 9 January 2020.

[2] D. Workman (2020), http://www.worldstopexports.com/natural-honey-exporters, accessed 9 January 2020.

[3] M.J.N. Nalda, J.L.B. Yague, J.C.D. Calva, et al. (2005), "Classifying honeys from the Soria province of Spain via multivariate analysis", *Anal. Bioanal. Chem.*, **382(2)**, pp.311-319, DOI: 10.1007/s00216-005-3161-0.

[4] C. Truzzi, S. Illuminati, A. Annibaldia, et al. (2014), "Physicochemical properties of honey from Marche, Central Italy: Classification of unifloral and multifloral honeys by multivariate analysis", *Natural Product Communications*, **9(11)**, pp.1519-1602.

[5] A.B. Manzanares, Z.H. Garcia, B.R. Galdon, et al. (2011), "Differentiation of blossom and honeydew honeys using multivariate analysis on the physicochemical parameters and sugar composition", *Food Chem.*, **126(2)**, pp.664-672, DOI: 10.1016/j.foodchem.2010.11.003.

[6] M. Oroian, S. Ropciuc (2017), "Honey authentication based on physicochemical parameters and phenolic compounds", *Comput. Electron. Agric.*, **138**, pp.148-156, DOI: 10.1016/j.compag.2017.04.020.

[7] P. Pohl (2009), "Determination of metal content in honey by atomic absorption and emission spectrometries", *Trends Analytical Chemistry*, **28(1)**, pp.117-128, DOI: 10.1016/j.trac.2008.09.015.

[8] International Honey Commission (2009), *Harmonised Methods of The International Honey Commission*, 63pp.

[9] J.W. White (1962), "Composition of American honeys", *Tech. Bull.*, **1261**, 124pp.

[10] CODEX Alimentarius (1981, 2001), *Standard for Honey - CXS 12-1981, Revised CODEX Standard for Honey, Standards and Standard Methods*, 7pp.

[11] X. Feas, J. Pires, A. Iglesias, et al. (2010), "Characterization of artisanal honey produced on the Northwest of Portugal by melissopalynological and physico-chemical data", *Food Chem. Toxicol.*, **48**, pp.3462-3470.

[12] S. Ouchemoukh, H. Louaileche, P. Schweitzer (2007), "Physicochemical characteristics and pollen spectrum of some Algerian honeys", *Food Control*, **18**, pp.52-58, DOI: 10.1016/j.foodcont.2005.08.007.

[13] M. Ewa, D. Beata, W. Rafal (2019), "Determination of the botanical origin of honeybee honeys based on the analysis of their selected physicochemical parameters coupled with chemometric assays", *FoodSci. Biotechnol.*, **28(5)**, pp.1307-1314, DOI: 10.1007/s10068-019-00598-5.

[14] M.N. Rashed, M.E. Soltan (2004), "Major and trace elements in different types of Egyptian mono-floral and non-floral bee honeys", *J. Food Compos. Anal.*, **17**, pp.725-735, DOI: 10.1016/j.jfca.2003.10.004.

[15] Vietnam Ministry of Health (2011), *QCVN 8-2:2011/BYT, National Technical Regulation on The Limits of Heavy Metals Contamination in Food.*

DOI: 10.31276/VJSTE.63(4).23-27

Adsorptive removal of methyl orange and methylene blue from aqueous solutions with *Acacia crassicarpa* activated carbon

Tue Ngoc Nguyen[1*], Khanh Quoc Dang[2], Duc Trung Nguyen[1]

[1]*School of Chemical Engineering, Hanoi University of Science and Technology, 1 Dai Co Viet Street, Bach Khoa Ward, Hai Ba Trung District, Hanoi, Vietnam*

[2]*School of Materials Science and Engineering, Hanoi University of Science and Technology, 1 Dai Co Viet Street, Bach Khoa Ward, Hai Ba Trung District, Hanoi, Vietnam*

Received 1 July 2021; revised 20 September 2021; accepted 29 September 2021

Abstract:

In this study, the activated carbon was used to create from *Acacia crassicarpa* bark was prepared and it was analysed for the potential development of low-cost, carbon-based adsorbents that remove industrial dyes from aqueous solutions. The adsorbents were characterised by utilising a variety of spectroscopy techniques and surface analyses. The adsorption of methyl orange (MO) and methylene blue (MB) onto the material was investigated under optimal experimental conditions including temperature, adsorbent dosage, and initial concentration of chemicals. It was observed that the Langmuir isotherm model adequately matched the adsorption data. The maximum adsorption capacities predicted by the Langmuir isotherm were found to be 10.36 mg.g^{-1} for MO and 15.34 mg.g^{-1} for MB, respectively. The adsorbents were able to remove the cationic dye more effectively than the anionic dye. The authors expected that this study's findings will be helpful in scaling up the production in the future of low-cost adsorbents using *Acacia crassicarpa* for the removal of cationic and anionic dyes.

Classification number: **2.2**

1. Introduction

A germ-free environment and safe drinking water are fundamental necessities that support healthy life. Currently, clean water is a vital element of domestic usage and it is employed in industrial and agricultural applications. However, existing suitable water sources can be contaminated by bacteria, microbes, and/or industrial waste containing organic pollutants, heavy metals, and various anions [1-5]. Two of the most commonly used dyes in biology, medicine, and textile industries are the chemical indicators MB and MO, both of which can cause various health problems like abdominal disorders if digested [6, 7]. Additionally, the presence of MB and MO in water, even at low concentrations, can absorb a major portion of sunlight and thus reduce sunlight penetration that can decrease the dissolved oxygen in water and hinder the growth of aquatic biota [6, 8]. Therefore, it is crucial to remove MB and MO dye molecules from industrial effluent before being discharged into the environment. Therefore, removing dyes from aqueous solutions has become an immense challenge that has attracted great interest.

Various physical, chemical, and even biological techniques such as biosorption, chemical oxidation, coagulation, membrane filtration, photodegradation, and adsorption have been employed to remove these organic pollutants from aqueous environments. However, adsorption has been known as the most effective, simple, and inexpensive technique as it is one of the most studied dye removal methods for water treatment [9, 10]. Recently, carbon-based materials like activated carbon (AC) have been used extensively as adsorbents due to their advantages in specific surface area, weight, mechanical strength, and electronic characteristics. With the purpose of improving the performance of carbon-based materials, a number of studies employing AC originating from low cost agricultural waste have been established [11]. Among biomass and agricultural wastes, *Acacia crassicarpa* bark is one alternative low cost material that can be used for AC preparation. Not only does this precursor have a large organic content and is locally available, there are large amounts of this agricultural waste available from industries that can be transformed into a value-added product. In addition, only small sample sizes of coffee grounds are needed to prepare the activation process. To the best of our knowledge, no studies of *Acacia crassicarpa* activated carbon (ACAC) have been published for MB and MO adsorption.

[*]*Corresponding author: Email: tue.nguyenngoc@hust.edu.vn*

Based on these factors, this paper aims to prepare and evaluate the dye removal potential of a novel, low cost, and green activated carbon originating from *Acacia crassicarpa* bark for removing MO and MB dyes from aqueous solutions. Two dye wastewaters containing MO and MB were adsorbed by the materials and the equilibrium of the dye adsorption process was thoroughly studied. The obtained results were used to assess the adsorption isotherm of the materials to determine optimal parameters.

2. Materials and method

2.1. Experimental materials

The chemicals used herein were all commercial products. All chemical reagents were of analytical grade and used without further purification. Chemicals were purchased from the Xilong Company in China. MB and MO, which have the chemical formula of $C_{16}H_{18}ClN_3S$ (MW of 319.85 g.mol^{-1}, λ_{max} of 668 nm) and $C_{14}H_{14}N_3NaO_3S$ (MW of 327.33 g.mol^{-1}, λ_{max} of 464 nm), respectively, were selected as the adsorbates in this research work.

2.2. Preparation of AC

Preparation of AC from *Acacia crassicarpa* bark: *Acacia crassicarpa* bark was collected from Nghe An province, Vietnam. The collected bark were washed several times with distilled water to remove any dirt. It was then air dried at 105°C for 24 h to a constant weight. The obtained dried solids were ground into a fine powder and then sieved to 43 µm. Then, the dried powder was loaded into a programmable tube furnace and heated up to 400°C under purified Ar gas flow (120 cm^3.min^{-1}) for organic phase removal. The resulting solid was denoted as ACAC-1. The next step was the carbonization process. First, the precursor was introduced to a sample holder that was placed in a rotary tube furnace. The operating conditions were increased from room temperature to 600°C with a pre-selected heating rate of 2, 3, and 4°C min^{-1} under Ar flow of 30 ml.min^{-1}. At 600°C, the temperature was subsequently increased to 1150°C with a heating rate of 5°C min^{-1} and was kept fixed for 1 h. The corresponding AC from the three different temperature rates were denoted as ACAC-2, ACAC-3, and ACAC-4 for 2, 3, and 4°C min^{-1}, respectively. The four samples then were measured using X-ray diffraction (XRD), Brunauer-Emmett-Teller (BET) analysis, and elemental analysis. After that, the ACAC-3 sample underwent a second carbonization process in which the temperature was first increased to 600°C and then increased to 1160°C with heating rates of 3°C min^{-1} and 5°C min^{-1}, respectively. The resulting solid was denoted as ACAC-5. Sample ACAC-5 was then carbonized with the same procedure as the previous ACAC-3. The resulting AC sample was denoted as ACAC-6. Afterward, all AC samples were washed with distilled water repetitively for 24 h until the sample colour was unchanged. The washed carbon was impregnated with NaOH 10% with a ratio of 1:5, then washed again with distilled water until pH 7 and vacuum-dried at ambient temperature (20°C) to become activated carbon.

2.3. Characterization of the AC

Elemental analysis integrated with IR spectroscopy was used to determine the components of the synthesized ACs. BET measurements were conducted to measure the surface area of all the AC samples. Scanning electron microscopy (SEM) was used to observe the surface morphology and surface texture of the materials. To study the changes in the microstructures of the four AC samples, an analysis was performed on measurements from high-resolution XRD. The carbon content was determined from IR measurements on a CS744 carbon/sulfur analyser via combustion.

2.4. Adsorption experiments

First, we chose two different dyes, MB and MO, to test the adsorption performance of the selected adsorbents. MB showed a positive charge in solution as it is a cationic dye, while MO showed a negative charge in solution as it is an anionic dye. A temperature of 25°C and pH of 7.0 were fixed throughout all experiments. First, 2.0-3.0 mg of the adsorbents were dispersed into 50 ml each of two dyes with various initial concentrations. Volumetric flasks were ultrasonicated for 1 h, then shaken in a gas bath thermostatic oscillator with a shaking speed of 300 rpm until equilibrium was reached. When the adsorption equilibrium was reached, the amount of residual dye concentration was determined at their specific wavelength (664 nm for MB and 464 nm for MO) using a UV-Vis spectrophotometer. The concentrations of the dyes were estimated using linear regression equations obtained by plotting its calibration curve. The amount of the two dyes adsorbed by the adsorbent (q_e, mg.g^{-1}) was calculated by the following mass balance formula:

$$q_e = \frac{(C_o - C_e)V}{W}$$

where C_0 (mg.l^{-1}) and C_e (mg.l^{-1}) are the initial and equilibrium concentrations of MB or MO, respectively, *V* is the volume of the solution (L), and *M* is the weight of the adsorbent (g). The two isotherm models of Freundlich and Langmuir were used to evaluate the adsorption equilibrium characteristics of MB and MO on the two carbon-based materials. All isotherm models were fit to experimental data using linear equations, which are shown in Table 1.

Table 1. Adsorption isotherm models and their linear equations.

Isotherm models	Equations
Langmuir adsorption isotherm	$\frac{C_e}{q_e} = \frac{1}{q_{max} K_L} + \frac{C_e}{q_{max}}$
Freundlich adsorption isotherm	$\log q_e = \log K_F + \frac{1}{n} \log C_e$

In the equations of Table 1, q_{max} (mg.g^{-1}) is adsorption constant related to the adsorption capacity, k_L (l.g^{-1}) is the adsorption constant related to the energy of adsorption, K_F is the adsorption constant related to adsorption capacity (mg.g^{-1}) (l.mg^{-1})$^{1/n}$ and n is the adsorption constant measuring the adsorption intensity.

3. Results and discussion

As mentioned above, the structural characteristics of the ACAC samples were analysed using SEM, BET, and the CS744 carbon/sulfur analyser.

3.1. Elemental analysis

The carbon contents of the ACAC samples are presented in Fig. 1. According to the IR measurement of the CS744 carbon/sulfur analyser, the different heating rates of ACAC-1 to ACAC-4 lead to different carbon contents that increased from 63.63 to 79.93%, respectively. Sample ACAC-3 was then selected to proceed further because of its high carbon content. After two carbonization processes on ACAC-4, 89.32% C was achieved.

Pre-treatments were applied prior to the carbonization process to ensure the stability and preservation of the precursor structure during the subsequent carbonization. In fact, specialized pre-treatments can be used to enhance the carbon content in prepared materials in terms of stability and separation performance. The first carbonization process facilitates stabilization of the precursor's asymmetric structure and provides dimensional stability in order to withstand the high temperatures of the subsequent carbonization steps. In the following carbonization process, mostly heteroatoms existing in polymeric macromolecules were removed and subsequently a stiff and cross-linked carbon matrix was obtained. The carbon matrix with an amorphous porous structure formed from the evolvement of gaseous products and the reconfiguration of the crystalline structure during carbonization.

On the other hand, the variation of carbon content in the ACAC samples represents an interaction between temperature and heating rate on the yield of carbon content. The carbonization of the AC at 600ºC is dominated by the depolymerization reaction and decomposition of volatile matter to form solid carbon. The heating rate affects the rate of volatile evolution from the bark. In more detail, heating rates at temperatures above 400°C favour rapid volatile evolution. The resulting carbon content comes from the process that dominates, i.e., either the formation of solid carbon or the removal. A lower heating rate therefore allows equilibrium reactions to promote higher carbon content. With an increase in heating rate up to 3ºC.min^{-1}, the condensation reaction dominates the carbonization process and the fixed carbon content continues to rise. As seen in Fig. 1, the carbon content tends to increase when the temperature was below 600ºC and the heating rate was less than 3ºC. min^{-1}. When the heating rate rose above 3ºC.min^{-1}, the carbon content decreased from 79.93% for ACAC-3 to 74.09% for ACAC-4. The reason being is that at high heating rates, molecular disruption is steadfast and volatile fragments are consequently released so quickly that successive adjustments and equilibrium, leading to further primary reactions that yield char, have less opportunities to take place. When the heating rate rises further, the condensation reaction gradually slows down and the rate of formation of fixed carbon decreases, these processes are accompanied with the result of reduced fixed carbon content.

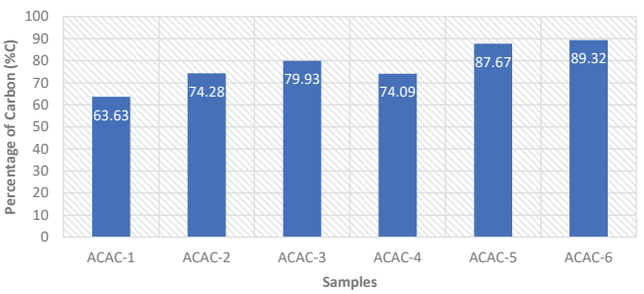

Fig. 1. The percentage of carbon element in the six ACAC samples.

To study changes in the microstructures of the ACAC samples, XRD analysis was carried out. As shown in Fig. 2, the ACAC samples all primarily contained carbon and calcium carbonate (18.18, 34.15, 47.17, and 50.96º according to the JCPDS:01-078-4614). From the XRD spectrum, ACAC-1 does not exhibit distinct peaks corresponding to a typical carbon material, thus, no discrete mineral phase was formed. Additionally, the hump in the 2θ range from 20 to 30° suggests a high degree of disorder in the carbonaceous material. Thus, ACAC-1 has a completely amorphous structure as expected with organic materials. In the XRD spectra of ACAC-3 and ACAC-4, a distinct peak of carbon appears that corresponds to the presence of crystal phase. After the carbonization processes, ACAC-5 and ACAC-6 show very well defined peaks of carbon at 2θ values of 26.26, 29.20, 43.27 , 47.26, and 48.52º (reference to the patterns JCPDS:04-019-9068, 01-089-8495, 04-007-2136, and 04-013-5952). These diffraction peaks indicate that these samples have a turbostratic structure.

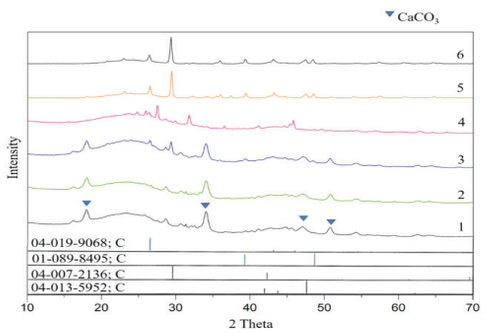

Fig. 2. XRD spectra of ACAC with four different settings. Numbers 1 through 6 represent the six ACAC samples.

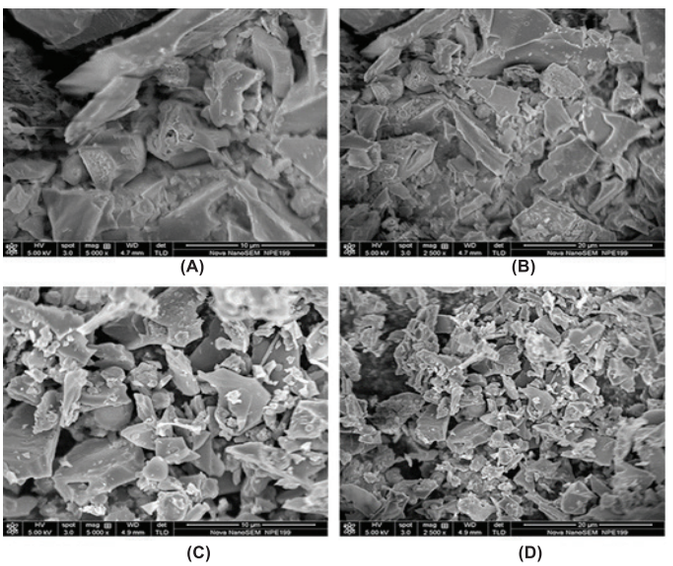

Fig. 3. SEM micrographs of four the ACAC samples: (A) and (B) are ACAC-1; (C) and (D) are ACAC-4.

Figure 3 is an SEM image of the ACAC samples before and after the first carbonization process, respectively. A porous structure of the ACAC samples was not clearly observed by SEM and their surface is also covered by significant amount of impurities. Using ImageJ software, the particle size fraction of ACAC-1 from Fig. 3 was 3.51 µm and the particle size fraction of ACAC-4 was 1.84 µm. This suggests that the surface area of ACAC-4 increased in comparison to ACAC-1. Based on these results, ACAC-4 went through two carbonization processes and the surface area of the final product was measured by the BET method.

3.2. The pore structure analysis

The pore size distributions of ACAC-6 were analysed and the summarized results are presented in Fig. 4. The diameter of a copper atom is roughly 0.257 nm, and since the average pore diameter of ACAC is 10 µm, the copper atoms easily remain in the pores of the activated carbon. Sample ACAC-6 showed an average S_{BET} of 363.56 $m^2.g^{-1}$. According to the obtained results, the adsorption capacity of the adsorbent was determined to not only depend on surface properties, but also pore structure. The use of ultrasonic power can contribute to making new pores on the surface of activated carbon, which improves MB removal. Besides, as shown in Fig. 4, most of the pores fall into a diameter category of 1-2.5 µm. According to Kasaoka, et al., the pore diameter of an adsorbent must be at least 1.7 times larger than the adsorbate so that adsorption becomes possible [12]. In this case, the diameters of both MB and MO are about 0.8 nm, while the average pore size of ACAC is 2.00 µm; thus, it can efficiently adsorb both MB and MO molecules.

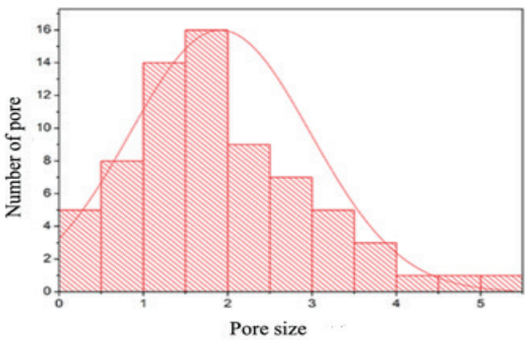

Fig. 4. The distribution of the pores and their sizes in sample ACAC-6.

3.3. Adsorption isotherm

As mentioned before, the adsorption isotherm is a vital tool that explains the relationship between adsorbate molecules and the adsorbent surface. It describes how adsorbate molecules are distributed on the surface of the adsorbent. The obtained parameters from the two models for ACAC-6 are summarized in Table 2. From the results, the correlation coefficient (R^2) of the Langmuir isotherm is the largest, which indicates that adsorption depends on the interaction between the homogeneous and the monolayer coverage of MB and MO onto the two studied materials. Additionally, a characteristic parameter of the Langmuir isotherm was also determined, i.e., the dimensionless factor R_L also known as the separation factor, which can be calculated by the following equation:

$$R_L = \frac{1}{1 + K_L C_0}$$

where C_0 is the initial concentration of MB (or MO) and k_L is the Langmuir constant.

Table 2. Langmuir and Freundlich parameters for MB and MO adsorption on the ACAC-6.

	Langmuir coefficients		
Adsorbates	q_m ($mg.g^{-1}$)	K_L ($l.g^{-1}$)	R^2
MB	15.34	1.11	0.9921
MO	10.36	1.04	0.9104
	Freundlich coefficients		
	n	K_F	
MB	3.66	8.14	0.8922
MO	2.96	3.87	0.6070

The value of R_L is associated with the type of isotherm: unfavourable (R_L>1), linear (R_L=1), favourable (0<R_L<1), or irreversible (R_L=0) [13]. The R_L values of MB adsorption onto activated carbons are determined to be in the range of 0.04-0.15 for ACAC-6, which represents that the Langmuir adsorption isotherm is favourable. The Langmuir and Freundlich isotherms for MB and MO adsorption onto ACAC-6 are shown in Fig. 5 and Fig. 6, respectively.

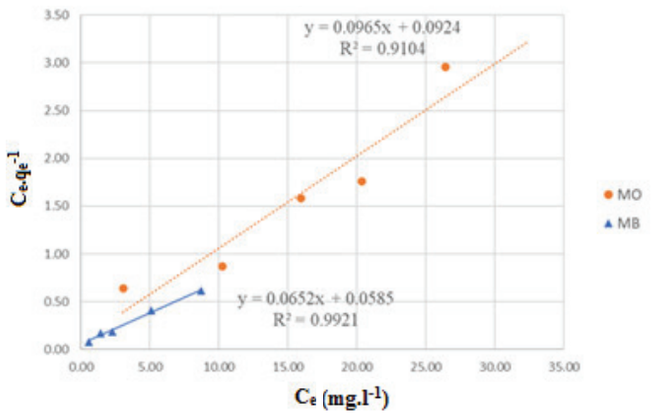

Fig. 5. Langmuir adsorption isotherm for MB and MO removal using ACAC-6.

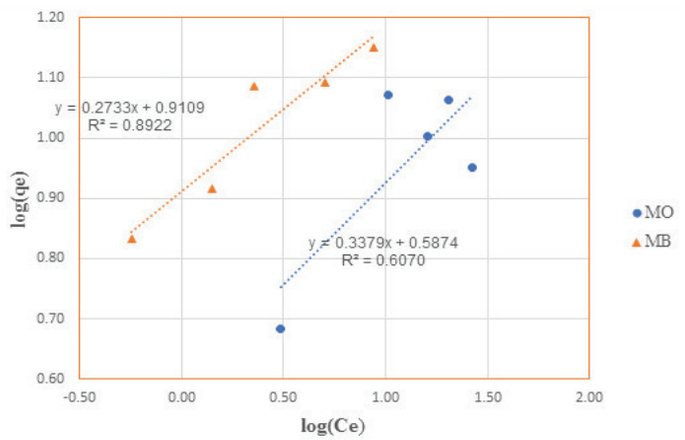

Fig. 6. Freundlich adsorption isotherm for MB removal using ACAC-6.

4. Conclusions

The removal of the industrial dyes MB and MO by using activated carbon originating from *Acacia crassicarpa* agricultural waste was investigated. Adsorption experiments were performed and the maximum adsorption capacity was determined by the adsorption of MB and MO. The experimental data fit the Langmuir isotherm model indicating a monolayer distribution of dye molecules over the surface of the activated carbon. The Langmuir maximum adsorption capacity was determined as 15.34 mg.g^{-1} for MB and 10.36 mg.g^{-1} for MO. Based on all results, ACAC can be regarded as a potential adsorbent for the removal of MB dye from aqueous solutions.

CRedit author statements

Tue Ngoc Nguyen, Khanh Quoc Dang, Duc Trung Nguyen: Conceptualization, Methodology, Data curation, Formal analysis, Conceptualization, Methodology, Writing - Original draft preparation, Writing - Review & Editing.

ACKNOWLEDGEMENTS

This research is funded by the Hanoi University of Science and Technology (HUST) under project number T2020-TT-009. We acknowledge the support of the SAHEP project for performing the testing analyses at the School of Materials Science and Engineering, Hanoi University of Science and Technology.

COMPETING INTERESTS

The authors declare that there is no conflict of interest regarding the publication of this article.

REFERENCES

[1] I. Ismail, A.S. Fawzy, N.M. Abdel-Monem, et al. (2012), "Combined coagulation flocculation pre treatment unit for municipal wastewater", *J. Adv. Res.*, **3**(**4**), pp.331-336, DOI: 10.1016/j.jare.2011.10.004.

[2] M. Ghaedi, A.G. Nasab, S. Khodadoust, et al. (2015), "Characterization of zinc oxide nanorods loaded on activated carbon as cheap and efficient adsorbent for removal of methylene blue", *J. Ind. Eng. Chem.*, **21**, pp.986-993, DOI: 10.1016/j.jiec.2014.05.006.

[3] M. Ibrahim, A.A. Shaltout, D.E. Atta, et al. (2009), "Removal of COOH, Cd and Pb using water hyacinth: FTIR and flame atomic absorption study", *J. Iran. Chem. Soc.*, **6**(**2**), pp.364-372, DOI: 10.1007/BF03245846.

[4] G. Sharma, A. Kumar, M. Naushad, et al. (2018), "Fabrication and characterization of Gum arabic-*cl*-poly(acrylamide) nanohydrogel for effective adsorption of crystal violet dye", *Carbohydr. Polym.*, **202**, pp.444-453, DOI: 10.1016/j.carbpol.2018.09.004.

[5] M. Naushad (2014), "Surfactant assisted nano-composite cation exchanger: Development, characterization and applications for the removal of toxic Pb^{2+} from aqueous medium", *Chem. Eng. J.*, **235**, pp.100-108, DOI: 10.1016/j.cej.2013.09.013.

[6] M.Z. Alam, S. Ahmad, M. Ahmad (2010), "Mutagenicity and genotoxicity of tannery effluents used for irrigation at Kanpur, India", *Ecotoxicol. Environ. Saf.*, **73**(**7**), pp.1620-1628, DOI: 10.1016/j.ecoenv.2010.07.009.

[7] M. Bahrami, A. Nezamzadeh-Ejhieh (2015), "Effect of the supported ZnO on clinoptilolite nano-particles in the photodecolorization of semi-real sample bromothymol blue aqueous solution", *Mater. Sci. Semicond. Process.*, **30**, pp.275-284, DOI: 10.1016/j.mssp.2014.10.006.

[8] S. Sohrabnezhad, A. Pourahmad (2010), "Comparison absorption of new methylene blue dye in zeolite and nanocrystal zeolite", *Desalination*, **256**(**1-3**), pp.84-89, DOI: 10.1016/j.desal.2010.02.009.

[9] C. Leodopoulos, D. Doulia, K. Gimouhopoulos, et al. (2012), "Single and simultaneous adsorption of methyl orange and humic acid onto bentonite", *Appl. Clay Sci.*, **70**, pp.84-90, DOI: 10.1016/j.clay.2012.08.005.

[10] M. Rafatullah, O. Sulaiman, R. Hashim, et al. (2009), "Adsorption of copper (II), chromium (III), nickel (II) and lead (II) ions from aqueous solutions by meranti sawdust", *J. Hazard. Mater.*, **170**(**2-3**), pp.969-977, DOI: 10.1016/j.jhazmat.2009.05.066.

[11] K. Bedin, A.C. Martins, A.L. Cazetta, et al. (2016), "KOH-activated carbon prepared from sucrose spherical carbon: adsorption equilibrium, kinetic and thermodynamic studies for Methylene Blue removal", *Chem. Eng. J.*, **286**, pp.476-484, DOI: 10.1016/j.cej.2015.10.099.

[12] S. Kasaoka, Y. Sakata, E. Tanaka, et al. (1987), "Design of molecular sieving carbon-studies on adsorption of various dyes in liquid phase", *Nippon Kagaku Kaishi*, **12**, pp.2260-2266 (in Japanese).

[13] S. Guo, W. Li, L. Zhang, et al. (2009), "Kinetics and equilibrium adsorption study of lead(II) onto the low cost adsorbent - *Eupatorium adenophorum spreng*", *Process Saf. Environ. Prot.*, **87**(**5**), pp.343-351, DOI: 10.1016/j.psep.2009.06.003.

DOI: 10.31276/VJSTE.63(4).28-35

Effects of compressing parameters and $Mg(OH)_2$ content on mechanical properties and flame retardancy of rice straw-fibre reinforced composites

Doan Van Hong Thien[1], Thao Phuong Nguyen[1], Mong Linh Nguyen Thi[1], Ngoc Tuyet Tran[1], Thanh Nhan Le[1], Trung Nam Nguyen[1], Manh Can Le[1], Chanh-Nghiem Nguyen[2], Dan-Thuy Van-Pham[1*]

[1]Department of Chemical Engineering, Can Tho University, Campus II, 3/2 Street, Xuan Khanh Ward, Ninh Kieu District, Can Tho City, Vietnam
[2]Department of Automation Technology, Can Tho University, Campus II, 3/2 Street, Xuan Khanh Ward, Ninh Kieu District, Can Tho City, Vietnam

Received 19 February 2021; revised 2 May 2021; accepted 14 May 2021

Abstract:
Rice straw fibre was utilized for fabricating unidirectional (UD) composites. In this study, the effects of compression temperature (160, 170, 180°C), duration (2, 5, 10, 15, and 20 min), pressure (100, 125, and 150 $kg.cm^{-2}$), and fibre volume fraction (20, 30, 40, and 50%) on the mechanical properties of composites were investigated, respectively. The composite with optimal mechanical properties was prepared at a temperature of 180°C, pressure of 125 $kg.cm^{-2}$ for 10 min, and at a fibre volume fraction of 40%. $Mg(OH)_2$ was found to be an appropriate additive to enhance the flame retardancy of the composite. Interestingly, this agent also improved the mechanical and thermal insulation properties of the obtained composite at a ratio of 20% $Mg(OH)_2$. The impact strength reached its highest value of 31.1 $kJ.m^{-2}$, which is approximately 2.5 higher than that value at 10% and 30% $Mg(OH)_2$, respectively. The 20% $Mg(OH)_2$ added composite showed the best thermal insulation ability. The flame endurance of the specimen was rated as HB, V0, and 5VB standards.

Keywords: **flame retardancy, poly(vinyl chloride), rice straw, thermal insulation.**

Classification number: **2.3**

1. Introduction

Rice straw is a typical agricultural residue that represents about 45% of the rice production volume [1], and is abundant in rice-growing countries such as India and Vietnam. Although rice straw possesses the ability to become a value-added by-product [2], it has been poorly treated. Traditionally, rice straw can be utilized as an animal feed or fuel source, but it is mainly incinerated and discarded back to the field resulting in not only a waste of resources but also environmental pollution [3]. Therefore, an appropriate method to utilize rice straw is needed in order to prevent this seasonal environmental pollution. In recent years, plenty of studies have been conducted in order to put rice straw in use. In particular, rice straw has been considered as a promising source to produce bioethanol via fermentation [4], agriculture compost [5], biodegradable fibre, or mostly as a composite reinforcement [6]. However, most of the aforementioned studies require rice straw to be chemically modified, which is expensive, time consuming, and may be harmful to the environment due to the use of chemicals.

In this study, rice straw fibres were used not only as fillers but also reinforcement materials for a poly(vinyl chloride) (PVC) matrix. Moreover, the high silica content and porous structure of rice straw fibres are considered to be an advantage aiming to improve the flame retardancy of the material. Among other kinds of polymers, PVC was chosen based on its unique ability to be processed at low temperatures. Besides, the significant amount of chlorine in PVC can retard fires from both starting and spreading [3]. To further increase the flame retardancy of the composite, $Mg(OH)_2$ was added to the components. Among the other inorganic flame retardants, $Mg(OH)_2$ was chosen due to the ability to endothermically decompose into MgO and release water vapor [7]. As the heat is absorbed by the decomposition reaction, the flame ignition of the associated components is delayed. At the same time, MgO acts as a barrier to prevent further interaction between the combustible components and oxygen. Besides, the released vapor water can not only cool down the combustion area but also partially dilute the combustible gases. Moreover, the flame retardant additive $Mg(OH)_2$ can be guaranteed to withstand the composite fabrication process since it starts to decompose at around 300-340°C. After the composites

*Corresponding author: Email: vpdthuy@ctu.edu.vn

were produced, their stability, mechanical and thermal properties, and flammability were investigated for selective formulation purposes.

2. Materials and methods

2.1. Materials

Rice straw was obtained directly from a field in the Hong Dan district, Bac Lieu province. $Mg(OH)_2$ was purchased from the CEMACO company (Vietnam). Commercial PVC powder was provided by the TPC Vina company with properties as shown in Table 1.

Table 1. Properties of PVC powder.

Property	Value
Density	1.45-1.50 $g.cm^{-3}$
Tensile strength	500-700 $kg.cm^{-2}$
Flexural strength	800-1,200 $kg.cm^{-2}$
Compressive strength	800-1,600 $kg.cm^{-2}$
Modulus of Elasticity	4,000-10,000 $kg.cm^{-2}$
Elongation at break	10-25%
Coefficient of linear expansion	0.00006-0.00007
Thermal conductivity	$3.8\text{-}4*10^{-4}$ $cal.(cm.s.°C)^{-1}$

2.2. Rice straw mat preparation

After collecting raw rice straw from the field, the flower and leaf were removed and only the body was used. The body was then cleaned with water, oven-dried to expel moisture, disentangled, and cut into pieces 3-4 cm in length. Finally, a mould of evenly distributed rice straw was hot compressed by using a hydraulic press machine (PAN STONE P-100-PCD, Taiwan) under different conditions to form unidirectional fibre mats. The optimum conditions for fibre mat preparation were at a temperature of 130°C and a pressure of 50 $kg.cm^{-2}$ for 60 s. Under the mentioned conditions, lignin plays the role of adhesive in the rice straw-fibre mat, which is called a preform.

2.3. PVC film preparation

To investigate the optimum condition to prepare the PVC film, PVC powder was hot compressed under various conditions by using a hydraulic press machine (PAN STONE P-100-PCD, Taiwan) as well. The optimum conditions for PVC film preparation were carried out at 180°C and a pressure of 100 $kg.cm^{-2}$ for 30 s. After that, in order to increase the flame retardancy of the material, a film comprising PVC and $Mg(OH)_2$ with various ratios was fabricated by following the optimum condition.

2.4. Composite preparation

To prepare the rice straw composite, the prepreg was firstly prepared by compressing one layer of rice straw mat sandwiched by two layers of PVC film. Then, the final composite was made by pressing the prepregs between the hot plates, followed by decreasing the pressure to cool down the composite. Finally, all of the excess amounts of rice straw were removed from the composite. In this study, the effects of compressing temperature, duration, pressure, fibre ratio, and $Mg(OH)_2$ content on the mechanical properties of the obtained composites were successively investigated. Moreover, the effects of $Mg(OH)_2$ content on thermal properties and flammability were studied.

2.5. Measurements of mechanical properties

Tensile strength: Tensile strength property was determined by using the Zwick/Roell BDO - FB050TN testing machine following the ASTM D638-04 standard, in which the rectangle specimens of 115x15x3 mm were used, and the number of tests was five.

Flexural strength: Flexural strength measurements have been carried out by using the Zwick/Roell BDO - FB050TN testing machine in accordance with ASTM D790M/84. The total number of tests was five and the used sample dimensions were 45x15x3 mm.

Impact strength: Impact strength measurements were conducted by using the Zwick/Roell BPI – 50COMC testing machine according to ASTM D 256-04 standard. Five replicates were carried out with a sample size of 65x15x3 mm and the 45° V-notch located at the position of 20% width.

Thermal insulation test: The thermal insulation test was conducted in the system consisting of two chambers, as shown in Fig. 1. The sample is placed in between two chambers. When heat is continuously provided into chamber 1 by the heat source, the temperature differential is determined by measuring the temperature at chamber 1 and chamber 2 for different periods.

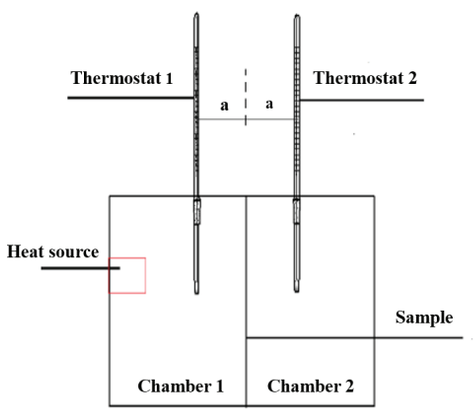

Fig. 1. Thermal insulation test setting.

Combustion test: The combustion tests were performed with respect to HB, HB45, HB75 standards (Fig. 2A), V0, V1, V2 standards (Fig. 2B), and 5VA, 5VB standards (Fig. 2C).

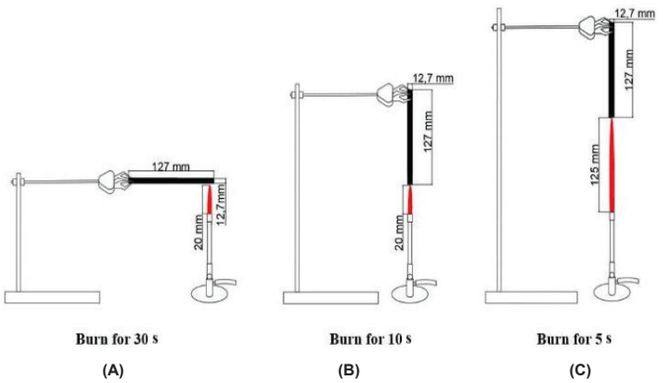

Fig. 2. Flame retardancy tests regarding (A) HB, HB45, HB75 standards, (B) V0, V1, V2 standards, and (C) 5VA, 5VB standards.

3. Results and discussion

3.1. Structure of extracted rice straw fibres

By using SEM and chemical composition determination, rice straw fibres, as well as other lignocellulosic fibres, are found to be mainly constituted of cellulose, hemicellulose, and lignin [6, 8, 9]. As a microscopic object can be better visualized by its best-focused image [10] or all-in-focused image [11], the obtained rice straw fibres were imaged by using an optical microscope (Nikon, ECLIPSE LV100POL, Japan) that was equipped with an autofocusing module [12] to create the best-focused image for better visibility of the fibre (Fig. 3).

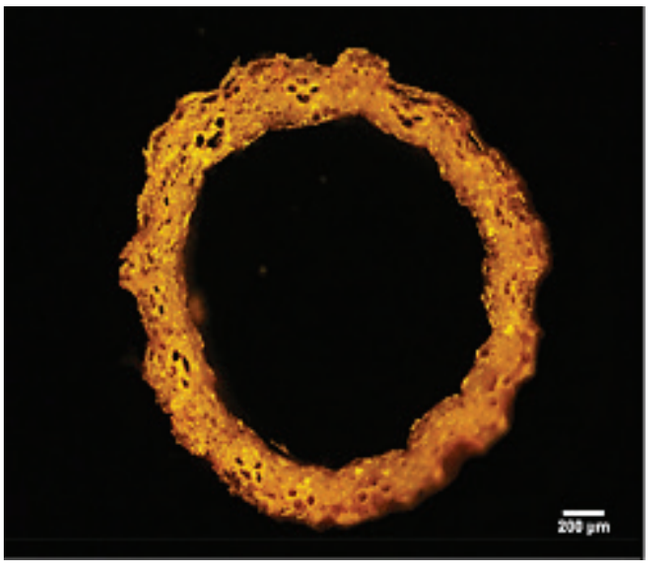

Fig. 3. All-in-focus image of rice straw with porous structure.

3.2. Effects of compressing temperature on the mechanical properties of composite

To evaluate the effects of compressing temperature on the formation of the rice straw composite, mechanical tests (e.g., tensile strength, flexural strength, and impact strength) for the compression temperature variations (from 150 to 190°C) were conducted while the compression duration, pressure, and rice straw ratio were fixed at 20 min, 100 kg.cm^{-2}, and 50%, respectively. However, the composite at a pressing temperature of 150°C was separated into layers and the one at a pressing temperature of 190°C was burned, so those samples were unable to be tested.

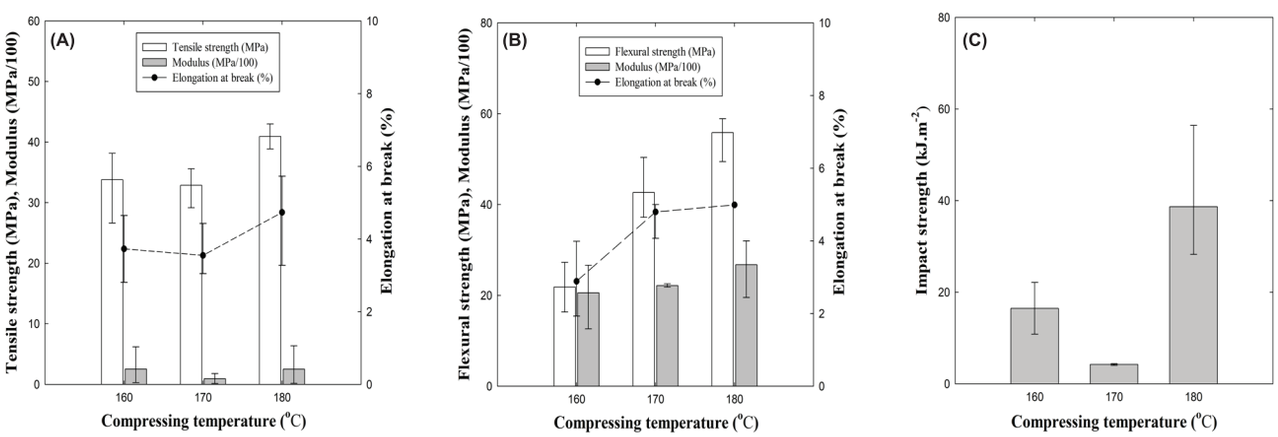

Fig. 4. Effect of compressing temperature on (A) tensile strength, (B) flexural strength, and (C) impact strength of rice straw composite.

The effects of the compression temperature on the tensile strength, flexural strength, and impact strength are shown in Fig. 4. There was a common trend observed of the mechanical properties of the rice straw composite regarding the pressing temperature. Specifically, as the pressing temperature increased, the mechanical strengths also increased, as well as the elastic moduli and the elongation at break. However, the tensile strength and the impact strength fluctuated as the pressing temperature went up, which is likely caused by the poor dispersion of the rice straw in the composite. The results show that the tensile strength, which represents the strength of the material, sharply rose approximately by 17.5% when the temperature was increased from 160□ (σ=33.79x10^{-2} MPa) to 180^{o}C (σ=40.39x10^{-2} MPa). Also, the elongation at break, which represents the ductility of the material, expanded from 3.73 to 4.73% while the elastic modulus remained unchanged. In case of the flexural strength, which is defined as the maximum amount of force a material can bear without breaking or permanently deforming, as the pressing temperature increased, the flexural strength and elongation at break values significantly increased to approximately 61 and 42%, respectively. Besides, the elastic modulus was slightly changed from 20.56x10^{-2} MPa at 160□ to 26.74x10^{-2} MPa at 180□. The rise of the tensile and flexural strength indicates that the interfacial adhesion between the rice straw mat and PVC increases with the increment in the compressing temperature. However, the impact strength, which corresponds to the capability of the material to resist a sudden stress or force, first declined as the compression temperature was raised from 160 to 170^{o}C. Then, it bounced back to peak at 180^{o}C (E=38.66 kJ.m^{-2}). This behaviour could be explained by the fact that at the low compression temperature of 160^{o}C, the PVC was not completely melted resulting in plastic lumps in the composite. When the compression temperature was raised to 170^{o}C, the polymer was completely melted but did not fully interact with the rice straw mat. Hence, the impact strength fell off. Eventually, 180°C was chosen as an adequate compression temperature to fabricate the composite. At this temperature, the heat effectively melted the PVC but did not burn the fibre leading to an increment in the interfacial adhesion between the rice straw mat and PVC.

3.3. Effects of compression duration on the mechanical properties of composite

In an attempt to analyse the effect of the compression duration on the rice straw composite formation, the composites were prepared with the compression duration varies from 2 to 25 min, while the pressing temperature, pressure, and rice straw ratio were fixed at 180^{o}C, 100 kg.cm^{-2}, and 50%, respectively. However, as the pressing duration reached 25 min, the composite was burned. Therefore, the mechanical strength tests were conducted for the composites which were pressed for 2 to 20 min.

Figure 5 illustrates the mechanical strength (e.g., tensile strength, flexural strength, and impact strength) of the rice straw composite subjected to different compression durations. While the tensile strength, flexural strength, elastic moduli, and the elongation at break show the same declining tendencies; the impact strength demonstrated the opposite trend in which the impact strength increased when the compression duration rose. As the compression duration increased from 2 to 20 min, both the tensile strength and flexural strength showed similar trends in which these were increased (2 to 5 min) then were strongly declined to 30.46 and

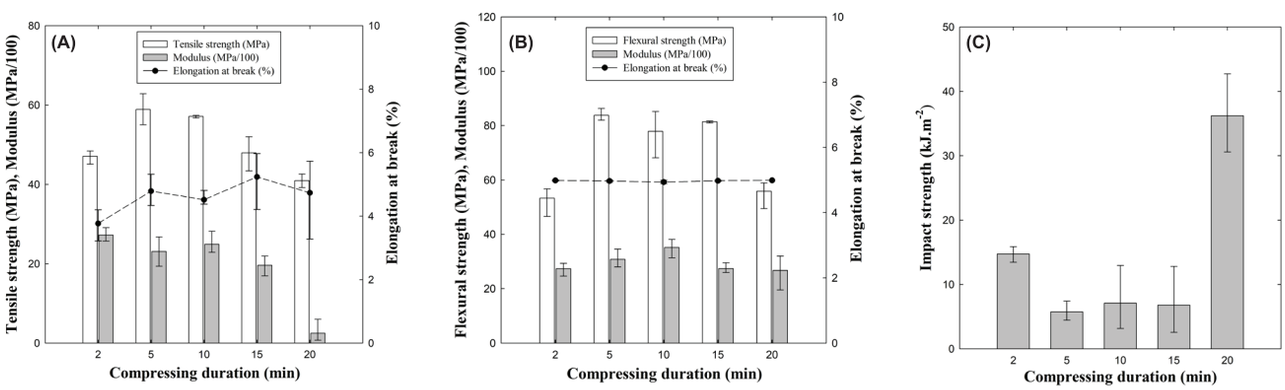

Fig. 5. Effect of pressing duration on (A) tensile strength, (B) flexural strength, and (C) impact strength of rice straw composite.

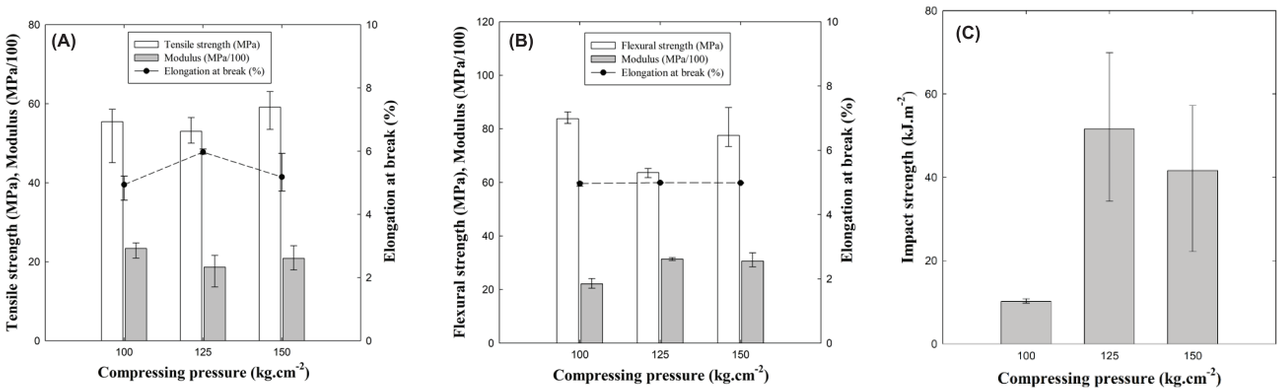

Fig. 6. Effect of compression pressure on (A) tensile strength, (B) flexural strength, and (C) impact strength of rice straw composite.

33.37%, respectively. In addition, the elastic modulus for both the tensile strength and flexural strength peaked at a compression duration of 10 min, after that the elastic moduli started to decrease. This behaviour implies that 10 min is a sufficient compression duration for the rice straw composite fabrication since below which the PVC was not sufficiently melted resulting in an enhancement of the interfacial adhesion between PVC and the fibres and above which the rice straw started to deform. In contrast to the tensile and flexural strength, the value for impact strength peaked at 20 min compression time. At which, the matrix of PVC and fibres was the strongest. However, as the composite was targeted to be used as a construction material in which the elastic moduli of the tensile strength and the flexural strength were prioritized over the impact strength, 10 min was chosen as an adequate compression duration. At this compression duration, the composite possessed the highest flexibility and sufficient hardness.

3.4. Effects of compression pressure on the mechanical properties of composite

The effect of compression pressure on the preparation of the rice straw composite was evaluated by fixing the pressing conditions at 180°C for 20 min and rice straw ratio at 50% with the variation of compression pressure ranging from 50 to 150 kg.cm^{-2}. Nevertheless, the composites were separated into layers when the compression pressure below 75 kg.cm^{-2} was applied, and those samples were unable to be tested. The effect of compression pressure on the mechanical properties of the rice straw composite can be seen in Fig. 6. As can be seen in the figure, there is almost no distinct difference in tensile strength when the compression pressure was increased. Nevertheless, at the compression pressure of 125 kg.cm^{-2}, the material possessed the highest values for both impact and flexural strength modulus indicating sufficient interfacial adhesion between PVC and the rice straw. When a stronger compression pressure was applied (e.g., 150 kg.cm^{-2}), the rice straw tended to displace to the sides leading to a slight fall in impact strength. In addition, since the material was targeted to be used as a construction material for ceilings, the flexural strength modulus was the key factor of material and thus the compression pressure of 125 kg.cm^{-2} was chosen as the optimum condition. At this pressure, the consumed energy is lower than at a compression pressure at 150 kg.cm^{-2} but the material still possessed adequate mechanical properties.

3.5. Effects of rice straw fibre on the mechanical properties of composite

As the compression conditions were determined, the effect of the rice straw ratio on the mechanical properties of the composite was measured with a variety of rice straw ratios (20 to 60%). However, when the rice straw ratio was 60%, the amount of polymer (PVC) was not sufficient to create the composite. Therefore, the sample with the rice straw ratio of 60% was unqualified to be tested.

Figure 7 shows the effect of rice straw ratio on the tensile, flexural, and impact strength of the composite. Predictably, adding rice straw into the formulation significantly influenced the mechanical strength of the composite. As the former ratio rose, the latter proportionally declined. Importantly, when the rice straw ratio was increased from 40 to 50%, the elongation at break values for both tensile strength and flexural strength sharply decreased emphasizing a reduction in the ductility of the material. In the case of impact strength, at low rice

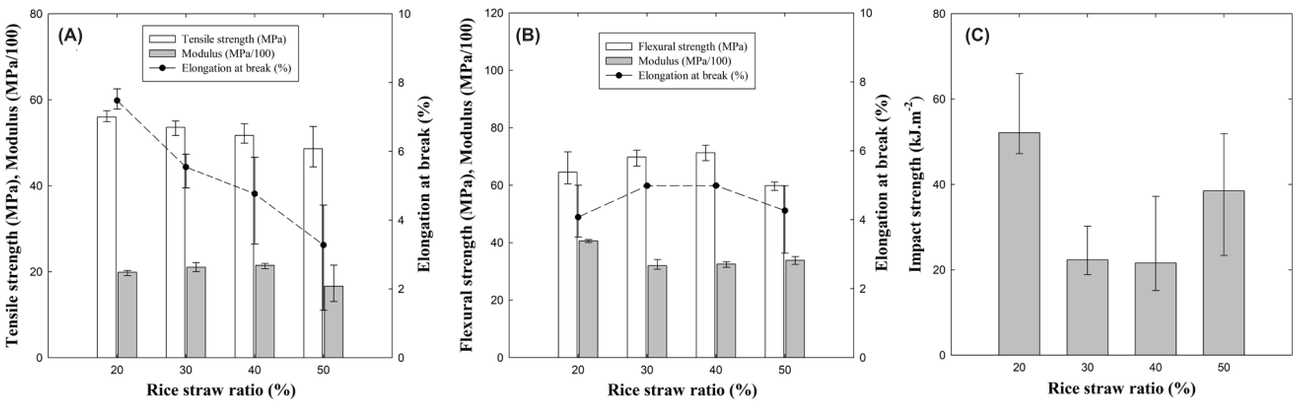

Fig. 7. Effect of rice straw ratio on (A) tensile strength, (B) flexural strength, and (C) impact strength of rice straw composite.

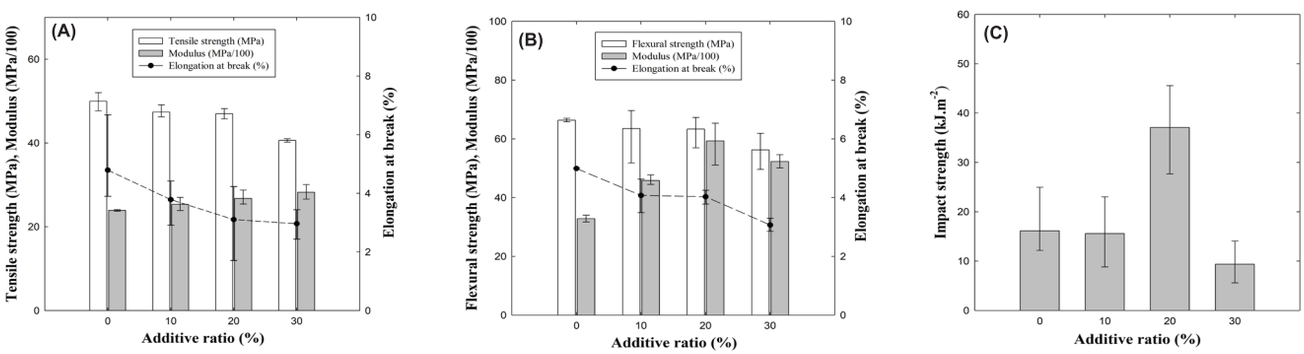

Fig. 8. Effect of additive on (A) tensile strength, (B) flexural strength, and (C) impact strength of rice straw composite.

straw content (e.g., 20%), PVC may have completely filled in the voids between the fibres and formed a homogeneous matrix. This matrix was weakened as the rice straw content increased. However, as the ratio of rice straw reached 50%, the value of impact strength rose again as the fibre became dominant in the composite. Eventually, a rice straw ratio of 40% was chosen to fabricate the composite since that composite consisted of the largest amount of rice straw while still meeting the mechanical standards for use as a construction material.

3.6. Effects of additive on the mechanical properties of composite

To analyse the effect of the addition of an additive on the rice straw composite formation, which is used to enhance the flame retardancy of the composite, the composites with a rice straw ratio of 40% were prepared at 180°C and 125 kg.cm^{-2} for 10 min with amounts of $Mg(OH)_2$ additive varying from 0 to 30 wt%.

In order to improve the flame retardancy ability of the composite, $Mg(OH)_2$ was added to the composite fabrication process. The effect of the flame-retardant additive on the mechanical properties of the composite can be seen in Fig. 8. When the additive powder was added into the mixture, it could fill into the voids created by the rice straw and PVC leading to an increment in the tensile and flexural strength moduli, as well as the impact strength. In particular, at a ratio of 20% additive, the impact strength reached its highest value of 31.1 kJ.m^{-2}, which is approximately 2.5 and 4 times higher than that value at 10% and 30% additive, respectively. When the additive content was increased further to 30% in PVC, the material started to become weak as the excess amount of $Mg(OH)_2$ hindered the interaction between the PVC and rice straw. Therefore, 20% of $Mg(OH)_2$ in PVC was chosen as the optimum ratio to be added to the rice straw composite.

3.7. Thermal insulation ability

Figure 9 reveals the thermal insulation ability of the rice straw composite. Clearly, the composite shows the ability to insulate heat even in the absence of a flame retardant additive (e.g. $Mg(OH)_2$). When heat is continuously provided to the system, the heat is immediately transferred from chamber 1 to chamber 2

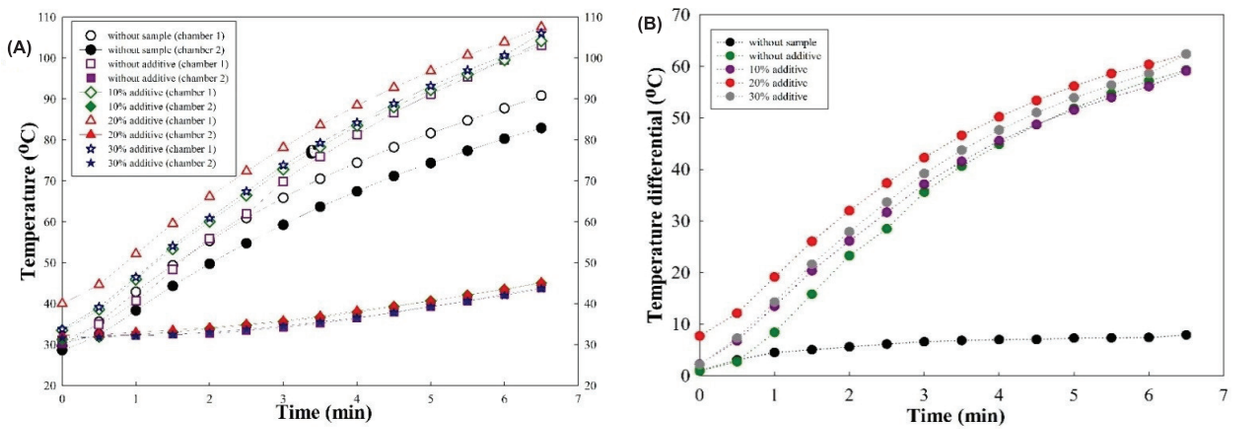

Fig. 9. Thermal insulation ability of the rice straw composite.

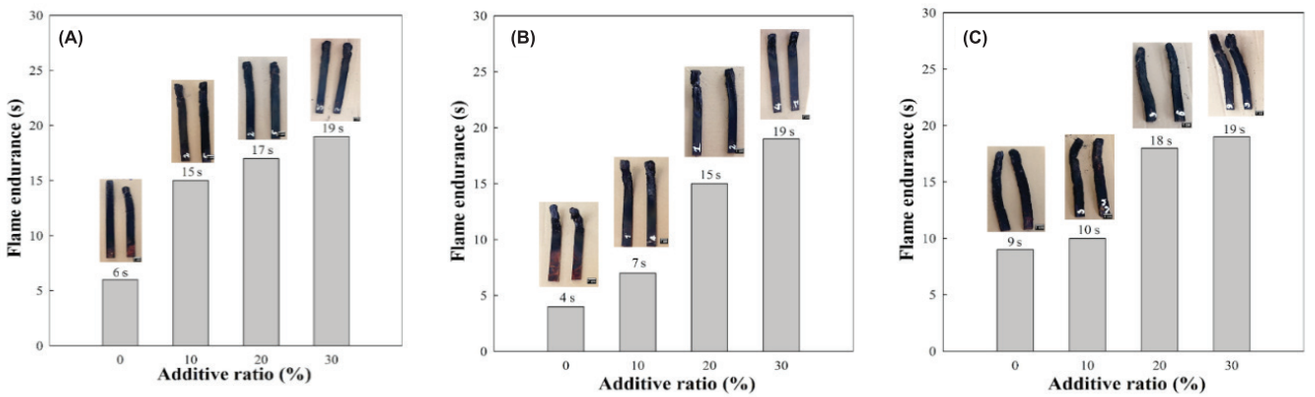

Fig. 10. Combustion tests regarding to (A) HB, HB45, HB75, (B) V0, V1, V2, and (C) 5VA, 5VB standards.

without any obstacles so that the temperature differential between the two chambers was negligible. When a rice straw composite was placed in between chamber 1 and chamber 2, the heat at chamber 1 is insulated leading to a noticeable temperature differential. Consequently, the thermal insulation ability of the rice straw is proven. Moreover, when a flame retardant chemical (e.g. $Mg(OH)_2$) was incorporated into the formulation, the ability of the rice straw composite to insulate heat improved further. It is worth noting that the ratio of 20 wt% $Mg(OH)_2$ in PVC shows the best result, which corresponds to the mechanical properties.

3.8. Flame retardancy ability

Figure 10 (A-C) represent the results of the horizontal, vertical, and 5V combustion tests, respectively. In general, as the flame-retardant additive ratio increased, the flame endurance, which is defined as the burning duration the specimen could bear before starting to deform, also increased for all three types of combustion tests. When the specimen was horizontally combusted by the 20 mm flame for 30 s, the specimen burned independently to the specimen thickness. Therefore, one could rate it as HB. In the case of the combustion tests regarding the V0, V1, V2 standards, in which the specimen was combusted vertically by the 20 mm flame for 10 s, the specimen self-extinguished within 10 s without dropping. Hence, one could rate it as V0. Finally, when the specimen was subjected to 5VA, 5VB combustion tests, the specimen could be classified as 5VB since it was not burned with flaming and glowing combustion, as well as dripping did not occur.

4. Conclusions

UD rice straw fibre-reinforced PVC composites were successfully prepared by a common compression moulding method. Composites at a fibre volume fraction of 40% prepared at a temperature at 180°C and pressure of 125 $kg.cm^{-2}$ for 10 min possessed the best possible mechanical properties. It was found that the flame-retardant additive $Mg(OH)_2$ did not only enhance the tensile strength and flexural strength moduli, but also

improved the ability to insulate heat and retard a flame. The obtained composites with 20 wt% $Mg(OH)_2$ in PVC showed the best result in mechanical properties as well as thermal insulation ability. Moreover, the flame endurance of the specimen was rated as HB, V0, and 5VB standards.

CRediT author statements

Doan Van Hong Thien: Formal analysis, Validation; Thao Phuong Nguyen: Writing - Original draft, Visualization; Mong Linh Nguyen Thi: Investigation, Formal analysis, Validation; Ngoc Tuyet Tran: Investigation, Formal analysis, Validation; Thanh Nhan Le: Investigation, Formal analysis, Validation; Trung Nam Nguyen: Investigation, Formal analysis, Validation; Manh Can Le: Investigation, Formal analysis, Validation; Chanh-Nghiem Nguyen: Formal analysis, Visualisation; Dan-Thuy Van-Pham: Writing - Original draft, Conceptualization, Methodology, Supervision, Writing - Review and editing.

COMPETING INTERESTS

The authors declare that there is no conflict of interest regarding the publication of this article.

REFERENCES

[1] R. Khandanlou, M.B. Ahmad, K. Shameli, et al. (2014), "Mechanical and thermal stability properties of modified rice straw fiber blend with polycaprolactone composite", *Journal of Nanomaterials*, **2014(7)**, pp.1-9, DOI: 10.1155/2014/675258.

[2] P. Fu, S. Hu, J. Xiang, et al. (2009), "Mechanism study of rice straw pyrolysis by fourier transform infrared technique", *Chinese Journal of Chemical Engineering*, **17(3)**, pp.522-529, DOI: 10.1016/S1004-9541(08)60240-2.

[3] M. Molaverdi, K. Karimi, S. Mirmohamadsadeghi (2019), "Improvement of dry simultaneous saccharification and fermentation of rice straw to high concentration ethanol by sodium carbonate pretreatment", *Energy*, **167(C)**, pp.654-660, DOI: 10.1016/j.energy.2018.11.017.

[4] M.R. Swain, A. Singh, A.K. Sharma, et al. (2019), *Chapter 11 - Bioethanol Production from Rice- and Wheat Straw: An Overview*, Bioethanol Production from Food Crops, Academic Press, pp.213-231.

[5] E. Mahmoud, N.A. El-Kader (2015), "Heavy metal immobilization in contaminated soils using phosphogypsum and rice straw compost", *Land Degradation & Development*, **26(8)**, pp.819-824, DOI: 10.1002/ldr.2288.

[6] N.D. Vu, H.T. Tran, T.D. Nguyen (2018), "Characterization of polypropylene green composites reinforced by cellulose fibers extracted from rice straw", *International Journal of Polymer Science*, **2018(4)**, DOI: 10.1155/2018/1813847.

[7] W. Meng, W. Wu, W. Zhang, et al. (2019), "Bio-based $Mg(OH)_2$@M-Phyt: Improving the flameretardant and mechanical properties of flexible poly(vinyl chloride)", *Polymer International*, **68(10)**, pp.1759-1766, DOI: 10.1002/pi.5885.

[8] X. Chen, J. Yu, Z. Zhang, et al. (2011), "Study on structure and thermal stability properties of cellulose fibers from rice straw", *Carbohydrate Polymers*, **85(1)**, pp.245-250, DOI: 10.1016/j.carbpol.2011.02.022.

[9] D.T. Van-Pham, M.T. Nguyen, C.N. Nguyen, et al. (2018), "Effects of processing parameters on mechanical properties and structure of banana fiber-reinforced composites", *Journal of Renewable Materials*, **6(6)**, pp.662-670, DOI: 10.7569/JRM.2018.634107.

[10] D.-T. Van-Pham, T.Y.N. Pham, M.C. Tran, et al. (2020), "Extraction of thermally stable cellulose nanocrystals in short processing time from waste newspaper by conventional acid hydrolysis", *Mater. Res. Express*, **7(6)**, DOI: 10.1088/2053-1591/ab9668.

[11] D.T.V. Pham, Q.H. Le, T.N. Lam, et al. (2020), "Four-factor optimization for PET glycolysis with consideration of the effect of sodium bicarbonate catalyst using response surface methodology", *Polymer Degradation and Stability*, **179**, DOI: 10.1016/j.polymdegradstab.2020.109257.

[12] C.N. Nguyen, K. Ohara, E. Avci, et al. (2012), "Real-time precise 3D measurement of micro transparent objects using All-In-Focus imaging system", *Journal of Micro-Nano Mechatronics*, **7(1)**, pp.21-31, DOI: 10.1007/s12213-012-0041-5.

DOI: 10.31276/VJSTE.63(4).36-41

Clinical and subclinical characteristics of brain-dead donors for liver transplantation in Viet Duc University Hospital

Thanh Khiem Nguyen[1*], Hong Son Trinh[2], Gia Anh Pham[3], Ham Hoi Nguyen[1], Trung Nghia Bui[3], Manh Thau Cao[3], Quang Nghia Nguyen[3], Viet Khai Ninh[3], Tuan Hiep Luong[4], Tien Quyet Nguyen[3]

[1]Bach Mai Hospital, 78 Giai Phong Street, Phuong Mai Ward, Dong Da District, Hanoi, Vietnam
[2]Vietnam National Coordinating Centre for Human Organ Transplantation, 40, Trang Thi Street, Hang Bong Ward, Hoan Kiem District, Hanoi, Vietnam
[3]Viet Duc University Hospital, 40 Trang Thi Street, Hang Bong Ward, Hoan Kiem District, Hanoi, Vietnam
[4]Hanoi Medical University, 1 Ton That Tung Street, Trung Liet Ward, Dong Da District, Hanoi, Vietnam

Received 6 September 2021; revised 8 November 2021; accepted 19 November 2021

Abstract:

Since 2010, 49 cases of liver transplants from brain-dead donors were performed at Viet Duc University Hospital. This study is a descriptive cross-section cohort study with a combined analysis of retrospective and prospective occurrences of a series of cases of liver procurement from brain-dead donors in Viet Duc University Hospital from March 2010 to March 2020. The results of this study showed several features: the average age of the brain-dead donors was 29.8±10.9 (18-69), donors were mostly male (7.17/1, 87.8%), and the main cause of brain death was head trauma. Clinically, 40.8 and 63.3% of the subjects were hypothermic and diagnosed with diabetes insipidus, however, the subjects were all well resuscitated before procurement. Therefore, haemodynamic indices and temperatures were maintained at stable levels and there was no statistically significant difference. In subclinical aspects, haemoglobin and platelet levels decreased significantly but remained within the target criteria during resuscitation while blood sodium levels increased significantly during resuscitation when compared with levels at the time of admission ($p<0.001$) thus corresponding to diabetes insipidus. In general, 44.90% of donors were within the ideal standard, and in the extended standard group, the highest rate was electrolyte disorders (32.65%). In conclusion, there are many variations in clinical and paraclinical body signs as well as homeostasis in the brain-dead donors. Of these signs, the most prominent were changes in haemodynamics, temperature, urine output, complete blood count, blood clotting, and blood sodium levels. These are all factors that are included in the criteria to consider the selection of a liver donor.

Keywords: **brain-dead donors, clinical and subclinical characteristics, liver transplantation.**

Classification number: **3.2**

1. Introduction

Organ transplantation in general, and liver transplantation in particular, is one of the most outstanding medical achievements of the past few decades. However, since its inception, the transplant field has always faced the problem of scarcity of donated organs for all organs and especially the liver. The graft can be the whole liver from a deceased donor (including brain death and cardiac death) or a partial liver from a living donor. Trends in the use of donated organs differ in each region due to cultural issues. For example, in Asia, the main source of liver donation comes from living donors, however, donations from brain dead donors have also been increasing over time [1].

Donor selection is an important first step in obtaining a good quality graft. Ideal criteria of a deceased donor include young age, brain death due to trauma, stable haemodynamics, no hypernatremia, etc., which helps to achieve very good results after transplantation but also limits the number of donor organs [2, 3]. Recently, an expanded criteria of brain-dead donors has been introduced in order to maximize organ donation sources, which includes accepting donors who are elderly, had cardiac arrest, persistent hypotension, severe hypernatremia, or liver steatosis [4, 5]. Rationally considering the clinical and subclinical factors of brain-dead donors helps to balance these two factors while maximizing the quantity of donor organs and ensuring successful results after transplantation. In Vietnam,

*Corresponding author: Email: nguyenthanhkhiemvd@gmail.com

clinical and subclinical changes are mainly considered in terms of anaesthesia and resuscitation [6, 7]. T.H. Son, et al. (2016, 2017) [8, 9] was the first authors interested in factors affecting donor selection, but this was a study on donors in France. Therefore, we carried out this study to evaluate clinical and subclinical characteristics of brain-dead subjects at Viet Duc University Hospital.

2. Subjects and methods

2.1. Subjects

There were 49 subjects all over 18 years old, diagnosed with brain-death, and underwent multiple organ procurement with recipients of orthotopic liver transplantation at the Viet Duc University Hospital from May 2010 to May 2020.

Selection criteria: Donors who were over 18 years old with severe cerebral injuries (e.g., head trauma, cerebral vascular accident, ruptured cerebral vascular aneurysm…) and diagnosed brain-dead according to Ministry of Health's criteria. The livers were procured and transplanted to the corresponding recipient in Viet Duc University Hospital with complete medical records.

2.2. Methods

Descriptive, cross-sectional study of a series of cases.

Variables:

- General characteristics: age, gender, body mass index, ABO blood type, history (diabetes, hypertension, alcoholism...), and cause of brain death (traumatic brain injury, ruptured brain aneurysm, or cerebrovascular accident).

- Clinical and subclinical signs:

+ Heart rate, mean systolic blood pressure (SBP), average temperature, urine output in 1 h (starting at the time of admission but before brain-death test and organ procurement).

+ Rate of cardiac arrest, hypotension (mean BP<70 mm Hg), use of vasopressors, diabetes insipidus (Seckl's criteria: urine >3 l per day, urine osmolality <300 mOsm/kg, blood sodium >145 mEq/l).

+ Status of bacterial and viral infections: pneumonia, bacteraemia (sepsis), hepatitis B, hepatitis C, etc.

+ Haematology - biochemistry: haemoglobin, prothrombin time, PT-INR index, the amount of blood and serum transfused during resuscitation, kidney function tests (urea, creatinine), liver enzymes (AST/ALT), bilirubin, and blood sodium and potassium levels.

- Rate of extended criteria donor (mostly according to Briceno criteria: donor >60 years, ICU stay >4 days, hypotensive episodes <60 mmHg >1 h, bilirubin >2.0 mg/dl, ALT >170 U/l and/or AST >140 U/l, the use of dopamine doses >10 µg/kg per min and peak serum sodium >160 mEq/l).

Data analysis: using SPSS 20.0 software.

3. Results

Table 1. General characteristics of donors.

Mean age	29.8±10.9 (18-69); age group <40 (81.6%)
Gender	Male/female: 7.17/1 (87.8%)
BMI (kg/m²)	21.11±2.24 (17.58-27.80)
ABO blood types	O/A/B/AB: 55.1/14.3/26.5/4.1 (%)
Medical history	Hypertension/alcoholism/diabetes: 2.04/4.08/2.04 (%)
Brain-dead cause	Head trauma/ruptured cerebral aneurysm/cerebral infarction: 89.8/8.2/2.0 (%)

Table 1 revealed that the average age of donors was 29.8±10.9 and the working age (18-69 years old) was the majority. The male-to-female sex ratio was 7.17/1, the average BMI was 21.11±2.24, and the most frequent brain-death cause was head trauma (89.8%).

Table 2. Clinical signs of the donors.

Index	At admission	Before brain-dead test	Before procurement	p-value
Heart rate (per min)	98.1±22.5	104.5±19.4	101.7±28.7	0.447
Mean SBP (mmHg)	87.1±16.9	85.5±12.3	88.3±24.5	0.834
Temperature (°C)	36.6±0.6	36.1±1.2	36.4±1.6	0.121
Amount of urine (ml per hour)	330.0±278.1	663.2±405.9	480.0±312.8	0.039

As shown in Table 2, the subjects were resuscitated well before procurement, haemodynamic indices and temperature were maintained at stable levels, and there was no statistically significant difference, however, the urine volume increased during resuscitation which represented the progression of diabetes insipidus (p=0.039).

Table 3. Clinical changes of the donors.

Systemic disorders	Number (n)	Ratio (%)
Cardiac arrest (n=49)	2	4.1
Hypotension (n=49)	11	22.45
Use of vasopressors (n=49)	46	93.9
Diabetes insipidus (n=35)	31	63.3
Hypothermia (n=48)	20	41.7

All cases of cardiac arrest and hypotension were well resuscitated and remained stable until aortic clamping (Table 3).

Table 4. Bacterial and viral infection's status of donors.

Bacterial and viral infections		Number (n)	Ratio (%)
Sepsis		1	2.0
Viral infection	Hepatitis B	0	0
	Hepatitis C	2	4.1

According to Table 4, there was 1 patient with sepsis with the following blood culture results: *Klebsiella pneumoniae*, *Pseudomonas aeruginosa*, and *Actinobacteria baumannii*. There were 2 donors who had antibodies against hepatitis C, but no virus was found in their blood.

Table 5. Donor's haematology test results.

Index	At admission	Before brain-dead test	Before procurement	p-value
Haemoglobin (g/l)	120.73±27.80	114.06±17.00	105.72±14.41	0.014
White blood cells (G/l)	19.14±6.49	15.90±4.85	14.16±3.97	<0.001
Platelet (T/l)	174.42±69.53	127.41±86.05	121.01±55.70	0.004
Prothrombin (s)	15.22±2.17	17.02±3.18	15.92±2.65	0.009
PT-INR	1.27±0.20	1.77±2.37	1.34±0.23	0.005

The haemoglobin and platelet levels decreased significantly but remained within the target criteria during resuscitation. Prothrombin time and PT-INR were severely disturbed but were also adjusted to the target before organ procurement (Table 5).

Table 6. Amount of blood products transfused during resuscitation.

Blood products	Number (n-%)	Amount of transmission (ml)		
		Minimum	*Maximum*	*Mean*
Red blood cells (ml)	28/49 (57.1%)	250	3200	1026.79±604.69
Platelets (ml)	2/49 (4.1%)	250	500	375.00±125.00
Plasma (ml)	21/49 (42.9%)	200	1350	551.25±315.44

In 57.1% of cases, red blood cells were transfused preoperatively, the average volume of infusion was 1026.79 ml, and only 2 cases required platelet transfusion with an average volume of 375 ml (Table 6).

Table 7. Biochemical test results.

Index	At admission	Before brain-dead test	Before procurement	p-value
Na (mmol/l)	141.86±8.12	153.30±10.58	149.35±10.37	<0.001
Ure (mmol/l)	5.96±2.94	5.49±3.44	4.49±3.07	0.166
Creatinine (µmol/l)	102.16±65.18	94.46±36.74	82.77±23.86	0.234
AST (U/l)	104.89±181.48	71.32±74.98	52.64±41.18	0.168
ALT (U/l)	62.04±83.48	45.97±59.27	39.17±45.13	0.307
Total Bil (µmol/l)	13.97±8.63	18.50±9.21	17.39±9.33	0.108
Directed bil (µmol/l)	3.21±1.70	5.23±3.36	5.38±3.23	0.01
Albumin (g/l)	30.91±6.72	26.58±5.01	31.14±8.61	0.007

In Table 7, blood sodium levels increased significantly during resuscitation compared with the time of admission ($p<0.001$) corresponding to diabetes insipidus. The mean ALT/AST increased, but within the resuscitation target, and this index tended to improve during resuscitation.

Table 8. Liver characteristics of donors on ultrasound and computerized tomography.

Characteristics		Ultrasound	Computerized tomography
Number		46/49 (93.9%)	4/49 (8.16%)
Liver parenchyma	Normal	44 (95.7%)	4 (100%)
	Cirrhosis	0	0
	Steatosis	2 (4.3%)	0
	Liver trauma	0	0
Anatomical variation of hepatic artery		0/46	0/4
Anatomical variation of portal vein		0/46	0/4
Bile duct dilatation		0/46	0/4

Ultrasound is the main test to examine the organs before surgery (Table 8).

Table 9. Criteria for selection of liver donors.

Donor's selective criteria		n	%
Standard criteria		22	44.90
Extended criteria	Age >60	1	2.04
	ICU stay >4 days	3	6.12
	SBP <70 mmHg lasting at least 1 h	1	2.04
	Hepatitis C	2	4.08
	Blood sodium >160 mmol/l	16	32.65
	AST >170 U/l and/or ALT >140 U/l	6	12.24
	Sepsis	1	2.04
	BMI>28, Hb <70 g/l, ICU >7 days, Dopamine >10 µg/kg/min, total Bilirubin >34 mmol/l, PaO_2 <80 mmHg, liver steatosis >30%	0	0

44.90% of donors were within the ideal standard. In the extended standard group, the highest rate was electrolyte disorders (32.65%) (Table 9).

4. Discussion

In our study, the average age of donors was 29.8±10.9 years, the lowest was 18 years old, the highest was 69 years old, and up to 81.6% of the donors had the ideal age of under 40 years old (Table 1). The average age in our study was much lower than other studies around the world. The mean age of organ donors in Korean and French populations in the statistics of T.H. Son, et al. (2016) [8], D.H. Jung, et al. (2015) [10] were 48 and 58, respectively. We chose donors at a young age, mainly under 40, because liver transplantation has only been developed in Vietnam for about 10 years and a qualified result from the quality of the transplant is needed. In

general, age will partially affect liver volume, liver perfusion, and a mild increase in fibrosis [11].

The proportion of male brain-dead donors accounted for 7.17/1 more than 87.8% in our study (Table 1) and this can be explained by the fact that most of the organ donors at Viet Duc University Hospital had brain death caused by traumatic brain injury, which is predominate in males. Research by D.V. He, et al. (2005) [12] on the epidemiology of traumatic brain injury at Viet Duc University Hospital showed that the male rate accounted for 79.4%. Research by T.H. Son, et al. (2016) [8] on liver donors in Strasbourg (France) showed that the proportion of men accounted for only 54.1%, much lower than in our study, and this difference was explained by the cause of brain death with the highest rate in Strasbourg being by cerebrovascular accident (62.2%) - a disease with an equal prevalence between the two genders. However, this result also showed that the cause of brain death due to stroke in our country has not been paid enough attention.

A stable donor's systemic status is an important factor in optimising the graft's function. In our study, the average heart rate fluctuated between 98-104 beats per minute, the mean blood pressure of above 80 mmHg was maintained relatively constantly, and there was no difference between these values at the time of admission, the time of brain-death test, and before organ procurement (Table 2). The results were within the haemodynamic stability criteria for brain-dead donors per the 2007 Paris Organ Transplantation Conference [13]. This demonstrates that brain death resuscitation is effective in maintaining haemodynamics. During the resuscitation process, we recorded 11 cases (22.45%) with hypotension, but they were all resuscitated well afterwards and maintained haemodynamically stable until organ removal (Table 3). In order to maintain haemodynamic stability during resuscitation, most subjects must take vasopressors and the rate of vasopressors in our study was 93.9%. Our results on heart rate-average blood pressure, rate of haemodynamic disturbances, as well as the rate of vasopressor use are similar to those of [14], but on an in-depth study on resuscitation. The author analysed in more detail the different time points from the time the patient was admitted to the hospital to the time of organ removal thereby showing that the rate of haemodynamic disturbances at the time of admission was the highest at 21.3%, and the rate of using vasopressor at the highest point was 100%.

A dysfunctional hypothalamus after brain death leads to impaired thermoregulatory function. Hypothermia increases diuresis, interferes with coagulation, increases the risk of arrhythmias, and increases the risk of infection [15]. In our study, the average temperature was kept relatively constant during the resuscitation process and ranged from 36.00 to 37.2^{o}C, and the difference in temperature between the time points from admission to before surgery was not statistically significant (Table 2). Our average temperature was similar to the study of Dung (2019) [14] (36.41±1.31^{o}C). During the resuscitation process, we also actively implemented measures to prevent hypothermia such as warming and supplying warm fluids.

Diabetes insipidus is very common in subjects with brain-death due to damage to the posterior pituitary hypothalamus [16]. In S.M. Kazemeyni, et al. (2008) [17], the rate of diabetes insipidus in brain-dead subjects was 70.2%, and our statistics show similar results with a rate of 63.3% (Table 3). In addition, our results also showed that the mean urine volume during resuscitation and before organ procurement significantly increased compared to hospital admission (p=0.039) (Table 2). This demonstrates that despite the resuscitation, hypothalamic damages are always progressive in brain-dead people.

Infection is a common condition in subjects with brain-death because of severe systemic conditions, coordinative damages, and long hospital stays with invasive therapies. A study by [8] recorded that 6.76% of brain-dead subjects had sepsis and their livers were still taken for transplantation. Our study recorded 1 case of bacteraemia in which antibiotics were used according to the antibiogram (Table 4). The rest were given prophylactic antibiotics during resuscitation. Sepsis is not a contraindication for organ donation with appropriate preoperative and postoperative antibiotics along with adjustment of immunosuppressive regimens for recipients after surgery. However, there are reports that lead to mixed opinions when there are recipients with hepatic artery occlusion as the cause is believed to be the result of bacteraemia caused by *E. coli* of the donor [18, 19].

There is a great deal of evidence that there were no differences in survival between the two groups of grafts taken from anti-HCV-positive donors and anti-HCV-negative donors. People previously infected with the hepatitis C virus in the blood are considered a contraindication for liver donation. However, in the new era of antiviral hepatitis C drugs, even brain-dead donors with the hepatitis C virus in their blood can be considered for liver transplantation to non-hepatitis C-infected recipients, and of course were treated with anti-hepatitis C drugs after transplantation [20]. Our study recorded 2 cases with positive anti-HCV tests, however, no virus was detected in the blood count and both grafts were transplanted to subjects with hepatitis C (Table 4). That was a reasonable selection of liver donors in the context that the organ resources are always lacking and need to be utilised to the fullest extent while ensuring the safety of the recipients.

Hypernatremia is a common condition in brain-dead people, which is a consequence of diabetes insipidus. Hypernatremia is also a common concern in brain-dead donors because some studies have suggested that it affects graft function and increases graft mortality. It is hypothesized that high levels of sodium in donor blood lead to increased osmotic pressure, cellular oedema, and exacerbation of cellular injury upon reperfusion. In our study, the average sodium concentration at the time of the brain-death test and before surgery was 153.30 mmol/l and 149.35 mmol/l, respectively, and the ratio of sodium max >160 mmol/l was 32.65% (Table 7). Our results are the same as in the study of E. Totsuka, et al. (1999) [21] with an average blood sodium concentration of 153.5 mmol/l and of R.S. Magus, et al. (2010) [22] with a maximum blood sodium concentration >160 of 36%. Our study also showed that blood sodium at the time of the brain-death test and before organ procurement was both high and significantly increased compared with at the time of hospital admission (141.85 mmol/l) with $p<0.001$. Thus, despite intensive resuscitation, blood sodium disorder still worsens corresponding to the state of diabetes insipidus.

Elevating liver enzymes in brain-dead donors is often a consequence of trauma, hypoxia, anaemia, haemodynamic instability, and sometimes toxicity and drug side effects. In our study, the mean values of AST and ALT increased slightly and tended to decrease over time to near normal levels (52.64 U/l and 39.17 U/l respectively) at times before organs procurement (Table 7). There were only 6 cases where maximum AST and ALT levels increased higher than the standard values for the ideal donor (AST >170 U/l and/or ALT >140 U/l) (Table 9). This result was different from the study of R.S. Magus, et al. (2015) [23] with the percentage of donors with ALT >500 U/l up to 7%. This difference is mainly caused by the donors in this study having a relatively large proportion of asphyxiation (anoxia), and this group often had elevated liver enzymes.

Total bilirubin levels greater than 34 µmol/l are considered an exaggerating factor [24]. In our study, the mean bilirubin concentration was in the normal range (from 13.97 to 18.59 µmol/l), there was no difference between during the time from hospital admission to organ removal, and there were no cases of bilirubin concentration exceeding the ideal standard (Tables 7-9). Our average bilirubin concentration was similar to the study of D.J. Carpenter, et al. (2019) [25], however, this study had 7.6% Bilirubin cases within the extended criteria. This can also be explained because the cause of brain death in this study was more than 20% asphyxiation and 44.6% stroke. Stroke subjects often have a high average age with systemic diseases such as diabetes and dyslipidaemia affecting liver quality, while asphyxiation is the cause of hypoxia in the liver.

The implementation of preoperative imaging facilities were used to evaluate the imaging features of the transplant organ for surgery such as liver volume, anatomical variations of the hepatic hilum, and liver steatosis [26]. All of our subjects had at least one preoperative imaging method to evaluate the morphological characteristics of the organs, which was mainly abdominal ultrasound, however, only 4 cases (8.16%) were imaged with a CT scan. Accordingly, in 100% of subjects no liver damage was detected (parenchyma and hepatic hilum components) on ultrasound or computed tomography while 2 cases (4.17%) had grade I liver steatosis images on ultrasound. Compared with macroscopic results from surgery and pathology, the sensitivity of ultrasound on the diagnosis of liver steatosis was 2/13 (15.38%) and the specificity was 2/2 (100%). We could not find any studies in the English literature that used ultrasound to assess the liver status of brain-dead donors before surgery. At centres in France, CT scans of the whole body are often applied to assess both brain death and the status of the organs to be removed. The study of A. Tache, et al. (2016) [27] showed that abdominal CT excluded two donors that had severe liver steatosis (>60%), and found that 10% of the donors had anatomical variations of the hepatic arteries. However, in our study, the liver donors were mainly traumatized at a younger age, thus the role of preoperative screening with imaging tools was reduced. The use of ultrasound for screening is also reasonable as bedside ultrasound helps to limit the need to move, which aggravates the whole-body condition.

The consideration of clinical features was completed so that we can choose a reasonable liver donor. In the first stage, we selected the ideal donor according to Feng's criteria (age <40 years, brain death due to trauma, haemodynamic stability, no liver steatosis, no chronic liver disease as well as communicable diseases) [28]. However, over time, when the demand for transplants remained very high and we mastered the techniques of organ procurement and transplantation as well as resuscitation, we gradually began using donors at an expanded standard. Based on Bricano's expanded criteria combined with some other updated studies [5, 29, 30], we selected an extended criteria to apply to our research. Accordingly, 55.10% of donors were in the expanded criteria, with the highest rate being hypernatremia (32.65%) followed by elevated liver enzymes (12.24%) (Table 9). Our study results are consistent with the study of S. Gruttadauria, et al. (2008) [29] with the proportion of subjects with ideal criteria also approximately 50%. However, this study also had statistics on the rate of risk factors of which the highest percentage was the electrolyte disorder (32.65%). This result was consistent with the characteristics of the cause of brain death differ between developed and developing countries with mainly young subjects having brain death due to traumatic brain injury.

Conclusions

There are many variations in the clinical and subclinical signs of the body as well as homeostasis in brain-dead donors of which the most prominent are changes in haemodynamics, temperature, urine output, complete blood count, blood clotting, and blood sodium

levels. These are all factors that are included in the criteria to consider the selection of a liver donor. Resuscitation to limit these changes helps to obtain more organ resources as well as a good quality liver transplant.

CRedit author statements

Thanh Khiem Nguyen: Formal analysis, Validation, Supervision; Hong Son Trinh: Writing original draft, Visualisation; Gia Anh Pham: Investigation, Formal analysis, Validation; Ham Hoi Nguyen: Investigation, Formal analysis, Validation; Trung Nghia Bui: Investigation, Formal analysis, Validation; Manh Thau Cao: Investigation, Formal analysis, Validation; Quang Nghia Nguyen: Investigation, Formal analysis, Validation; Viet Khai Ninh: Formal analysis, Visualisation; Tuan Hiep Luong: Writing original draft, Conceptualisation; Tien Quyet Nguyen: Methodology, Writing - Review and editing.

COMPETING INTERESTS

The authors declare that there is no conflict of interest regarding the publication of this article.

REFERENCES

[1] C.L. Chen, S.C. Kabiling, A.M. Concejero (2013), "Why does living donor liver transplantation flourish in Asia?", *Nature Reviews Gastroenterology & Hepatology*, **10(12)**, pp.746-751, DOI: 10.1038/nrgastro.2013.194.

[2] New York State Department of Health Workgroup (2005), "Workgroup on expanded criteria organs for liver transplantation", *Liver Transplantation*, **11**, pp.1184-1192.

[3] S. Feng, N.P. Goodrich, J.L.B. Gresham, et al. (2006), "Characteristics associated with liver graft failure: The concept of a donor risk index", *Am. J. Transplant.*, **6(4)**, pp.783-790, DOI: 10.1111/j.1600-6143.2006.01242.x.

[4] M. Cescon, G.L. Grazi, A. Cucchetti, et al. (2008), "Improving the outcome of liver transplantation with very old donors with updated selection and management criteria", *Liver Transplantation*, **14(5)**, pp.672-679, DOI: 10.1002/lt.21433.

[5] H. Furukawa, M. Taniguchi, M. Fujiyoshi, et al. (2012), "Experience using extended criteria donors in first 100 cases of deceased donor liver transplantation in Japan", *Transplantation Proceedings*, **44(2)**, pp.373-375, DOI: 10.1016/j.transproceed.2012.01.010.

[6] C.T.A. Dao, et al. (2012), "Clinical and laboratory characteristics and methods of resuscitation anesthesia for organ transplantation in brain-dead organ donors", *Journal of Military Pharmaco - Medicine*, Special Issue of Organ Transplantation, **5(3)**, pp.35-45 (in Vietnamese).

[7] M.X. Hien, et al. (2012), "Study on the change of some organ functions and the timing of organ transplantation in brain dead subjects", *Journal of Military Pharmaco - Medicine*, **5(6)**, pp.83-90 (in Vietnamese).

[8] T.H. Son, N.T. Khiem (2016), "Clinical characteristics of brain-dead donor in 2014 at Hepato-Biliary-Pancreatic Surgery Department, Hautepierre Hospital, Strasbourg, France", *Journal of Practical Medicine*, **5(1011)**, pp.102-107 (in Vietnamese).

[9] T.H. Son, et al. (2017), "Research on brain-dead donors who were donated by family in Vietnam from April 23, 2008 to August 19, 2016", *Journal of Practical Medicine*, **2(1035)**, pp.50-56 (in Vietnamese).

[10] D.H. Jung, S. Hwang, C.S. Ahn, et al. (2015), "Safety and usefulness of warm dissection technique during liver graft retrieval from deceased donors", *Transplantation Proceedings*, **47(3)**, pp.576-579, DOI: 10.1016/j.transproceed.2014.12.043.

[11] T. Yandza, et al. (2003), "Update on the selection criteria for cadaveric donors for liver transplantation", *Gastroenterol. Clin. Biol.*, **27(2)**, pp.163-175 (in French).

[12] D.V. He, et al. (2005), "Epidemiological characteristics of traumatic brain injury at Viet Duc University Hospital", *Journal of Medical Research, Hanoi Medical University*, **39(6)**, pp.90-97 (in Vietnamese).

[13] F. Durant, J.F. Renz, B. Alkofer, et al. (2008), "Report of the Paris consesus meeting on expanded critia donors in liver transplantation", *Liver Transplantation*, **14(12)**, pp.1694-1707, DOI: 10.1002/lt.21668.

[14] D.T.K. Dung (2019), "Study on the effectiveness of organ function resuscitation in potential organ donors", *Clinical Research Institute 108 of Medicine and Pharmacy*, **9(6)**, pp.88-97 (in Vietnamese).

[15] J. Wong, H.L. Tan, J.P.S. Goh (2017), "Management of the brain dead organ donor", *Trends in Anaesthesia and Critical Care*, **13**, pp.6-12, DOI: 10.1016/j.tacc.2016.11.004.

[16] A.M. Ranasinghe, R.S. Bonser (2011), "Endocrine changes in brain death and transplantation", *Best Practice & Research Clinical Endocrinology & Metabolism*, **25(5)**, pp.799-812, DOI: 10.1016/j.beem.2011.03.003.

[17] S.M. Kazemeyni, F. Esfahani (2008), "Influence of hypernatremia and polyuria of brain-dead donors before organ procurement on kidney allograft function", *Urol. J.*, **5(3)**, pp.173-177.

[18] R.P. Pauly, D. Rayner, A.G. Murray, et al. (2004), "Transplantation in the face of severe donor sepsis: Pushing the boundaries?", *Am. J. Kidney Dis.*, **44(4)**, pp.e64-e67.

[19] K.E. Doucette, M.A. Saif, N. Kneteman, et al. (2013), "Donor-derived bacteremia in liver transplant recipients despite antibiotic prophylaxis", *American Journal of Transplantation*, **13(4)**, pp.1080-1083, DOI: 10.1111/ajt.12133.

[20] J.F. Crismale, J. Ahmad (2019), "Expanding the donor pool: Hepatitis C, hepatitis B and human immunodeficiency virus-positive donors in liver transplantation", *World J. Gastroenterol.*, **25(47)**, pp.6799-6812, DOI: 10.3748/wjg.v25.i47.6799.

[21] E. Totsuka, F. Dodson, A. Urakami, et al. (1999), "Influence of high donor serum sodium levels on early postoperative graft function in human liver transplantation: Effect of correction of donor hypernatremia", *Liver Transplantation and Surgery*, **5(5)**, pp.421-428, DOI: 10.1002/lt.500050510.

[22] R.S. Mangus, J.A. Fridell, R.M. Vianna, et al. (2010), "Severe hypernatremia in deceased liver donors does not impact early transplant outcome", *Transplantation*, **90(4)**, pp.438-443, DOI: 10.1097/TP.0b013e3181e764c0.

[23] R.S. Mangus, J.A. Fridell, C.A. Kubal, et al. (2015), "Elevated alanine aminotransferase (ALT) in the deceased donor: Impact on early post-transplant liver allograft function", *Liver International*, **35(2)**, pp.524-531, DOI: 10.1111/liv.12508.

[24] J. Briceño, T. Marchal, J. Padillo, et al. (2002), "Influence of marginal donors on liver preservation injury", *Transplantation*, **74(4)**, pp.522-526, DOI: 10.1097/00007890-200208270-00015.

[25] D.J. Carpenter, M.C. Chiles, E.C. Verna, et al. (2019), "Deceased brain dead donor liver transplantation and utilization in the united states: Nighttime and weekend effects", *Transplantation*, **103(7)**, pp.1392-1404, DOI: 10.1097/TP.0000000000002533.

[26] H.K. Kanduri, A. Xire, S.C.G. Kurelli, et al. (2019), "Role of imaging in pre-hepatic transplantation evaluation", *Radiology of Infectious Diseases*, **6(4)**, pp.133-141, DOI: 10.1016/j.jrid.2020.02.004.

[27] A. Tache, N. Badet, A. Azizi, et al. (2016), "Multiphase whole-body CT angiography before multiorgan retrieval in clinically brain dead patients: Role and influence on clinical practice", *Diagnostic and Interventional Imaging*, **97(6)**, pp.657-665, DOI: 10.1016/j.diii.2015.06.024.

[28] N.T. Quyet (2010), *Research and Implementation of Liver-Kidney Transplantation from Brain-Dead Donors,* State-level project code KC10.25/06-10, Ministry of Science and Technology.

[29] S. Gruttadauria, G. Vizzini, D. Biondo, et al. (2008), "Critical use of extended criteria donor liver grafts in adult-to-adult whole liver transplantation: A single-center experience", *Liver Transplantation*, **14(2)**, pp.220-227, DOI: 10.1002/lt.21359.

[30] N. Goldaracena, E. Quinonez, P. Mendez, et al. (2012), "Extremely marginal liver grafts from deceased donors have outcome similar to ideal grafts", *Transplantation Proceedings*, **44(7)**, pp.2219-2222, DOI: 10.1016/j.transproceed.2012.07.113.

DOI: 10.31276/VJSTE.63(4).42-46

Study on α-glucosidase inhibitory activity of 40 kinds of vegetables, tubers, and fruits in An Giang

Thi-My-Linh Lam[1], Minh-Tuan Le[2], Manh-Ha Bui[3*]

[1]Faculty of Education, An Giang University, Vietnam National University - Ho Chi Minh City, 18 Ung Van Khiem Street, Dong Xuyen Ward, Long Xuyen City, An Giang Province, Vietnam
[2]Faculty of Agriculture and Natural Resources, An Giang University, Vietnam National University - Ho Chi Minh City, 18 Ung Van Khiem Street, Dong Xuyen Ward, Long Xuyen City, An Giang Province, Vietnam
[3]Department of Environmental Sciences, Saigon University, 273 An Duong Vuong Street, Ward 3, District 5, Ho Chi Minh City, Vietnam

Received 6 January 2020; revised 28 February 2020; accepted 13 March 2020

Abstract:

A study on the α-glucosidase inhibitory activity of 40 kinds of vegetables, tubers, and fruits found in the An Giang province was conducted. The results indicated that all 40 extracted samples displayed α-glucosidase inhibitory activity at a concentration of 250 µg ml^{-1}, 36 extracted samples showed an inhibition rate greater than 50% at 250 µg ml^{-1}, 25 extracted samples had over 50% at 100 µg ml^{-1}, 17 extracted samples possessed more than 50% at 50 µg ml^{-1}, 7 extracted samples sampled showed over 50% at 25 µg ml^{-1}, 5 extracted samples were greater than 50% at 10 µg ml^{-1}, and 1 extracted sample was greater than 50% at 1 µg ml^{-1}. Among the 40 samples, those taken from the seeds of *Areca catechu*, the fruits of *Cassia grandis*, the fruits of *Syzygium cumini*, the seeds of *Glycine max*, and the stems of *Enydra fluctuans* exhibited the strongest α-glucosidase inhibitory activity in methanol, with IC_{50} values of 0.15, 2.54, 4.05, 5.17 and 8.68 µg ml^{-1}, respectively, which were stronger than the positive control acarbose with an IC_{50} value of 214.5 µg ml^{-1}.

Keywords: **An Giang, α-glucosidase, *Areca catechu*, *Cassia grandis*, fruit, *Glycine max* and *Enydra fluctuans*, *Syzygium cumini*, tuber, vegetable.**

Classification number: **3.3**

1. Introduction

Diabetes is a disease known for symptoms of characteristically high blood sugar levels due to a lack of insulin with or without insulin resistance. Individuals with diabetes not only have high blood sugar but also have high sugar levels in their urine, so-called diabetes mellitus. Besides, diabetes also causes dangerous complications such as cardiovascular risks, stroke, and chronic kidney disease. Diabetes includes two types and diabetes type 2 accounts for about 90% of the total number of cases [1]. In the body, the small intestinal cell membrane secretes the α-glucosidase enzyme that plays a role in the hydrolysis of carbohydrates from food into oligosaccharides. Then, these hydrolysed oligosaccharides turn into glucose and enter the bloodstream via the small intestinal membrane to feed the body's cells. When the body has a metabolic disorder, carbohydrates and blood sugar levels will rise and lead to diabetes. By inhibiting the activity of the α-glucosidase enzyme, hydrolysis of carbohydrates slows down and blood sugar levels reduce [1].

Therefore, the search for vegetables, tubers, and fruits with the ability to inhibit the α-glucosidase enzyme may have significance in new diabetes treatments. Consequently, in this study, we conducted a screening of the α-glucosidase enzyme inhibitory activity of some vegetables, tubers, and fruits found in the An Giang province to further guide the research of diabetes treatments.

2. Materials and methods

2.1. Sample preparation

The 40 samples of vegetables, tubers, and fruits in this study were purchased in the An Giang province during the month of 1/2019 (Table 1) and were identified by Dr. Luong Minh Chau, Institute of Rice in the Mekong delta. These samples (of vegetables, tubers, and fruits) were selected according to three criteria: folk criteria (used to treat diabetes mellitus), references, and random selection. The dried vegetables, tubers, and fruits were minced, and then simmered under circulation 3 times with the solvent methanol for 3 h. The extracted samples were collected and concentrated at low pressure to obtain samples in a methanol solvent.

*Corresponding author: Email: manhhakg@sgu.edu.vn

Table 1. The list of 40 vegetables, tubers, fruits in An Giang.

Number	Science name	Familia	Parts used	Selection criteria
1	*Abelmoschus esculentus* L.	Malvaceae	Fruits	1
2	*Allium ramosum* L.	Alliaceae	Stems	3
3	*Amaranthus tricolor* L.	Amaranthaceae	Stems	3
4	*Asparagus officinalis* L.	Asparagaceae	Stems	3
5	*Azadirachta indica* A.	Meliaceae	Leaves	1
6	*Basella alba* L.	Basellaceae	Stems	1
7	*Benincasa hispida* Thunb	Cucurbitaceae	Fruits	3
8	*Brassica integrifolia (West.) O.E. Schulz*	Brassicaceae	Stems	3
9	*Brassica juncea* L. Czern	Brassicaceae	Stems	3
10	*Brassica rapa chinensis*	Brassicaceae	Stems	3
11	*Brassica rapa* subsp. *pekinensis* Lour.	Brassicaceae	Stems	3
12	*Cassia grandis* L.F.	Fabaceae	Fruits	3
13	*Centella asiatica* L.	Apiaceae	Stems	2
14	*Colocasia esculenta* L.	Araceae	Tubers	3
15	*Cucumis sativus* L.	Cucurbitaceae	Fruits	1
16	*Cucurbita pepo L.*	Cucurbitaceae	Fruits	2
17	*Eichhornia crassipes* M.	Pontederiaceae	Stems	3
18	*Enydra fluctuans* Lour.	Asteraceae	Stems	2
19	*Areca catechu* L.	Arecaceae	Seeds	3
20	*Glycine max* L. Merr.	Fabaceae	Seeds	3
21	*Ipomoea batatas* L.	Convolvulaceae	Tubers	1
22	*Ipomoea batatas* L.	Convolvulaceae	Stems	1
23	*Lagenaria siceraria* M.	Cucurbitaceae	Fruits	3
24	*Luffa cylindrica* L. M.	Cucurbitaceae	Fruits	1
25	*Momordica charantia* L.	Cucurbitaceae	Stems	2
26	*Momordica charantia* L.	Cucurbitaceae	Fruits	2
27	*Momordica charantia* L.	Cucurbitaceae	Seeds	2
28	*Morus alba* L.	Moraceae	Fruits	2
29	*Musa balbisiana* Colla	Musacea	Young fruits	1
30	*Peperomia pellucida* L.	Piperaceae	Stems	1
31	*Perilla frutescens* L.	Lamiaceae	Stems	3
32	*Phaseolus vulgaris* L.	Fabaceae	Fruits	3
33	*Piper sarmentosum* R.	Piperaceae	Stems	1
34	*Raphanus sativus* L.	Brassicaceae	Tubers	3
35	*Sauropus androgynus* L.	Phyllantheae	Stems	1
36	*Solanum lycopersicum* L.	Solanaceae	Fruits	3
37	*Solanum melongena* L.	Solanaceae	Fruits	3
38	*Spinacia oleracea* L.	Amaranthaceae	Stems	1
39	*Syzygium cumini* L.	**Myrtaceae**	Fruits	2
40	*Vigna unguiculata* sp.	Fabaceae	Fruits	3

1-folk criteria; 2-references; 3-random selection.

2.2. Process of inhibitory activity testing α-glucosidase enzyme

Methodological basis:

The *α*-glucosidase enzyme catalyses *p*-nitrophenyl-*α*-D-glucopyranoside into *α*-D-glucose and *p*-nitrophenol, which has a light yellow colour and maximum absorbance in the optical spectrum at 401 nm [2]. In the presence of enzyme inhibitors, the intensity of the absorption of the solution will decrease. Based on the absorption intensity of the solution with and without a sample, the percentage of inhibition of the *α*-glucosidase enzyme of the sample can be calculated. Construction of the line of representation between percent inhibitors and concentration of inhibitors determines the IC_{50} values, which is the concentration of the sample at which 50% of the enzymes are inhibited. Samples with higher activity have lower IC_{50} values.

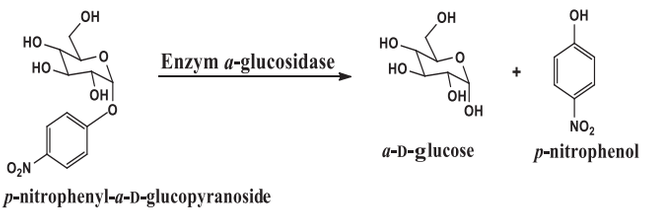

Diagram 1. Hydrolysis of the *α*-glucosidase enzyme with *p*-nitrophenyl-*α*-D-glucopyranoside substrate.

Chemicals:

- Phosphate buffer solution 0.01 M with pH=7.0

- *α*-glucosidase enzyme solution 0.1 U ml^{-1}

- *p*-nitrophenyl-*α*-D-glucopyranoside background solution 1.5 mM

- Na_2CO_3 solution 0.1 M

All the chemicals were supplied from Aldrich-Sigma.

Activation test procedure:

The sample was dissolved in a phosphate buffer, to which 50 µl of the enzyme was added and mixed well. After incubation at 37ºC for 5 min, 50 µl of background solution was added, mixed well, and incubated again at 37°C for 30 min. At the end of the second incubation period, 375 µl of Na_2CO_3 was added and the optical density of the solution was measured at a wavelength of 401 nm. Each sample was measured at 5 different concentrations (250, 100, 50, 25, 10 µg ml^{-1}), along with a blank sample that was similar to the test samples. Still, the enzyme solution was replaced with a phosphate buffer solution. The average of three optical density measurements at each concentration was calculated as the inhibitory percentage value (I%).

3. Results and discussion

The results of the enzyme *α*-glucosidase inhibitory activity of the 40 vegetables, tubers, and fruits from the An Giang province are presented in Table 2.

Table 2. The results of α-glucosidase enzyme inhibition activity of the 40 vegetables, tubers, fruits from the An Giang province.

Number	Samples	Inhibition (%)					IC_{50} (µg ml^{-1})
		250 (µg ml^{-1})	*100 (µg ml^{-1})*	*50 (µg ml^{-1})*	*25 (µg ml^{-1})*	*10 (µg ml^{-1})*	
1	*Abelmoschus esculentus*	*	96.89±0.71	78.71±1.45	49.74±0.98	24.67±0.99	25.22
2	*Allium ramosum*	*	87.51±0.81	60.96±1.19	40.43±1.13	31.06±1.51	36.65
3	*Amaranthus tricolor*	17.93±1.65	1.39±0.66	-	-	-	>250
4	*Asparagus officinalis*	*	96.01±0.85	62.72±0.46	22.01±0.97	1.6±0.58	42.19
5	*Azadirachta indica*	87.6±0.68	39.77±1.04	5.77±0.82	-	-	132.08
6	*Basella alba*	98.77±0.25	32.49±0.88	15.37±0.83	3.36±1.3	-	139.63
7	*Benincasa hispida* Thunb	*	54.47±0.73	22.87±0.8	7.1 ± 1.7	-	92.93
8	*Brassica integrifolia*	46.8±1.09	19.27±1.48	7.1±1.79	-	-	>250
9	*Brassica juncea*	*	51.52±1.01	23.43±0.53	6.46±0.48	-	97.29
10	*Brassica rapa chinensis*	93.02±0.63	40.5±0.86	18.19±0.91	7.95±0.85	-	127.13
11	*Brassicarapa* subsp. *pekinensis*	*	68.16±1.33	37.16±1.79	7.81±1.02	-	70.72
12	*Centella asiatica*	*	75.15±0.66	26.4±1.15	2.6±0.9	-	74.21
13	*Colocasia esculenta*	*	67.3±0.92	46.44±0.83	15.69±0.58	6.16±0.63	58.53
14	*Cucumis sativus*	23.78±0.98	3.57±1.63	-	-	-	>250
15	*Cucurbita pepo*	*	97.12±0.36	55.58±0.51	27.27±1.25	1.92±0.76	45.07
16	*Eichhornia crassipes*	*	73.44±1.34	28.04±0.77	11.39±0.93	-	74.18
17	*Ipomoea batatas*	81.57±0.15	33.5±0.91	27.28±0.95	10.8±0.52	3.54±1.41	151.50
18	*Ipomoea batatas*	*	86.61±0.86	76.09±1.01	58.47±0.78	49.22±0.73	11.26
19	*Lagenaria siceraria*	*	96.39±1.25	69.28±0.96	23.2±1.33	4.09±0.24	39.54
20	*Luffa cylindrica*	*	97.88±0.38	82.66±0.92	34.45±0.86	15.04±2.02	33.07
21	*Momordica charantia*	*	93.36±1.31	71.22±0.85	44.45±1.59	29.2±0.57	30.18
22	*Momordica charantia*	95.88±0.64	31.84±1.01	19.65±1.61	-	-	142.54
23	*Momordica charantia*	*	*	89.16±2.45	40.39±1.22	12.51±0.99	29.93
24	*Morus alba*	*	59.98±1.43	34.22±1.24	16.4±1.06	2.65±1.3	80.63
25	*Musa balbisiana*	*	*	97.7±0.15	68.06±0.97	26.65±0.74	18.46
26	*Peperomia pellucida*	96.09±0.38	39.65±1.55	21.13±1.39	12.28±0.91	-	126.76
27	*Perilla frutescens*	*	51.78±0.71	20.19±1.13	11.34±0.73	3.31±1.05	97.18
28	*Phaseolus vulgaris*	*	97.04±0.43	64.63±1.21	17.67±0.72	6.96±1.16	42.21
29	*Piper sarmentosum*	76.56±0.88	22.76±1	19.68±1.44	11.28±1.17	1.19±0.91	175.94
30	*Raphanus sativus*	98.68±0.27	48.71±0.97	5.62±1	-	-	103.86
31	*Sauropus androgynus*	96.78±0.51	26.72±1.17	17.41±1.42	2.25±1.21	-	149.84
32	*Solanum lycopersicum*	36.84±0.77	8.31±0.86	-	-	-	>250
33	*Solanum melongena*	98.34±0.44	41.77±1.43	15.84±1.15	-	-	121.82
34	*Spinacia oleracea*	45.78±1.64	13.38±1.07	3.08±1.08	-	-	>250
35	*Vigna unguiculata*	*	99.9±0.2	77.36±1.19	49.4±1.9	2.39±1.35	38.75
		-	10 (µg ml^{-1})	5 (µg ml^{-1})	2.5 (µg ml^{-1})	1.0 (µg ml^{-1})	
36	*Cassia grandis*	*	97.14±0.61	83.29±0.8	49.45±1.9	23.17±2.43	2.54
37	*Enydra fluctuans*	*	55.91±2.13	33.58±1.05	11.71±1.13	-	8.68
38	*Glycine max*	*	79.49±0.86	48.93±2.22	24.15±2.74	11.3±1.43	5.17
39	*Syzygium cumini*	*	98.59±0.73	64.6±1.27	26.34±1.12	9.79±1.53	4.05
		-	1.0 (µg ml^{-1})	0.5 (µg ml^{-1})	0.25 (µg ml^{-1})	0.1 (µg ml^{-1})	
40	*Areca catechu*	*	95.99±0.37	84.59±0.45	59.5±0.91	44.92±0.62	0.15
Acarbose							214.5

-: enzyme inhibitor concentration lower than 1% (I<1%); *: enzyme inhibitor concentration is higher than 100% (I>100%).

The results of this study showed that of the 40 samples of vegetables, tubers, and fruits, all 40 samples had inhibitory activity at a concentration of 250 µg ml^{-1}, while 36 samples had greater than 50% inhibition at a concentration of 250 µg ml^{-1}, 25 samples had greater than 50% inhibition at a concentration of 100 µg ml^{-1}, and 17 samples had greater than 50% inhibition at a concentration of 50 µg ml^{-1}. At lower concentrations, 7 samples had greater than 50% inhibition at a concentration of 25 µg ml^{-1}, 5 samples had greater than 50% inhibition at a concentration of 10 µg ml^{-1}, and 1 sample had greater than 50% inhibition at a concentration of 1 µg ml^{-1}. Of the 40 samples, the 5 with the most robust inhibition activity of the α-glucosidase enzyme should be further

tested at lower concentrations, as the IC_{50} values of the 5 samples were 0.15, 2.54, 4.05, 5.17, and 8.68 µg ml^{-1}, respectively, which is much stronger than the positive control (IC_{50} value of acarbose was 214.5 µg ml^{-1}).

Areca catechu (areca nut, Fig. 1) is very popular in South Asia and the seed of these trees has been employed as traditional medicine. A lot of compounds have been identified from *Areca catechu* such as steroids, tannins, flavones, alkaloids, fatty acids, and triterpenes, which could be notable pharmacological activities [3].

Fig. 1. *Areca catechu.*

Cassia grandis (Fig. 2) has been found in the Mekong Delta for a long time. According to the dictionary of medicinal plants [4, 5] and accessible experience in Vietnam, *Cassia grandis* has a variety of medicinal uses. Its fresh leaves cure dermatophytosis, its green fruit cures dysentery, and its ripe fruit cures bone aches and pains. Meanwhile, chemical investigations of this plant are still limited. Besides traditional uses of the plant as in Vietnam, and particularly in South America where it is said to be the origin of *Cassia grandis*, its ripe fruits are a good remedy for people suffering from anaemia. Recent biological studies showed that this plant possesses several biological activities such as antimicrobial effects on saltwater shrimp, anti-diabetic, antioxidant, anti-inflammatory, analgesic, and hepatoprotective activity, etc. Preliminary chemical screening tests showed the presence of almost 9 large groups of natural compounds: flavonoid, anthracoid, alkaloid, steroid, terpenoid, glycoside, tannin, saponin, and coumarin [6].

Fig. 2. *Cassia grandis*.

Syzygium cumini (jambolan, Fig. 3) is one of the most commonly used anti-diabetic medicines. A lot of research shows that this plant contains anthocyanin, glucoside, ellagic acid, isoquercetin, kaemferol, and myricetin. Muniappan Ayyanar and Pandurangan Subash-Babu (2012) [7] found that alcaloid, jambosine, and glycoside jambolin or antimellin in *Syzygium cumini's* seed is a natural medicine.

Fig. 3. *Syzygium cumini*.

Glycine max (soybean, Fig. 4) is a globally grown legume, including Vietnam. Ghahari, et al. [8] studied the chemical composition of soybean oil and showed its antioxidant and antibacterial effects on various agriculturally harmful pathogens. By gas chromatography combined with mass spectrometry, the authors identified 40 components in soybean oil, accounting for 96.68% of the total amount of oil. In particular, the main components were carvacrol (13.44%), (E, E)-2.4-decadienal (9.15%), *p*-allylanisole (5.65%), *p*-cymene (4.87%), and limonene (4.75%). By disk diffusion and minimum inhibitory concentration techniques, the antibacterial activity of soybean oil was determined. In addition, the antioxidant activity of soybean oil was assessed by catalase, peroxidase, superoxide effuse and 2,2-diphenyl-1-picrylhydrazyl (DPPH) assays. The oil showed significant activity against *Pseudomonas syringae* subsp. syringae, *Rathayibacter toxicus* with MIC = 25 µg ml^{-1}, and *Pyricularia oryzae* with MIC = 12.5 µg ml^{-1}. In addition, the free radical scavenging capacity of the essential oil was determined with an IC_{50} value of 162.35 µg ml^{-1}. The results suggest that this plant may be a potential

source of biocide, thus beneficial for economical and environmentally friendly disease control strategies. It may also be a good candidate for further biological and pharmacological investigations [8].

Fig. 4. ***Glycine max*.**

Enhydra fluctuans (Fig. 5), a natural vegetable, is used in Vietnamese meals. The *Enhydra fluctuans* belongs to the Asteraceae family and is gaining interest because of some of its amazing benefits to human health. According to folk medicine, its leaves have a slightly bitter taste, cure inflammation and skin diseases, can be used as a laxative, and to treat bronchitis, nervous affections, leucoderma, and biliousness. Some extracted compounds such as β-carotene, saponins, cholesterol, glucoside, and boostydrin are the main components in these plants. This vegetable has some great uses such as an antioxidant, for liver protection, central nervous system inhibition, and pain relief. The amazing pharmacological effects of this vegetable help scientists open up research pathways into herbs that can treat diseases without causing unwanted side effects that are caused by some synthetic drugs in use today [9].

Fig. 5. ***Enhydra fluctuans*.**

4. Conclusions

Results of the screening of the inhibitory activity of the α-glucosidase enzyme from the 40 samples of vegetables, tubers, and fruits showed that 1 sample had an IC_{50} value <1 µg ml^{-1}, 4 samples had IC_{50} values <10 µg ml^{-1}, 20 samples had IC_{50} values from 100 to 10 µg ml^{-1}, 10 samples had IC_{50} values from 250 to 100 µg ml^{-1}, and 5 samples had IC_{50} values >250 µg ml^{-1}. The positive control in this study was acarbose and 35 of the 40 samples had an α-glucosidase enzyme inhibitory activity stronger than the positive control, especially the seeds of *Areca catechu*, the fruits of *Cassia grandis*, the fruits of *Syzygium cumini*, the seeds of *Glycine max,* and the stems of *Enydra fluctuans*. These research results create a basis for the study of isolated substances originating from strong active samples and contribute to the investigation of diabetes treatments derived from herbs, which can have reduced side effects compared with synthesized active substances.

CRedit author statements

Thi-My-Linh Lam, Minh-Tuan Le, Manh-Ha Bui: Conceptualisation, Methodology, Data curation, Formal analysis, Conceptualisation, Methodology, Writing - Original draft preparation, Writing - Review & Editing.

COMPETING INTERESTS

The authors declare that there is no conflict of interest regarding the publication of this article.

REFERENCES

[1] T.K. Nguyen, T.T.B. Diep, T.B.T. Dang, et al. (2006), *Endocrinology*, Ho Chi Minh city University of Medicine and Pharmacy, Medicine Publisher.

[2] H.T. Nguyen, S.M. Kim (2009), "Three compounds with potent *a*-glucosidase inhibitory activity purified from sea cucumber *Stichopus japonicus*", *Symposium Food Consumer Insights in Asia: Current Issues and Future*, pp.112-122.

[3] W. Peng, Y.J. Liu, N. Wu, et al. (2015), "*Areca catechu* L. (*Arecaceae*): A review of its traditional uses, botany, phytochemistry, pharmacology and toxicology", *J. Ethnopharmacol.*, **164**, pp.340-356, DOI: 10.1016/j.jep.2015.02.010.

[4] H.H. Pham (2003), *Vietnamese Plants*, **Vols**. **I-II-III**, Young Publishers (in Vietnamese).

[5] H.B. Do (2006), *Medicinal Plants and Medicinal Animals in Vietnam*, **Vols**. **1-2-3**, Scientific and Technical Publishing House (in Vietnamese).

[6] Q.L. Ngo (2017), *Chemical Investigation of Cassia Grandis L.F (fabaceae) in Mekong Delta*, Dissertation in Natural Products Chemistry, University of Science and Technology.

[7] M. Ayyanar, P. Subash-Babu (2012), "*Syzygium cumini* (L.) Skeels: A review of its phytochemical constituents and traditional uses", *Asian Pac. J. Trop. Biomed.*, **2(3)**, pp.240-246, DOI: 10.1016/S2221-1691(12)60050-1.

[8] S. Ghahari, H. Alinezhad, G.A. Nematzadeh, et al. (2017), "Chemical composition, antioxidant and biological activities of the essential oil and extract of the seeds of *Glycine max* (Soybean) from North Iran", *Curr. Microbiol.*, **74(4)**, pp.522-531, DOI: 10.1007/s00284-016-1188-4.

[9] R. Ali, M. Billah, M. Hassan, et al. (2013), "*Enhydra fluctuans* Lour: A review", *Research J. Pharm. and Tech.*, **6(9)**, pp.927-929.

DOI: 10.31276/VJSTE.63(4).47-54

In silico screening of drug inhibitors of SARS-CoV-2 RNA-dependent RNA polymerase target

Thanh Tung Bui[1*], Bao Kim Nguyen[1], Minh Ngoc Le[1], The Toan Nguyen[2], The Hai Pham[3]

[1]University of Medicine and Pharmacy, Vietnam National University - Hanoi,
144 Xuan Thuy Street, Dich Vong Hau Ward, Cau Giay District, Hanoi, Vietnam
[2]Key Laboratory for Multiscale Simulation of Complex Systems, University of Science, Vietnam National University - Hanoi,
334 Nguyen Trai Street, Thanh Xuan Trung Ward, Thanh Xuan District, Hanoi, Vietnam
[3]Hanoi University of Pharmacy,
13-15 Le Thanh Tong Street, Phan Chu Trinh Ward, Hoan Kiem District, Hanoi, Vietnam

Received 22 December 2020; revised 28 February 2021; accepted 12 March 2021

Abstract:

Objectives: The COVID-19 pandemic triggering acute respiratory syndrome has become a major global health concern. After one year into this pandemic, special therapies for COVID-19 remain an unprecedented challenge to mankind and finding drugs to treat this disease is extremely urgent. The SARS-CoV-2 RNA-dependent RNA polymerase (RdRp) enzyme that regulates viral replication has been examined as a potential therapeutic target for the inhibition of SARS-CoV-2 infection. In this study, the authors evaluated the ability of RNA-dependent RNA polymerase drug inhibitors by using an *in silico* molecular docking model. Methods: the 3D structure of RdRp enzyme (PDB ID:6M71, resolution of 2.90 Å) was derived from the Protein Data Bank RCSB. The ligand structures were collected from DrugBank for the RdRp target. Molecular docking was done by AutoDock Vina software. Lipinski's rule of five is used to compare compounds with drug-like and non-drug-like properties. Pharmacokinetic parameters of potential compounds were evaluated using the pkCSM tool. Results: based on the DrugBank database, we collected 192 antiviral molecules and compared them to remdesivir, which has inhibitory activity with this protein target. Results showed that 26 out of 192 compounds have a higher ability to inhibit the SARS-CoV-2 RdRp enzyme than remdesivir. Next, 6 drugs were selected by visually inspecting the docking results with focus on the main interaction between crucial residues at the binding site of the SARS-CoV-2 RdRp enzyme. For the visual inspection, the existence of polar interactions with ASP760 and ASP761 were utilised as the preference criterion. Finally, Lipinski's rule of 5 criteria and absorption, distribution, metabolism, excretion and toxicity (ADMET) profile analysis suggested five drugs that have good pharmacokinetic properties. Conclusions: these drugs were dihydroergotamine, sofosbuvir, nilotinib, tipranavir, and darunavir and may be used as anti-SARS-CoV-2 agents.

Keywords: ***in silico*****, molecular docking, remdesivir, RNA-dependent RNA polymerase (RdRp), SARS-CoV-2.**

Classification number: **3.3**

1. Introduction

Since COVID-19 acute respiratory syndrome was first discovered in Wuhan city, Hubei province, China, the scientific community, as well as the entire human race, has come face-to-face with an unprecedented challenge to find treatments for this disease. As of October 28th, 2020, there have been 43,540,739 reported cases and 1,16,650 deaths globally (WHO 2020) as the virus continues to rapidly spread [1]. In Vietnam, 1,094 cases and 35 deaths have been reported. One of the biggest concerns of this disease is that its symptoms are often very diverse and manifest differently in each patient. Clinical symptoms are usually noticed 5-to-6 days after infection but the incubation period can be up to 14 days [2]. Fever, coughing, and fatigue are among the most common symptoms. There have been patients with no reported symptoms but suddenly deteriorate rapidly with severe hypoxia that can lead to other diseases and even death [3, 4].

SARS-CoV-2 has a 29.9 kb-size positive-sense RNA genome. It is composed of 14 open reading frames (ORFs), which encode a total of 27 proteins that are further divided into structural and non-structural proteins

Corresponding author: Email: tungasia82@gmail.com

(NSPs) [5]. RNA-dependent RNA polymerase (RdRp) is an important enzyme to the viral RNA life cycle as it is involved in the transcription and translation of the SARS-CoV-2 genome. This enzyme is the cleavage product of polyproteins 1a and 1ab from ORF1a and ORF1ab [6]. Therefore, RdRp is considered to be a major target for antiviral inhibitors.

Molecular docking is a modelling technique that predicts the position and favourable configuration of a substrate molecule (ligand) binding to a protein molecule (target). This *in silico* method saves significant time and cost in the screening of compounds compared with experimental methods.

The rapid spread of COVID-19 has emphasised the need for the global development of coronavirus vaccines and therapies. Therefore, we investigated potential drugs to inhibit RNA-dependent RNA polymerase (RdRp) for COVID-19 treatment. Our research focused on antiviral compounds that were collected from DrugBank with keyword "antiviral". DrugBank is a pharmaceutical knowledge base that has enabled significant advancements in the field of data-driven medicine [7]. Remdesivir is an antiviral drug that has been approved by the Food and Drug Administration (FDA) for the treatment of COVID-19 requiring hospitalisation [8]. Thus, to evaluate the ability of these compounds to inhibit SARS-CoV-2 RdRp, remdesivir was used as a positive control.

2. Materials and methods

2.1. Structure-based virtual screening (SBVS)

Virtual screening is presently a worthy solution to the discovery of new hits. The database of 192 antiviral chemical compounds, available from DrugBank, was chosen for SBVS studies. From this subset, molecular docking using AutoDock Vina was used to select the compounds based on binding energies lower than that of remdesivir. Next, the compounds were selected by visually inspecting the docking results with focus on the main interaction between crucial residues at the binding site of the SARS-CoV-2 RdRp enzymes. For the visual inspection, the existence of polar interactions with ASP760 and ASP761 were utilised as the preference criterion. Finally, the authors performed Lipinski's rule of five and the prediction of ADMET for hit compounds.

2.2. Protein receptors preparation

The 3D structure of the RNA-dependent RNA polymerase (RdRp) enzyme (PDB ID: 6M71, resolution of 2.90 Å) was derived from the Protein Data Bank RCSB [9]. All water molecules and co-crystal were removed from the protein molecule using Discovery Studio Visualizer 4.0 software. After that, hydrogen atoms will be added to the protein before regenerating the active site using MGL AutoDock tools 1.5.6 software. Furthermore, the MOE SiteFinder algorithm was used to classify the RdRp binding pocket. The grid center for 6M71 was set as X=121, Y=120, and Z=125 (Angstrom), length 30 Å X 30 Å X 30 Å with the distance between grid cells is 1 Å [10]. The protein is then saved in PDBQT format to prepare for the docking program.

2.3. Ligands preparation

The ligand structures were collected from DrugBank for the RNA-dependent RNA polymerase enzyme (RdRp) target involved 192 antiviral compounds. The structures were downloaded from DrugBank in the simplified molecular-input line-entry system (SMILES) format and then converted into 3D structures in PDB format using MOE software [7]. After that, the ligands were optimised by Avogadro software using Conjugate Gradients and converted to PDBQT format using AutoDock tools software.

2.4. Performance of molecular docking

These collected compounds were docked into the active site using AutoDock Vina software. The ligand-protein interaction energy is calculated by the scoring function of AutoDock Vina.

2.5. Lipinski's rule of five

Lipinski's rule of five is used to compare drug-like and non-drug-like molecules [11]. It is widely employed to evaluate a potential molecule for use as a therapeutical drug. This rule acts as a filter that screens promising compounds with particular pharmacological characteristics. In this work, we used an online tool to evaluate Lipinski's rule of five [12]. The chemical structures were downloaded from the PubChem database and set at pH 7.0 [13].

2.6. Prediction of ADMET by computational analysis

In order to analyse the physiochemical efficiency of the five above-mentioned drugs to inhibit the target protein, we used *in silico* ADMET profiling. An ADMET profile involves five parameters: absorption, distribution, metabolism, excretion, and toxicity, which all play a significant role to demonstrate the likelihood of success of a drug. Drug absorption depends on factors including

membrane permeability, intestinal absorption, levels of skin permeability, and as a substrate or inhibitor of the P-glycoprotein. Drug distribution relies on factors like the blood-brain barrier (logBB), central nervous system (CNS) permeability, and volume of distribution (VDss). Based on the cytochrome (CYP) models for substrate or inhibition (CYP2D6, CYP3A4, CYP1A2, CYP2C19, CYP2C9, CYP2D6, and CYP3A4), metabolism is expected. Based on the total clearance model and the renal OCT2 substrate, excretion is expected. Based on salmonella typhimurium reverse mutation assay (AMES) toxicity, human ether-a-go-go-related gene (hERG) inhibition, hepatotoxicity, and skin sensitisation, the toxicity of drugs is expected. These criteria have been determined and their standard ranges have been tested for compliance. ADMET profiling was predicted using the pkCSM tool [14]. The canonical SMILES molecular structures of collected compounds were retrieved from the DrugBank database [7].

3. Results

3.1. Binding pocket

Using the MOE SiteFinder to find the RdRp binding pocket, we found these essential acid amines: ASP760, ASP761, ASP623, ASP452, TYR455, TYR456, ARG553, PRO620, ARG624, GLU811, TYR619, PRO620, LYS621, CYS622, ASP623, SER681, LYS798, GLU811, and SER814 were all involved at the active site. Fig. 1 illustrates the active site or binding pocket of RdRp in the yellow box.

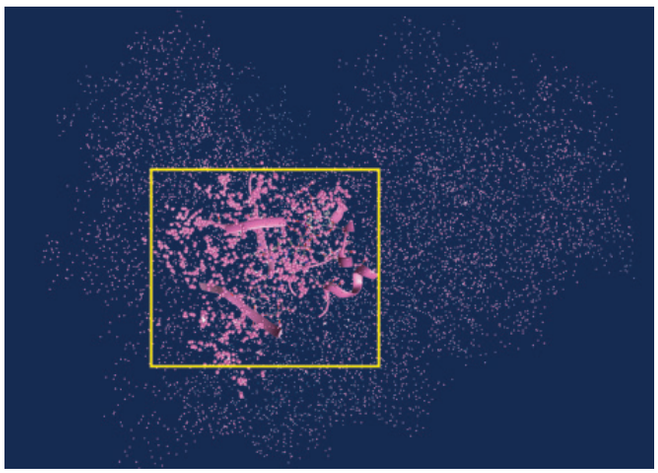

Fig. 1. The binding pocket of SARS-CoV-2 RdRp.

3.2. Binding energy

Figure 2 presents the SBVS workflow employed to find hits as SARS-CoV-2 RdRp enzyme inhibitors.

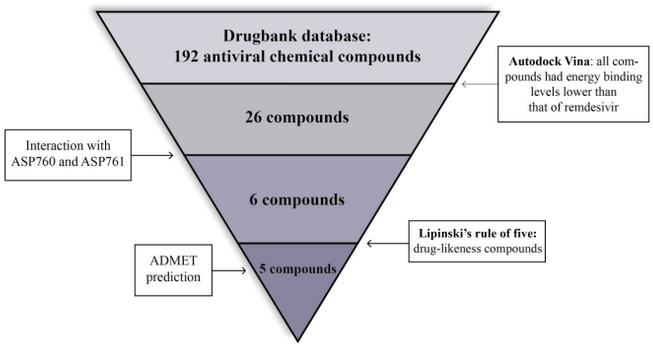

Fig. 2. The structure-based virtual screening workflow.

After preparing the ligands, we docked the 192 antiviral drugs retrieved with RNA-dependent RNA polymerase enzyme to screen target inhibitory activity.

Remdesivir is an antiviral drug that has been approved by the FDA for the treatment of COVID-19 requiring hospitalisation [8]. As an RNA polymerase (RdRp) inhibitor, it can inhibit coronavirus replication in respiratory epithelial cells [15]. Therefore, in this study, we compared the docking scores of the ligands with remdesivir to evaluate the compounds' abilities to inhibit RNA-dependent RNA polymerase enzyme. A.A. Elfiky (2020a) [16] also reported that remdesivir has a binding energy with the SARS-CoV-2 RdRp target of -7.6 kcal/mol. Fig. 3 shows the interaction between remdesivir and the RdRp enzyme.

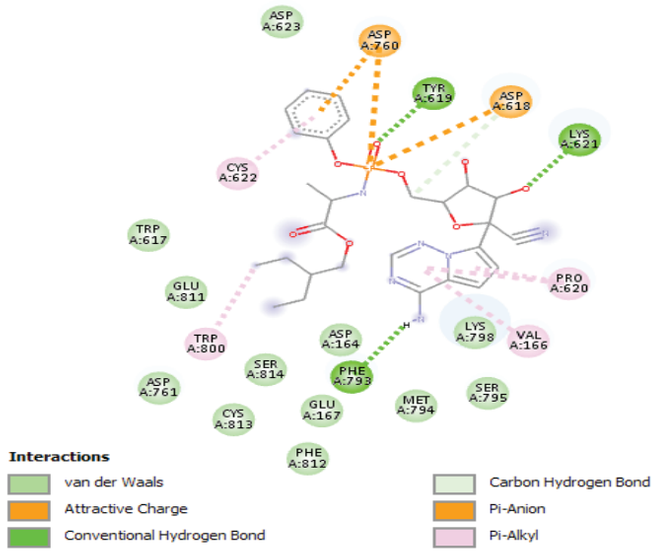

Fig. 3. Interaction between remdesivir and RdRp enzyme.

From the results of docking 192 drugs, we obtained 26 drugs with lower binding energy levels than remdesivir (-7.6 kcal/mol). Ligand-amino acid interactions of these 26 compounds are shown in Table 1.

Table 1. Ligand-amino acid interactions of 26 scoring antiviral drugs against the RdRp enzyme.

No	Name	Binding energy (kcal/mol)	Involved amino acids
1	Dihydroergotamine	-9.4	ASP760, ASP761, LYS621, ARG553, GLU811, LYS798, LYS551
2	Sofosbuvir	-9.4	ASP760, ASP761, ASO618, TYR619, CYS622, GLU811, TRP800, SER814, CYS813
3	Nilotinib	-8.8	ASP760, ASP761, LYS621, ARG553, ARG624, TYR455, TYR619, ASP623, SER814, PRO620
4	Inarigivir	-8.6	ASP760, ASP761, ARG553, ASP623, ALA554, ASP452, ARG624, SER814, CYS813, GLU811, TRP800
5	Tipranavir	-8.2	ASP760, ASP761, LYS621, ARG553, ARG624, ASP618, ASP452, TYR455, PRO620, GLU811, CYS622
6	Darunavir	-7.7	ASP760, ASP761, LYS621, ARG553, CYS622, TYR455, ARG624, ASP623, TYR619
7	Golvatinib	-9.3	ASP623 ARG624, LYS621, ARG553, THR680, TYR456, SER681, SER682
8	Beclabuvir	-9	ARG553, LYS621, CYS622, ASP164, ASN552
9	Nafamostat	-8.7	LYS621, VAL166, LYS798, TRP800, TRP617, GLY811
10	Bictegravir	-8.6	ARG624, ASP623, LYS621, ARG553, CYS 622, TYR619
11	Baloxavir marboxil	-8.2	ASP623, ASN691, CYS622, ASP760, ARG553,LYS621
12	Avatrombopag	-8.2	PRO620, VAL166, LYS521, TYR455, ARG553, ARG555, ARG836
13	Adarotene	-8.1	VAL166, PRO620, LYS621, ARG624
14	Delavirdine	-8	THR556, ARG553, LYS621, TYR619
15	Dolutegravir	-8	TYR619, ASP760, CYS622, LYS621, ARG553, ARG624, ASP623
16	Aplaviroc	-8	ARG553, LYS621, TYR455, GLU811, TRP617
17	Deferasirox	-8	ASP618, TYR619, CYS622, PRO620, LYS621, ARG553
18	Raltegravir	-7.9	ASN691, ALA688, THR556, ARG553, LYS621, TYR455, ASP623
19	Doravirine	-7.9	ARG553, ARG624, ASP623, TYR619, CYS622, ASN691, ASP760
20	Pritelivir	-7.9	LYS798, PRO620, LYS621, ASP623, ARG553, TYR455
21	Elsulfavirine	-7.9	ARG553, CYS622, ASP164, ASN552, THR556, ARG553, LYS621, TYR619
22	PF-232798	-7.9	ARG624, ASP623, LYS621, ASP761
23	Pranlukast	-7.8	ASP623, ARG555, ARG553, ARG624, ASP452, TYR455, LYS621
24	BMS-488043	-7.8	ASP623, CYS622, ASP761, GLU811, TRP617, TRP800, ALA762
25	Nelfinavir	-7.7	ARG553, TYR619, LYS621, PRO620, VAL166, SER795, PHE793
26	Benperidol	-7.7	VAL166, LYS798, PRO620, SER795, PHE793, LYS621, ARG553, ARG624

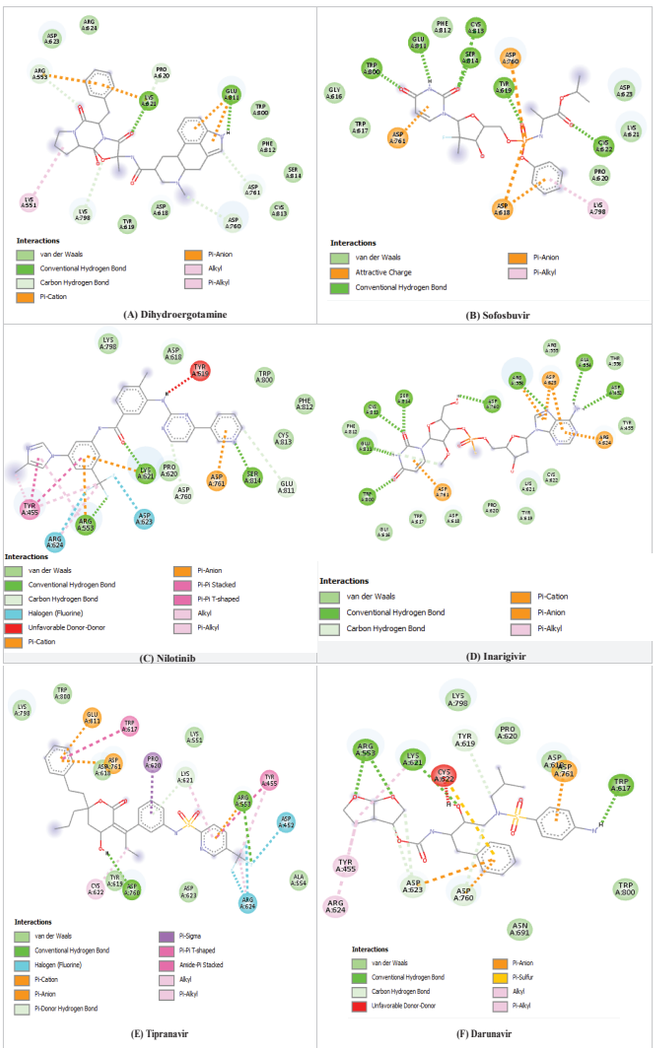

Fig. 4. Interactions between dihydroergotamine, sofosbuvir, nilotinib, inarigivir, tipranavir, and darunavir with the RdRp enzyme (A-F).

ASP760 and ASP761, two aspartate residues, are the main catalytic residues of RdRp [17, 18]. These two residues are exceptionally conserved in all coronaviruses. As a selection criterion, the presence of polar interactions with ASP760 and ASP761 was used. Six compounds were selected based on the main interaction between these essential residues at the binding site of SARS-CoV-2 RdRp enzyme. Fig. 4 shows the interaction between dihydroergotamine, sofosbuvir, nilotinib, inarigivir, tipranavir, darunavir, and the RdRp enzyme target.

3.3. Lipinski's rule of five

Lipinski's rule of five is used to distinguish between drug-like and non-drug-like molecules. It predicts high probabilities of drug-like effectiveness or failure for molecules complying with 2 or more of the following

rules: molecular mass (MW) below 500 Dalton; high lipophilicity (expressed as logP below 5); less than 5 donors of hydrogen bonds (HBD); less than 10 acceptors of hydrogen bonds (HBA1); and a molar refractivity (MR) between 40-130.

Table 2. The result of Lipinski's rule of five.

No	Drugs	Molecular weight	HBD	HBA1	logP	MR	Drug-likeness
1	Dihydroergotamine	583.0	3	9	1.498670	155.963348	Yes
2	Sofosbuvir	529.0	3.0	12.0	1.999300	123.152649	Yes
3	Nilotinib	529.0	2	7	6.356432	140.482941	Yes
4	Inarigivir	587.0	6	16	-0.876200	132.885513	No
5	Tipranavir	602	2.0	7.0	8.406303	152.331619	Yes
6	Darunavir	547.0	4	10	3.456099	141.639954	Yes

Among the 6 potential drugs, 5 of them satisfied more than 2 criteria, which we then suggest are potential candidates. These candidates are sofosbuvir, dihydroergotamine, nilotinib, tipranavir, and darunavir (Table 2). Then, we focus on analysing the pharmacokinetic properties including absorption, distribution, metabolism, excretion, and toxicity of these drugs.

3.4. Prediction of absorption, distribution, metabolism, excretion and toxicity (ADMET) profile

The prediction of absorption, distribution, metabolism, excretion, and toxicity profile of five selected drugs are shown in Table 3.

4. Discussion

4.1. Structure-based virtual screening and molecular docking

Comparing the interactions of the 5 drugs with remdesivir, we can see that their bonds to the RdRp enzyme have similarities with remdesivir. This is demonstrated by their association with several important amino acids such as LYS621, ASP761, ARG553, and especially the π-anion bond with ASP760. In addition, these drugs also bind to many other amino acids such as TYR619, PRO620, ASP618, CYS622, etc. In recent studies, they demonstrated the same residues to bind strongly within the active sites of RdRp [17, 19].

Analysing the binding energy and interaction of the ligand-amino acid, we found that all five drugs had COVID-19 therapeutic potential. Dihydroergotamine and sofosbuvir, which had the lowest binding energy to SARS-CoV-2 RdRp (-9.4 kcal/mol), was docked into the active site of the enzyme in a similar manner to remdesivir. Dihydroergotamine was observed to interact via carbon hydrogen bonds to ASP760 and ASP761 along with π-anion electrostatic bonds to GLU811 and LYS621. On the other hand, sofosbuvir could bind to the

Table 3. The result of ADMET profile.

Properties	Dihydro-ergotamine	Sofosbuvir	Nilotinib	Tipranavir	Darunavir
Absorption					
Water solubility (log mol/l)	-2.941	0.953	-2.899	-5.181	-3.358
Caco-2 permeability (log Papp in 10^{-6} cm/s)	0.271	0.472	1.385	0.664	0.493
Intestinal absorption (human) (% absorbed)	64.091	64.308	99.538	98.275	75.477
Skin permeability (log Kp)	-2.735	-2.736	-2.735	-2.735	-2.739
P-glycoprotein substrate	Yes	Yes	Yes	Yes	Yes
P-glycoprotein I inhibitor	Yes	Yes	Yes	Yes	Yes
P-glycoprotein II inhibitor	Yes	No	Yes	Yes	No
Distribution					
VDss (human) (log l/kg)	1.301	-0.728	-0.547	-0.04	0.602
Fraction unbound (human) (Fu)	0.301	0.08	0.243	0	0.055
BBB permeability	-0.532	-1.873	-0.684	-1.368	-1.111
CNS permeability (log PS)	-2.693	-4.343	-2.052	-3.063	-3.519
Metabolism					
CYP2D6 substrate	No	No	No	No	No
CYP3A4 substrate	Yes	No	Yes	Yes	Yes
CYP1A2 inhibitor	No	No	No	No	No
CYP2C19 inhibitor	No	No	Yes	Yes	No
CYP2C9 inhibitor	Yes	No	Yes	Yes	No
CYP2D6 inhibitor	No	No	No	No	No
CYP3A4 inhibitor	Yes	No	Yes	Yes	Yes
Excretion					
Total clearance (log ml/min/kg)	0.67	-0.106	0.406	0.131	0.622
Renal OCT2 substrate (human)	No	No	Yes	No	No
Toxicity					
AMES toxicity	No	No	No	No	No
Max. tolerated dose (human) (log mg/kg/day)	0.135	1.049	0.199	-0.354	-0.763
HERG I inhibitor	No	No	No	No	No
HERG II inhibitor	Yes	No	Yes	Yes	No
Oral rat acute toxicity (LD_{50}) (mol/kg)	2.714	2.31	2.489	2.367	2.107
Oral rat chronic toxicity (LOAEL) (log mg/kg bw/day)	3.131	1.824	0.923	2.326	2.775
Hepatotoxicity	Yes	Yes	Yes	Yes	Yes
Skin sensitisation	No	No	No	No	No
T. Pyriformis toxicity (log ug/l)	0.285	0.283	0.285	0.286	0.289
Minnow toxicity (log mM)	1.74	1.023	1.301	-2.023	0.61

interface active pocket of the SARS□CoV-2 by conventional hydrogen bonding through TYR619, CYS622, and GLU811 as well as π-anion bonds through ASP760, ASP761, and ARG553. Nilotinib also interacted with SARS-CoV-2 RdRp by a conserved binding pattern. It was found that this compound had interacted with carbon hydrogen bonds to ASP760 and GLU811 along with π-anion bonds to ASP761, LYS621, and ARG553. Tipranavir and Darunavir had high binding energies to the viral RdRp through some of the same amino acids such as hydrogen bonds with ARG553, π-anion electrostatic bond with ASP761, and other interactions with ASP760, LYS621, and CYS622. For Tipranavir, hydrogen and π-anion bonds with ASP760 and ASP761, respectively, were observed with a docking score of -8.2 kcal/mol. The binding energy and the interaction of the ligand-amino acid between Darunavir and SARS-CoV-2 exhibited an inhibitory ability against COVID-19 of Darunavir. Both Tipranavir and Darunavir exhibited two π-anion interactions with ASP760 and ASP761 with docking score of -7.7 kcal/mol.

Our docking findings revealed that dihydroergotamine (DHE) is a semi-synthetic ergot alkaloid that exhibits high affinities against RdRp with docking binding energies of -9.4 kcal/mol, which is similar to the research result of S. Gul, et al. (2020) [20]. Previous studies using *in silico* models have also shown the SAR-CoV-2 inhibitory potential of DHE due to interactions within the binding pocket through a good number of hydrogen bonds and hydrophobic interactions [20, 21]. In the research of A. Gupta, et al. (2020) [22] using molecular mechanics Poisson-Boltzmann surface area (MM/PBSA), DHE had the lowest binding free energy of -17.9 kcal/mol among the final set of surveyed drugs. Thus, it is suggested that a strong interaction between SARS-CoV-2 and DHE exists. Sofosbuvir is a virus inhibitor of great interest among direct-acting antivirals currently in development [23]. Sofosbuvir was also shown to have an ability to bind to the SARS□CoV□2 RNA□dependent RNA polymerase and inhibit enzyme activity [24]. Previous studies reported that sofosbuvir may be a possible candidate in the treatment of COVID-19 based on the similarity of HCV and coronavirus replication systems [25-28]. Nilotinib is another potential compound that showed strong binding energy towards SAR-CoV-2 RdRp. A recent study by Z. Ruan, et al. (2020) [24] showed the binding energy between nilotinib and the active site of the SARS-CoV-2 RdRp enzyme to be -8.4 kcal/mol, which is similar to our result of -8.8 kcal/mol. Noticeably, nilotinib should be able to inhibit SARS□CoV□2 replication in *in vitro*, both in Vero□E6 and in Calu□3 cells, with a half maximal effective concentration (EC_{50}) evaluated at 1.44 and 3.06 μM, respectively [29]. Also, some recent publications demonstrated that Tipranavir could serve as a potential COVID-19 medicinal product, with additional validation studies, because of interactions with the main protease and RNA-dependent RNA polymerase of SARS-CoV-2 [30, 31]. Finally, darunavir exhibited inhibitory ability against COVID-19 in our research. This drug has been carried out in many studies and shows signs of improvement in COVID-19 treatment [32-34].

All five drugs mentioned have been approved by the FDA for antiviral treatment. Due to the COVID-19 pandemic, the option of these FDA-approved drugs is a wise decision in this current emergency because they have already been tested prior to FDA approval.

Each of the five drugs have been shown to treat many diseases as well as inhibit viruses. Dihydroergotamine is a semi-synthetic ergot alkaloid that has been widely used in the treatment of migraines [35]. Sofosbuvir is a hepatitis C virus inhibitor of great interest among direct-acting antivirals currently in development [23]. Nilotinib is a tyrosine kinase inhibitor used to treat chronic myelogenous leukemia [36]. Tipranavir is a new protease inhibitor that, by blocking HIV-1 and HIV-2 proteases, is highly selective for therapeutic intervention in the viral life cycle [37, 38]. As darunavir's high genetic barrier and potency, it is a protease inhibitor for the successful treatment of HIV-1 infection in both naive and experienced subjects [39, 40]. Thus, these medications propose their reuse for new health complications. The benefits associated with repurposed drugs include safety for human use, no escalating cost, and a reduced timeline for its development [41].

4.2. ADMET prediction

The absorption of drugs is predicted based on membrane permeability, intestinal absorption, skin permeability levels, and P-glycoprotein substrate or inhibitor. When the Papp coefficient is $>8\times10^{-6}$, the predicted value is >0.90. Hence, the compound has high Caco-2 permeability and is simple to absorb [42]. Nilotinib was predicted to have high Caco-2 permeability. The intestinal absorption (human) percentage of all mentioned compounds is comparatively high: sofosbuvir (67.308%), dihydroergotamine (64.091%), nilotinib (99.538%), tipranavir (98.275%), and darunavir (75.477%). Concerning skin permeability, a compound with log Kp>-2.5 is understood as having very poor skin permeability [42]. However, none of the drugs were considered to have low skin permeability. P-glycoprotein is a member of the superfamily of ABC transporters that can excrete drugs or other exogenous chemicals from cells. The results suggest that sofosbuvir, dihydroergotamine, and nilotinib may be actively exuded from cells by P-glycoprotein. Dihydroergotamine, tipranavir, and nilotinib were predicted to be a P-glycoprotein inhibitor.

The distribution of medication depends on factors that consist of the blood-brain barrier (logBB), CNS permeability, and the volume of distribution (VDss). The distribution extent is a parameter to signify the distribution of medication

in numerous tissues *in vivo*. VDss is considered low if it is below 0.71 l/kg (log VDss<-0.15) and high if it is above 2.81 l/kg (log VDss>0.45) [43]. The results confirmed that the distribution volume of dihydroergotamine and darunavir were high whereas the VDss of sofosbuvir and nilotinib were -0.728 and -0.547, respectively, and lower than -0.15. For a given drug, a log BB <-1 is considered to poorly cross the blood-brain barrier [43]. Sofosbuvir, tipranavir, and darunavir were predicted to have difficulty crossing the blood-brain barrier. For CNS permeability, sofosbuvir, tipranavir, and darunavir were predicted to be unable to penetrate the central nervous system (CNS) (logPS is <-3) while dihydroergotamine and nilotinib may penetrate the CNS.

Metabolism is anticipated based on the CYP fashions for substrate or inhibition (CYP2D6, CYP3A4, CYP1A2, CYP2C19, CYP2C9, CYP2D6, and CYP3A4). A significant detoxification enzyme in the body, primarily found in the liver, is cytochrome P450. The two main isoforms of cytochrome P450 that are responsible for drug metabolism are CYP2D6 and CYP3A4 [44]. The results confirm that sofosbuvir is not a substrate for the two subtypes. However, all four remaining compounds were substrates for CYP3A4. This suggests that nilotinib, dihydroergotamine, darunavir, and tipranavir may be metabolised in the liver. The prediction demonstrates that the total clearance of dihydroergotamine is the best observed by means sofosbuvir, tipranavir, nilotinib, and darunavir.

The toxicity profile of these compounds were also analysed. The toxicities of these drugs are expected based on their AMES toxicities, hERG inhibition, hepatotoxicities, and skin sensitization. Almost all of these compounds were observed to inhibit the human ether-a-go-go-related gene II (hERG II) except for sofosbuvir and darunavir. The toxicity prediction from the AMES test (*Salmonella typhimurium* reverse mutation assay) indicated that all the compounds could be considered as non-mutagenic agents. High toxicities were shown for all the compounds in *Tetrahymena pyriformis*. All the compounds may not affect skin sensitisation.

Although these above-mentioned drugs were approved by the FDA, we used ADMET prediction to re-evaluate their structural alerts of toxicity. Nilotinib, tipranavir, and dihydroergotamine were observed to be hERG II inhibitors, which is the principal cause for the development of acquired long QT syndrome leading to fatal ventricular arrhythmia. All five drugs are the substrates of P-glycoprotein, which are easily transported in the body but may have hepatotoxicity.

5. Conclusions

Our research is to screen existing approved drugs by the FDA and suggest their reuse for new medical complications. This current research screened 192 antiviral drugs from the DrugBank database for inhibition of the SARS-CoV-2 virus. We showed that five FDA-approved drugs found after virtual screening showed stable interaction with key residues of the RdRp enzyme including dihydroergotamine, sofosbuvir, nilotinib, tipranavir, and darunavir, which inhibited viral proliferation. ADMET predictions demonstrated some structural alerts of toxicity in these drugs. In conclusion, based on our findings, we suggest that these five promising drugs should be further studied *in vitro*, *in vivo,* and in clinical trials to combat this widespread infection.

CRedit author statements

Thanh Tung Bui: Conceptualisation, Methodology, Writing - Original draft preparation, Writing - Review & Editing; Bao Kim Nguyen, Minh Ngoc Le, The Toan Nguyen, The Hai Pham: Conceptualization, Methodology, Data curation, Formal analysis, Writing - Review & Editing.

COMPETING INTERESTS

The authors declare that there is no conflict of interest regarding the publication of this article.

REFERENCES

[1] Ministry of Health (2020), *Information on Acute Respiratory Infections COVID-19*, https://ncov.moh.gov.vn (in Vietnamese), accessed 22 December 2020.

[2] N. Chams, S. Chams, R. Badran, et al. (2020), "COVID-19: A multidisciplinary review", *Frontiers in Public Health*, **8**, DOI: 10.3389/fpubh.2020.00383.

[3] M. Cevik, C.G.G. Bamford, A. Ho (2020), "COVID-19 pandemic - A focused review for clinicians", *Clin. Microbiol. Infect.*, **26(7)**, pp.842-847, DOI: 10.1016/j.cmi.2020.04.023.

[4] J.F.W. Chan, S. Yuan, K.H. Kok, et al. (2020), "A familial cluster of pneumonia associated with the 2019 novel coronavirus indicating person-to-person transmission: A study of a family cluster", *The Lancet*, **395(10223)**, pp.514-523, DOI: 10.1016/S0140-6736(20)30154-9.

[5] A. Wu, Y. Peng, B. Huang, et al. (2020), "Genome composition and divergence of the novel coronavirus (2019-nCoV) originating in China", *Cell Host & Microbe*, **27(3)**, pp.325-328, DOI: 10.1016/j.chom.2020.02.001.

[6] Y. Gao, L. Yan, Y. Huang, et al. (2020a), "Structure of the RNA-dependent RNA polymerase from COVID-19 virus", *Science*, **368(6492)**, pp.779-782, DOI: 10.1126/science.abb7498.

[7] D.S. Wishart, Y.D. Feunang, A.C. Guo, et al. (2018), "DrugBank 5.0: A major update to the DrugBank database for 2018", *Nucleic Acids Res.*, **46(D1)**, pp.D1074-D1082, DOI: 10.1093/nar/gkx1037.

[8] D. Rubin, K. Chan-Tack, J. Farley, et al. (2020), "FDA approval of remdesivir - A step in the right direction", *The New England Journal of Medicine*, **383(27)**, pp.2598-2600, DOI: 10.1056/NEJMp2032369.

[9] Y. Gao, L. Yan, Y. Huang, et al. (2020b), "SARS-CoV-2 RNA-dependent RNA polymerase in complex with cofactors", *RCSB Protein Data Bank*, DOI: 10.2210/pdb6M71/pdb.

[10] S. Singh, F. Sk, A. Sonawane, et al. (2020), "Plant-derived natural polyphenols as potential antiviral drugs against SARS-CoV-2 via RNA- dependent RNA polymerase (RdRp) inhibition: An *in-silico* analysis", *Journal of Biomolecular Structure and Dynamics*, pp.6249-6264, DOI: 10.1080/07391102.2020.1796810.

[11] C.A. Lipinski (2004), "Lead- and drug-like compounds: the rule-of-five revolution", *Drug Discovery Today: Technologies*, **1(4)**, pp.337-341, DOI: 10.1016/j.ddtec.2004.11.007.

[12] B. Jayaram, T. Singh, G. Mukherjee, et al. (2012), "*Sanjeevini:* A freely accessible web-server for target directed lead molecule discovery", *BMC Bioinformatics*, **13**, DOI: 10.1186/1471-2105-13-S17-S7.

[13] E.E. Bolton, J. Chen, S. Kim, et al. (2011), "PubChem3D: A new resource for scientists", *Journal of Cheminformatics*, **3**, DOI: 10.1186/1758-29463-32.

[14] D.E.V. Pires, T.L. Blundell, D.B. Ascher (2015), "pkCSM: Predicting smallmolecule pharmacokinetic and toxicity properties using graph-based signatures", *J. Med. Chem.*, **58(9)**, pp.4066-4072, DOI: 10.1021/acs.jmedchem.5b00104.

[15] C.J. Gordon, E.P. Tchesnokov, J.Y. Feng, et al. (2020), "The antiviral compound remdesivir potently inhibits RNA-dependent RNA polymerase from Middle East respiratory syndrome coronavirus", *J. Biol. Chem.*, **295(15)**, pp.4773-4779, DOI: 10.1074/jbc.AC120.013056.

[16] A.A. Elfiky (2020a), "Ribavirin, remdesivir, sofosbuvir, galidesivir, and tenofovir against SARS-CoV-2 RNA dependent RNA polymerase (RdRp): A molecular docking study", *Life Sciences*, **253**, DOI: 10.1016/j.lfs.2020.117592.

[17] S.O. Aftab, M.Z. Ghouri, M.U. Masood, et al. (2020), "Analysis of SARS-CoV-2 RNA- dependent RNA polymerase as a potential therapeutic drug target using a computational approach", *Journal of Translational Medicine*, **18**, DOI: 10.1186/s12967-020-02439-0.

[18] X. Xu, Y. Liu, S. Weiss, et al. (2003), "Molecular model of SARS coronavirus polymerase: implications for biochemical functions and drug design", *Nucleic Acids Research*, **31(24)**, pp.7117-7130, DOI: 10.1093/nar/gkg916.

[19] J. Ahmad, S. Ikram, F. Ahmad, et al. (2020), "SARS-CoV-2 RNA dependent RNA polymerase (RdRp) - A drug repurposing study", *Heliyon*, **6(7)**, DOI: 10.1016/j.heliyon.2020.e04502.

[20] S. Gul, O. Ozcan, S. Asar, et al. (2020), "*In silico* identification of widely used and well-tolerated drugs as potential SARS-CoV-2 3C-like protease and viral RNA-dependent RNA polymerase inhibitors for direct use in clinical trials", *Journal of Biomolecular Structure & Dynamics*, **39(17)**, pp.6772-6791, DOI: 10.1080/07391102.2020.1802346.

[21] A.B. Gurung, M.A. Ali, J. Lee, et al. (2020), "*In silico* screening of FDA approved drugs reveals ergotamine and dihydroergotamine as potential coronavirus main protease enzyme inhibitors", *Saudi J. Biol. Sci.*, **27(10)**, pp.2674-2682, DOI: 10.1016/j.sjbs.2020.06.005.

[22] A. Gupta, H.X. Zhou (2020), "Profiling SARS-CoV-2 main protease (M^{PRO}) binding to repurposed drugs using molecular dynamics simulations in classical and neural network-trained force fields", *ACS Combinatorial Science*, **22(12)**, pp.826-832, DOI: 10.1021/acscombsci.0c00140.

[23] M. Bourliere, S.C. Gordon, S.L. Flamm, et al. (2017), "Sofosbuvir, velpatasvir, and voxilaprevir for previously treated HCV infection", *N. Engl. J. Med.*, **376(22)**, pp.2134-2146, DOI: 10.1056/NEJMoa1613512.

[24] Z. Ruan, C. Liu, Y. Guo, et al. (2020), "SARS-CoV-2 and SARS-CoV: Virtual screening of potential inhibitors targeting RNA-dependent RNA polymerase activity (NSP12)", *Journal of Medical Virology*, **93(1)**, pp.389-400, DOI: 10.1002/jmv.26222.

[25] A. Nourian, H. Khalili (2020), "Sofosbuvir as a potential option for the treatment of COVID-19", *Acta Biomed.*, **91(2)**, pp.236-238, DOI: 10.23750/abm.v91i2.9609.

[26] R. Gupta, P. Dhamija (2020), "Sofosbuvir for COVID-19 infection: A potential candidate", *Indian J. Pharmacol.,* **52(3)**, pp.232-233, DOI: 10.4103/ijp.IJP_675_20.

[27] A.A. Elfiky (2020b), "Anti-HCV, nucleotide inhibitors, repurposing against COVID-19", *Life Sciences,* **248**, DOI: 10.1016/j. lfs.2020.117477.

[28] B. Sayad, M. Sobhani, R. Khodarahmi (2020), "Sofosbuvir as repurposed antiviral drug against COVID-19: Why were we convinced to evaluate the drug in a registered/approved clinical trial?", *Arch. Med. Res.*, **51(6)**, pp.577-581, DOI: 10.1016/j.arcmed.2020.04.018.

[29] V. Cagno, G. Magliocco, C. Tapparel, et al. (2020), "The tyrosine kinase inhibitor nilotinib inhibits SARS-CoV-2 *in vitro*", *Basic & Clinical Pharmacology & Toxicology*, **128(4)**, pp.621-624, DOI: 10.1111/bcpt.13537.

[30] P. Indu, M.R. Rameshkumar, N. Arunagirinathan, et al. (2020), "Raltegravir, indinavir, tipranavir, dolutegravir, and etravirine against main protease and RNA- dependent RNA polymerase of SARS-CoV-2: A molecular docking and drug repurposing approach", *J. Infect. Public Health*, **13(12)**, pp.1856-1861, DOI: 10.1016/j.jiph.2020.10.015.

[31] Y. Kumar, H. Singh, C.N. Patel (2020), "*In silico* prediction of potential inhibitors for the main protease of SARS-CoV-2 using molecular docking and dynamics simulation based drug-repurposing", *J. Infect. Public Health*, **13(9)**, pp.1210-1223, DOI: 10.1016/j.jiph.2020.06.016.

[32] E.J. Kim, S.H. Choi, J.S. Park, et al. (2020), "Use of darunavir-cobicistat as a treatment option for critically ill patients with SARS-CoV-2 infection", *Yonsei Med. J.*, **61(9)**, pp.826-830, DOI: 10.3349/ymj.2020.61.9.826.

[33] T.U. Singh, S. Parida, M.C. Lingaraju, et al. (2020), "Drug repurposing approach to fight COVID-19", *Pharmacol. Rep.*, **72(6)**, pp.1479-1508, DOI: 10.1007/s43440-020-00155-6.

[34] E. Meriglier, C. Rivoisy, M. Hessamfar, et al. (2021), "Safety of hydroxychloroquine and darunavir or lopinavir in COVID-19 infection", *J. Antimicrob. Chemother*, **76(2)**, pp.482-486, DOI: 10.1093/jac/dkaa441.

[35] J.R. Saper, S. Silberstein (2006), "Pharmacology ofdihydroergotamine and evidence for efficacy and safety in migraine", *Headache*, Suppl. 4, pp.S171-S181, DOI: 10.1111/j.1526-4610.2006.00601.x.

[36] E. Jabbour, J. Cortes, H. Kantarjian (2010), "Nilotinib for the treatment of chronic myeloid leukemia: An evidence-based review", *Core Evidence*, **4**, pp.207-213, DOI: 10.2147/ce.s6003.

[37] S. Thaisrivongs, J.W. Strohbach (1999), "Structure-based discovery of tipranavir disodium (PNU-140690E): A potent, orally bioavailable, nonpeptidic HIV protease inhibitor", *Biopolymers*, **51(1)**, pp.51-58, DOI: 10.1002/(SICI)1097-0282(1999)51:1<51::AID-BIP6>3.0.CO;2-U.

[38] Z. Temesgen, F. Cainelli, S. Vento (2005), "Tipranavir", *Drugs Today (Barc)*, **41(11)**, pp.711-720, DOI: 10.1358/dot.2005.41.11.937960.

[39] V. Spagnuolo, A. Castagna, A. Lazzarin (2018), "Darunavir for the treatment of HIV infection", *Expert Opin. Pharmacother.*, **19(10)**, pp.1149-1163, DOI: 10.1080/14656566.2018.1484901.

[40] E.D. Deeks (2014), "Darunavir: A review of its use in the management of HIV-1 infection", *Drugs*, **74(1)**, pp.99-125, DOI: 10.1007/s40265-013-0159-3.

[41] S. Pushpakom, F. Iorio, P.A. Eyers, et al. (2019), "Drug repurposing: Progress, challenges and recommendations", *Nat. Rev. Drug Discov.*, **18(1)**, pp.41-58, DOI: 10.1038/nrd.2018.168.

[42] Y. Han, J. Zhang, C.Q. Hu, et al. (2019), "*In silico* ADME and toxicity prediction of ceftazidime and its impurities", *Front. Pharmacol.*, DOI: 10.3389/fphar.2019.00434.

[43] D.E.V. Pires, T.L. Blundell, D.B. Ascher (2015), "pkCSM: Predicting smallmolecule pharmacokinetic and toxicity properties using graph-based signatures", *J. Med. Chem.*, **58(9)**, pp.4066-4072, DOI: 10.1021/acs.jmedchem.5b00104.

[44] C. Prakash, A. Kamel, D. Cui, et al. (2000), "Identification of the major human liver cytochrome P450 isoform(s) responsible for the formation of the primary metabolites of ziprasidone and prediction of possible drug interactions", *British Journal of Clinical Pharmacology*, **49**, Suppl. 1, pp.35S-42S, DOI: 10.1046/j.1365-2125.2000.00151.x.

DOI: 10.31276/VJSTE.63(4).55-61

The antidepressant-like effects of an n-butanol fraction of *Ocimum sanctum* Linn. extract in unpredictable chronic mild stress-induced depression in mice

Thu Hien Nguyen[1], Thi Xoan Le[1*], Van Tai Nguyen[2], Thi Nguyet Hang Pham[2], Minh Khoi Nguyen[2], Matsumoto Kinzo[3, 4]

[1]Department of Pharmacology and Biochemistry, National Institute of Medicinal Materials, 3B Quang Trung Street, Trang Tien Ward, Hoan Kiem District, Hanoi Vietnam
[2]Department of Phytochemistry, National Institute of Medicinal Materials, 3B Quang Trung Street, Trang Tien Ward, Hoan Kiem District, Hanoi Vietnam
[3]Center for Supporting Pharmaceutical Education, Daiichi University of Pharmacy, 22-1 Mukaino, Minami Ward, Fukuoka City, Japan
[4]Graduate School of Pharmaceutical Sciences, Daiichi University of Pharmacy, 22-1 Mukaino, Minami Ward, Fukuoka City, Japan

Received 14 July 2021; revised 25 August 2021; accepted 8 September 2021

Abstract:

We previously reported that *Ocimum sanctum* Linn. (OS) ethanolic extract and its n-butanol fraction (OS-B) could improve depression-like behaviour in olfactory bulbectomized mice. The present study aims to clarify the antidepressant-like effects of OS-B and the possible mechanism of its action using mice subjected to unpredictable chronic mild stress (UCMS). UCMS mice were administered daily with OS-B (50 mg/kg, 100 mg/kg, p.o.) or imipramine (IMP, 8 mg/kg, i.p.), a reference drug. The UCMS-induced anhedonia in mice was analysed by the sucrose preference test, while behavioural despair was assessed using the tail suspension test (TST) and forced swimming test (FST). Locomotor activities and grooming behaviour of mice were elucidated using the open-field test (OFT). The UCMS procedure for 5 weeks induced anhedonia, and this symptom was significantly ameliorated by the administration of OS-B (100 mg/kg) as well as IMP during the UCMS period. Moreover, the OS-B and IMP treatment attenuated the UCMS-induced enhancement of behavioural despair in the TST and FST. In OFT, mice subjected to UCMS showed a decrease in grooming behaviour, and the effect of UCMS was reversed by OS-B and IMP administrations. No significant difference in locomotor activities between each animal group was observed. The amelioration effects of OS-B and IMP on UCMS-induced behavioural despair in the TST were abolished by administrating of ρ-chlorophenylalanine (PCPA, 80 mg/kg, i.p), a tryptophan hydroxylase inhibitor, and α-methyl-ρ-tyrosine (AMPT, 100 mg/kg), a tyrosine hydroxylase inhibitor. The present results suggest that OS-B attenuates UCMS-induced depression-like symptoms via monoaminergic systems including in the noradrenergic, dopaminergic, and serotonergic system.

Keywords: **antidepressant, monoaminergic system, *Ocimum sanctum*, serotonergic system, unpredictable chronic mild stress.**

Classification number: **3.3**

1. Introduction

Depression is currently one of the leading causes of the worldwide burden of disease. It is one of the most common psychiatric disorders characterised by psychological, behavioural, and physiological symptoms [1]. Lines of evidence have demonstrated that the monoaminergic-sympathetic nervous systems play essential roles in the depressive pathophysiology and antidepressant therapy [2]. The regulation of mood was significantly influenced by the monoaminergic system on the brain circuit especially serotonin, norepinephrine, and dopamine [3, 4]. In fact, prescription antidepressants such as tricyclics, monoamine oxidase inhibitors, selective serotonin reuptake inhibitors, and selective noradrenaline reuptake inhibitors, almost solely focus on enhancing monoamine transmitter function [4]. However, the treatment of depression with conventional antidepressants has many adverse effects [5, 6]. Therefore, daily intake of herbs with the potential to affect monoaminergic neurotransmitter systems may offer an effective strategy for treating and preventing depressive disorders associated with various stressors.

OS has various medicinal properties in the traditional system of medicine. It is also used as herbal tea or spice in Southeast Asian countries, including Vietnam. Many studies reveal that OS has a unique combination of actions

*Corresponding author: Email: xoanle@nimm.org.vn

that include anti-inflammatory [7], anti-dementia [8, 9], anxiolytic and antidepressant [10], as well as antioxidant effects [11, 12], etc. Regarding its chemical properties, OS reportedly contains a volatile oil, flavonoids (luteolin, apigenin, orientin, vicenin, cirsimaritin, isothymusin, luteolin-7-*O*-glucuronide and apigenin-7-*O*-glucuronide) [11, 13, 14], glycoglycerolipids (ocimumoside A and B) [15], and triterpenoids (ursolic acid and oleanolic acid) [16]. In the previous study, we demonstrated that ethanolic extract of OS ameliorated cognitive dysfunction and neuro-histological damages in olfactory bulbectomized (OBX) mice via enhancing the central cholinergic systems and VEGF expression [17]. Moreover, it was found that the ethanolic extract of OS improved depression-like behaviour in OBX mice [18]. Our findings suggested that the anti-depression effect of the OS ethanol extract was due to chemical constituents fractionated by n-BuOH, but not n-hexane or ethyl acetate [19]. However, the mechanism underlying the antidepressant effect of the OS-B fraction is unclear.

Because the development of depression was closely related to socio-environmental chronic stressors, a variety of stress-based animal models have been used to explore the antidepressant potential of herbal medicines and their mechanisms of action. Based on the stress hypothesis of depression, the UCMS model has been employed as a useful model with predictive validity, face validity, and construct validity [20]. In UCMS-induced depression-like behaviour, dysfunction of monoaminergic systems is reportedly one of the most relevant biological factors [21, 22]. In the present work, we aimed to examine the antidepressant-like effect and the underlying mechanism of OS-B using a UCMS model of depression. Our results suggested that OS-B exhibits anti-depressive effects at least in part via noradrenergic, dopaminergic, and/or serotonergic systems.

2. Materials and methods

2.1. Animals

Male *Swiss albino* mice (5-6 weeks old) were supplied from the National Institute of Hygiene and Epidemiology, Hanoi, Vietnam. Animals were housed for at least one week before experiments. Mice had free access to tap water and conventional rodent food. Housing was kept under standardized conditions with temperature 25±1°C, humidity 65-75% and photoperiod 12:12 (lights on at 7:00 A.M.). All behavioural tests were performed in the light phase, between 9:00 and 18:00. The present studies were conducted in accordance with the Guiding principles for the care and use of animals (NIH publication #85-23, revised in 1985) and were approved by the Institutional Animal Use and Care Committees of the National Institute of Medicinal Materials (NIMM), Hanoi, Vietnam.

2.2. Preparation of plant extract

OS was collected in Hanoi and identified by Dr. Pham Thanh Huyen (Department of Medicinal Plant Resources, NIMM, Vietnam). The voucher specimen (voucher #NIMM-16474B) was deposited at NIMM. The preparation of OS-B has been described previously [19]. Briefly, the aerial part of OS (4 kg) was extracted 3 times with 70% ethanol under reflux for 2 h. Each extract was combined, filtered using a filter paper (Whatman® qualitative filter paper, Grade 93, 580×580 cm, Merck, Darmstadt, Germany), and concentrated at 50°C under a vacuum yielding two litres of aqueous extract. The resultant extract was successively partitioned three times with n-hexane, ethyl acetate (EtOAc), and n-butanol (BuOH). Thereafter, the BuOH phase was evaporated and then dried in a vacuum oven at 50°C to obtain a 68-g n-BuOH fraction (OS-B). The chemical profile of OS-B was conducted using high-performance liquid chromatography (HPLC) as previous described [17]. The HPLC analysis exposed that the OS-B contained 5.82% luteolin-7-*O*-glucuronide, 2.26% apigenin-7-*O*-glucuronide, 0.15% apigenin, 0.45% luteolin, 1.00% ursolic acid, and 0.87% oleanolic acid (see supplemental data).

2.3. UCMS procedure and drug administration

The UCMS procedure reported by D. Mizuki, et al. (2014) [23] was used with minor modification. Mice were subjected to different unpredictable mild stressors such as: 18 h of isolation, food and water deprivation before sucrose preference test (SPT), 36 h of light exposure, 24 h of cage tilting at 45°, 24 h of exposure to an empty bottle, 3 h of confinement in a cramped jar for each mouse, a 24 h period of a wet cage (200 ml water/50 g rice husk), 3 h of a rat singing sound (playing a video record), and 24 h of paired caging. On average, the animals were exposed to two of these stressors at different times every day, which was randomly scheduled over 1 week. The stress process was repeated throughout 5 weeks before the behavioural tests. The UCMS was still in progress during the testing stages, excluding testing days to avoid affecting the test results. The non-stress control group was housed under normal conditions.

The aforementioned OS-B was freshly suspended in distilled water and administered at doses of 50 mg/kg/day (OS-B 50) and 100 mg/kg/day (OS-B 100) (p.o.). Imipramine (IMP; Sigma Chemical Co, St. Louis, MO, USA) was dissolved in 0.9% saline and administered at doses of 8.0 mg/kg/day (i.p.). Non-stressed and the UCMS control group mice were administered daily with tap water by oral route (p.o.). On the day of the behavioural tests, OS-B and IMP were administered for 60 and 30 min, respectively, before the test. This procedure is summarised in Fig. 1.

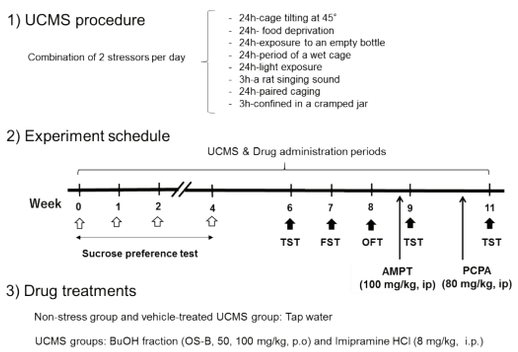

Fig. 1. Schematic drawing of the experimental protocol.

In week 0, *Swiss albino* mice were separated into non-stress and UCMS groups. The UCMS procedure was started from week 0 to week 11. The UCMS group was given tap water or butanol fraction of OS (OS-B, 50 and 100 mg/kg/day, p.o.) or imipramine HCl (IMP, 8 mg/kg, i.p.). The sucrose preference test was conducted weekly from week 0 to week 4 during the UCMS exposure. The depression-like behaviours were assessed using a TST, force swimming test (FST), and an open field test (OFT). 4 h before the drug administration on the week 9, OS-B 100- and IMP-treated group mice were pre-treated with a single dose of α-methyl-ρ-tyrosine (AMPT) (100 mg/kg, i.p.). Ten days after the AMPT treatment, the OS-B 100- and IMP-treated group mice were administered with ρ-chlorophenylalanine (PCPA) (80 mg/kg, i.p.) for 4 consecutive days before subjected to TST.

2.4. Behavioural performances

Sucrose preference test (SPT): SPT was used to assess as an index of anhedonia. The tests were conducted once before starting the UCMS procedure (week 0) and during UCMS induction (5 times in total) according to the previous report [24] with slight modification. The animals were trained to consume a 2% sucrose solution for a 48-h period without food and water before the first SPT at week 0. In the SPT, mice were separately placed in a cage and deprived of water and food for 18 h. The mice then received tap water or a 2% sucrose (w/v) solution from two drinking nozzles set at the cage for 1 h. The positions of the nozzles were randomly switched. The amounts of 2% sucrose solution and the weight of each mouse were recorded. The sucrose preference of each mouse was calculated with the following formula:

$$\text{Sucrose intake (g/kg b.w.)} = [0.02 \times V\,(\text{ml})]/[0.001 \times m\,(\text{g})]$$

TST: At week 6, TST was conducted as previously described [18, 23, 25]. Briefly, each mouse was suspended by adhesive tape, which was placed approximately 2 cm from the tip of the tail. The mouse's head was above the floor 40 cm. This short-term inescapable stress led to characteristic behaviour immobility. The animal behaviour was video-recorded during a 6-min period and then the mice were returned to the home cage. Immobility time was analysed for the last 5 min and defined as a state with a movement speed of no more than 0.05 cm^2/s using the Any-maze Video Tracking System (ver. 4.99, Stoelting Co., IL, USA).

FST: One week after the TST, mice were subjected to FST. In this test, each mouse was forced to swim in clear plexiglass cylinders (internal diameter: 12 cm, height: 24 cm) containing water (18 cm deep) at 20±1°C. The behaviours of each mouse were video-recorded from above for 6 min. The immobility duration was calculated using Any-maze Video Tracking System (ver. 4.99, Stoelting Co., IL, USA). Immobility was determined when the animals ceased struggling and showed floating motionless in the water with minimum movements to keep the nose above water surface [26].

OFT: Spontaneous motor activity of animals was elucidated in the open field. The activity was video-recorded, and then the effects of test drugs were elucidated using the Digiscan Infrared Photocell system (Omnitech Electronics, Columbus, OH), which consisted of 40×40×50 cm plexiglass arenas with black floors fitted into infrared beams dividing the space into 16 equal squares. This system calculated the number of times that the animal interrupted infrared beams during a 10-min observation period. Measurement parameters were horizontal activity (units) and vertical activity (units). The vertical activity was defined as the number of times the animal interrupted the horizontal beam sensor. In addition, the total duration (seconds) that the animal spent grooming was scored as an index of UCMS-induced stress response by two experienced observers in a blind manner. The floor of the apparatus was cleaned with 70% ethanol before testing the next mouse.

2.5. Pharmacological treatments

α-methyl-ρ-tyrosine (AMPT, Sigma Chemical Co, St. Louis, MO, USA), an inhibitor of tyrosine hydroxylase, a rate-limiting enzyme for noradrenaline and dopamine synthesis [27] and DL-ρ-chlorophenyl alanine (PCPA, Acros Organics, Switzerland), an inhibitor of tryptophan hydroxylase (TPH) involved in the serotonin synthesis [28], were used to explore the role of serotonergic and noradrenergic system in the antidepressant-like actions of OS-B. AMPT and PCPA and were dissolved in saline with 1% Tween 80. On week 9, OS-B 100- and IMP-treated group mice were treated with a single dose of AMPT (100 mg/kg, i.p.) 4 h before the drug administration. Sixty minutes after the administration, the mice were subjected to TST. Ten days after AMPT treatment, the OS-B 100- and IMP-treated mice groups were administered with PCPA (80 mg/kg, i.p.) for 4 consecutive days. Thirty min after the last PCPA administration, mice were administrated the test drug treatment and, after 60 min, were submitted to the TST (Fig. 1).

2.6. Data analysis

All the results obtained in current study were represented as the mean ±S.E.M. The comparisons between all the groups were performed by one-way ANOVA followed by post hoc Student-Newman-Keuls test (SPSS 22.0). A p value of <0.05 was regarded significant.

3. Results

3.1. Effects of OS-B and IMP on UCMS-induced anhedonia using the sucrose preference test (SPT)

SPT was conducted weekly to assess anhedonia of UCMS-exposed mice. As shown in Fig. 2, no significant difference in sucrose consumption from week 0 to week 3 was found between each animal group. However, the sucrose consumption at week 4 markedly decreased in the vehicle-treated UCMS group as compared to non-stress group mice, indicating UCMS-induced anhedonia symptom. IMP treatment significantly suppressed the increase in sucrose intake at week 4 in UCMS-exposed groups. OS-B (50 and 100 mg/kg) also dose-dependently reversed UCMS-induced decrease in sucrose intake.

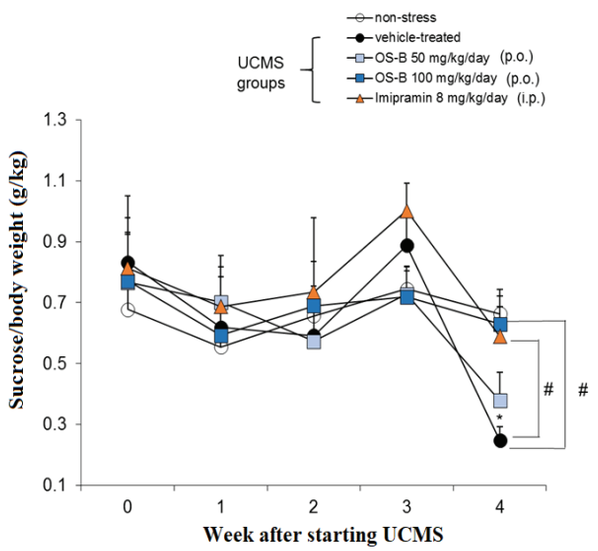

Fig. 2. The effects of OS-B (50 and 100 mg/kg) on UCMS-induced depression-like behaviours in the SPT. Sucrose preference of each animal group was weekly measured before and during 4-week UCMS procedure (n=9-10). *p<0.05 vs. non-stress group; #p<0.05 vs. UCMS control group.

3.2. Effects of OS-B and IMP on UCMS-induced depression-like behaviour in TST and FST

Depression-like behaviours of UCMS mice were analysed by the TST and FST. As shown in Fig. 3, the vehicle-treated UCMS group showed significantly longer immobility time than the non-stress group (p<0.01, p<0.05, respectively) in TST and FST, indicating a depression-like symptom. IMP treatment markedly decreased the immobility time of UCMS mice in both TST and FST. The OS-B (50 and 100 mg/kg)-treated UCMS group significantly and dose-dependently decreased the immobility time when compared with the UCMS control group mice.

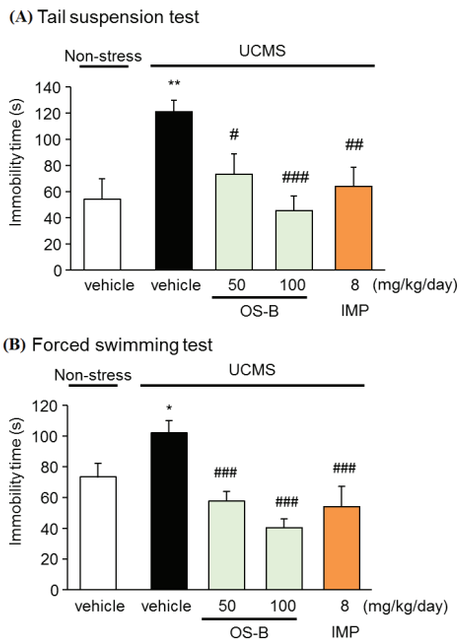

Fig. 3. The effects of OS-B (50 and 100 mg/kg) on UCMS-induced depression-like behaviour in the TST and the FST. The immobility time of each animal group in the TST **(A)** and FST **(B)** was calculated as an index of depression-like behaviour at weeks 6 and 7, respectively, during the UCMS procedure (n=9-10). *p<0.05, **p<0.01 vs. non-stress mice, #p<0.05, ##p<0.01 and ###p<0.001 vs. UCMS control group.

3.3. Effects of OS-B and IMP on locomotor activity and grooming behaviour of UCMS mice in the OFT

The OFT was conducted to determine the locomotor activity of the UCMS mice, so that false-positive results can be excluded. As shown in Fig. 4A1-2, no significant difference between each animal group in the horizontal and vertical activity, indicating that neither IMP nor OS-B affected the locomotor activity of UCMS mice.

Besides, the time the animals spent grooming was manually recorded since a decrease of grooming behaviour in the OFT is likely related to less motivation or interest in daily performance, such as the maintenance of minimal personal care, which is a symptom of depression [29]. As shown in Fig. 4B, mice subjected to UCMS treatment clearly showed decreased time spent grooming. Moreover, the administration of OS-B (50, 100 mg/kg) and imipramine significantly prolonged the time of self-grooming in UCMS-exposed mice.

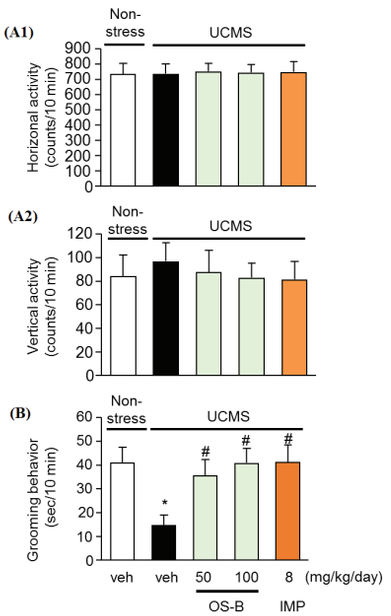

Fig. 4. The effects of OS-B (50 and 100 mg/kg) and IMP on locomotor activity and grooming behaviours of UCMS mice. Horizontal activity **(A1)** and vertical activity **(A2)**, **(B)** grooming behaviours expressed as a total accumulated time during a 10-min session (n=9-10), *p<0.05 vs. non-stress group, #p<0.05 vs. UCMS control group.

3.4. Involvement of monoaminergic system in the antidepressant-like effects of OS-B

AMPT, a tyrosine hydroxylase inhibitor, and PCPA, a tryptophan hydroxylase inhibitor, were used to clarify the implication of monoaminergic systems in the antidepressant-like effects of OS-B. The UCMS control group displayed remarkably longer immobility duration than the non-stress group ($p<0.05$) in the TST conducted at week 9 and 11 after starting the UCMS exposure. However, pre-treatment with AMPT (100 mg/kg, i.p.) completely abolished the suppressing effects of OS-B and IMP on the immobility of UCMS mice in the TST (Fig. 5A). The antidepressant-like effects of OS-B (100 mg/kg) and IMP on UCMS mice in the TST were also reversed by pre-treatment of UCMS mice with PCPA (80 mg/kg, i.p.) (Fig. 5B).

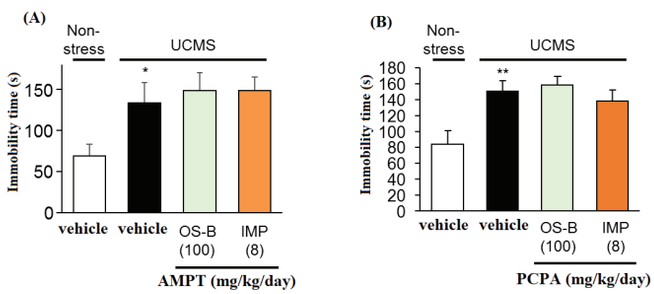

Fig. 5. The effect of the pre-treatment with α-methyl-ρ-tyrosine (AMPT, 100 mg/kg, i.p.) (A) and DL-ρ-chlorophenyl alanine (PCPA, 80 mg/kg, i.p.) (B) on OS-B induced antidepressant-like effects in the TST. n=9-10, *p<0.05, **p<0.01 vs. non-stress group. No significant difference between OS-B and IMP vs. non-stress group.

4. Discussion

The present study using a UCMS-exposed animal model of depression demonstrated that OS-B exhibited anti-depression-like effects the same as imipramine, a typical antidepressant drug, via the serotonergic and noradrenergic systems. Thus, it is likely that the daily OS administration is beneficial for preventing/improving core symptoms in patients with depressive disorders.

In this study, we employed the UCMS to induce depression-like behaviours in mice because the UCMS procedure, the UCMS-induced pathophysiological features, and the susceptibility to antidepressant drugs are associated with human depression. These features of the UCMS-exposed animal provide a rationale to use as an animal model with constructive, face, and predictive validities of depression. Using the UCMS model, we found that the daily treatment of the UCMS-exposed animals with OS-B (50 and 100 mg/kg) and imipramine dose-dependently reversed the UCMS-induced anhedonia. Indeed, anhedonia was detected as a gradual decrease in sucrose consumption in the animals exposed to the UCMS procedure. Anhedonia is one of the most prominent symptoms observed in humans with depressive illness [30] and is reportedly linked to dysfunctions in the reward-related processes. The dopaminergic system, in particular, plays an important role in predicting reward, generating motivation, and responding to conditioned incentive stimuli [31]. Downregulation of dopaminergic systems has been observed in animals subjected to chronic mild stress [32] and patients with depression [33]. Considering these findings, it is likely that OS-B can ameliorate anhedonia, probably, by affecting the dopaminergic systems implicated in the reward-related process in the brain.

The present study also revealed the antidepressant-like actions of OS-B in the TST and FST. As shown in Fig. 3, vehicle-treated UCMS mice showed a markedly exacerbated behavioural despair response measured as a prolonged immobility time in these tests, compared to non-stress mice. These data indicate that the UCMS-exposed mice are more susceptible to stressful stimuli than non-stressed control animals. Moreover, when administered daily during a UCMS exposing period, OS-B and imipramine almost completely prevented the exacerbation of behavioural despair responses to stressors in the TS and FST. These results are consistent with our previous study in which OS and OS-B ameliorated behavioural despairs exhibited by OBX animals, an animal model of dementia patients with depression [19]. Thus, our findings suggest that OS-B acts like an antidepressant-like drug and protects animals from being vulnerable to stressors.

Moreover, it should be noted that, in the present study, the immobility time of 100 mg/kg/day OS-B- and 8.0 mg/kg/day imipramine-treated UCMS groups showed less than that of the non-stress group. These data raise the possibility that OS-B, at a daily dose of 100 mg/kg, may exhibit a psychostimulant activity in the UCMS animals, thereby apparently reducing the immobility time

of UCMS animals in the TST and FST. However, this possibility seems to be little, if any, because OS-B (50-100 mg/kg/day, p.o.) had no effects on the spontaneous motor activity of the UCMS animals in the OFT. Rather, an interesting finding in the OFT is that the administration of OS-B and imipramine significantly reversed the USMC-induced decrease in the time animals spent grooming. Recent evidence indicates that a decrease in grooming behaviour in UCMS animals is associated with reduced motivation and a decrease in self stimulatory behaviour, or reduced sensitivity to pleasure, and is representative of anhedonia, a core symptom of depression [29]. Taken together, the findings in the OFT further support the idea that OS-B possesses the antidepressant activity in the UCMS animals like imipramine.

We also investigated whether monoaminergic systems are involved in the antidepressant-like effects of OS-B in UCMS animals because monoaminergic systems in the brain play an essential role in the clinical effects of various typical and atypical antidepressant drugs including imipramine. For this aim, we employed AMPT and PCPA, inhibitors for catecholamine and serotonin biosynthesis, respectively, because lines of evidence have demonstrated that depletion of monoamines by AMPT and PCPA antagonize the effects of antidepressant drugs on behavioural despairs in rodents [34-37]. The present results showed that the ameliorative effects of 100 mg/kg/day OS-B and 8 mg/kg/day imipramine on behavioural despairs detected in TST were completely abolished in the UCMS group treated with AMPT and PCPA. These findings strongly suggest that OS-B exerts the antidepressant-like action in UCMS animals in a manner depending on the levels of endogenous monoamines in the brain as imipramine does. This idea seems to explain the mechanism underlying the aforementioned ameliorative action of OS-B on anhedonia observed in UCMS animals. In addition, according to E.J. Richard, et al. (2016) [38], the anti-stress activity of *Ocimum sanctum* standardized extract (ociglycoside-I (>0.1% w/w), rosmarinic acid (>0.2% w/w), and triterpene acids such as oleanolic acid and ursolic acid (>2.5% w/w)) in chronic variable stress rats was contributed by inhibiting blood cortisol release, blocking corticotropin-releasing hormone receptor type 1, and obstructing activities of 11β-hydroxysteroid dehydrogenase type 1 and catechol-O-methyltransferase *in vitro*. Therefore, it cannot be denied that OS-B actions could be not only dependent on the monoaminergic system but also due to the other mechanisms.

It is still unclear whether the monoamine-dependent antidepressant-like effects of OS-B in the UCMS model of depression share the same mechanism as imipramine and other antidepressant drugs targeting monoaminergic systems and monoamine transporters in particular. In our preliminary study using an OBX model [19], we found that some major constituents of OS such apigenin, luteolin, and apigenin-7-*O*-β-D-glucuronide played a role in the antidepressant effects of OS-B. Moreover, several previous studies reported that apigenin possesses pharmacological and neurochemical effects associated with improvement of depression, such as increasing noradrenalin activity, inhibiting monoamine oxidase activities, and stimulating an L-tyrosine uptake [39]. In addition, luteolin reportedly exerts antidepressant-like effects via inhibiting and downregulating plasma membrane monoamine transporter [40]. Thus, it is likely that these chemical constituents of OS-B are involved in the monoamine-dependent antidepressant-like effects of OS-B. Nevertheless, further investigations are required to clarify the exact molecular mechanism(s) and chemical constituent(s) that account for OS-B's preventive and ameliorative effects on depression-related symptoms caused in the USCM animals.

5. Conclusions

In summary, the results of this study suggest that OS-B could prevent/ameliorate UCMS-induced depression-like symptoms and its actions are involved neurotransmitter systems included in the noradrenergic, dopaminergic and serotonergic systems.

CRedit author statements

Thu Hien Nguyen, Thi Xoan Le, Van Tai Nguyen: Conceptualisation, Methodology, Data curation, Formal analysis, Writing - Review & Editing; Thi Nguyet Hang Pham, Minh Khoi Nguyen, Matsumoto Kinzo: Conceptualisation, Methodology, Writing - Original draft preparation, Writing - Review & Editing.

ACKNOWLEDGEMENTS

This research is funded by the Vietnam National Foundation for Science and Technology Development (NAFOSTED) under grant number 106-YS.05-2016.22.

COMPETING INTERESTS

The authors declare that there is no conflict of interest regarding the publication of this article.

REFERENCES

[1] GBD 2017 Disease and Injury Incidence and Prevalence Collaborators (2018), "Global, regional, and national incidence, prevalence, and years lived with disability for 354 diseases and injuries for 195 countries and territories, 1990-2017: A systematic analysis for the global burden of disease study 2017", *The Lancet*, **392(10159)**, pp.1789-1858, DOI: 10.1016/S0140-6736(18)32279-7.

[2] R. Jankord, J.P. Herman (2008), "Limbic regulation of hypothalamo-pituitary-adrenocortical function during acute and chronic stress", *Annals of The New York Academy of Sciences*, **1148**, pp.64-73, DOI: 10.1196/annals.1410.012.

[3] B. Dell'Osso, M.C. Palazzo, L. Oldani, et al. (2011), "The noradrenergic action in antidepressant treatments: pharmacological and clinical aspects", *CNS Neuroscience & Therapeutics*, **17(6)**, pp.723-732, DOI: 10.1111/j.1755-5949.2010.00217.x.

[4] M. Hamon, P. Blier (2013), "Monoamine neurocircuitry in depression and strategies for new treatments", *Progress in Neuro-Psychopharmacology and Biological Psychiatry*, **45**, pp.54-63, DOI: 10.1016/j.pnpbp.2013.04.009.

[5] J. Moncrieff, I. Kirsch (2005), "Efficacy of antidepressants in adults", *BMJ*, **331(7509)**, pp.155-157, DOI: 10.1136/bmj.331.7509.155.

[6] J. Read, J. Williams (2018), "Adverse effects of antidepressants reported by a large international cohort: Emotional blunting, suicidality, and withdrawal effects", *Current Drug Safety*, **13(3)**, pp.176-186, DOI: 10.2174/1574886313666180605095130.

[7] S.S. Choudhury, L. Bashyam, N. Manthapuram, et al. (2014), "*Ocimum sanctum* leaf extracts attenuate human monocytic (THP-1) cell activation", *Journal of Ethnopharmacology*, **154(1)**, pp.148-155, DOI: 10.1016/j.jep.2014.03.049.

[8] V.V. Giridharan, R.A. Thandavarayan, T. Konishi (2015), "*Ocimum sanctum* Linn. (Holy Basil) to improve cognition", *Diet and Nutrition in Dementia and Cognitive Decline*, Academic Press, pp.1049-1058, DOI: 10.1016/B978-0-12-407824-6.00098-7.

[9] S. Sampath, S.C. Mahapatra, M.M. Padhi, et al. (2015), "Holy Basil (*Ocimum sanctum* Linn.) leaf extract enhances specific cognitive parameters in healthy adult volunteers: A placebo controlled study", *Indian J. Physiol. Pharmacol.*, **59(1)**, pp.69-77.

[10] M. Chatterjee, P. Verma, R. Maurya, et al. (2011), "Evaluation of ethanol leaf extract of *Ocimum sanctum* in experimental models of anxiety and depression", *Pharmaceutical Biology*, **49(5)**, pp.477-483, DOI: 10.3109/13880209.2010.523832.

[11] M.A. Kelm, M.G. Nair, G.M. Strasburg, et al. (2000), "Antioxidant and cyclooxygenase inhibitory phenolic compounds from *Ocimum sanctum* Linn.", *Phytomedicine*, **7(1)**, pp.7-13, DOI: 10.1016/S0944-7113(00)80015-X.

[12] M. Shivananjappa, M. Joshi (2012), "Aqueous extract of tulsi (*Ocimum sanctum*) enhances endogenous antioxidant defenses of human hepatoma cell line (HepG2)", *Journal of Herbs, Spices & Medicinal Plants*, **18(4)**, pp.331-348, DOI: 10.1080/10496475.2012.712939.

[13] A.G.R. Nair, R. Gunasegaran, B.S. Joshi (1982), "Chemical investigation of certain South Indian plants", *Indian J. Chem.*, **21**, pp.979-980, DOI: 10.1002/ptr.1399.

[14] P.U. Devi, K.S. Bisht, M. Vinitha (1998), "A comparative study of radioprotection by *Ocimum* flavonoids and synthetic aminothiol protectors in the mouse", *The British Journal of Radiology*, **71(847)**, pp.782-784, DOI: 10.1259/bjr.71.847.9771390.

[15] P. Gupta, D.K. Yadav, K.B. Siripurapu, et al. (2007), "Constituents of *Ocimum sanctum* with antistress activity", *Journal of Natural Products*, **70(9)**, pp.1410-1416, DOI: 10.1021/np0700164.

[16] D. Sarkar, A. Srimany, T. Pradeep (2012), "Rapid identification of molecular changes in Tulsi (*Ocimum sanctum* Linn) upon ageing using leaf spray ionization mass spectrometry", *Analyst*, **137(19)**, pp.4559-4563, DOI: 10.1039/c2an35655d.

[17] X.T. Le, H.T. Nguyen, T.V. Nguyen, et al. (2021), "*Ocimum sanctum* Linn. extract improves cognitive deficits in olfactory bulbectomized mice via the enhancement of central cholinergic systems and VEGF expression", *Evidence-Based Complementary and Alternative Medicine*, **2021**, DOI: 10.1155/2021/6627648.

[18] N.H. Anh, L.T. Xoan (2015), "Antidepressant-like effect of *Ocimum sanctum* in Olfactory Bulbectomized mice", *Journal of Medicinal Materials*, **20(5)**, pp.311-316.

[19] X.L. Thi, H.N. Thu, H.P Nhu, et al. (2020), "Putative constituents contributing to the antidepressant-like effects of *Ocimum sanctum* in olfactory bulbectomized-mice", *Journal of Medicinal Materials*, **25(3)**, pp.186-192.

[20] C.H. Duman (2010), "Models of depression", *Vitamins & Hormones*, **82**, pp.1-21.

[21] S. Bekris, K. Antoniou, S. Daskas, et al. (2005), "Behavioural and neurochemical effects induced by chronic mild stress applied to two different rat strains", *Behavioural Brain Research*, **161(1)**, pp.45-59, DOI: 10.1016/j.bbr.2005.01.005.

[22] A. Ahmad, N. Rasheed, P. Gupta, et al. (2012), "Novel ocimumoside A and B as anti-stress agents: Modulation of brain monoamines and antioxidant systems in chronic unpredictable stress model in rats", *Phytomedicine*, **19(7)**, pp.639-647, DOI: 10.1016/j.phymed.2012.02.012.

[23] D. Mizuki, K. Matsumoto, K. Tanaka, et al. (2014), "Antidepressant-like effect of *Butea superba* in mice exposed to chronic mild stress and its possible mechanism of action", *Journal of Ethnopharmacology*, **156**, pp.16-25, DOI: 10.1016/j.jep.2014.08.014.

[24] S. Daodee, O. Monthakantirat, K. Ruengwinitwong, et al. (2019), "Effects of the ethanol extract of *Dipterocarpus alatus* leaf on the unpredictable chronic mild stress-induced depression in ICR mice and its possible mechanism of action", *Molecules*, **24(18)**, DOI: 10.3390/molecules24183396.

[25] P. Sithisarn, P. Rojsanga, S. Jarikasem, et al. (2013), "Ameliorative effects of *Acanthopanax trifoliatus* on cognitive and emotional deficits in olfactory bulbectomized mice: an animal model of depression and cognitive deficits", *Evidence-Based Complementary and Alternative Medicine*, **2013**, DOI: 10.1155/2013/701956.

[26] R. Linge, A. Pazos, A. Diaz (2013), "Social isolation differentially affects anxiety and depressive-like responses of bulbectomized mice", *Behavioural Brain Research*, **245**, pp.1-6, DOI: 10.1016/j.bbr.2013.01.041.

[27] D.H. Park, D.M. Stone, H. Baker, et al. (1994), "Early induction of rat brain tryptophan hydroxylase (TPH) mRNA following parachlorophenylalanine (PCPA) treatment", *Molecular Brain Research*, **22(14)**, pp.20-28, DOI: 10.1016/0169-328x(94)90028-0.

[28] R.N. Brogden, R.C. Heel, T.M. Speight, et al. (1981), "α-Methyl-p-tyrosine: A review of its pharmacology and clinical use", *Drugs*, **21(2)**, pp.81-89, DOI: 10.2165/00003495-198121020-00001.

[29] J.C. Frisbee, S.D. Brooks, S.C. Stanley, et al. (2015), "An unpredictable chronic mild stress protocol for instigating depressive symptoms, behavioral changes and negative health outcomes in rodents", *Journal of Visualized Experiments*, **106**, DOI: 10.3791/53109.

[30] P. Willner (2017), "The chronic mild stress (CMS) model of depression: History, evaluation and usage", *Neurobiology of Stress*, **6**, pp.78-93, DOI: 10.1016/j.ynstr.2016.08.002.

[31] A.D. Avakian, A. Markou (2012), "The neurobiology of anhedonia and other reward-related deficits", *Trends in Neurosciences*, **35(1)**, pp.68-77, DOI: 10.1016/j.tins.2011.11.005.

[32] G.D. Chiara, G. Tanda (1997), "Blunting of reactivity of dopamine transmission to palatable food: A biochemical marker of anhedonia in the CMS model?", *Psychopharmacology*, **134(4)**, pp.351-353, DOI: 10.1007/s002130050465.

[33] J.C. Pruessner, F. Champagne, M.J. Meaney, et al. (2004), "Dopamine release in response to a psychological stress in humans and its relationship to early life maternal care: A positron emission tomography study using [11C] raclopride", *Journal of Neuroscience*, **24(11)**, pp.2825-2831, DOI: 10.1523/JNEUROSCI.3422-03.2004.

[34] M.G.D. Montis, C. Gambarana, D. Meloni (1993), "Alpha-methyl-para-tyrosine antagonizes the effect of chronic imipramine on learned helplessness in rats", *European Journal of Pharmacology*, **249(2)**, pp.179-183, DOI: 10.1016/0014-2999(93)90430-p.

[35] S.S. Hamada, A. Suzuki, Y. Ueda, et al. (2017), "Serotonergic and dopaminergic systems are implicated in antidepressant-like effects of chotosan, a Kampo formula, in mice", *Journal of Pharmacological Sciences*, **133(2)**, pp.110-113, DOI: 10.1016/j.jphs.2017.01.002.

[36] H.L. Miller, P.L. Delgado, R.M. Salomon, et al. (1996), "Effects of α-methyl-para-tyrosine (AMPT) in drug-free depressed patients", *Neuropsychopharmacology*, **14(3)**, pp.151-157, DOI: 10.1016/0893-133X(95)00072-L.

[37] R.W. Lam, E.M. Tam, A. Grewal, et al. (2001), "Effects of alpha-methyl-para-tyrosine-induced catecholamine depletion in patients with seasonal affective disorder in summer remission", *Neuropsychopharmacology*, **25(1)**, pp.97-101, DOI: 10.1016/S0893-133X(01)00337-2.

[38] E.J. Richard, R. Illuri, B. Bethapudi, et al. (2016), "Anti-stress activity of *Ocimum sanctum*: possible effects on hypothalamic-pituitary-adrenal axis", *Phytotherapy Research*, **30(5)**, pp.805-814, DOI: 10.1002/ptr.5584.

[39] T. Nakazawa, T. Yasuda, J. Ueda, et al. (2003), "Antidepressantlike effects of apigenin and 2,4,5-trimethoxycinnamic acid from *Perilla frutescens* in the forced swimming test", *Biological and Pharmaceutical Bulletin*, **26(4)**, pp.474-480, DOI: 10.1248/bpb.26.474.

[40] S. Zhu, S. Lei, S. Zhou, et al. (2019), "Luteolin shows antidepressant-like effect by inhibiting and downregulating plasma membrane monoamine transporter (PMAT, *Slc29a4*)", *Journal of Functional Foods,* **54**, pp.440-448, DOI: 10.1016/j.jff.2019.01.048.

DOI: 10.31276/VJSTE.63(4).62-65

Effects of different shrimp extracts on *Vibrio parahaemolyticus* growth and virulence

Nguyen Thuan Thien Truong, The Hao Nguyen, Cong Chinh Bui, Thi Thu Hoai Nguyen*

School of Biotechnology, International University, Vietnam National University - Ho Chi Minh City, Quarter 6, Linh Trung Ward, Thu Duc City, Ho Chi Minh City, Vietnam

Received 12 March 2020; revised 26 May 2020; accepted 8 June 2020

Abstract:

***Vibrio parahaemolyticus* is the main causative agent of acute hepatopancreatic necrosis disease (AHPND) in shrimp. This study aimed to investigate how shrimp extracts affect the growth and virulence of an AHPND-causative strain known as *V. parahaemolyticus* XN9. To this end, the bacteria was cultured in media containing 3% extract of each of five shrimp types and their growth kinetics were compared against that from bacteria grown in brain-heart infusion (BHI) media. Eight-hour growth curves were constructed using the plate-counting method. The activity of five extracellular enzymes that contribute to bacterial virulence was examined using the agar-based method. The results showed that *V. parahaemolyticus* XN9's growth was strongly enhanced in all five shrimp extract media with the highest increase (25% greater than the BHI medium) found in the giant tiger prawn extract. Additionally, all the shrimp extracts boosted the extracellular enzymatic activity of *V. parahaemolyticus* XN9, although to different extents. In summary, the shrimp extracts, particularly that from the prawns, not only promoted the viability and growth of *V. parahaemolyticus* XN9 but also its extracellular enzymatic activities.**

Keywords: **extracellular enzymes, growth curve, shrimp extracts, viability, *Vibrio parahaemolyticus*, virulence factors.**

Classification number: **3.5**

1. Introduction

Vibrio parahaemolyticus is a Gram-negative, halophilic, non-spore-forming, curved, rod-shaped marine bacterium [1]. This bacterium is versatile in its ability to live as a free organism or as a parasite of marine or fresh-water zooplankton, fish, shellfish, and shrimp [2]. It has been reported as the leading food-born gastroenteritis causative agent in humans [3]. In addition, *V. parahaemolyticus* was also identified as the pathogen of AHPND, previously named the early mortality syndrome (EMS), which has caused serious damage to the global shrimp production in the last decade [4]. The disease was first identified in China in 2009 where it quickly spread to Vietnam in 2010, followed by Malaysia in 2011, Thailand in 2012, and finally expanded to the Western hemisphere after that [5]. A Vietnamese study in 2018 showed that this bacterium is highly ubiquitous in water samples (78.1%) and seafood (86.2%) from the Mekong delta [6]. In the region of Hanoi, *V. parahaemolyticus* was also found to be dominantly present in shrimp samples (>90%) [7]. Fortunately, not all of the *V. parahaemolyticus* strains are pathogenic. It has been proven that only a specific set of *V. parahaemolyticus,* those that produce the $PirA^{vp}$/$PirB^{vp}$ toxin, can cause AHPND [4, 8]. The ability to generate this binary toxin is determined by the genes located in a large plasmid residing within the bacterial cells. Genotyping analysis of the plasmid revealed the close relationship of Vietnamese AHPND isolates with the ones from China and Thailand [9]. However, the ability of *V. parahaemolyticus* to cause disease may also have contributions from other virulence factors [5]. Previous data indicated that extracellular enzymes are an important part of the bacterium's virulence [10-13]. Unfortunately, the study of the expression and activity of these enzymes is limited as the experimental outcome is greatly affected by the culture conditions. Many studies have shown that taking *V. parahaemolyticus* out of its inherent natural environment, specifically a shrimp or oyster body, would significantly affect its physiology, growth and virulence when stored or grown in nutrient media [14-18]. Therefore, in this study, we used the extracts of different shrimps that are potential hosts of *V. parahaemolyticus* to investigate the impact of these extracts on the growth and extracellular enzymatic activity of *V. parahaemolyticus*. Five shrimp types were used in the study, including white-leg shrimp (*Litopenaeus vannamei* or formerly called *Penaeus vannamei*), red-leg shrimp (a variety of *Penaeus vannamei*), giant tiger prawn (*Penaeus monodon*), giant river prawn (*Macrobrachium rosenbergii*), and greasyback shrimp (*Metapenaeus ensis*), which are AHPND-affected and major cultured shrimp. The results of this study would assist virulence research of *V. paraheamolyticus*.

2. Materials and methods

2.1. Materials

V. parahaemolyticus XN9 was generously provided by Nha Trang University, Khanh Hoa, Vietnam. The bacterial identity and association to AHPND was confirmed in the previous study [19]. Five kinds of shrimp including white-leg shrimp (*Litopenaeus*

*Corresponding author: Email: ntthoai@hcmiu.edu.vn

vannamei), red-leg shrimp (a variety of *Litopenaeus vannamei*), greasyback shrimp (*Metapenaeus ensis*), giant river prawn (*Macrobrachium rosenbergii*), and giant tiger prawn (*Penaeus monodon*) were purchased fresh from the Binh Dien market, Ho Chi Minh city, Vietnam in 2018.

2.2. Preparation of shrimp-extract containing media

The preparation of the shrimp extract media was adapted from the chopped meat culture protocol with modifications [20]. In brief, the shrimp were washed in distilled water, then grounded into a paste using blender and cooked at 60°C for 1 h. The obtained shrimp pastes were dried at 80°C and ground again to achieve shrimp extract powders. The drying time was adjusted to be around 3 h so that the net weight of the achieved shrimp extract powder was about 30% of the initial fresh shrimps' weight. The powders were then stored at 4°C for later use. The media was prepared with 3% shrimp extracts and 2.5% NaCl. The control medium to be used was BHI (Himedia, India) with 2.5% NaCl supplemented. All the media were adjusted to pH 7.0.

2.3. Growth analysis of V. parahaemolyticus under different shrimp extracts

The plate counting method was used to build the growth curve of *V. parahaemolyticus*. The formula $\mu=(\log_{10} X-\log_{10} X_0)/t\times2.303$ was applied where μ is the specific growth rate (SGR), X is the cell number or cell mass at a certain time, X_0 is the initial cell number or cell mass, and t is the time [21]. In short, an overnight culture at 30°C of *V. parahaemolyticus* XN9 in BHI broth (Himedia, India) with 2.5% NaCl supplemented was used to inoculate 50 ml in either BHI broth (Himedia, India) with 2.5% NaCl supplemented or in the medium containing 3% extract of either white-leg shrimp, red-leg shrimp, greasyback shrimp, giant river prawn, or giant tiger prawn. The initial OD was adjusted to an $OD_{620\ nm}$ of 0.05. The culture was incubated at 30°C under static conditions for 8 h. After each hour, 100 µl of culture was taken out to be plated on BHI agar.

2.4. Extracellular enzymatic activity analysis of V. parahaemolyticus under different shrimp extracts

Caseinase, hemolysin, lipase, gelatinase, and chitinase were examined using the agar-based method [22, 23]. To achieve this, *V. parahaemolyticus* XN9 was inoculated and cultured in either BHI broth (Himedia, India) with 2.5% NaCl supplemented or in a medium containing 3% extract of either white-leg shrimp, red-leg shrimp, greasyback shrimp, giant river prawn, or giant tiger prawn. The culture was incubated at 30°C, under static conditions and overnight. After that, the overnight culture was diluted to OD_{620nm}=0.05 and 10 µl of this suspension was dropped onto the surface of the BHI agar containing either 1.5% (w/v) skim milk, 2.0% gelatin (w/v), sheep blood agar, tributyrin agar, or 5% colloidal chitin for caseinase, gelatinase, hemolysin, lipase, and chitinase testing, respectively. The plates were incubated at 30°C overnight for the caseinase and gelatinase testing and for 48 h for the hemolysin, lipase, and chitinase testing. While *Vibrio cholerae* VCTC2012 (obtained from Vietnam type culture collection, kindly provided by Namkhoa Ltd, Vietnam) was used as a positive control for caseinase, gelatinase, hemolysin, and chitinase testing, *Staphylococcus aureus* ATCC 29213 (purchased from Lan Oanh Ltd, Vietnam) was used for lipase testing. After incubation, clear halos around the colonies were observed, which indicated that the activity of the testing enzyme was measurable. In the case of gelatinase, to observe the activity of the enzyme, the agar surface was immersed in saturated ammonium sulfate [$(NH_4)_2SO_4$] (JHD, China) that forms a cloudy precipitate with the remaining gelatin and results in a clear halo zone indicating where the gelatin was digested. The experiments were performed in triplicate.

2.5. Data analysis

The enzymatic activity (EA) was calculated as $EA=\frac{D-d}{2}$, in which *D* is the diameter of both the bacterial drop and the zone around the bacterial drop (mm) and *d* is the diameter of the bacterial drop itself (mm). The EA is graded as follows: (–) when no visible halo is present, (+) when the EA value is limited to 1-2 mm, and (++) when the EA value is greater than or equal to 2 mm [22]. Each test was performed in triplicate and the obtained data were analysed using one-way ANOVA (Excel software, Microsoft). The means were also analysed using t-tests ($p<0.05$) to compare the variation between the extracellular enzymatic activity of each test and the corresponding standard condition (2.5% NaCl, pH 8.5, 120 rpm and 30°C).

3. Results

3.1. Growth kinetics of V. parahaemolyticus XN9 in BHI and in media containing different shrimp extracts

The growth curves of *V. parahaemolyticus* XN9 in the different tested media are constructed and presented in Fig. 1. In all the tested media, *V. parahaemolyticus* reached a stationary phase after 5 h. After 8 h, *V. parahaemolyticus* XN9 reached a much higher CFU in all the shrimp extract media compared to the BHI medium (Fig. 1). The growth in BHI was monitored further for more than 24 h in the optimizing step, but no particular

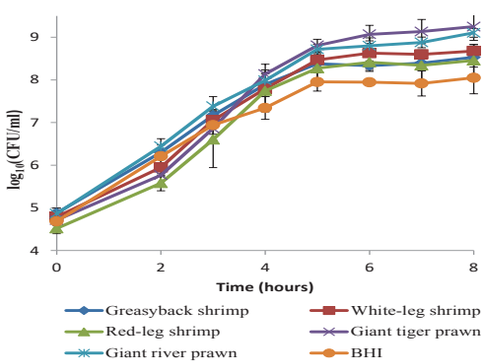

Fig. 1. Growth of *V. parahaemolyticus* XN9 in different media. *V. parahaemolyticus* XN9 was cultured in either BHI or a medium containing either greasyback shrimp, white-leg shrimp, red-leg shrimp, giant river prawn, or giant tiger prawn extract. The culture was carried out at 30°C, under static conditions, and observed for 8 h.

activity was observed after the bacteria reached its stationary phase (data not shown).

The calculated SGR also showed that *V. parahaemolyticus* XN9 grew very well in all shrimp extract media compared to the BHI medium (Table 1). While SGR in BHI was only 1.51±0.05 (h^{-1}), SGR in greasyback shrimp, white-leg shrimp, red-leg shrimp, giant river prawn, and giant tiger prawn media were all higher with SGR values of 1.61±0.01, 1.69±0.04, 1.73±0.10, 1.81±0.03, and 1.89±0.04 (h^{-1}), respectively. Therefore, except for greasyback shrimp, the SGR of *V. parahaemolyticus* XN9 in the other four tested shrimp extracts were significantly higher when compared to the BHI medium ($p<0.05$). The giant tiger prawn was the best medium, which brought about an increase of SGR by 25% followed immediately by giant river prawn at 20%.

Table 1. Effect of different shrimp extracts on specific growth rate (SGR) of *V. parahaemolyticus* XN9. The specific growth rate was calculated after 5 h, just before reaching the stationary phase. The values are expressed in mean ± standard deviation (SD).

Types of medium	SGR (h^{-1})
BHI	1.51±0.05
White-leg shrimp	1.69±0.04
Red-leg shrimp	1.73±0.10
Giant tiger prawn	1.89±0.04
Greasyback shrimp	1.61±0.01
Giant river prawn	1.81±0.03

3.2. Extracellular enzymatic activity of V. parahaemolyticus XN9 in BHI and in media containing different shrimp extracts

The extracellular enzymatic activity of *V. parahaemolyticus* (caseinase, gelatinase, lipase, hemolysis, and chitinase) in the presence of 5 different shrimp extracts media were examined. As a result, activity was observed in caseinase, gelatinase, and lipase for all the tested media but no activity was observed in hemolysin and chitinase (Fig. 2). While caseinase and gelatinase showed no significant difference in activity between the BHI and other shrimp extract media, the lipase activity, in contrast, was significantly higher in all shrimp extracts compared to BHI ($p<0.05$). Besides, the giant tiger prawn and giant river prawn, again, were the best media to promote the activity of the extracellular enzymes in *V. parahaemolyticus* (Fig. 2).

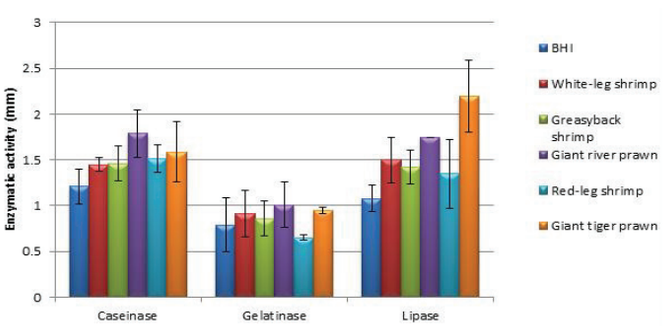

Fig. 2. Extracellular enzymatic activity of *V. parahaemolyticus* XN9 in different tested media. Hemolysin and chitinase did not express activity in any media thus were not shown.

4. Discussion

V. parahaemolyticus is ubiquitous in marine and estuarine environments. It can colonize multiple aquatic animals and cause disease in these animals and sometimes in humans, too. While the human isolates can survive well with *in vitro* culturing conditions, the strains that cause the disease in shrimp normally do not and require different optimal culture conditions [14, 24]. Their growth and viability are highly affected by culture conditions like salinity, pH, temperature, and medium type [25, 26]. In this study, we saw a significant improvement in the viability and growth of *V. parahaemolyticus* XN9, a shrimp disease-causing strain, when cultured in shrimp extract media compared to the optimal artificial culture medium [14]. Especially, prawn extracts including giant tiger and river prawn were the two extracts that strongly promoted the growth rate of the bacterium. The data suggests that the shrimp-adapted isolates should be cultured and studied using host-extract containing media.

Regarding extracellular enzymatic activity, our results also present strong activity of lipase, caseinase, and gelatinase when *V. parahaemolyticus* was precultured in shrimp extract media. As the number of bacteria was adjusted before the enzymatic testing, the activity of the enzymes seemed to be due to the bacterial cells themselves and not their quantity. The increase of lipase, caseinase, and gelatinase can provide an explanation for the improved growth and viability of *V. parahaemolyticus* when cultured in shrimp extracts. Additionally, the observed increase also implicated that the virulence of *V. parahaemolyticus* can be increased when existing with its hosts. Lipase, for example, was a common virulence factor of *V. parahaemolyticus* with about 80% of *V. parahaemolyticus* having lipase [13], while proteases (caseinase, gelatinase) were shown to be important to the pathogenesis of *Vibrio* [11, 27]. The increase of the enzyme is associated with the increased pathogenicity of the *Vibrio* species [11, 27].

On the other hand, no activity from hemolysin and chitinase was observed in *V. parahaemolyticus* XN9 in our study. Regarding hemolysin of *V. parahaemolyticus*, both thermostable direct hemolysin (TDH) or TDH-related hemolysin (TRH) are considered as major virulence factors of *V. parahaemolyticus* because of their ability to effectively induce cell lysis [2]. However, not all pathogenic strains contained hemolysins and, while 90% of human clinical isolates are hemolysin producers, shrimp disease-causing isolates are not [6, 19, 28]. Chitinase, on the other hand, was not investigated much as a virulence factor in *V. parahaemolyticus*. It seems that the chitinase-encoding gene lies on a prophage-like element and multiple genes are involved in the chitin-degrading ability of *V. parahaemolyticus* [29, 30]. The chitinase activity requires proper conditions to be induced [30] and thus it is understandable if it was not observed under our study settings.

5. Conclusions

In summary, our study showed that the media containing shrimp extract not only enhanced the viability of *V. parahaemolyticus* XN9, but also improved its production of virulence factors, especially

the giant tiger prawn and giant river prawn extracts. Therefore, it is suggested that shrimp extracts have the potential to replace conventional nutrient ingredients in preparation media, which assists the study of *V. parahaemolyticus* in laboratory conditions.

CRedit author statements

Nguyen Thuan Thien Truong, The Hao Nguyen: Conceptualisation, Methodology, Data curation, Formal analysis, Writing - Review & Editing; Cong Chinh Bui, Thi Thu Hoai Nguyen: Conceptualisation, Methodology, Writing - Original draft preparation, Writing - Review & Editing.

COMPETING INTERESTS

The authors declare that there is no conflict of interest regarding the publication of this article.

REFERENCES

[1] C.A. Broberg, T.J. Calder, K. Orth (2011), "*Vibrio parahaemolyticus* cell biology and pathogenicity determinants", *Microbes. Infect.*, **13(12-13)**, pp.992-1001, DOI: 10.1016/j.micinf.2011.06.013.

[2] D. Ceccarelli, L. Calegari, F. Asconeguy, et al. (2013), "Distribution and dynamics of epidemic and pandemic *Vibrio parahaemolyticus* virulence factors", *Front. Cell. Infect. Microbiol.*, **3**, DOI: 10.3389/ fcimb.2013.00097.

[3] E. Scallan, P.M. Griffin, F.J. Angulo, et al. (2011), "Foodborne illness acquired in the United States-major pathogens", *Emerg. Infect. Dis.*, **17(1)**, pp.7-15, DOI: 10.3201/eid1701.P11101.

[4] C.T. Lee, I.T. Chen, Y.T. Yang, et al. (2015), "The opportunistic marine pathogen *Vibrio parahaemolyticus* becomes virulent by acquiring a plasmid that expresses a deadly toxin", *Proc. Natl. Acad. Sci. U.S.A*, **112(34)**, pp.10798-10803, DOI: 10.1073/pnas.1503129112.

[5] P. Li, L.N. Kinch, A. Ray, et al. (2017), "Acute hepatopancreatic necrosis disease-causing *Vibrio parahaemolyticus* strains maintain an antibacterial type VI secretion system with versatile effector repertoires", *Appl. Environ. Microbiol.*, **83(13)**, DOI: 10.1128/AEM.00737-17.

[6] T.T.H. To, Y. Haruka, N.K. Thuan, et al. (2018), "Prevalence of *Vibrioparahaemolyticus* in seafood and water environment in the Mekong delta, Vietnam", *J. Vet. Med. Sci.*, **80(11)**, pp.1737-1742, DOI: 10.1292/jvms.18-0241.

[7] V.T. Tra, L. Meng, D. Pichpol, et al. (2016), "Prevalence and antimicrobial resistance of *Vibrio* spp. in retail shrimps in Vietnam", *Berl. Munch. Tierarztl. Wochenschr.*, **129(1-2)**, pp.48-51.

[8] R. Sirikharin, S. Taengchaiyaphum, P. Sanguanrut, et al. (2015), "Characterization and PCR detection of binary, pir-like toxins from *Vibrio parahaemolyticus* isolates that cause acute hepatopancreatic necrosis disease (AHPND) in shrimp", *PLOS ONE*, **10(5)**, DOI: 10.1371/journal. pone.0126987.

[9] J.E. Han, K.F. Tang, D.V. Lightner (2015), "Genotyping of virulence plasmid from *Vibrio parahaemolyticus* isolates causing acute hepatopancreatic necrosis disease in shrimp", *Dis. Aquat. Organ.*, **115(3)**, pp.245-251, DOI: 10.3354/dao02906.

[10] K. Kadokura, A. Rokutani, M. Yamamoto, et al. (2007), "Purification and characterization of *Vibrio parahaemolyticus* extracellular chitinase and chitin oligosaccharide deacetylase involved in the production of heterodisaccharide from chitin", *Appl. Microbiol. Biotechnol.*, **75(2)**, pp.357-365, DOI: 10.1007/s00253-006-0831-6.

[11] S. Miyoshi (2013), "Extracellular proteolytic enzymes produced by human pathogenic *vibrio* species", *Front. Microbiol.*, **4**, DOI: 10.3389/ fmicb.2013.00339.

[12] R. Wang, L. Sun, Y. Wang, et al. (2018), "Influence of food matrix type on extracellular products of *Vibrio parahaemolyticus*", *BMC Microbiol.*, **18(1)**, DOI: 10.1186/s12866-018- 1207-7.

[13] R.A. Costa, L.M.C. Amorim, R.L. Araujo, et al. (2013), "Multiple enzymatic profiles of *Vibrio parahaemolyticus* strains isolated from oysters", *Rev. Argent. Microbiol.*, **45(4)**, pp.267-270, DOI: 10.1016/S0325-7541(13)70035-X.

[14] P.T.L. Anh, L.Q. Khang, N.T. Thuc, et al. (2018), "Optimizing conditions for *Vibrio parahaemolyticus* culture and preservation", *7th International Conference on The Development of Biomedical Engineering in Vietnam*, pp.681-684, DOI: 10.1007/978-981-13-5859-3_115.

[15] H. Fujikawa, B. Kimura, T. Fujii (2009), "Development of a predictive program for *Vibrio parahaemolyticus* growth under various environmental conditions", *Biocontrol. Sci.*, **14(3)**, pp.127-131, DOI: 10.4265/bio.14.127.

[16] B. Liu, H. Liu, Y. Pan, et al. (2016), "Comparison of the effects of environmental parameters on the growth variability of *Vibrio parahaemolyticus* coupled with strain sources and genotypes analyses", *Front. Microbiol.*, **7**, DOI: 10.3389/fmicb.2016.00994.

[17] W.B. Whitaker, M.A. Parent, L.M. Naughton, et al. (2010), "Modulation of responses of *Vibrio parahaemolyticus* O3:K6 to pH and temperature stresses by growth at different salt concentrations", *Appl. Environ. Microbiol.*, **76(14)**, pp.4720-4729, DOI: 10.1128/AEM.00474-10.

[18] S.A. Soto-Rodriguez, R.L. Olvera, D.A. Palacios-Gonzalez, et al. (2019), "Characterization and growth conditions of *Vibrio parahaemolyticus* strains with different virulence degrees that cause acute hepatopancreatic necrosis disease in *Litopenaeus vannamei*", *J. World Aquacult. Soc.*, **50(4)**, pp.1-14, DOI: 10.1016/j. aquaculture.2016.12.022.

[19] N.N. Vu, P.T.T. Huyen, L.N.M. Tien, et al. (2017), "Investigating the production of extracellular enzymes of various *Vibrio parahaaemolyticus* isolates in Vietnam", *J. Biotechnol.*, **15(4)**, pp.703-710, DOI: 10.15625/1811-4989/15/4/13413.

[20] M.K. Bacic, C.J. Smith (2008), "Laboratory maintenance and cultivation of bacteroides species", *Curr. Protoc. Microbiol.*, **13**, DOI: 10.1002/9780471729259. mc13c01s9-13C.1.

[21] I. Pepper, C. Gerba, J. Brendecke (2011), *Environmental Microbiology: A Laboratory Manual, 2nd Edition*, Elsevier, 232pp.

[22] A.B. Vermelho, M.N. Meirelles, A. Lopes, et al. (1996), "Detection of extracellular proteases from microorganisms on agar plates", *Mem. Inst. Oswaldo. Cruz.*, **91(6)**, pp.755-760, DOI: 10.1590/s0074-02761996000600020.

[23] K. Ohishi, K. Murase, T. Ohta, et al. (2000), "Cloning and sequencing of a chitinase gene from *Vibrio alginolyticus* H-8", *J. Biosci. Bioeng.*, **89(5)**, pp.501-505, DOI: 10.1016/s1389-1723(00)89106-9.

[24] R. Paranjpye, O.S. Hamel, A. Stojanovski, et al. (2012), "Genetic diversity of clinical and environmental *Vibrio parahaemolyticus* strains from the Pacific Northwest", *Appl. Environ. Microbiol.*, **78(24)**, pp.8631-8638, DOI: 10.1128/AEM.01531-12.

[25] J. Lee (2009), *Laboratory Studies of Growth Conditions of Vibrio Parahaemolyticus in Pacific Oyster (Crassostrea gigas) with International Considerations to Shellfish-associated Illnesses in South Korea*, An Undergraduate Thesis, Oregon State University, 153pp.

[26] J.A. Gooch, A. DePaola, J. Bowers, et al. (2002), "Growth and survival of *Vibrio parahaemolyticus* in postharvest American oysters", *J. Food Prot.*, **65(6)**, pp.970-974, DOI: 10.4315/0362-028x-65.6.970.

[27] G. Osei-Adjei, X. Huang, Y. Zhang (2018), "The extracellular proteases produced by *Vibrio parahaemolyticus*", *World J. Microbiol. Biotechnol.*, **34(5)**, DOI:10.1007/s11274-018-2453-4.

[28] P. Raghunath (2014), "Roles of thermostable direct hemolysin (TDH) and TDH-related hemolysin (TRH) in *Vibrio parahaemolyticus*", *Front. Microbiol.*, **5**, DOI: 10.3389/fmicb.2014.00805.

[29] D. Castillo, K. Kauffman, F. Hussain, et al. (2018), "Widespread distribution of prophage-encoded virulence factors in marine *Vibrio* communities", *Sci. Rep.*, **8(1)**, DOI: 10.1038/s41598-018- 28326-9.

[30] T. Hirano, M. Okubo, H. Tsuda, et al. (2019), "Chitin heterodisaccharide, released from chitin by chitinase and chitin oligosaccharide deacetylase, enhances the chitin-metabolizing ability of *Vibrio parahaemolyticus*", *J. Bacteriol.*, **201(20)**, DOI: 10.1128/JB.00270-19.

DOI: 10.31276/VJSTE.63(4).66-71

Evaluating the potential of aquaculture in the Hoa Binh reservoir with carrying capacity and water quality indices

Diep Thi Ngoc Phan[1*], Binh Duc Nguyen[2], Paul Liew[1], Ha Thi Thu Pham[3], Tung Thanh Nguyen[1], Hieu Trung Nguyen[4]

[1]Vietnam Institute for Fisheries Economics and Planning, 10 Nguyen Cong Hoan Street, Ngoc Khanh Ward, Ba Dinh District, Hanoi, Vietnam
[2]Research Institute for Aquaculture Number 1, Dinh Bang Ward, Tu Son City, Bac Ninh Province, Vietnam
[3]University of Science, Vietnam National University - Hanoi, 334 Nguyen Trai Street, Thanh Xuan Trung Ward, Thanh Xuan District, Hanoi, Vietnam
[4]Research Institute for Aquaculture Number 2, 116 Nguyen Dinh Chieu Street, Da Kao Ward, District 1, Ho Chi Minh City, Vietnam

Received 26 March 2021; revised 8 May 2021; accepted 21 May 2021

Abstract:

Not only does the Hoa Binh reservoir play essential roles in water storage for electricity generation and flood regulation, but also it has great potential to aid aquaculture production. Presently, aquaculture production sits at around 9,200 tons/year; however, a recent MARD circular (#16 in 2015) estimated that maximum production would approach 10,000 tons/year in the productive photic zone. This paper supports increased capacity towards a sustainable commodity production model by optimizing production levels and farming practices. To reach this goal, it is necessary to determine water quality parameters using the Relative Water Quality Index (ReWQI) and carrying capacity (CC) analysis. Data was obtained from 30 sites at upstream, midstream, and downstream sections of the reservoir during the 2019 dry and wet seasons. The results from the ReWQI reflected good water quality potential (rated between 92-100) for aquaculture. The total nitrogen (TN) and total phosphorus (TP) levels of 10,794.9 kg/day and 1,965.4 kg/day, respectively, indicate high biological productivity resulting in strong fish growth potential. CC analysis and overall water quality reflect the potential for sustainable and increased productivity to 22,730.4 tons/year, which is an increase in production of over 13,200 tons/year compared to the current period. To reach a higher yield of 40 kg/year/m^3 within each cage (5,040 kg/cage/year), the corresponding increase in number needs to be 4,510 cages based on a common cage size of 126 m^3 (6x6x3.5 m). In order to reach these future production goals, this work concludes that the local government should begin spatial planning decisions based on appropriate cage allocation and distribution with respect for regular monitoring of water quality and nutrient load capacity of the environment to reach sustainable aquaculture development.

Keywords: **aquaculture, carrying capacity, Hoa Binh reservoir, water quality index.**

Classification number: **5.1**

1. Introduction

Aquaculture in the Hoa Binh reservoir plays important roles in the nourishment and poverty alleviation of its local people. Hydropower development in the reservoir has created substantial revenue for Hoa Binh province and lent support to other economic sectors such as tourism and fish transportation, all of which have a positive impact on local fishers. In 2019, the Hoa Binh reservoir had 4,670 fish cages that reached an output of approximately 9,200 tons [1]. According to the province's socio-economic development plan, aquaculture output of the reservoir is expected to increase to over 10,000 tons [2]. Aquaculture in the Hoa Binh reservoir is expected to develop towards efficient commodity production along sustainable goals [3]. However, in recent years, aquaculture has been threatened by the deterioration of reservoir water quality due to waste produced by activities such as tourism, water transport, aquaculture itself, as well as from unregulated waste and human activity from upstream sources. This waste has contributed to worsening water quality in the reservoir and consequently affects aquaculture [4]. Given this situation, farm managers should ask themselves two questions: 1) is the water quality suitable for aquaculture and 2) what are the maximum and sustainable aquaculture potentials of the reservoir? To answer these questions, it is necessary to evaluate the required suitability of water quality for aquaculture, determine the CC of the aquatic environment, and determine the maximum output that could be produced in the basin. Water quality for

*Corresponding author: Email: diepphan2014@yahoo.co.uk

aquaculture is assessed using the ReWQI [5, 6] while CC is calculated using an FAO tool in combination with the Legovic model [7]. ReWQI is selected to assess the quality of water in the Hoa Binh reservoir because it summarizes the results of water quality parameters and dispenses identifiable results (such as Poor, Moderate, and Good) for water quality [8-10]. The ReWQI also takes into account the different qualities of water sampled from different parts of the reservoir, as well as a number of water quality parameters chosen for that site.

In aquaculture, CC is understood as the ability of the aquatic environment to sustainably support the biological load caused by aquaculture operations [11]. Environmental carrying capacity (ECC) modelling incorporates the ReWQI and CC results to better understand the impact of human generated activities on the sustainability of the reservoir. The ECC is used because it determines nutrient and pollution impacts along with input thresholds that the reservoir can withstand [12]. Aquaculture carrying capacity (ACC) is the main metric that determines the productivity level of farming within the threshold as set by the ECC. This value should not exceed the tolerance of the ECC in that area (based on the permissible limits of environmental quality standards). This analysis also includes two important indicators: TN and TP. These are essential components of aquaculture feed as well as indicators of natural organic matter in the reservoir. Together, these elements contribute to algal growth and primary production capacity of a water body [13, 14].

This study contributes to the project titled "Research solutions to develop aquaculture in large reservoirs towards efficient and sustainable commodity production" developed by MARD. The result of this study will lead to follow-up studies on detailed spatial planning for aquaculture, re-arrangement of cages, and identification of suitable locations for aquaculture.

2. Materials and methods

2.1. Study area

The Hoa Binh hydropower reservoir (Fig. 1) was built between 1979-1984 with a basin area of 53,600 km² and volume of 9.45 billion m³ based on an average water level of 117 m. The reservoir has a multi-purpose design: it serves as a power generator that supplies electricity to the countryside, as well as a flood controller, natural disaster reducer, and a water supply for downstream areas [15]. The length of the reservoir is approximately 230 km and starts from the hydroelectric dam to the upper region of the Da river. Its location is 20°48'30.06" N; 105°19'23.53" E to 20°48'27.32" N; 105°5'42.22" E. Its rich aquatic diversity is attributed to the surrounding high mountains and thousands of hectares of vegetation and forests with high canopy coverage [16]. The main aquaculture species are *Bagarius bagarius*, *Mausoleum, yellow mausoleum, American catfish, red carp, black carp, and sturgeon* [16, 17].

2.2. Materials

In this study, eight water quality parameters (pH, temperature, DO, $N\text{-}NH_4^+$, $N\text{-}NO_2^-$, $N\text{-}NO_3^-$, TN, and TP) were sampled and analysed in June (dry season) and October (wet season) in 2019. Samples were taken at 2 depths (0.5 and 6 m) at 30 sites in across the upstream, midstream, and downstream areas of the reservoir (Fig. 1). Over the two seasons, 120 samples were collected and stored based on the Guidance of the National standards TCVN 6663-6:2008 [18], TCVN 5994:1995 [19], and TCVN 6663-3:2016 [20]. They were analysed based on the guide of APHA (2017) [21]. All collected samples were analysed at the Centre for Environment and Disease Monitoring in Aquaculture, Research Institute for Aquaculture No. 1 (RIA1).

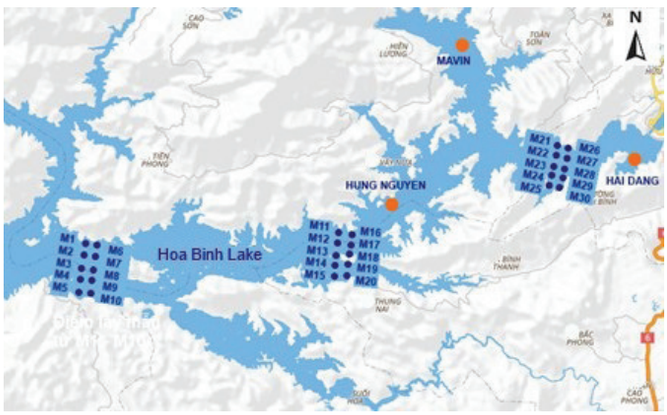

Fig. 1. A map of the Hoa Binh hydropower reservoir displaying the 30 monitoring sites (blue dots).

2.3. The ReWQI method

In this study, the ReWQI method is selected for analysis [5, 6]. The advantages of the ReQWI include the following: 1) the monitoring parameters do not coincide with the parameters defined in the issued guidelines of Vietnam WQI as well as other methods, which are difficult to apply; 2) the hierarchical scale depends on the survey parameter ($n \geq 2$), which is not self-regulating and therefore has no ambiguity; and 3) the weight is calculated according to the environmental standards of each unique parameter so it is not subjective and does not suffer from the virtual effect [5, 6].

The water quality parameters consist of pH, temperature, DO, $N\text{-}NH_4^+$, $N\text{-}NO_2^-$, $N\text{-}NO_3^-$, TN, and TP. In addition, Grade A1 surface water from the National Technical Regulations on Surface Water Quality (QCVN 08-MT:2015/BTNMT) and National Technical Regulations on Freshwater Fish Cage Culture - Conditions for Food Safety and Environmental Protection (QCVN 02-22:2015/BNNPTNT) are chosen for this evaluation. To analyse water quality parameters, the ReWQI equation is applied:

$$ReWQI = 100 * (1 - \frac{p_k}{p_n})$$

where $P_k = \sum_1^k W_i(q_i - 1)$; k is the number of parameters that do not fulfil the environmental standards ($qi>1$); $P_n = P_k + P_m$; n is the total number of observation parameters; $P_m = \sum_{i=1}^{m_1} W_i q_i + \sum_{i=1}^{m_2} W_i(1 - q_i)$; m_1 is the number of parameters with q_i=1; and m_2 is the number of parameters with q_i<1.

According to H.N. Pham (2020) [6], ReWQI is calculated using 5 steps given below:

Step 1. Calculate the individual indices or sub-indices, q_i, with the 6 water quality parameters pH, temperature, DO, N-NH_4^+, N-NO_2^-, and N-NO_3^-. These parameters are divided into 3 main groups:

Group 1: lower environmental standard: N-NH_4^+, N-NO_2^-, N-NO_3^-.

Group 2: upper environmental standard: DO.

Group 3: permitted standard in the fragment [a, b]: pH and temperature.

Step 2: Calculate the temporary weight W_i^*.

Step 3: Calculate the final weight W_i of each parameter i.

Step 4: Calculate the ReWQI.

Step 5: Apply the hierarchical rating scale (Table 1) for assessing water quality.

The water quality assessment hierarchy (5 levels) depends on *n* of the ReWQI. The calculation results of the rating scale of ReWQI (with n=6) are shown in Table 1.

Table 1. Hierarchical rating scale for assessing water quality with n=6.

ReWQI	Water quality	Colour	
92<ReWQI≤100	Good	Green	
83≤ReWQI≤92	Moderate	Yellow	
50<ReWQI≤83	Fair	Orange	
17<ReWQI≤50	Poor	Red	
0≤ReWQI≤17	Very poor	Brown	

The ReWQI value of each monitoring site is compared with the classification in Table 1 to infer the water quality for that monitoring site.

In this study, the assessment of ReWQI gives an overall picture of the water quality at the surface and middle stratum of the fish cage culture area in Hoa Binh reservoir and serves as an indicator of pollution in cage culture areas and further zones for water quality. Consequently, the assessment guides managers to develop workable solutions to reduce pollution and plan for appropriate aquaculture development in Hoa Binh reservoir.

2.4. Calculating carrying capacity

In this study, carrying capacity is calculated by combining the FAO carrying capacity tool, the T. Legović, et al. (2008) method [7], and the method devised by D.T. Tran, et al. (2012) [14]. Considering that most of the lake is viable for aquaculture, this tool can be used efficiently and quickly to test multiple new sites for cage farming suitability. This tool helps build a relationship between the human, terrestrial, and aquatic farming pressures on the reservoir and makes an effort to strike a balance in a sustainable way. A few standard parameters are entered into the equation to determine acceptable maximum levels of production that do not adversely affect the ecosystem and hydrology of the reservoir. The aquaculture carrying capacity can be defined as:

$$ACC=ECC/PL$$

in which ACC is the aquaculture carrying capacity; ECC is the environmental carrying capacity of TN or TP; and PL is the pollutant load of TN or TP. The ECC is defined as:

$$ECC=(C_{max}-C_o)x(1+R)xVx10^{-3}$$

in which C_{max} is the concentration of organic and inorganic nutrient loads in the environmental standard (mg/l); C_o is the concentration of nutrients at the time of the study (mg/l); R is the water exchange rate of the basin; and V is the average volume of the water body (m^3) [13, 14].

The total human, cattle, and poultry populations, as well as the reservoir area, were entered into a spreadsheet using the T. Legović, et al. (2008) model [7].

2.5. Discharge sources from livestock, human

The nutrient load from $PL_{CN/H}=NxPL_i$

in which $PL_{CN/H}$ is nutrient load from livestock, people (kg/year); N is the population number (person), total cattle and poultry; PL_i is nutrient load rate i (kg/cattle or kg/poultry per year) [22]. Nutrient discharge rate in domestic wastewater: Acceptable treatment of TN is 1.0 and TP is 0.25; primary treatment of TN is 2.0 and TP is 0.5; untreated TN is 4.0 and TP is 1.0 [23].

2.6. Discharge sources from agriculture

$PL_{NN}=SxPL_i$

Similarly, agriculture discharge was calculated as: PL_{NN} is the nutrient discharge load from agriculture (kg/year); S is land use (km^2); PL_i is nutrient load rate is according to different kinds of cultural land use (kg/km^2/year) [7, 22, 24, 25].

3. Results

3.1. Results of assessing the suitability of water quality for aquaculture using ReWQI

Based on data from the 30 monitored sites, water quality is more suitable at 0.5 m than 6 m in both dry and wet season. The maximum value of ReWQI at the sites at 0.5 m was 100 in both dry and wet seasons. The ReWQI at the 6 m depth ranged from 71 to 91 in the dry season and from 70 to

91 in the wet season in 2019. The results in Fig. 2 show that, water quality at the 30 sites during dry and wet seasons are at a "Good" level for aquaculture at 0.5 m. The ReWQI at 30 sites at 6 m are categorized as "Moderate" and "Fair" for aquaculture species. Among them, 18 sites had their water quality index categorized as "Moderate", and 12 sites categorized as "Fair" in the dry season. In the wet season, 15 sites were categorized as "Moderate" and 15 sites categorized as "Fair" water quality.

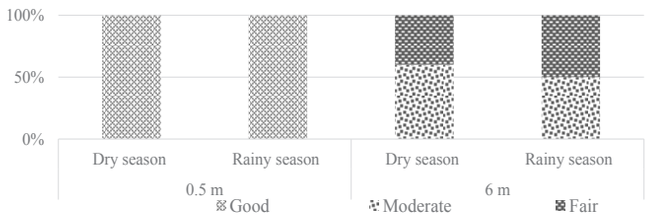

Fig. 2. Comparing water quality in 0.5 and 6 m depths.

In summary, the water quality at surface layer (0.5 m) is highly suitable for aquaculture. In the middle layer (6 m), water quality was "Moderate" to "Fair", consequently, the fish cages may require added aeration to improve the conditions.

3.2. Results of assessing the maximum aquaculture production by environmental carrying capacity assessment tool

Results of assessment of nutrient/pollutant load into Hoa Binh reservoir: Anthropogenic sources accounted for 75% of the nutrient load, while the remaining 25% was from general agriculture such as rice farming and horticulture. The total nutrient loads from residential, livestock and agriculture waste are 4,647.4 kg TN/day and 1,918.0 kg TP/day respectively. In comparison, the dry season produced 1,859.0 kg TN/day and 767.2kg TP/day with the wet season producing 7,435.8 kg TN/day and 3,068.7 kg TP/day. The total pollutant load of waste from tourist activity was 1,946.4 kg TN/day and 486.6 kg TP/day during dry and wet seasons. The total pollutant load from discharge to the reservoir 566.1 kg TN/day and 440.3 kg TP/day in dry season; and 2,012.9 kg TN/day and 1,258.1 kg TP/day in the wet season. The total pollutant load of waste from aquaculture for TN was 6,423.5 kg/day and TP 271.3 kg/day. Emission factors for 1 ton of fish over one-year culture period was 0.857 kg/day/ton for TN and 0.036 kg/day/ ton for TP. Cage fish farming takes place directly on the reservoir surface all year-round, so the amount of waste from aquaculture was divided equally for the dry and wet seasons: TN was 6,423.5 kg/day and TP was 271.3 kg/day.

Results of ECC in Hoa Binh reservoir: The water exchange rate (R) was 2.359 in dry season and 8.089 in wet season and TN and TP in the reservoir were at oligotrophic levels (in the dry season, TN was 0.018 mg/l and TP was 0.015 mg/l; during the wet season TN was 0.012 mg/l and TP was 0.010 mg/l) [26, 27]). ECC calculations show that, in the dry season, TN was 34,214.6 kg/day and TP was 4,030.5 kg/day. In the wet season, TN was 109,696.6 kg/day and TP was 14,136.2 kg/day.

Results of ACC: Based on a safety factor range from 0.3 to 0.7 in accordance with Circular 76/2017/TT-BTNMT [28], we chose a safety factor of 0.6 (60%). From results in Table 2, the Load ratio relative to ECC in the dry season was 31.6 and 9.8% in the wet season, which is within the 60% safety factor. Therefore, the amount of acceptable waste allowed to enter the reservoir in the dry season is 9,733.9 kg/day; while in the rainy season, the amount of waste permitted into the reservoir is 47,999.4 kg/day. With a Nutrient load rate of TN at 0.856 kg/day/ton fish, the ACC in dry season is 11,365.2 tons/season (productivity 2.8 tons/year) and the rainy season is 56,043.8 tons/season (productivity 13.82 tons/year).

Table 2. ECC aquaculture based on total nitrogen values.

Indicator	Unit	Dry season	Wet season
ECC	kg/day	34,214.6	109,696.6
ECC at 60% (ECC_{60})	kg/day	20,528.8	65,818.0
Total pollutant load ($\sum Q$)	kg/day	10,794.9	17,818.6
Load ratio relative to ECC	%	31.6	9.8
The amount of waste allowed into the reservoir: $ECC_{aquaculture}=ECC_{60}-\sum Q$	kg/day	9,733.9	47,999.4
Nutrient load rate from aquaculture (PL)	kg/day/ton fish	0.856	
$ACC=ECC_{aquaculture}/PL$	ton/season	11,365.2	56,043.8
	ton/year	22,730.4	112,087.5
Productivity (area 8,110 ha)	ton/ha/year	2.80	13.82

In this study, the TN/TP ratio in the dry and wet seasons is 1.2, which is less than 10, indicating that TN is the limiting factor of the reservoir and a major factor affecting the growth of algae in the reservoir [27]. ACC in the dry season is 22,730.4 and 112,087.5 tons/year in the wet season. Consequently, the output of 22,730.4 tons/year in the dry season is determined as the ACC for aquaculture production in Hoa Binh reservoir.

According to Vietnam Standards (QCVN 02-22:2015/MARD), the density of cages in the flowing water area can occupy a maximum of 0.2% of the water surface area, equating to 162,200 m^2. The size of a common cage with dimensions of 6x6x3.5 m has a volume of 126 m^3. From Table 3, we can calculate the fish capacity for each cage at between 35-40 kg/year/m^3. This yield was consistent with the survey carried out by V.T. Phan, et al. (2018) [29] as well as the Research Institute for Aquaculture No. 2 in 2019 [30] and L.V. Dieu (2020) [31]. We can also calculate the number of cages required for the lake, as described in Table 3.

Table 3. Number of cages allowed to be installed in Hoa Binh reservoir.

Cage surface area	Cage volume	Weight of fish per m^3	Fish weight per cage per year	Production threshold of fish in kg per year	Number of cages in reservoir	Surface area of cages in reservoir
m^2	m^3	kg/m^3	kg/cage/year	Ton/year	cages	m^2
(a)	(b)	(c)	(d=bxc)	(e)	(f=e/d)	(g=fxa)
		20	2,520		9,020	324,720.0
		25	3,150		7,216	259,776.0
36	126	30	3,780	22,730.4	6,013	216,468.0
		35	4,410		5,154	185,554.3
		40	5,040		4,510	162,360.0
36	126	50	6,300	22,730.4	3,608	129,888.0

Based on the surface area capacity of the lake, it can be seen that the maximum number of cages is 4,510 cages (volume of 126 m^3/cage) with a suitable water surface area of 162,360.0 m^2. The productivity of cages can vary depending on the cultured species and the production capacity of the farm, but the maximum is 40 kg/m^3.

4. Discussion

The results of the 2019 assessment of surface water quality at 30 monitoring points in Hoa Binh reservoir show that surface (0.5 m) water quality was categorized as "Good" for aquaculture while the middle layer (6 m) was deemed "Moderate" or "Fair" for aquaculture. The significance of the ReWQI as a practical tool is its combination of multiple water parameters such as pH, temperature, DO, $N\text{-}NH_4^+$, $N\text{-}NO_2^-$, and $N\text{-}NO_3^-$ into one metric. Meanwhile, the ECC index is measured against multiple pollution factors and their thresholds. By combining these indicators, this study is able to more accurately determine the extent and potential for aquaculture capacity. The parameters TN and TP are limiting factors and the difference in water quality between the two water depths suggests that there are other factors that still need to be considered when analysing the benefits of this tool; these factors include, for example, population changes, point source and non-point sources of pollution, as well as unpredictably low water levels filling the dam. Combining these data would enable managers to determine the future rate of expansion and evaluate the choice of other suitable aquaculture sites based on site characteristics and proximity to human activity. Comparing studies from 1992 to 2010 and in 2018 [15], water quality in the Hoa Binh reservoir has tended to deteriorate somewhat. This makes it increasingly necessary to maintain environmental monitoring and provide recommendations when the conditions are not suitable for aquaculture.

Depending on the fish species, an annual production of 22,730.4 tons/year measured during the dry season was preferred as the target range rather than 112,087.50 tons/year during the wet season due to the fact that the annual growth cycle of fish production takes approximately twelve to fifteen months. This conservative but realistic estimate is due to the fact that cages cannot be restocked with juvenile fish during the higher water levels in the wetter months. This is also due to the fact that TN is a limiting factor affecting biological growth in the reservoir throughout most of the year. Thus, the recommended potential for annual aquaculture production was determined to be 22,730.4 tons/year. At this stage, farmers should not target the higher ACC value, however, future farming methods using different species may be able to overcome this limitation. The suggested maximum number of cages is therefore 4,510 for the reservoir with an annual production target of 5,040 kg per cage per year based on approximately 35 to 40 kg/m^3 of fish per cage at the grow out stage.

It is therefore our recommendation that farmers need to apply appropriate fish density and improve feed formulations and feed controls to avoid negatively affecting water quality in order to sustainably cultivate fish [32]. In addition, coordinated cage placement would take advantage of freshwater flows and oxygen renewal in accordance with better management practices as a means of improving ecological and economic sustainability in farming practices. Aquaculture-based nutrient load sources of TN in the reservoir are 6,423.5 kg/day during the dry season and similar during the wet season. While suitable water quality is evident in the surface trophic layer, the nature of the aquatic environment means that it is difficult to determine where or how nitrification negatively impacts production. Future research would include monitoring water quality data in order to plan ahead and detect future spikes in nutrient loads compared with the existing data.

This is the first study on carrying capacity in the Hoa Binh reservoir, and, as such, only answers the question of how many tons of aquatic products can be raised in the reservoir in accordance with the environmental load. In order to determine the area and quantity to be farmed in each specific location, it is necessary to identify the potential sites for farming along with detailed spatial planning to distribute the number of cages accordingly. This study is part of a result of a project at the ministerial level of agriculture. Thus, VIFEP/MARD can use these results for follow-up studies. Based on these results, MARD should propose regulations that allow fish to be raised to the threshold of an environmental carrying capacity instead of the regulations in the National Technical Regulation Number 02-22:2015 of MARD on "freshwater fish cage culture - conditions for food safety and environmental protection".

5. Conclusions

The multiple competing functions of the hydropower reservoir between farming and human activity requires careful planning based on reliable data and forecasting. Based on the two research questions stated in the introduction regarding suitable water quality and maximizing aquaculture potential, this study proves that planners and farmers can be guided to utilize aquatic resources responsibly and should be provided with data that is relevant and practical. The expansion of aquaculture should be considered against these findings and therefore determine the pace and volume of this development. Since water quality indirectly impacts farmers and their profits, these findings will help determine how intensively fish cages should be managed when considering water

quality, pollutant loads, pollutant sources, and environmental carrying capacity. Regular monitoring of increases in P and N, as well as water quality indices in the designated sites along the reservoir, would dictate decision making for more productive sites for cage culture. Further eutrophication cannot be eliminated totally, therefore, monitoring is required to mitigate the negative effects of poor water quality.

CRedit author statements

Diep Thi Ngoc Phan, Binh Duc Nguyen, Paul Liew: Conceptualisation, Methodology, Data curation, Formal analysis, Writing - Review & Editing; Ha Thi Thu Pham, Tung Thanh Nguyen, Hieu Trung Nguyen: Conceptualisation, Methodology, Writing - Original draft preparation, Writing - Review & Editing.

COMPETING INTERESTS

The authors declare that there is no conflict of interest regarding the publication of this article.

REFERENCES

[1] Hoa Binh Fisheries Department (2020), *Report on The Implementation Results of The Tasks in The First 9 Months of The Year, and Key Tasks in The Last 3 Months of 2020* (in Vietnamese).

[2] Ministry of Agriculture and Rural Development (2015), *National Technical Regulation on Freshwater Fish Cage Culture - Conditions for Food Safety and Environmental Protection* (in Vietnamese).

[3] Ministry of Agriculture and Rural Development (2017), *Decision No. 3710/QD-BNN-KHCN dated September 15, 2017, Approving The Content and Funding of Scientific Research and Test Production Projects at Ministry level Will Begin from 2018* (in Vietnamese).

[4] Directorate of Fisheries, Ministry of Agriculture and Rural Development (2018), *Report on The Pilot Project on Protection, Regeneration and Development of Aquatic Resources in The Da River Basin in The Area of Hoa Binh Reservoir in The Period of 2018-2022* (in Vietnamese).

[5] H.N. Pham, L.K. Dong, V.A.T. Pham, et al. (2015), *Guidance on Assessing The Quality of The Air, Water and Soil Environment Using a Single and Composite Index,* Vietnam Education Publishing House, 199pp (in Vietnamese).

[6] H.N. Pham (2020), "Relative water quality index (ReWQI) - A new method for aggregate water quality assessment", *Water and Environment Journal,* **34(S1)**, pp.873-883, DOI: 10.1111/wej.12586.

[7] T. Legovic, R. Palerud, G. Christensen, et al. (2009), "A model to estimate aquaculture carrying capacity in three areas of The Philippines", *Science Diliman*, **20(2)**, pp.31-40.

[8] R.A. Deininger (1980), "A water quality index for rivers", *Water International*, **5(3)**, pp.16-21.

[9] A. Lumb, T.C. Sharma, J.F. Bibeault (2011), "A review of genesis and evolution of water quality index (WQI) and some future directions", *Water Quality, Exposure and Health*, **3(1)**, pp.11-24, DOI: 10.1007/s12403-011-0040-0.

[10] P.T.M. Hanh, S. Sthiannopkao, D.T. Ba, et al. (2011), "Development of water quality indexes to identify pollutants in Vietnam's surface water", *Journal of Environmental Engineering*, **137(4)**, pp.273-283, DOI: 10.1061/(asce)ee.1943-7870.0000314.

[11] L.G. Ross, T. Telfer, L. Falconer, et al. (2013), *Site Selection and Carrying Capacities for Inland and Coastal Aquaculture: FAO/Institute of Aquaculture, University of Stirling, Expert Workshop, 6-8 December 2010, Stirling, The United Kingdom of Great Britain and NorThern Ireland*, Food and Agriculture Organization of The United Nations, Rome.

[12] C.W. McKindsey, H. Thetmeyer, T. Landry, et al. (2006), "Review of recent carrying capacity models for bivalve culture and recommendations for research and management", *Aquaculture*, **261(2)**, pp.451-462, DOI: 10.1016/j.aquaculture.2006.06.044.

[13] J.S. Alabaster (1986), *Review of The State of Water Pollution Affecting Inland Fisheries in SouTheast Asia*, Food and Agriculture Organizatin of The United Nations, 25pp.

[14] D.T. Tran, V.M. Tran, T.T.T. Cao, et al. (2012), *Carrying Capacity in Halong - Bai Tu Long Bay*, Publishing House for Science and Technology, DOI: 10.13140/RG.2.1.1489.6883.

[15] K.D. Nguyen, Q.T. Doan (2018), "Water quality of Hoa Binh reservoir", *Conference: International Symposium on Lowland Technology (ISLT) 2018*, 9pp.

[16] Hoa Binh PPC (2014), *Resolution No. 12. Development of Raising Fish in Cages and Cages of Hoa Binh Hydropower Reservoir, Period 2014-2020* (in Vietnamese).

[17] Hoa Binh PPC (2018), *Decision No. 3118/QD-UBND, Approving The Project on Reviewing and Adjusting The Master Planning of The Agriculture Sector of Hoa Binh Province to 2020, Planning Toward 2030* (in Vietnamese).

[18] Ministry of Natural Resources and Environment (2018), *Water Quality - Sampling Part 6: Guidance on Sampling of Rivers and Streams* (in Vietnamese).

[19] Ministry of Natural Resources and Environment (1995), *Water Quality Sampling - Guidance on Sampling from Natural Lakes and Man-Made Lake* (in Vietnamese).

[20] Ministry of Natural Resources and Environment (2016), *Water Quality - Sampling - Part 3: Preservation and Handling of Water Samples* (in Vietnamese).

[21] E.W. Rice, R.B. Baird, A.D. Eaton (2017), *Standard Methodsfor The Examination of Water and Wastewater, 23rd Edition*, American Water Works Association, 1796pp.

[22] World Health Organization (1982), "Rapid assessment of sources of air, water, and land pollution", *Yogyakarta: Gadjah Mada University Press*, 113pp.

[23] World Bank (1993), *Pilot Application of Selected Aquaculture Planning and Management Tools in Indonesia, Thailand and Vietnam.*

[24] R.W. Howarth, G. Billen, D. Swaney, et al. (1996), "Regional nitrogen budgets and riverine N and P fluxes for The drainages to The North Atlantic Ocean: Natural and human influences", *Biogeochemistry*, **35**, pp.75-139, DOI: 10.1007/BF02179825.

[25] I. Valiela, G. Collins, J. Kremer, et al. (1997), "Nitrogen loading from coastal watersheds to receiving estuaries: New method and application", *Ecological Applications*, **7(2)**, pp.358-380, DOI: 10.1890/1051-0761(1997)007[0358:NLFCWT]2.0.CO;2.

[26] R.J. Davies-Colley, M.E. Close (1990), "Water colour and clarity of New Zealand rivers under baseflow conditions", *New Zealand Journal of Marine and Freshwater Research*, **24(3)**, pp.357-365, DOI: 10.1080/00288330.1990.9516430.

[27] University of Florida (2000), *A Beginner's Guide to Water Management Nutrients*, 37pp.

[28] Ministry of Natural Resources and Environment (2017), *Circular 76/2017/TT-BTNMT, Regulations Assessing The Capacity of Rivers to Receive Wastewater*, 12pp (in Vietnamese).

[29] V.T. Phan, V.T. Tran, T.N.D. Phan (2018), *Current Status Assessment of Aquaculture Development in Reservoirs with Area >5,000 ha,* Vietnam Institute for Economics and Planning, 79pp (in Vietnamese).

[30] Research Institute for Aquaculture No. 2 (2019), *Management, Rearangement, Stabilizing The Fish Cage Farming Area in Tri An Reservoir* (in Vietnamese).

[31] L.V. Dieu (2020), *Environmental Capacity Assessment of Pleikrong Hydropower Reservoir*, Vietnam Institute of Economics and Planning, 63pp (in Vietnamese).

[32] D. Hlavac, Z. Adamek, P. Hartman, et al. (2014), "Effects of supplementary feeding in carp ponds on discharge water quality: A review", *Aquacult. Int.*, **22(1)**, pp.299-320, DOI: 10.1007/s10499-013-9718-6.

DOI: 10.31276/VJSTE.63(4).72-78

An empirical relationship between $PM_{2.5}$ and aerosol optical depth from MODIS satellite images for spatial simulation over Ho Chi Minh city

Vo Quoc Bao[1, 2], Tran Thi Van[1, 2*]

[1]*Faculty of Natural Resources and Environment, Ho Chi Minh City University of Technology, 268 Ly Thuong Kiet Street, Ward 14, District 10, Ho Chi Minh City, Vietnam*
[2]*Vietnam National University - Ho Chi Minh City, Linh Trung Ward, Thu Duc City, Ho Chi Minh City, Vietnam*

Received 17 March 2021; revised 2 May 2021; accepted 13 May 2021

Abstract:

Air quality in megacities has been a pressing concern of environmental managers and scientists for decades. Indeed, particulate matter (PM), especially $PM_{2.5}$, is considered a dangerous particle that is harmful to human health. The current sparse monitoring network in Ho Chi Minh city (HCMC) does not accurately reflect the spatial distribution of fine particles in ambient air. Therefore, this research examines the relationship between ground-based station data and aerosol optical depth (AOD) imagery from the Moderate Resolution Imaging Spectroradiometer (MODIS) onboard the Terra/Aqua satellite to establish a $PM_{2.5}$ distribution map of HCMC. $PM_{2.5}$ concentration values monitored from two ground stations were collocated by time and space with Terra/MODIS AOD data from the period of 2016-2020. Pairs of values were checked for correlation and then fit to several regression functions. The most suitable function was chosen to simulate the quantified $PM_{2.5}$ distributions in the study area. A high correlation between $PM_{2.5}$ concentrations and AOD at the wavelength of green light (R^2=0.810) was found with a linear regression model. The results showed that the highest concentration of $PM_{2.5}$ was in February, and the mean value was higher than QCVN 05:2013 (32.5 µg/m^3 compared with 25 µg/m^3, annual mean). These results support the need for essential air quality monitoring in HCMC.

Keywords: **aerosol optical depth (AOD), air pollution, MODIS, $PM_{2.5}$.**

Classification number: **5.1**

1. Introduction

Fine particles possessing an aerodynamic diameter of less than 2.5 µm, also known as $PM_{2.5}$, are generated by both human-made and natural sources with the majority being from human-made activities like vehicle engines, power generation, and urban heat. [1]. According to World Health Organization (WHO), there is no safe threshold for inhaling these fine particles, either short term or long term, that avoids any adverse effects. Indeed, long-term exposure will increase specific age mortality risks especially to the elderly, children, and those with respiratory or cardiovascular diseases that place these individuals in risky health conditions. Besides this, the WHO report also states that fine particle exposure in high concentration can worsen lung and heart conditions, increase the number of hospital admissions, and even cause death [2]. In HCMC, rapidly increasing transportation density and numerous under-invested industrial parks are raising the air quality index higher year by year. According to the report of Green ID (2018a) [3] about the air quality in HCMC, the number of hours of which the air quality index was classified at an unhealthy level occupied 28.3% of the first trimester of 2018, which is much higher than the same period in 2016 and 2017 (0.6 and 9.6%, respectively). Understandably, the density of dust particle dispersion in the atmosphere continues to grow and become an enormous challenge for local authorities in charge of controlling and monitoring air quality.

In general, megacities of developing countries are still prioritizing economic growth over the environment and, in those cases, networks of fine particle monitoring stations remain limited. HCMC is no exception to this. The installation of only a few $PM_{2.5}$ ground-based stations restricts a thorough assessment of time-space dynamics of fine particles. Therefore, the real-time database of available $PM_{2.5}$ monitoring stations in the research area combined with a remote sensing technique brings a promising method to estimate $PM_{2.5}$ concentrations over the whole city.

An atmospheric remote sensing technique-based index called the AOD is currently being used in scientific research to examine the dispersion of particles of various sizes over large or small areas. AOD, sometimes known as the optical thickness (τ), is a measure of beam solar attenuation due to obstruction from dust or haze. In other words, AOD tells

*Corresponding author: Email: tranthivankt@hcmut.edu.vn

us how much direct sunlight reaches the Earth's surface after it is absorbed or scattered by dust particles. AOD is a dimensionless number and is determined by the amount of aerosol in an atmospheric vertical column from the Earth's surface to the top of the atmosphere over different wavelengths [4]. From an observer on the ground, an AOD of less than 0.1 is considered clean with characteristics of a clear blue sky, bright sun, and maximum visibility. As AOD increases to 0.5, 1.0, or even greater than 3.0, aerosols become so dense that the sun is obscured [5].

Some epidemiological studies on the health effects of air pollution were conducted by using measures of $PM_{2.5}$ collected from sparse networks of stationary ground monitors as the exposure metric [6-8]. However, such in-situ $PM_{2.5}$ monitoring stations gives data that represents only a small surrounding zone. Meanwhile, patients could come from other areas, so their acquired particulate-matter related diseases might not originate from the measured area. Therefore, to enhance the reliability of the association between $PM_{2.5}$ and hospital admissions, $PM_{2.5}$ data should be extracted from many more sources. In other words, there should be $PM_{2.5}$ data available for the whole research area and even its vicinity. Nowadays, to build a map of $PM_{2.5}$ dispersions, numerous studies aimed at finding the association between $PM_{2.5}$ and AOD have been conducted using high spatial-temporal coverage of satellite aerosol products. For example, I. Wijeratne (2003) [9] carried out research to find the relationship between AOD, which was computed from Landsat-7/ETM+, and polluted substances including PM_{10}, CO, NO, NO_2, SO_2, NH_3, O_3 and black particles (BP) and then mapped the urban air pollution dispersion across the Netherlands. Another research project from N. Kumar (2007) [10] examined the empirical relationship between $PM_{2.5}$ concentrations and MODIS-retrieved AOD (5-km spatial resolution) in the Delhi metropolitan area. A grid of 1×1.5 km^2 overlaid the research area, and $PM_{2.5}$ monitored at 113 sites were collocated by time and space with the AOD computed by using data from MODIS on the Terra satellite. The research showed a significant positive association between $PM_{2.5}$ and AOD, and 1% change in AOD explained the 0.52 ± 0.202% and 0.39 ± 0.15% change in $PM_{2.5}$ monitored within ±45 and 150 min intervals, respectively, of AOD data. The advantage of the above studies in predicting $PM_{2.5}$ concentrations is the support from plenty of real ground-based fine particle data to enhance the accuracy and dependability of the regression model. Besides regression analysis methods, some scientists have utilized simulation models to detect the variation tendency of the $PM_{2.5}$/AOD ratio of research areas, then verifying it by surfaced-measured $PM_{2.5}$ data. The chemical transport model (CTM) has been widely used by many researchers as global scale model [11-13]. Another model called geographically weighted regression (GWR), which is often used on a regional scale, has also been coming up in a lot of research [14-16]. These two models have been employed to construct the map of both horizontal and vertical distributions of $PM_{2.5}$ during the study period, and each model has certain advantages and limitations.

In Vietnam, especially HCMC, there are few studies on $PM_{2.5}$. Due to its distinctive characteristics like small size, light weight, and long retention time, V.D. Xuan, et al. (2017) [17] came up with a comprehensive research plan to investigate the elements in particles and predict the source of $PM_{2.5}$ generations. N.T.H. Giang, et al. (2014) [18] has also conducted research to investigate roadside levels and traffic emission rates of $PM_{2.5}$ in HCMC. However, no previous research has simulated $PM_{2.5}$ distributions over that area. Currently, since the in situ $PM_{2.5}$ monitoring stations are very sparsely distributed, there are some limitations like missing input data for simulation models, which typically demand a large amounts and variations of data to obtain an accurate simulation. Therefore, remote sensing technology that has been applied worldwide is used to examine and simulate particles over HCMC. T.T. Van, et al. (2014) [19] simulated the spatial distribution of PM_{10} across HCMC on a Landsat image in 2003. The research exploited the correlation of airborne particle - PM_{10} and AOD from Landsat to establish a map of PM_{10} dispersion in the atmosphere. The research rudimentarily showed the potential application of remote sensing technology in monitoring dust particles in the air. Four years after the first trial, to evaluate the increasing level, T.T. Van, et al. (2018) [20] expanded the research by building an additional map of PM_{10} distribution in 2015 over HCMC. The 2015 PM_{10} pollution level was more serious when compared with the map from 2003.

In this research, regional ground-based $PM_{2.5}$ concentrations are estimated directly from MODIS-based AOD by regression analysis. Then, $PM_{2.5}$ are simulated on MODIS imagery on 5 representative days for each month in the dry season.

2. Data and methods

2.1. Data

The data for this research comes from 2 main sources: (a) ground-based $PM_{2.5}$ concentrations from 2 in-situ, real-time monitoring stations at the United State (US) Consulate and Environmental Source Samplers, Inc, respectively, in HCMC and (b) MODIS based-AOD extracted from the Terra/Aqua satellite.

Ground-based $PM_{2.5}$ concentrations:

- $PM_{2.5}$ data were extracted from a continuous ambient monitoring station located at the US Consulate in HCMC (coordinates: 10°46'59.9 N, 106°42'03.2 E). Besides this, fine particle concentration was also collected from a different monitoring station invested by the company Environmental

Source Samplers (coordinates: 10°48'54.5 N, 106°43'11.0 E). Both ground-based stations record 24-h atmospheric $PM_{2.5}$ data with high accuracy.

- The Terra satellite housing MODIS circles earth every day and passes over the research area at a certain time interval. The Terra satellite acquires daily images of HCMC at the period of 10:00-11:00 am (Vietnam Time Zone, UTC+7), while the Aqua satellite does so between 2:00-3:00 pm. Therefore, in this research, $PM_{2.5}$ data were extracted within this time interval for data synchronization. Furthermore, MODIS image quality significantly depends on weather and cloud coverage, so dust particle data were collected on clear-sky days of the dry season from January to April (2016-2020).

MODIS Imagery based-AOD: The aerosol optical depth of the MODIS's Terra and Aqua satellites is computed by the National Aeronautics and Space Administration (NASA) through two important algorithms, namely, Dark Target and Deep Blue. AOD retrieved from MODIS imagery has a spatial resolution of 3 km and is stored online for free download. On the satellite, there are seven spectral bands with wavelengths of 0.47, 0.55, 0.66, 0.865, 1.24, 1.64 and 2.13 µm measured by MODIS. However, scattering and absorption of both molecules and aerosols in the atmosphere are only important and occur in visible and near-infrared regions [21]. Besides, research works by T.T. Van, et al. (2012, 2014) [19, 22] on PM_{10} distribution from SPOT 5 and Landsat satellite imagery also stated that airborne particulate matter showed better scattering at visible wavelengths. Therefore, this research focused on measuring and assessing the strength of the relationship between MODIS-AOD at 3 wavelengths, namely, 0.47, 0.55 and 0.66 µm, and the corresponding $PM_{2.5}$ concentration data.

2.2. Methods

There are two types of spatial resolutions for MODIS-AOD, which are 10 km and 3 km. In this research, since the simulated area was a city and not an entire region, 3-km spatial resolution was used to ensure the highest accuracy for the correlation investigation.

In this study, MODIS-based AOD at the coordinates of 2 ground-based continuous $PM_{2.5}$ monitoring stations in HCMC were extracted. Besides this, $PM_{2.5}$ data from the two stations at the time the MODIS satellite passed and scanned the research area were collected. The majority of the acquired data was in the dry season when the weather was cloudless. Since the resolution of MODIS imagery was quite low (3 km in space), some retrieved AOD values were not located exactly at the coordinates of the $PM_{2.5}$ stations, but they were not greater than a distance of 1.5 km. Additionally, since the monitoring device gives 1 h worth of data, there is a slight discrepancy compared with the time the MODIS imagery was acquired (less than 30 min).

The main research method in this work is correlation analysis, which is a statistical technique that is used to measure how strongly a pair of 2 variables are related to each other. In this research, 2 variables were specifically determined by real-time measurement values of $PM_{2.5}$ and AOD from MODIS. An advantageous result in correlation analysis allowed the next step of using a regression function to simulate $PM_{2.5}$ concentration distributions across the study area. The dataset was divided into two parts: training data (55 values in the stage of 2016-2019) to establish the model and testing data (8 values in 2020) to check the reliability and accuracy of the model.

Firstly, a Q-Q test was conducted to check the normal distribution of all datasets. All data that included real-time $PM_{2.5}$ concentrations and MODIS-AOD of 3 different wavelengths (0.47, 0.55 and 0.66 µm) were tested to assess if they are normally distributed.

Pearson analysis is the next step to check the correlation between two quantitative and continuous variables, which are $PM_{2.5}$ data and AOD, in this research. The purpose of employing the Pearson analysis was to check the strength of the relationship between $PM_{2.5}$ and AOD at the 3 types of wavelengths mentioned above. The Pearson coefficient (R) ranges from -1 to +1. The closer R is to +1 or -1, the more closely AOD and $PM_{2.5}$ are related (SPSS tutorial) [23].

Based on the Pearson's coefficient of correlation analysis, any wavelengths that show AOD is not correlated with $PM_{2.5}$ are removed. Conversely, the remaining AODs that show high correlation with $PM_{2.5}$ are applied to build the regression model using the least squares method. Besides, in our research, we examined the test not only with linear models, but other regression models (Table 1), to find the best-fit function. All steps were conducted by statistical software (SPSS). In SPSS analysis, selecting the best model that mathematically describes the relationship between two variables is based on three criteria. Here, the Sig Anova and Sig coefficient (or p-value) results from SPSS must be less than 5% (significant level). This means the null hypothesis can be discarded and that there exists an association between the two variables. After that, R^2 was the final criterion used to determine the best model.

Finally, to verify the feasibility of the regression model, root mean square error (RMSE) in Eq. 1 was used to compare the deviation between $PM_{2.5}$ computed by the regression model and the real $PM_{2.5}$ data from the testing dataset. Keep in mind that AOD represents a vertical column of aerosol from the Earth's surface to the satellite, which includes both particle and liquid droplets, and that $PM_{2.5}$ is mainly concentrated and dispersed near the ground and is almost always in particle form. Therefore, the elucidated relationship would be affected by these factors. RMSE is given by:

$$RMSE = \sqrt{\frac{1}{n}\sum(P_{cal} - P_{meas})^2} \quad (1)$$

where n is the number of samples, P_{cal} was the value of $PM_{2.5}$ calculated from the regression function and P_{meas} was the $PM_{2.5}$ that was measured by the ground-based monitoring stations.

Table 1. Equations of the different regression models between $PM_{2.5}$ and AOD (IBM) [24].

	Curve estimation regression models	Regression models $PM_{2.5}$ = f(AOD)
1.	Linear	$PM_{2.5}$=×AOD+β
2.	Logarithmic	$PM_{2.5}$=α×ln(AOD)+β
3.	Inverse	$PM_{2.5}=\frac{\alpha}{AOD}+\beta$
4.	Quadratic	$PM_{2.5}$=α×AOD^2+β×AOD+γ
5.	Cubic	$PM_{2.5}$=α×AOD^3+β×AOD^2+γ×AOD+ε
6.	Power	$PM_{2.5}$=AOD^{α}×β
7.	Compound	$PM_{2.5}$=α^{AOD}×β
8.	S-curve	$\ln(PM_{2.5})=\frac{\alpha}{AOD}+\beta$
9.	Logistic	$PM_{2.5}=\frac{1}{\alpha^{AOD}\times\beta+\frac{1}{\gamma}}$
10.	Growth	ln($PM_{2.5}$)=α×AOD+β
11.	Exponential	ln($PM_{2.5}$)=α×AOD+ln(β)

Results and discussion

Normal distribution test for $PM_{2.5}$ and AOD data

The probability Q-Q plot was used to check if $PM_{2.5}$ and AOD data were normally distributed. The results are shown in Fig. 1.

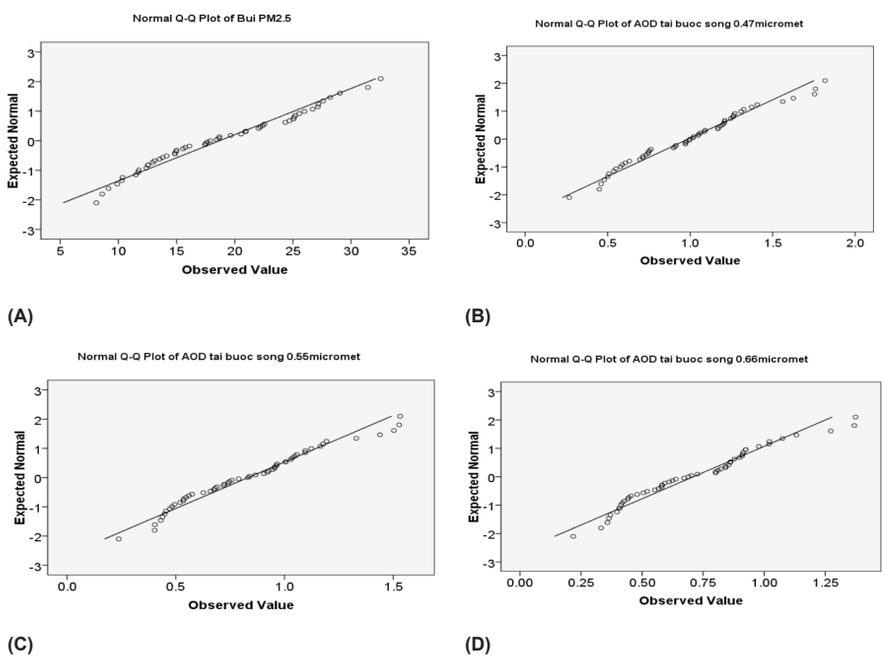

Fig. 1. Normal Q-Q Plot of (A) $PM_{2.5}$, (B) AOD-470 µm, (C) AOD-550 µm, and (D) AOD-660 µm.

If the datasets are closely distributed along the line in the Q-Q plots, it can be concluded that they have a normal distribution. In contrast, if the data points are scattered far from the line, it is obvious that the dataset is not normally distributed. The Q-Q plot for $PM_{2.5}$ and AOD in the 3 wavelengths (470, 550 and 660 µm) in Fig. 1 are dispersed very closely along the diagonal line in each case. Therefore, it was concluded that the dataset of $PM_{2.5}$ and the 3 AODs were normally distributed.

2.3. Pearson test to find the correlation between $PM_{2.5}$ and AOD

The correlation analysis between MODIS-AOD and $PM_{2.5}$ at 3 wavelengths (0.47, 0.55 and 0.66 µm) was a crucial and decisive stage of the research. In this step, since the datasets were quantitative variables, the Pearson test was selected to evaluate the correlation. The testing results are shown in Table 2.

Table 2. Correlation between $PM_{2.5}$ and AOD by Pearson test.

		AOD at the wavelength of 0.47 µm	AOD at the wavelength of 0.55 µm	AOD at the wavelength of 0.66 µm
$PM_{2.5}$	Pearson correlation	0.870**	0.900**	0.886**
	Sig. (2-tailed)	0.000	0.000	0.000

**: correlation is significant at the 0.01 level (2-tailed).

In general, the Pearson correlation analysis in Table 2 demonstrates positive relationships between $PM_{2.5}$ and AODs at 3 wavelengths with p=0.000. However, the $PM_{2.5}$ concentrations and AOD of green light (0.55 µm) indicated the most significant correlation at the 0.01 level (2-tailed) with R=0.900, while blue and red lights showed lower correlation levels of R=0.870 and 0.886, respectively. Therefore, we chose the green light AOD (0.55 µm) to build the regression model for $PM_{2.5}$.

2.4. Building the regression model for $PM_{2.5}$

After the Pearson correlation test, regression analysis was the next step to determine the most adequate model for this correlation. The regression models of $PM_{2.5}$ and AOD-0.55 µm built by SPSS are shown in Table 3.

Table 3. The regression models between $PM_{2.5}$ and AOD at wavelength of 0.55 µm.

Number	Models	R^2	Sig. (Anova)	Sig. (Coefficients)	
1	Linear	0.810	0.000	AOD Constant	0.000 0.003
2	Logarithmic	0.766	0.000	ln(AOD) Constant	0.000 0.000
3	Inverse	0.608	0.000	1/AOD Constant	0.000 0.000
4	Quadratic	0.812	0.000	AOD AOD^2 Constant	0.01 0.583 0.413
5	Cubic	0.821	0.000	AOD AOD^2 AOD^3 Constant	0.501 0.123 0.105 0.070
6	Power	0.773	0.000	ln(AOD) Constant	0.000 0.000
7	Compound	0.773	0.000	AOD Constant	0.000 0.000
8	S-curve	0.647	0.000	1/AOD Constant	0.000 0.000
9	Logistic	0.773	0.000	AOD Constant	0.000 0.000
10	Growth	0.773	0.000	AOD Constant	0.000 0.000
11	Exponential	0.773	0.000	AOD Constant	0.000 0.000

From Table 3, we could conclude that all models were suitable to use at a confidence of 95% because all sig. Anova results were less than 5%. However, the sig. coefficients of the quadratic and cubic models were greater than 5%, so these models were rejected. Among the remaining models, the inverse had the lowest R^2 (0.608) while linear had the highest value (0.810). Therefore, the linear model was selected to build the regression model with the standard error of 5.93 µg/m^3 (Eq. 2, Fig. 2) and it is given by:

$$PM_{2.5}=36.684\times AOD+6.839 \quad (2)$$

Equation 2 is applied to the testing dataset (8 values) to check the reliability of the regression model. The calculated $PM_{2.5}$ and the ground-based measured $PM_{2.5}$ are displayed in Table 4.

Table 4. Calculated and measured $PM_{2.5}$ of testing dataset.

Number	Date of simulation	Calculated $PM_{2.5}$ (µg/m^3)	Measured $PM_{2.5}$ (µg/m^3)
1	5-Jan 2020; 10:00	48.6	49.4
2	13-Jan 2020; 14:00	22.4	28.0
3	13-Feb 2020; 10:00	19.3	20.9
4	24-Feb 2020; 13:00	45.3	48.3
5	26-Feb 2020; 10:00	50.9	60.2
6	27-Feb 2020; 11:00	23.7	25.4
7	12-Mar 2020; 9:00	14.9	18.8
8	1-May 2020; 10:00	16.0	15.7

From Eq. 1, the RMSE of the testing dataset was 4.3 µg/m^3, which demonstrated that the deviation between calculated and measured $PM_{2.5}$ was not significant.

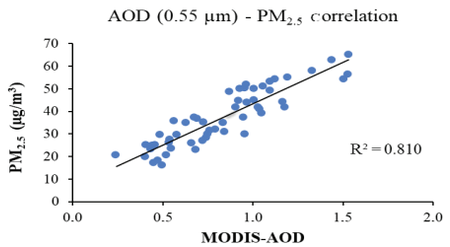

Fig. 2. Linear regression model between $PM_{2.5}$ and AOD at wavelength of 0.55 µm.

2.5. Mapping $PM_{2.5}$ distributions across HCMC

The regression model of $PM_{2.5}$ and AOD in the wavelength of 0.55 µm was employed to build a $PM_{2.5}$ map by ArcGIS. For an objective assessment, $PM_{2.5}$ was simulated at representative days in each month from December 2017 to April 2018.

The map of $PM_{2.5}$ distributions in HCMC was established on a MODIS satellite image at 10:00 am on representative days of each month in the dry season (Table 5). At this time, the industry was working, the traffic density was already high, and a circulation of trucks was allowed in the city; so 10:00 am could be considered as one of the largest dust generation times in a day. The map of Fig. 3 shows that $PM_{2.5}$ concentrations are higher at existing central districts such as districts 1, 3, 5, Tan Binh, Phu Nhuan and Go Vap. This could be explained by the tremendous intensity of transportation on main roads and infrastructure density in each section, especially at rush hour. Besides, some existing factories in industrial parks such as the Tan Binh, Tan Tao, and Le Minh Xuan industrial parks, have degraded emission treatment systems and discharge a large amount of gas that includes fine particles. In contrast, in suburban territories/districts such as Cu Chi, Binh Chanh, and Can Gio that have small traffic density and fewer construction, $PM_{2.5}$ tended to be lower. Especially, in the Can Gio district, the development of mangrove forests proved advantageous to the prevention of invading $PM_{2.5}$ from other areas.

Table 5. Statistics of $PM_{2.5}$ concentrations by representative days.

Dates	Mean	Max	Min
23-Dec-2017	19.9	28.9	10.34
03-Jan-2018	26.6	44.1	11.6
04-Feb-2018	32.5	49.7	16.6
11-Mar-2018	25.2	37.8	16.5
09-Apr-2018	24.1	41.7	14.1

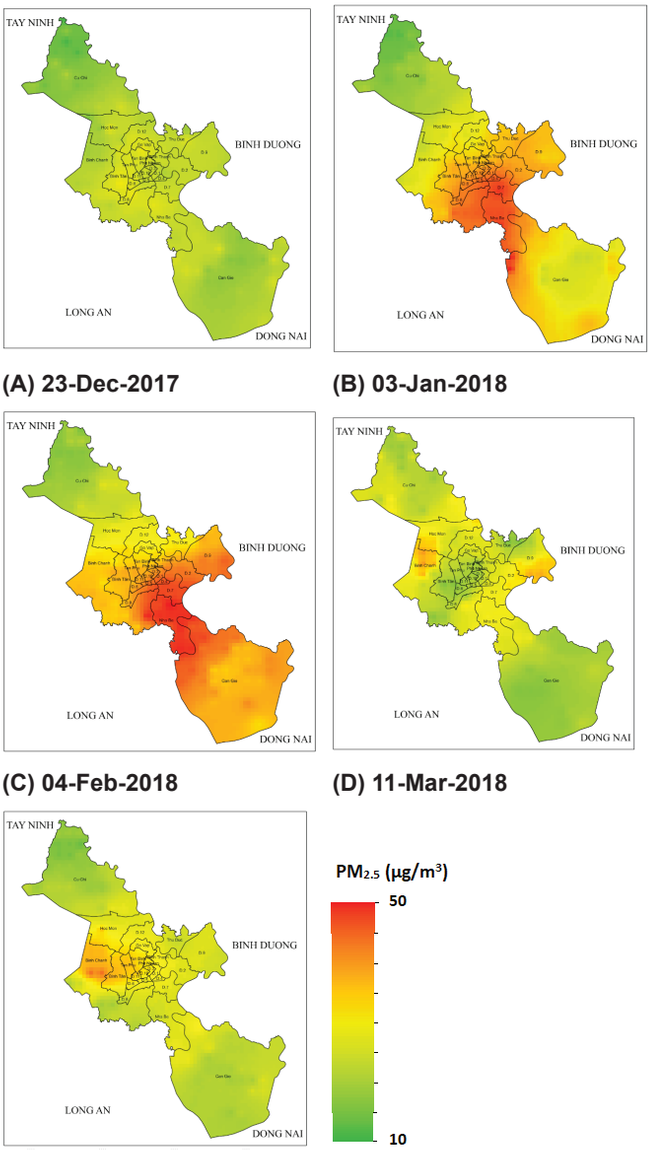

Fig. 3. $PM_{2.5}$ distributions over HCMC on (A) 23-Dec-2017, (B) 03-Jan-2018, (C) 04-Feb-2018, (D) 11-Mar-2018, and (E) 09-Apr-2018.

Binh Chanh and Cu Chi are known as two extensive land areas of HCMC where many industrial parks are on the plan of investment, so they can potentially become more and more polluted in the near future.

On 23-Dec-2017, since this is the transition time between the rainy and dry seasons, the average $PM_{2.5}$ over the entire HCMC was low (19.9 µg/m^3) (Table 5). However, $PM_{2.5}$ concentrations gradually increased over the next few months. At the peak of the dry season in February, the $PM_{2.5}$ mean was 32.5 µg/m^3, which is higher than the threshold specified in the National Technical Regulation on Ambient Air Quality, QCVN 05:2013 (25 µg/m^3, average in a year) [25]. In February, almost the entire south region of HCMC was ranked as a serious pollution area. The $PM_{2.5}$ concentrations at some places were at a high level with the highest value reached being 49.7 µg/m^3 (Table 5). Although these data are only for a few representative days for each month in the dry season, it showed that inside HCMC there are still areas that $PM_{2.5}$ concentrations exceeded Vietnamese standards every month (Fig. 3). With the rapid development of industry and economy, this is a serious warning of declining air quality in HCMC.

At present, the air quality in HCMC receives more and more concern from environmental management authorities and scientists alike. Many non-governmental organizations have been established with the purpose to prevent overwhelming air pollution and especially eliminate fine particles like $PM_{2.5}$ from the air. Although HCMC has been evaluated to be less polluted than Hanoi, the capital of Vietnam (Green ID, 2018b) [26], it is necessary to control and diminish the gas emissions generated from vehicles and industrial plants. Tackling the air pollution in HCMC is difficult to work and a long-term effort must be established and resolved in specific stages. Polluted substance dispersion surveillance is one of the first steps. In recent years, remote sensing has been demonstrated to be a distinctive tool for pollution monitoring.

In this research, remote sensing technology has been applied to simulate $PM_{2.5}$ concentrations on MODIS satellite images. Despite the low spatial resolution of MODIS satellite images, a daily image is nonetheless supplied so the progress of $PM_{2.5}$ distributions can be monitored, which allows time to find an appropriate treatment solution. Besides, to get more detailed $PM_{2.5}$ map, other higher resolution satellite images like Landsat or Sentinel can be used to build a city-level perspective of $PM_{2.5}$ dispersions.

The map of $PM_{2.5}$ distribution based on satellite images temporarily play an important role as the basis for environmental managers in HCMC to monitor the progress of fine particle generation in the atmosphere. Then, planning reasonable policies to firstly minimize the impact of $PM_{2.5}$ on human health and finally cut the sources of $PM_{2.5}$ emissions as much as possible for the purpose of sustainable development.

One more advantage of this research, when compared with others, is the accuracy. Since this research is based on the correlation between continuous quantitative variables, $PM_{2.5}$ data are being measured by continuous monitoring stations and AOD values from MODIS satellites are also being derived every day. Therefore, the more data received, the greater the accuracy of the model.

3. Conclusions

In this paper, the simulation of $PM_{2.5}$ via AOD from MODIS satellite imagery was derived from a simple regression model combined with remote sensing technology. Remote sensing is not a new tool to map particulate matter, but it is a cutting-edge technology that can be applied to many cities with sparse ground monitoring stations like HCMC. This research has had an initial success in verifying the assumption of an association between $PM_{2.5}$ concentrations and AOD. According to the correlation analysis result, $PM_{2.5}$ showed the best correlation with AOD at the green wavelength (0.55 µm) in form of linearity (R^2=0.810). On the scientific side, this research serves as a basis for further studies that apply remote sensing to air quality monitoring. For society, this research will help environmental managers as a reference source to issue policies that mitigate and prevent $PM_{2.5}$ emissions in HCMC.

CRedit author statements

Vo Quoc Bao, Tran Thi Van: Conceptualisation, Methodology, Data curation, Formal analysis, Writing - Review & Editing.

ACKNOWLEDGEMENTS

This research was funded by HCMC University of Technology, Vietnam National University, HCMC, under grant number T-MTTN-2020-39.

COMPETING INTERESTS

The authors declare that is no conflict of interest regarding the publication of this article.

REFERENCES

[1] GOV.UK (2019), *Public Health: Sources and Effect of $PM_{2.5}$, Local Air Quality Management (LAQM) Support*, Department for Environment Food & Rural Affairs.

[2] WHO (2005), *Air Quality Guidelines, Global Update 2005*, 496pp, WHO regional office for Europe.

[3] Green Innovation and Development Centre (2018a), *Current Status of Ambient Air Quality in HCMC - Quarter 1*, 3pp.

[4] Global Monitoring Laboratory, *SURFRAD Aerosol Optical Depth,* https://gml.noaa.gov/grad/surfrad/aod/, accessed 15 January 2021.

[5] NASA (2019), *Dark Target, Aerosol Retrieval Algorithm*, https:// darktarget.gsfc.nasa.gov/, accessed 15 January 2021.

[6] T. Lokman, A. Omar, K. Ferhat, et al. (2008), "Particulate matter ($PM_{2.5}$, $PM_{10-2.5}$, and PM_{10}) and children's hospital admissions for asthma and respiratory diseases: A bidirectional case-crossover study", *Journal of Toxicology and Environmental Health, Part A*, **71(8)**, pp.512-520, DOI: 10.1080/15287390801907459.

[7] Y. Guo, Y. Jia, Y. Pan, et al. (2009), "The association between fine particulate air pollution and hospital emergency room visits for cardiovascular diseases in Beijing, China", *Science of The Total Environment*, **407(17)**, pp.4826-4830, DOI: 10.1016/j.scitotenv.2009.05.022.

[8] C. Feng, J. Li, W. Sun, et al. (2016), "Impact of ambient fine particulate matter ($PM_{2.5}$) exposure on The risk of influenza like-illness: A time-series analysis in Beijing, China", *Environmental Health*, **15(1)**, pp.1-12, DOI: 10.1186/s12940-016-0115-2.

[9] I. Wijeratne (2003), *Mapping of Dispersion of Urban Air Pollution Using Remote Sensing Techniques and Ground Station Data*, Master Thesis, International Institute for Geo-Information Science and Earth Observation Enschede, The NeTherlands.

[10] N. Kumar (2007), "An empirical relationship between $PM_{2.5}$ and aerosol optical depth in Delhi Metropolitan", *Atmos. Environ.*, **41(21)**, pp.4492-4503, DOI: 10.1016/j.atmosenv.2007.01.046.

[11] Y. Liu, P. Koutrakis, R. Kahn (2007), "Estimating fine particulate matter component concentrations and size distributions using satellite-retrieved fractional aerosol optical depth: Part 2 - A case study", *J. Air Waste Manag. Assoc.*, **57(11)**, pp.1360-1369, DOI: 10.3155/1047-3289.57.11.1360.

[12] A.V. Donkelaar, R.V. Martin, M. Brauer, et al. (2010), "Global estimates of ambient fine particulate matter concentrations from satellite-based aerosol optical depth: Development and application", *Environ. Health Perspect.*, **118(6)**, pp.847-855, DOI: 10.1289/ehp.0901623.

[13] W.D. Nicolantonio, A. Cacciari (2010), "Modis multiannual observations in support of air quality monitoring in norThern Italy", *Italian Journal of Remote Sensing*, **43(3)**, pp.97-109, DOI: 10.5721/ItJRS20114337.

[14] X. Hu, L.A. Waller, M.Z.A. Hamdan, et al. (2013), "Estimating groundlevel PM_{25} concentrations in The souTheastern U.S. using geographically weighted regression", *Environmental Research*, **121**, pp.1-10, DOI: 10.1016/j.envres.2012.11.003.

[15] Z. Ma, X. Hu, L. Huang, et al. (2014), "Estimating groundlevel $PM_{2.5}$ in China using satellite remote sensing", *Environ. Sci. Technol.*, **48(13)**, pp.7436-7444, DOI: 10.1021/es5009399.

[16] W. Song, H. Jia, J. Huang, et al. (2014), "A satellite-based geographically weighted regression model for regional $PM_{2.5}$ estimation over The Pearl river delta region in China", *Remote Sens. Environ.*, **154**, pp.1-7, DOI: 10.1016/j.rse.2014.08.008.

[17] V.D. Xuan, T.C. Thanh (2017), "$PM_{2.5}$ personal exposure and sources of population living near 2 environment monitoring station in HCMC", *Science & Technology Development*, **20(M1)**, pp.26-34, DOI: 10.32508/stdjsee.v1iM1.434.

[18] N.T.H. Giang, N.T.K. Oanh (2014), "Roadside levels and traffic emission rates of $PM_{2.5}$ and BTEX in HCMC, Vietnam", *Atmospheric Environment*, **94**, pp.806-816, DOI: 10.1016/j.atmosenv.2014.05.074.

[19] T.T. Van, N.P Khanh, H.D.X. Bao (2014), "Remoted sensed aerosol optical thickness determination to simulate PM_{10} distribution over urban area of HCMC", *VNU Journal of Science*, **30(2)**, pp.62-72 (in Vietnamese).

[20] T.T. Van, N.H. Hai, V.Q. Bao, et al. (2018), "Remote sensing-based aerosol optical thickness for monitoring particular matter over The city", *The 2nd International Electronic Conference on Remote Sensing*, **2(7)**, DOI: 10.3390/ecrs-2- 05175.

[21] G. Camps-Valls, D. Tuia, L. Gomez-Chova, et al. (2011), *Remote Sensing Image Processing*, Morgan & Claypool Publishers, 192pp.

[22] T.T. Van, T.T. Binh, H.D.X. Bao (2012), "Study of dust pollution detecting ability in urban areas by remote sensing technology to support air environment observation", *Journal of Science and Technology Development*, **15(4)**, pp.33-47, DOI: 10.32508/stdj.v15i4.1822.

[23] SPSS Tutorial, *Pearson Correlations - Quick Introduction*, https://www.spss-tutorials.com/pearson-correlation-coefficient/, accessed 15 January 2021.

[24] IBM SPSS Statistics documentation, *Curve Estimation Regression*, https://www.ibm.com/docs/en/spss-statistics, accessed 15 January 2021.

[25] National Technical Regulation on Ambient Air Quality (2013), *QCVN 05:2013* (in Vietnamese).

[26] Green Innovation and Development Centre (2018b), *Update on Status of Air Quality in 1st Quarter 2018, Air Quality Report*, 3pp.

DOI: 10.31276/VJSTE.63(4).79-85

Rice straw open burning: Emissions, effects and multiple benefits of non-burning alternatives

Nguyen Thi Kim Oanh[1,2*]

[1]*Environmental Engineering and Management, School of Environment, Resources and Development, Asian Institute of Technology, Paholyothin Highway, Klong Luang District, Pathum Thani Province, Thailand*
[2]*Asian Institute of Technology Center in Vietnam, 8 Ton That Thuyet Street, My Dinh II Ward, Nam Tu Liem District, Hanoi, Vietnam*

Received 22 January 2021; revised 26 March; accepted 5 April 2021

Abstract:

Rice is one of the most important staple foods not just to people in Asia, but around the world. To meet domestic and export demands, farmers in Southeast Asia (SEA) grow 2-3 crop cycles per year, which leaves only a short period for land preparation. Field open burning of rice straw has been widely practiced to quickly clear the surface biomass for the next crop planting. However, this uncontrolled open combustion of rice straw releases large amounts of toxic air pollutants including key conventional pollutants along with carcinogenic compounds like dioxins, polycyclic aromatic hydrocarbons, and benzene, as well as major climate forcing agents. Emissions from rice straw open burning (RSOB) have been shown to significantly elevate ambient levels of $PM_{2.5}$ and surface ozone in adjacent urban areas. During the dry season, when stagnant meteorological conditions are prevalent, intensive open burning activities further intensify haze episodes. Rice straw, however, is a valuable resource that should be recovered and not disposed of by open burning. Indeed, several non-open burning alternatives are available that would bring in multiple benefits to air quality, climate, health, and economy. For example, the production of rice straw fuel pellets for cooking in clean gasifier cookstoves is one promising option. For the successful elimination of RSOB in SEA, technology development along with formulation and implementation of appropriate policies should be in place to mobilise active participation from all stakeholders.

Keywords: **co-benefits, cooking, rice straw open burning, rice straw pellet, toxic pollutants.**

Classification number: **5.3**

1. Introduction

Rice is the most popular crop in Asia with an annual production comprising of 90% of the world's total production. Rice is also the most important staple food in Asia as it provides 50-80% of the total calories consumed. Several countries in SEA are among the world's top ten rice exporters and, presently, the region collectively produces over 200 million metric tons (tonnes) of rice annually. To meet domestic and export demands, SEA farmers grow 2-3 crop cycles per year. Hence, there is only a short time period left to prepare the land for planting the next crop. Post-harvest RSOB has long been widely utilized by farmers in the region as it can quickly clear the surface biomass to facilitate land preparation. Survey results have shown that farmers in SEA prefer RSOB for land preparation because it requires less labor and also helps control undesirable weeds and pests along with providing ash as nutrients back into the soil [1]. Meanwhile, as farmers become wealthier and farming work becomes more mechanized, the demand for crop residue as cooking fuel or animal feedstock is declining. As a result, RSOB activity is now widespread and during the harvesting period the effects of smoke are felt on both local and regional scales, especially in the dry season.

By nature, RSOB is an uncontrolled combustion of vegetation biomass at low temperatures, hence, huge amounts of products of incomplete combustion (PIC) are released. These PIC are toxic air pollutants and include, for example, particulate matter (PM) that are mainly composed of fine inhalable particles or $PM_{2.5}$ (particles with aerodynamic diameters $\leq$2.5 µm) together with black carbon (BC) and organic carbon (OC) components (among others), gaseous pollutants of carbon monoxide (CO), and a range of volatile organic compounds (VOCs). A wide range of toxic and carcinogenic semi-volatile organic compounds (SVOCs that present in both PM and gas phases) such as polychlorinated dibenzo-*p*-dioxins and dibenzofurans (PCDD/PCDFs, hereafter referred to as dioxins), polycyclic aromatic hydrocarbons (PAHs), and organochlorinated pesticides are also found in RSOB smoke [2-13]. Many of these SVOCs are persistent organic pollutants that present over an extended time in the environment and have the ability to bioaccumulate in tissues, which makes them even of more of a health concern [14, 15].

It is worth mentioning that important greenhouse gases (GHGs) like methane (CH_4) and nitrous oxide (N_2O) are also emitted from RSOB. While a significant amount of CO_2 is

*Email: kimoanh@ait.asia

also released from the activity, the cycle is considered climate neutral because it is absorbed by the growth of the next crop. Besides, several toxic pollutants emitted from RSOB, so called "short-lived climate forcers" or "short-lived climate pollutants" (SLCPs), also have climate forcing effects. For example, BC is a strong climate warming agent while OC is a cooling agent [16]. In addition, pollutants released from RSOB can participate in chemical reactions in the atmosphere to form other pollutants that have both air quality and climate effects. As an example, VOCs and NOx in the presence of sunlight participate in photochemical reactions to form the tropospheric ozone, a secondary pollutant that is not only a strong GHG but also a toxic air pollutant to human health and plants and hence can reduce crop yield [17]. Nitrogen oxides (NO_x=NO+NO_2) and sulfur oxides (SO_x) released from the activity are important precursors of secondary inorganic particles, while VOCs are precursors of secondary organic particles. These secondary particles are formed in the atmosphere and they belong to the $PM_{2.5}$ size range.

There are two common burning methods for rice straw currently observed in SEA, namely pile burning and spread burning, which have different emission amounts per kg of rice straw burned [18, 19]. Pile burning is typically practiced after manual harvesting when RS is piled up at a paddy corner (or sometimes inside villages) and burned largely under smoldering conditions with a visible dense smoke plume, containing huge amounts of toxic pollutants (Fig. 1A). Spread burning (Fig. 1B) is normally applied in places where mechanical harvesting equipment is used. The combine harvesters cut the upper parts of rice plants and spread them in windrows while leaving the lower parts (or standing parts) virtually untouched. Spread burning fires normally consume most of the spreading RS but the standing parts, in many cases, are only partially burned especially when RS moisture is high. In Vietnam, pile burning is commonly practiced in the Red river delta region. Emissions from RSOB also strongly depend on the combustion conditions, which, in turn, depend on the moisture content of the RS and paddy soil (e.g., the higher moisture the more emissions), winds, and air humidity, among others.

Fig. 1. Rice straw field burning: (A) pile burning under smoldering conditions around Hanoi, Vietnam, May 2020 (Source: Dan Tri newspaper) **and (B) spread burning in Pathumthani, Thailand** (photo by author).

2. Results of emission factors from experimental studies

The results of emission factor measurements from the spread RSOB experiments conducted in Thailand [6, 18] are presented in Table 1 for particulate, gaseous, and SVOC pollutants. Other references quoted in Table 1 provide emission factors for RSOB but without indicating the burning methods, namely the spread or pile burning. The emission factors for burning of agricultural crop residues in general, compiled from different laboratory studies by M.O. Andreae, et al. (2001) [12], are also presented in Table 1.

Table 1. Emission factors of pollutants from RSOB (average ± SD), mass of pollutants (g or mg as specified) per kg of dry rice straw.

Pollutants		Rice straw		General agro residue (f)
		Spread RSOB [6, 18]	*Other data sources*	
Particulates				
$PM_{2.5}$, g/kg		8.3±2.2	3.8 (a)	3.9
EC, g/kg		0.53		0.69±0.13
OC, g/kg		2.78		3.3
Water soluble ions*, g/kg		1.5		
Levoglucosan, g/kg		0.47		0.27
Total elements**, g/kg		0.23		
Gaseous pollutants				
CO, g/kg		93±10	180±40 (b); 64±5 (c)	92±84
CO_2, g/kg		1177±140	1216±97 (b); 791±13 (c)	1515±177
Benzene, mg/kg		763±266	870±200 (b)	140
Toluene, mg/kg		232±3.4	1080±350 (b)	26
Ethylbenzene, mg/kg		nd		30
Xylenes, mg/kg		nd		10
SO_2, mg/kg		510±320	180±310 (g)	400
NOx mg/kg		490±210 (NO_2) 1120±480 (NOx)	790±50 (c, NO_2); 620±400 (b, NO)	2500±100 (NOx)
Aldehydes, mg/kg		147±8.0 (hood burning)	3170±880 (b, HCHO)	1400 (HCHO)
Semi-volatile organic compounds				
PAHs (16 USEPA), mg/kg	Particulate	34±35	1.02 (a); 18.6 (d); 3.0 (5% moist.) & 17.2 (20% moist.) (e)	
	Gaseous	230±333		
	Total	264±335	17.8 (a)	25
OCPs, mg/kg	Particulate	0.086±0.052		
	Gaseous	0.141±0.194		
	Total	0.227±0.20		

Data sources: a: [13]; b: [20], values for dry fuel, ash free; c: [21]; d: [22]; e: [23] for 5% and 20% moisture content of RS, included 9 PPAHs (Fth, BaA, BbF, BjF, BkF, BaP, IcdP, DahA and BghiP); f: [12]: estimates based on laboratory studies; g: [24].

*: total 9 water soluble ions (sodium, potassium, ammonium, magnesium, calcium, fluorite, chloride, nitrate, and sulfate).

**: total of 33 detected elements (including four more elements, i.e. Ca, Mg, Cl and K, than that presented in N.T.K. Oanh, et al. (2011) [18]).

There are very few experimental studies reporting emission factors of pile RSOB. N.T.K. Oanh, et al. (2011) [18] reported the emission factor of $PM_{2.5}$ for pile RSOB, which was about 18.3 g/kg of dry rice straw, i.e., more than two times greater than that of spread burning (8.3 g/kg). Based on the PM source profile reported in N.T.K. Oanh, et al. (2011) [18], the estimated emission factors of elemental carbon (EC, an operational definition of BC) is about 1.1 g/kg while that of OC is about 6.1 g/kg.

2.1. Emissions from RSOB and effects on local air quality

Emissions from RSOB in SEA and Vietnam: during 2010-2015, about 120 million tonnes of rice straw in SEA was disposed of annually by open burning with about 24 million tonnes from Vietnam alone [5]. Huge emissions are released from RSOB activity in SEA; roughly 1.8 million tonnes of $PM_{2.5}$, 12 million tonnes of CO, 65 g I-TEQ of dioxins (in the unit of toxicity equivalent, to the most toxic congener 2, 3, 7, 8-TCDD, based on the international toxicity scale), 25 thousand tonnes of PAHs, and 29 tonnes of OCPs, together with other toxic air pollutants such as benzene, toluene, and aldehydes (Table 2). By country, in the descending order, Indonesia, Vietnam, Myanmar, Thailand, and Philippines had the largest shares in RSOB emissions and collectively contributed more than 95% of the total SEA emissions from this activity. The emissions from RSOB in Vietnam typically contribute about 16-20% of the SEA's total and varies with pollutants.

N.T.K. Oanh, et al. (2018) [5] considered crop residue open burning (CROB) of the eight main crop types in SEA and reported that RSOB was the major contributor to CROB emissions by sharing 70-95% of the total amounts of different pollutants released. In 2010, CROB emissions in SEA contributed less than forest fires to the total emissions from these two major biomass open burning source categories (SUM=CROB+forest fires), i.e., CROB contributed about 10-43% to the SUM, varies with species. However, the shares of CROB emissions in the SUM differ significantly between countries. In Vietnam, for example, emissions from CROB were generally higher than the forest fires, i.e., sharing 49-92% of the SUM. In the Philippines, contributions from those two sources were in similar ranges, with the shares ranging between 33-69% that varies with species. However, forest fires had much higher contributions to the SUM in the countries of Indonesia, Thailand, and Myanmar [5]. It is worth emphasising that the effects of CROB emissions receive much less attention from society than catastrophic SEA transboundary haze events caused by forest fires.

Table 2. Annual emissions (in specified units) from RSOB in SEA and Vietnam averaged over the period 2010-2015.

Pollutants	Unit (*)	Vietnam	SEA
CO	Gg/yr	2258	12000
NO_x	Gg/yr	55	290
SO_2	Gg/yr	4.4	23
NMVOC	Gg/yr	170	890
NH_3	Gg/yr	100	500
PM_{10}	Gg/yr	330	2000
$PM_{2.5}$	Gg/yr	295	1800
BC	Gg/yr	13.6	70
OC	Gg/yr	228	800
CO_2	Gg/yr	28600	153900
CH_4	Gg/yr	100	520
N_2O	Gg/yr	2.4	13
Aldehydes	Gg/yr	3.6	19
Benzene	Gg/yr	18.5	97
Toluene	Gg/yr	5.6	29
PAHs	Gg/yr	6.4	25
OCPs	t/yr	5.5	29
Dioxins	g I-TEQ/yr	13	65

*Gg: thousand tonnes. Source: adapted from N.T.K. Oanh, et al. (2018) [5].

Effects of RSOB on ambient air quality: Several studies in SEA show evidence of the effects of RSOB emissions on local air quality. In Pathumthani, a large rice growing province of Thailand, RSOB is especially intensive during the dry months from November to April. The levels of carcinogenic PAHs measured in the ambient air of a rural area of Klong Luang (KL) district during the intensive RSOB days were above 400 ng/m^3 that is 60 times higher than the levels measured in the air in a remote site of Khao Yai (KY) national park [4]. The ambient profile of PAHs in KL during RSOB days (Fig. 2) shows a dominance of 4-ring compounds, most remarkably

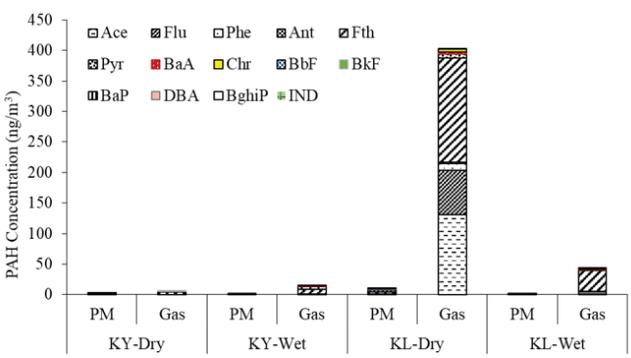

Fig. 2. PAHs levels and individual compound profiles in an intensive RSOB area (KL) and the remote national park (KY) during the dry and wet season (measurement data, extracted from Tipayarom and N.T.K. Oanh (2020) [4]).

fluoranthene, which indicates a strong influence of rice straw burning emissions on the PAH air quality [3, 25, 26]. The RSOB smoke in KL also contains high levels of OCPs (about 14 ng/m^3), which may be related to the re-emission of compounds accumulated in the paddy soil from the past applications.

Based on the analysis of mass and compositions of $PM_{2.5}$ measured in KL using the receptor modeling approach, ambient $PM_{2.5}$ levels show significant influence from RSOB. During the dry season, RSOB contributed about 14 µg/m^3 to the $PM_{2.5}$ mass concentration (40% of the total measured $PM_{2.5}$ mass), which is well above that estimated in the wet season with 4 µg/m^3 (25% of $PM_{2.5}$ mass) [27]. The air quality dispersion modeling using a 3D chemical transport model (CAMx-MM5) also revealed impacts on the surface ozone air quality by RSOB in the Bangkok metropolitan region [28]. The simulation results for an ozone episode in March showed that RSOB in the modeling domain would cause an increase in the hourly ozone, by an average 4 ppb with a maximum of 10 ppb, in the Rangsit station (located near KL), over the scenario with zero RSOB.

Exposure to RSOB smoke and potential health effects: Rice straw field burning emissions have been reported to induce high personal exposure to the toxic air pollutants in Asia, Europe, and the US [29-32]. However, the health effects specifically induced by RSOB have not been intensively studied. K. Torigoe, et al. (2000) [33] conducted a survey and revealed that emissions from RSOB in a study area in Japan possibly induced or exacerbated asthma attacks in children. The authors recommended the elimination of RSOB activity for the protection of the inhabitants' health, especially of children with asthma. Overall, intensive agricultural waste burning activities can affect air quality, human health, and the climate at continental and global scales [34, 35].

In SEA, large amounts of toxic air pollutants ($PM_{2.5}$, CO, VOCs, PAHs, OCPs, dioxins, etc.) are annually released from RSOB. The high levels of toxic air pollutants measured in areas with intensive RSOB activities suggest a high exposure risk and potential adverse health effects. The fact that agricultural land in Asia is widely distributed in suburban and rural areas, where people live and work, further intensifies the exposure risk. In some areas, such as the Red river delta of Vietnam, multiple small and short-lived RSOB fires can be densely seen during the harvesting months, hence, can seriously deteriorate air quality [36]. The emissions are widely dispersed to cause high air pollution levels not only in the rural areas where RSOB occurs but also in the adjacent urban areas [27, 37]. Furthermore, RSOB activity is more intensively practiced in the dry season when air pollution is already high due to the stagnant meteorological conditions and thus exaggerates haze episodes [4, 37].

Presently, the impacts of CROB including RSOB are often overlooked in many SEA countries and receive less concern from society as compared to catastrophic transboundary haze caused by forest fires. The negative impacts of RSOB, such as the effects of smoke on human health, should be widely disseminated to raise awareness and thereby encourage farmers to use non-open burning alternatives for crop residue management.

2.2. Non-burning alternatives for rice straw management

Non-burning alternatives: rice straw is a valuable resource that should be recovered rather than disposed of by open burning. There are non-open burning alternatives including off-site uses of RS as medium for mushroom cultivation, animal feed and bedding, garden mulching, or composting. Further, RS can be converted into biochar, processed fuel such as bioethanol or briquettes/pellets, and building materials [38, 39]. However, the labor and cost for collection and transportation of bulky loose RS remain a challenge. Other constraints exist, for example, the presence of a high silica (Si) content in RS affects the digestion capability of the livestock. The traditional uses of RS in handicraft making (hats, mats, and decoration items) or as construction material could be promoted but need suitable business models to sustain.

A promising alternative of "ploughing for on-site degradation" has been promoted in Thailand. Accordingly, the harvested paddy is ploughed using a powerful machine to incorporate RS into the soil following with the application of water, bio-extracted liquid, and bio-fertilizer to accelerate the degradation. However, local farmers do not generally prefer the method primarily because it still requires a considerable amount of time to make the paddy soil ready for the next crop plantation. In addition, the high cost of such a ploughing machine is also an issue. Therefore, most farmers still prefer to continue RS field burning activities. However, the results of a survey showed that the local farmers are indeed aware of the negative effects of RS field burning on paddy soil quality, e.g., the soil structure becomes hard after RSOB and some organic nutrient substances on the topsoil are burned to ash. The effects of smoke on human health are not yet recognized while those on the safety of on-road transport due to reduced visibility were of concern [40].

Cooking with loose RS in a simple tripod cookstove is traditionally practiced in rural areas of Asia [41, 42]. However, this low efficient cooking system consumes large amounts of fuel and generates huge amounts of emissions that affect both indoor and outdoor air quality. Some densification techniques can be applied to produce RS derived solid fuels that include, for example, roped/bundled straw, briquettes, and pellets, which have higher fuel density and are easier to store and transport than loose RS. Further, clean cookstoves can be used to effectively burn RS-derived fuel while generating less emissions. However, these conversion technologies are not yet fully developed or adapted for RS. Overall, the thermochemical conversion of RS into bioenergy is still not popularly applied

due to several technical constraints associated with RS's chemical and physical properties like high ash and silica content, rigorous crystalline structure, and low bulk density [42-44]. Combustion is the most mature technology used to generate energy from RS, but it also encounters several major shortcomings including corrosion/fouling of equipment due to high silica and potassium/alkali contents, ash accumulation and slagging, among others [44, 45].

Production of rice straw pellet fuel for cooking: Making RS pellets (pelletization) is one densification method to produce RS-derived solid fuel. This process can significantly increase the bulk density of RS, i.e. up to 600-700 kg/m^3 from, for example, 60-90 kg/m^3 of baled RS [46]. To improve the quality of the produced pellets, RS is usually mixed with woody/bamboo biomass and/or other additives. In particular, woody/bamboo biomass with its high lignin content and low ash content enhances the energy content and improves pellet durability while reducing its inorganic content [47].

The air quality team at the Asian Institute of Technology (AIT) has conducted research on RSOB emissions and assessed the associated impacts on air quality and climate forcing during the last 20 years. The AIRPET (Air pollution research project and network) from 2000-2010, sponsored by Swedish International Development Cooperation Agency (SIDA) and coordinated by AIT in collaboration with 6 Asian national research partners from China, India, Indonesia, Philippines, Thailand, and Vietnam [48], started emission characterization and modeling studies related to RSOB in SEA [49].

Recognizing RS as a valuable resource, the AIT team worked to identify alternatives that recover energy from this agricultural waste allowing farmers to commoditize waste that is prone to burning. In the Partnerships for Enhanced Engagement in Research (PEER) - SEA project "Assessment of impacts of the emission reduction measures of short-lived climate forcers on air quality and climate in SEA" (2012-2016) sponsored by U.S. Agency for International Development (USAID), the team quantified the RSOB emissions in SEA and assessed the impacts on air quality and climate forcing using the modeling tool [50]. A spin-off project under the Sustainable Mekong Research Network (SUMERNET) phase 3, sponsored by SIDA and titled "Turning rice straw into cooking fuel for air quality and climate co-benefit in selected Greater Mekong Subregion countries" (2016-2018), was conducted in cooperation with the Energy program at AIT and research partners in Thailand, Vietnam, and Cambodia to examine several options to turn RS into cooking fuel like RS bundles, briquettes, and pellets.

A laboratory scale pelletizing machine was developed in this project [51] and successfully produced RS pellets that can be burned effectively in a Mimimoto gasifier cookstove (GCS) (https://www.engineeringforchange.org/solutions/product/mimi-moto/). The GSC-pellet cooking system was

Fig. 3. (A) A pelletizing machine in an agricultural machinery company in Hanoi, (B) RS pellets produced, and (C) GCS-pellet cooking system demonstrated in Hanoi [52].

demonstrated at project sites in Cambodia, Thailand, and Vietnam and gained a general acceptance from farmers. A few shortcomings have been documented such as the strongly sintered ash remaining in GSC after pellet burning, which was difficult to remove from the stove and the ash material was found to be too hard for use for soil conditioning.

A supplementary award for PEER-SEA was provided to AIT for translating evidence-to-action in a demonstration project "Technology acceleration to transfer rice straw derived fuel and gasifier cookstove in Vietnam" (2017-2018). The project team successfully produced RS pellets using a full-scale prototype pelletizing machine in cooperation with the local project partners at the Hanoi National University and an agricultural machinery company in Hanoi (Fig. 3). The pellets burned well in the selected Mimimoto GCS without visible smoke. Certain modifications of feeding materials and pelletizing technical conditions make the ash soft enough to be removed easily from the stove and also to apply directly on soil. This cooking system has a high thermal efficiency, hence, consumes less fuel for cooking a meal. The emission measurements showed that the amount of $PM_{2.5}$ emitted from the cookstove when burning 1 kg of RS pellets was only about one-fifth (1/5) of that from RSOB pile burning. The RS pellets can be used for domestic cooking and are even more relevant for commercial cooking to substitute, for example, polluting honeycomb coal briquettes. Thus, this would reduce exposure to both indoor and outdoor air pollution and provide great health benefits.

The production of RS pellets and the selection of the optimal cookstove for burning the fuel create an opportunity to meaningfully recover this valuable agricultural waste and, at the same time, create an income source for farmers through selling RS and/or RS pellets. It provides an alternative to reduce RSOB and brings in benefits of clean air and climate though emission reduction. At the same time, RS pellet production helps cut down the consumption of fossil fuel (to reduce climate impacts) and wood fuel (to save trees), hence, providing multiple benefits.

A complete RS grinding-pelletizing machine should be further developed and demonstrated to bring the technology closer to end-users. Modifications to feeding material mixture compositions and the pelletizing technical conditions may be

exploited to produce pellets for other purposes like animal feedstock, organic fertilizers, and soil conditioners. The demand, willingness-to-pay by users, cost-benefit analysis, and potential environmental impacts should be analysed. Business models may be developed that involve participation of the private sector to produce and market RS pellets.

3. Conclusions

RSOB releases huge amounts of toxic air pollutants that seriously deteriorate local air quality not only in populated rural areas but also in nearby cities. Intensive RSOB in the dry period, when stagnant atmospheric conditions prevail, intensifies the formation of haze episodes. High levels of toxic and carcinogenic compounds in the ambient air during intensive burning periods indicate high exposure risks and potential adverse health effects.

Several non-burning alternatives are available to RSOB but certain constraints exist. The production of RS pellets for cooking fuel is a promising approach to minimize RSOB activities and gain multiple benefits. Further studies should include a detailed cost-benefit analysis of the application and should develop practical guidelines for the production of RS pellets with suitable physical and thermal characteristics of the fuel.

For successful elimination of RSOB in SEA, beside the technology development, formulation and implementation of appropriate policies should be in place to mobilise participation from all stakeholders. A strict "ban" on RSOB alone may not work effectively, but the enforcement should be done along with providing suitable and workable alternatives with subsidies/ incentives. Negative impacts of RSOB, specifically the effects of smoke on human health, should be widely disseminated to raise awareness and thereby encourage farmers to opt for non-open burning alternatives for rice straw management. The benefits brought about by non-open burning scenarios to ambient air quality and health should be demonstrated in future studies by using a detailed emission inventory and dispersion modelling approach. Suitable business models involving the private sector should be developed that incorporate sufficient incentives to encourage farmers to stop open burning.

ACKNOWLEDGEMENTS

The author, also the PI of the regional projects, would like to specially thank the sponsors of Swedish International Development Cooperation Agency for the generous funding supports to the AIRPET and SUMERNET projects, and U.S. Agency for International Development for the support to the SEA-PEER project with supplemental awards. The cooperation of AIT colleagues and national research partners from Thailand, Vietnam, Indonesia, and Cambodia, as well as the local company in Hanoi is highly acknowledged. The project activities would not be possible without the active participation from AIT students and project research staff.

COMPETING INTERESTS

The author declares that there is no conflict of interest regarding the publication of this article.

REFERENCES

[1] N.T.K. Oanh, D.A. Permadi, P.A. Salam, et al. (2019), "Assessment of co-benefits of using rice straw derived solid fuel for cooking to reduce emissions of agro-residue open burning in selected GMS countries", *Chapter 8, Development and Climate Change in The Mekong Region: Case Studies,* SIRD Publishing Co., Malaysia, 349pp.

[2] K. Anezaki, N. Kashiwagi (2021), "Daily variations and factors of atmospheric PCDD/Fs in post-harvest paddy fields: PCDD/F source estimation using a Bayesian semi-factor model", *Chemosphere*, **268**, DOI: 10.1016/j. chemosphere.2020.129292.

[3] C.T. Pham, Y. Boongla, T.D. Nghiem, et al. (2019), "Emission characteristics of polycyclic aromatic hydrocarbons and nitro-polycyclic aromatic hydrocarbons from open burning of rice straw in the north of Vietnam", *Int. J. Environ. Res. Public Health*, **16(13)**, pp.2343-2360, DOI: 10.3390/ijerph16132343.

[4] A. Tipayarom, N.T.K. Oanh (2020), "Influence of rice straw open burning on levels and profiles of semi-volatile organic compounds in ambient air", *Chemosphere*, **243**, DOI: 10.1016/j.chemosphere.2019.125379

[5] N.T.K. Oanh, D.A. Permadi, P.K. Hopke, et al. (2018), "Annual emissions of air toxics emitted from crop residue open burning in Southeast Asia over the period of 2010-2015", *Atmospheric Environment*, **187**, pp.163-173, DOI: 10.1016/j. atmosenv.2018.05.061.

[6] N.T.K. Oanh, A. Tipayarom, L.B. Thuy, et al. (2015), "Characterization of gaseous and semi-volatile organic compounds emitted from field burning of rice straw", *Atmospheric Environment*, **119**, pp.182-191, DOI: 10.1016/j.atmosenv.2015.08.005.

[7] X. Zhang, Y. Lu, Q.G. Wang, et al. (2018), "A high-resolution inventory of air pollutant emissions from crop residue burning in China", *Atmospheric Chemistry and Physics*, DOI: 10.5194/acp-2017-111.

[8] J. Jiminez, C. Claiborn, R. Dhammapala, et al. (2007), "Developing a source fingerprint for burning of wheat and Kentucky bluegrass stubble in Eastern Washington and Northern Idaho", *Environmental Science and Technology*, **41(22)**, pp.7824-7829.

[9] A.H. Miguel, A.E.F. Fernandez, P. Jaques, et al. (2004), "Seasonal variation of the particle size distribution of polycyclic aromatic hydrocarbons and of major aerosol species in Claremont, California", *Atmospheric Environment*, **38(20)**, pp.3241-3251, DOI: 10.1016/j.atmosenv.2004.03.008.

[10] M.D. Hays, P.M. Fine, C.D. Geron, et al. (2005), "Open burning of agricultural biomass: physical and chemical properties of particle-phase emissions", *Atmospheric Environment*, **39(36)**, pp.6747-6764, DOI: 10.1016/j.atmosenv.2005.07.072.

[11] B. Gullet, A. Touati (2003), "PCDD/F emissions from burning wheat and rice field residue", *Atmospheric Environment*, **37(35)**, pp.4893-4899, DOI: 10.1016/j. atmosenv.2003.08.011.

[12] M.O. Andreae, P. Merlet (2001), "Emission oftrace gases and aerosols from biomass burning", *Global Biogeochemical Cycles*, **15(4)**, pp.955-966, DOI: 10.5194/ acp-19-8523-2019.

[13] B.M. Jenkins, A.D. Jones, S.Q. Turn, et al. (1996), "Particle concentrations, gas-particle partitioning, and species intercorrelations for polycyclic aromatic hydrocarbons (PAH) emitted during biomass burning", *Atmospheric Environment*, **30(22)**, pp.3825-3835, DOI: 10.1016/1352-2310(96)00084-2.

[14] I.A.S. Hussein, M.S.M. Mansour (2016), "A review on polycyclic aromatic hydrocarbons: Source, environmental impact, effect on human health and remediation", *Egyptian Journal of Petroleum*, **25(1)**, pp.107-123, DOI: 10.1016/j.ejpe.2015.03.011.

[15] E.J. Mrema, F.M. Rubino, G. Brambilla, et al. (2013), "Persistent organochlorinated pesticides and mechanisms of their toxicity", *Toxicology*, **307**, pp.74-88, DOI: 10.1016/j.tox.2012.11.015.

[16] Intergovernmental Panel on Climate Change (2013), *Climate Change 2013: The Physical Science Basis*, Cambridge University Press, United Kingdom and New York, USA, 1535pp.

[17] N.T. Danh, L.N. Huy, N.T.K. Oanh (2016), "Assessment of rice yield loss due to exposure to ozone pollution in Southern Vietnam", *Science of The Total Environment*, **566-567**, pp.1069-1079, DOI: 10.1016/j.scitotenv.2016.05.131.

[18] N.T.K. Oanh, L.B. Thuy, D. Tipayarom, et al. (2011), "Source characterization of aerosol emission from field burning of rice straw", *Atmospheric Environment*, **45(2)**, pp.493-502, DOI: 10.1016/j.atmosenv.2010.09.023.

[19] K. Lasko, K. Vadrevu (2018), "Improved rice residue burning emissions estimates: Accounting for practice-specific emission factors in air pollution assessments of Vietnam", *Environmental Pollution*, **236**, pp.795-806, DOI: 10.1016/j.envpol.2018.01.098.

[20] T.J. Christian, B. Kleiss, R.J. Yokelson, et al. (2003), "Comprehensive laboratory measurements of biomass-burning emissions: 1. Emissions from Indonesian, African, and other fuels", *Journal of Geophysical Research*, **108(D23)**, pp.4719-4732, DOI: 10.1029/2003JD00354910.1029/2003JD003874.

[21] H. Zhang, X. Ye, J. Cheng, et al. (2008), "A laboratory study of agricultural crop residue combustion in China: Emission factors and emission inventory", *Atmospheric Environment*, **42(36)**, pp.8432-8441, DOI: 10.1016/j.atmosenv.2008.08.015.

[22] H. Keshtkar, L.L. Ashbaugh (2007), "Size distribution of PAH particulate emission factors from agricultural burning", *Atmospheric Environment*, **41(13)**, pp.2729-2739, DOI: 10.1016/j.atmosenv.2006.11.043.

[23] E. Sanchis, M. Ferrer, S. Calvet, et al. (2014), "Gaseous and particulate emission profiles during controlled rice straw burning", *Atmospheric Environment*, **98**, pp.25-31, DOI: 10.1016/j.atmosenv.2014.07.062.

[24] G. Cao, X. Zhang, S. Gong, et al. (2008), "Investigation on emission factors of particulate matter and gaseous pollutants from crop residue burning", *Journal of Environmental Sciences*, **20(1)**, pp.50-55, DOI: 10.1016/S1001-0742(08)60007-8.

[25] R.J. Sheesley, J.J. Schauer, Z. Chowdhury, et al. (2003), "Characterization of organic aerosols emitted from the combustion of biomass indigenous to South Asia", *Journal of Geophysical Research*, **108(D9)**, pp.4285-4300, DOI: 10.1029/2002JD002981.

[26] T. Korenaga, X. Liu, Z. Huang (2001), "The influence of moisture content on polycyclic aromatic hydrocarbons emission during rice straw burning", *Chemosphere Global Change Science*, **3(1)**, pp.117-122, DOI: 10.1016/S1465-9972(00)00045-3.

[27] D. Narita, N.T.K. Oanh, K. Sato, et al. (2019), "Pollution characteristics and policy actions on fine particulate matter in a growing Asian economy: The case of Bangkok metropolitan region", *Atmosphere*, **10(5)**, pp.227-245, DOI: 10.3390/atmos10050227.

[28] N.T.K. Oanh (2013), "Integrated approach to rice straw management for reduction of field burning activity", *Integrated Air Quality Management: Asian Case Studies,* CRC Press Boca Raton, USA, 424pp.

[29] K. Ravindra, T. Singh, S. Mor (2019), "Emissions of air pollutants from primary crop residue burning in India and their mitigation strategies for cleaner emissions", *Journal of Cleaner Production*, **208**, pp.261-273, DOI: 10.1016/j.jclepro.2018.10.031.

[30] M. Viana, J.M. Lopez, X. Querol, et al. (2008), "Tracers and impact of open burning of rice straw residues on PM in Eastern Spain", *Atmospheric Environment*, **42(8)**, pp.1941-1957, DOI: 10.1016/j.atmosenv.2007.11.012.

[31] C.F. Wu, J. Jimenez, C. Claiborn, et al. (2006), "Agricultural burning smoke in eastern Washington: Part II: Exposure assessment", *Atmospheric Environment*, **40(28)**, pp.5379-5392, DOI: 10.1016/j.atmosenv.2006.04.042.

[32] H.H. Yang, C.H. Tsai, M.R. Chao, et al. (2006), "Source identification and size distribution of atmospheric polycyclic aromatic hydrocarbons during rice straw burning period", *Atmospheric Environment*, **40(7)**, pp.1266-1274, DOI: 10.1016/j.atmosenv.2005.10.032.

[33] K. Torigoe, S. Hasegawa, O. Numata, et al. (2000), "Influence of emission from rice straw burning on bronchial asthma in children", *Pediatrics International*, **42(2)**, pp.143-150, DOI: 10.1046/j.1442-200x.2000.01196.x.

[34] UNEP-WMO (2011), *Integrated Assessment of Black Carbon and Tropospheric Ozone,* World Meteorological Organization and United Nations Environment Programme, 285pp.

[35] D. Shindell, J.C.I. Kuylenstierna, E. Vignati, et al. (2012), "Simultaneously mitigating near-term climate change and improving human health and food security", *Science*, **335(6065)**, pp.183-189, DOI: 10.1126/science.1210026.

[36] K. Lasko, K.P. Vadrevu (2018), "Biomass burning emissions variation from satellite derived land cover, burned area, and emission factors in Vietnam", *Land Atmospheric Research Applications in South and Southeast Asia*, pp.171-201, DOI: 10.1007/978-3-319-67474-2_9.

[37] D. Tipayarom, N.T.K. Oanh (2007), "Effects from open rice straw burning emission on air quality in the Bangkok metropolitan region", *ScienceAsia*, **33(3)**, pp.339-345, DOI: 10.2306/scienceasia1513-1874.2007.33.339.

[38] E.B. Belal (2013), "Bioethanol production from rice straw residues", *Brazilian Journal of Microbiology*, **44(1)**, pp.225-234, DOI: 10.1590/S1517-83822013000100033.

[39] J.Y. Park, R. Shiroma, M.I.A. Haq, et al. (2010), "A novel lime pretreatment for subsequent bioethanol production from rice straw-calcium capturing by carbonation (CaCCO) process", *Bioresource Technology*, **101(17)**, pp.6805-6811, DOI: 10.1016/j.biortech.2010.03.098.

[40] K. Kanokkanjana, A. Bridhikitti (2007), "Sustainable rice straw management for urban air pollution reduction in Bangbuathong, Nonthaburi province, Thailand", *Final Report of The CIDA-AIT Partnership*, Alumni demonstration project, Pathumthani Asian Institute of Technology, 23pp.

[41] L.N. Huy, N.T.K. Oanh, N.H. Phuc, et al. (2020), "Survey-based inventory for atmospheric emissions from residential combustion in Vietnam", *Environmental Science and Pollution Research*, **28**, pp.10678-10695, DOI: 10.1007/s11356-020-11067-6.

[42] N.N.H. Mai (2015), *Assessment of The Impact of Using Rice Straw Derived Cooking Fuel on The Emission of Air Pollution and Climate Forcers*, Master's Thesis, Asian Institute of Technology, 101pp.

[43] Y. Zhang, A. Ghaly, B.X. Li (2012), "Physical properties of rice residues as affected by variety and climatic and cultivation conditions in three continents", *American Journal of Applied Sciences*, **9(11)**, pp.1757-1768.

[44] M. Rozainee, S. Ngo, A. Salema, et al. (2008), "Effect of fluidising velocity on the combustion of rice husk in a benchscale fluidised bed combustor for the production of amorphous rice husk ash", *Bioresource Technology*, **99(4)**, pp.703-713, DOI: 10.1016/j.biortech.2007.01.049.

[45] M.C.M. Detras, M.V.P. Migo, N.V. Hung, et al. (2020), "Thermochemical conversion of rice straw", *Sustainable Rice Straw Management*, pp.43-64, DOI: 10.1007/978-3-030-32373-8_4.

[46] N.V. Hung, M.C.M. Detras, M.V. Migo, et al. (2020), "Rice straw overview: availability, properties, and management practices", *Sustainable Rice Straw Management*, pp.1-13, DOI: 10.1007/978-3-030-32373-8_1.

[47] Z. Liu, X. Liu, B. Fei, et al. (2013), "The properties of pellets from mixing bamboo and rice straw", *Renewable Energy*, **55**, pp.1-5, DOI: 10.1016/j.renene.2012.12.014.

[48] N.T.K. Oanh, N. Upadhyay, Y.H. Zhuang, et al. (2006), "Particulate air pollution in six Asian cities: Spatial and temporal distributions, and associated sources", *Atmospheric Environment*, **40(18)**, pp.3367-3380, DOI: 10.1016/j.atmosenv.2006.01.050.

[49] N.T.K. Oanh (2014), *Improving Air Quality in Asian Developing Countries: Compilation of Research Findings*, NARENCA, 435pp.

[50] D.A. Permadi, N.T.K. Oanh, R. Vautard (2018), "Assessment of emission scenarios for 2030 and impacts of black carbon emission reduction measures on air quality and radiative forcing in Southeast Asia", *Atmospheric Chemistry and Physics*, **18(5)**, pp.3321-3334, DOI:10.5194/acp-18-3321-2018.

[51] D.N. Cuong (2016), *A Study on Production and Combustion Behavior of Rice Straw Pellets*, Master's Thesis, Asian Institute of Technology, 140pp.

[52] PEER (2018), "Evidence-to-action supplements (sub-award)", *Assessment of Impacts of The Emission Reduction Measures of Short-Lived Climate Forcing Pollutants on Air Quality and Climate in Southeast Asia*, USAID/NAS, 30pp.

DOI: 10.31276/VJSTE.63(4).86-94

Establishing 3D hydrogeological solid model and database for sustainable groundwater management in the Vietnam Mekong delta

Vu Thanh Tam, Nguyen Ngoc Ha*, Ho Van Thuy

National Center for Water Resources Planning and Investigation, 93/95 Vu Xuan Thieu Street, Sai Dong Ward, Long Bien District, Hanoi, Vietnam

Received 19 May 2021; revised 29 July 2021; accepted 13 August 2021

Abstract:

The Vietnam Mekong delta (VMD) is a tide-dominated delta formed by the Mekong river system. The sediments are dominantly fine grained and were deposited in the receiving basin with slight inclination of pre-existing deposits in the East sea and gulf of Thailand. The VMD is homeland to about 18 million people that exploit about 4-6 million m^3/day of groundwater mainly for domestic use. In recent years, significant groundwater depletion has been occurring in many parts of the VMD due to excessive pumping. Consequently, the VMD has become increasingly faced with serious land subsidence, salt groundwater intrusion, and contamination. Establishing a 3D hydrogeological solid model and database are sorely needed to achieve sustainable groundwater management, and to serve as a basis for further in-depth analyses to quantify contributions from the above-mentioned hazards to current hydrogeological conditions. Therefore, a 3D hydrogeological solid model and database were built based on more than 1000 well logs available from the VMD. An areal distribution of the Holocene, Pleistocene, Pliocene, and Late Miocene subsurfaces from this 3D hydrogeological solid model and database showed zones of tectonic depression and uplift from Early Miocene - Quaternary. Also, the resulting areal distribution aquitards and aquifers thicknesses gave hints of ground saltwater intrusion and contamination.

Keywords: **groundwater extraction, subsurface modelling, Vietnam Mekong delta.**

Classification number: **5.3**

1. Introduction

The delta plain of the Mekong river is about 62,520 km^2 of which 52,100 km^2 is located in Vietnam, which is referred to as the VMD, and the remainder is located in Cambodia's territory. In Vietnam, the VMD spans 13 provinces with a population of 17.6 million [1]. The region represents a national rice bowl providing agricultural products not only for Vietnam but also other countries. In the VMD, the Bassac river known as the Hau river, runs along the development direction of the largest regional fault, which is 2,000 km long and vertically dipping down to 35 km deep. This fault line is internationally named the Mae Ping fault and also locally known as the Hau river fault for its part in Mekong delta [2, 3]. The VMD is known to be continuously sinking below sea level due to rising seawater levels and land subsidence. In many places within the delta, the land subsidence rate has been reported to be up to 10 cm/yr (Fig. 1A) [4], which is often linked to excessive groundwater pumping [5, 6]. The groundwater has been reported as being salty in many aquifers, especially in the coastal provinces of Ca Mau, Bac Lieu, Soc Trang, Tra Vinh, and Ben Tre [7, 8]. An example of the salt groundwater distribution is given in Fig. 1B. Therefore, this region is selected for 3D hydrogeological modelling that aims to: (i) Better understand the spatial distribution of hydrogeological units existing in the region, especially the appearance of the bedrocks on the surface ground in the provinces of Kien Giang, Binh Duong, and their dipping towards the Hau river and towards the coastal provinces of Ca Mau, Bac Lieu, Soc Trang, and Ben Tre. Insight into this spatial hydrogeological distribution can provide certain explanations of the groundwater salt intrusion and land subsidence appearances in the delta; and (ii) to achieve the first necessary step toward building a groundwater flow and transport model for the entire VMD.

*Corresponding author: Email: nnha@monre.gov.vn

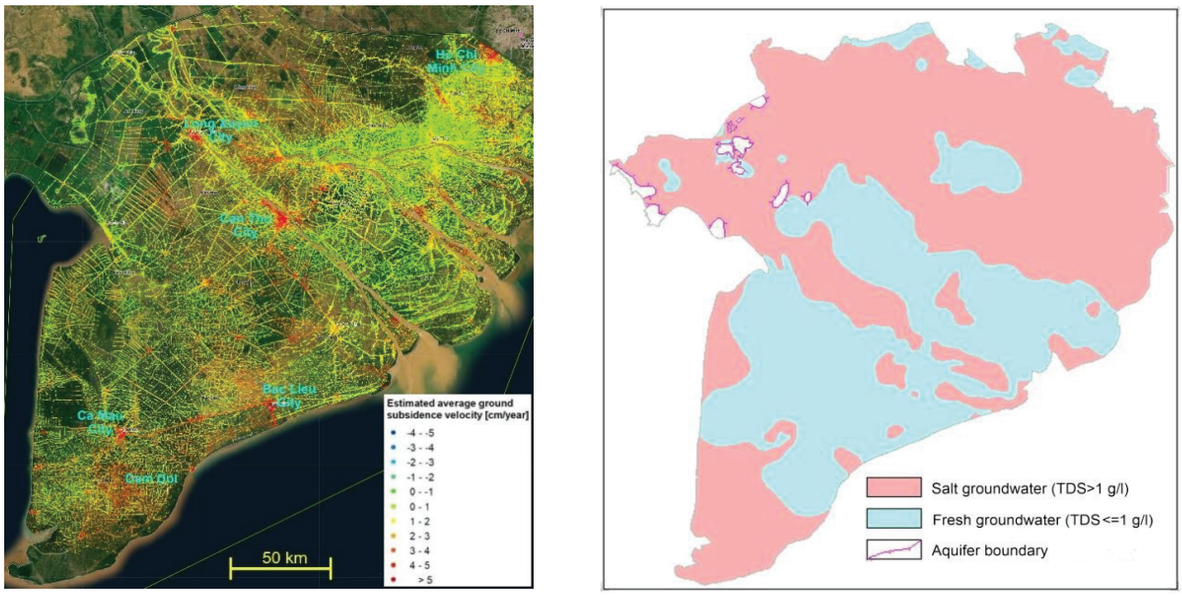

(A) **(B)**

Fig.1. (A) Land subsidence maps by Indra (2019) portraying Sentinel-1 imageries in the period 2014-2019 and (B) distribution of fresh and salt groundwater in aquifer 23 after DWRPIS [7].

Several 3D hydrogeological solid and groundwater flow models have been developed for the entire VMD. The first and most relatively complete one (in terms of modelling area and number of data used) is the groundwater model developed by the Division for Water Resources Planning and Investigation for the South (DWRPIS) [7]. The main objective of this model was to predict responses of the groundwater resources to several scenarios including future climate change and social-economic change in the VMD. This model was built on the basis of 903 well logs collected at that time in combination with Aquaveo GMS MODFLOW software with a 139(rows)x131(columns)x14(layers) cell grid with a cell resolution of 2x2 km^2. The modelling used the inversed distance weighting (IDW) interpolation method combined with am averaging and minimum thickness adjustment technique was applied to generate the top and bottom of all aquifers and aquitards. In this technique, when the interpolated bottom is higher than the interpolated top of an aquifer or aquitard, the top is adjusted by moving up half of a user-specified minimum thickness to above the interpolated value and moving down the bottom by the same interval to below the interpolated value. The minimum layer thickness (i.e., every layer must have a non-zero thickness everywhere in the modeling domain) is an essential requirement for a finite difference solution of the MODFLOW code. One major disadvantage of this modelling technique is the inability to delineate zones of "vertical hydrological window", i.e., zones where there is a direct connection between the aquifers, which occur in reality as they appear in well log G17-CM in Ca Mau city (Fig. 2).

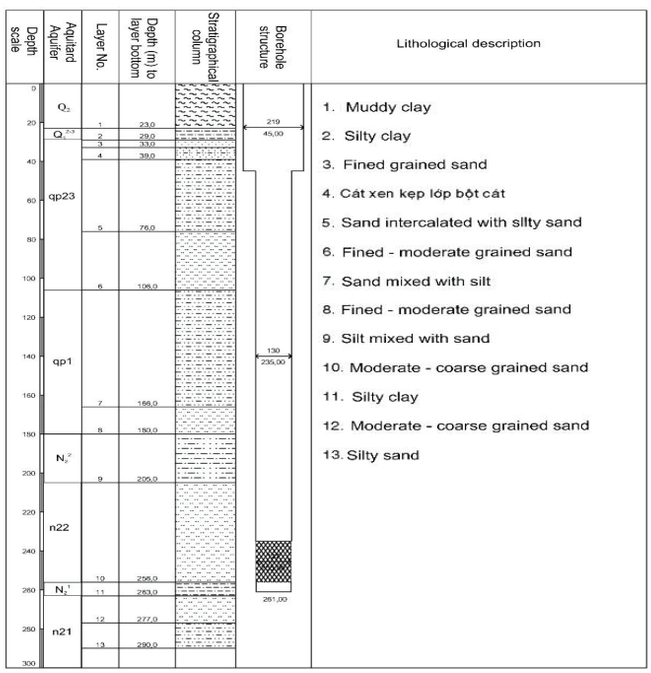

Fig. 2. The well log of borehole G17-CM in Ca Mau city shows the appearance of vertical hydrogeological windows at depth -23 m (no existence of aquifers qh or qp3, or aquitard Q13, and aquitard Q2 directly connecting with Q12-3), or at a depth -106 m (no aquitard Q11 separating aquifers qp23 with qp1).

At the same time as the above-mentioned modeling work was completed, a quasi-3D steady-state groundwater model of 410(rows)x308(columns) x8(layers) and cell resolution of 1x1 km^2 was developed by P. Vermeulen, et al. (2013) [9], which aimed to assess the groundwater resources in the VMD. This model was developed based on iMOD MODFLOW software and used only 95 boreholes collected from DWRPIS. Later, P.S.J. Minderhoud, et al. (2017) [6] built another 3D groundwater flow model to assess the impacts of the last 25 years of groundwater abstraction due to land subsidence in the VMD. This model is similar to Vermeulen's work in terms of modeling area, cell resolution, and data used, however, it is coupled with a 1D geotechnical subsidence module called SUB-CR. The simulated land subsidence rate was compared with the measured remotely using satellite-based synthetic aperture radar (SAR) imagery processed by interferometry (InSAR) for validation of the modelling. The results of this work implied that excessive pumping was the prevailing cause of land subsidence and groundwater level decline in the VMD, while neglecting other possible causes like tectonic displacement, surface loading, soil lithological properties, soil auto-compaction, and natural compaction. Indeed, it was later shown in a publication by C. Zoccarato, et al. (2018) [10] that the estimated average subsidence rate resulting from natural compaction of young Holocene sediments in the VMD can be as much as 2 mm/yr at the present shoreline and decreases gradually inland to 0.8 mm/yr towards the upper delta plain.

Very recently, J.L. Gunnink, et al. (2021) [11] produced a 3D groundwater salinity distribution and fresh groundwater volume model in the Mekong delta using a geostatistical analysis approach. One of the components of this research is the construction and update of the hydrogeological layer model (aquifers and aquitards discretized into voxels) from the existing model of P.S.J. Minderhoud, et al. (2017) [6]. Unlike other numerical groundwater flow and transport models, this research mainly used a point-based interpolation technique, namely, the ordinary kriging interpolation method, to generate a 3D groundwater salinity distribution per aquifer and aquitard, and to estimate the fresh groundwater volume per aquifer and per province for the entire VMD. Therefore, the saltwater transport pathway was not fully studied or clarified in this research work and questions such as how and where saltwater moves vertically (i.e., leaching through low permeable aquitard or flowing through vertical hydrogeological windows) remain unanswered.

Thus, a 3D hydrogeological solid model is an essential tool for various studies of groundwater resource and groundwater-related catastrophe management. However, in previous modelling works, the number of well logs was relatively sparse for such a large modelling area and, additionally, about two third of the boreholes do not reach the deepest aquifer. Therefore, existing 3D models do not give accurate local variations of thickness and subsurface of hydrogeological units as well as the possible existence of "vertical hydrogeological windows" in the groundwater system of the VMD. Since 2014, more water resource investigation projects with new, deep boreholes have been implemented by the National Center for Water Resources Planning and Investigation (NAWAPI). Indeed, well logs from these new boreholes were collected in this research. Besides, a sophisticated combination of the point IDW interpolation technique (for creating the tops and bottoms of hydrogeological units using measured data from the collected well logs) and the subsurface truncation method (the bottom elevation is lowered to the top elevation where the interpolated value of bottom is higher than the interpolated value of the bottom) are applied to this 3D solid modelling work to reveal zones of "vertical hydrogeological windows". Therefore, the 3D solid model and the associated database resulting from this research work is more detailed and accurate than the available ones as it overcomes the previously mentioned constraints. The 3D solid model is later applied to assess the contribution of tectonic vertical displacement to the current land subsidence status and to estimate possible pathways of salt and pollutant transport in the groundwater system in the VMD.

2. Study area

The VMD is a subaerial plain that has prograded ~220 km southeastward within the past 6,000-7,500 years [12, 13] and is tectonically controlled by three regional deep faulting systems: the NW-SE trending faults, the N-S trending fault, and SW-NE trending faults (Fig. 3). The Hau river runs along the development direction of the biggest regional fault and is about 2,000 km long and almost vertically dips down 35-70 km deep. It is internationally named Mae Ping fault and locally known as the Hau river fault for its part in the Mekong delta. The VMD is a tide-dominated delta formed by the Mekong river system. The study region is a flat lowland of 0.5-2.5 m elevation except for some hills and mountains of exposed bedrock in the northern parts of the Kien Giang and An Giang provinces. In the lowland area, the sediments are dominantly fine grained and were

deposited in the receiving basin with slight inclination of pre-existing deposits in the South China sea and gulf of Thailand.

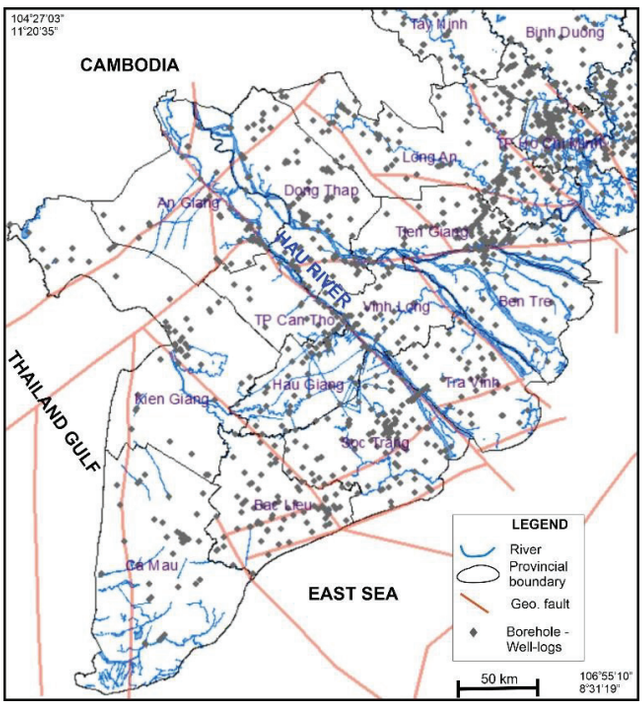

Fig. 3. Location of study region and selected boreholes for 3D hydrogeological model and geological faults adapted to Hoa (1996) [14] **and Trang (2019)** [13].

So far, through different hydrogeological mapping works at scales 1:50,000-1:200,000, the Vietnamese hydrogeologist association has conceptualized the whole unconsolidated sediments from the Late Miocene to the Quaternary in the VMD as being composed of 14 hydrogeological units, namely, the 7 aquitards (from top to bottom) Q_2, Q_1^3, Q_1^{2-3}, Q_1^1, N_2^2, N_2^1, and N_1^3, and the 7 aquifers qh, qp3, qp23, qp1, n22, n21, and n13. Deeper unconsolidated sediments of Middle Miocene N_1^{2-3} have been observed in few geological-hydrogeological wells and/or petroleum exploration wells near the Hau river in the provinces of Hau Giang and Ben Tre. For example, clayish silt aged N_1^{2-3} below a depth of -495 m in borehole 17-III-NB (Hau Giang province); or a set of intercalated layers of clay, silt, and sand aged Neogene (?) at depths of -508 to -798 m found in the 1190-m deep petroleum exploration well HG1 in Hau Giang province. However, because of the very small number of such deep wells that enable the characterization of deeper water-bearing porous formations, the porous groundwater system of 14 hydrogeological units is conceptualized to overlie much less permeable Paleozoic - Cenozoic bedrocks as appearing in a number of well logs from the provinces of An Giang, Kien Giang, Ca Mau, and Bac Lieu.

In the VMD, groundwater is a very important source of water for domestic use as well as for aquaculture-agricultural production demands. The total number of licensed production wells (i.e., wells of pumping discharge ≥10 m^3/day) in the region is 9,287 with an abstracted volume of 1.97×10^6 m^3/day [15]. A recent detailed investigation in Ca Mau province shows the actual abstracted volume (i.e., including also unlicensed production wells of pumping rate <10 m^3/day) is 426.4×10^3 m^3/day while the licensed abstraction volume is only 143.9×10^3 m^3/day [16]. Therefore, it is roughly estimated that the actual abstracted volume is 2-3 times higher than the licensed volume. This huge abstraction volume has been causing deep cones of groundwater depletion in aquifers qp23, qp1, and n22 where most of the production wells are being pumped.

3. Data overview and remarks

The baseline of this work is the well log dataset of the NAWAPI. This dataset consists of 1,545 well logs of geological-hydrogeological investigative boreholes drilled across 19 provinces of the Southern Plain of Vietnam, and most of them were collected during the implementation of the project "Assessment of impact of global climate change to the groundwater resources in the Vietnam Mekong delta, proposal of resilient measures" [7] and the project "Groundwater resources compilation - mapping scaled 1:200,000 for provinces of Vietnam" [8]. The abovementioned dataset does not include all available well logs since only the deepest well logs for each national groundwater monitoring station are input into the dataset (each is often composed of 3-6 boreholes monitoring different aquifers, which are located few meters distant from each other).

For 3D hydrogeological modelling, 1,214 boreholes located in the study region were selected from the abovementioned well log dataset, and each well log contains a downhole hydrogeological stratification and lithological description of every drilling interval of a borehole. An example of a well log is shown in Fig. 1A, and a quick check of these well logs shows that many of them do not seem to be very reliable as they exhibit very similar lithological sequences and the hydrogeological units found in the lithological description of these well logs were not distinguished. This check also demonstrates that a small number of well logs do not have geographic coordinates, or the specified coordinates do not match the specified locality name. Hence, 331 well logs with

questionable information were discarded. Fig. 3 shows the location of the 1,214 well logs selected for the modelling.

It should be noted that only 436 out of 1,214 boreholes were drilled through the 14 hydrogeological units. In the study region, the deepest well (drilling depth -558.79 m), which does not reach the bottom of aquifer n13, is Q618070 in the Soc Trang province. So, the uncertainty of the modeling increases with depth.

It is observed that the selected boreholes are not equally distributed spatially in the study region as most production wells are found near cities or townships. In addition, high lithological heterogeneity and sudden change in thickness of lithological layers are observed in some places. Therefore, bumpy interpolation of the top and bottom surfaces of the hydrogeological units in some places are expected due to these aforementioned factors.

From an individual well log sheet of the selected dataset, the following information are extracted and input into an MS Excel file, which is later imported to ArcGIS software for building the 3D hydrogeological solid model and GIS database: (i) Name, x-y coordinate, and z-value (ground elevation) of the borehole and (ii) name of hydrogeological unit (for instance aquitard Q2, aquifer qh, etc.), bottom elevation, thickness, and lithological description in top-down order until the bottom of the borehole.

4. Building the 3D hydrogeological solid model and database

As mentioned earlier, the Vietnam Hydrogeological Society has so far been conceptualizing the entirety of the unconsolidated sediments aged from Neogene to Quaternary in the VMD as a system of 7 aquifers and 7 aquitards. This system of stratification has appeared in most groundwater resource investigation projects or research publications for the study area, for example, in [7, 8, 17]. This stratification is based on a vertical distribution of lithological composition and the geological age of the soil layers appearing in the well logs. As a rule-of-thumb often exerted in practice, a layer or consecutive layers of fine grains (i.e., clay, silt, loam-silt) with a total thickness ≥5 m is stratified as an aquitard, and vice versa for an aquifer. In reality, that rule has been loosely applied to individual well logs based on personal expertise, and often without a reference to surrounding boreholes. This can result in a sudden change in thickness of a hydrogeological unit when a 3D stratification solid model is built. In this work, we still follow the abovementioned rule, but with careful verification and reference to nearby well logs as described in more detail in the following paragraphs. The building process of the 3D hydrogeological solid model and GIS database is shown in Fig. 4.

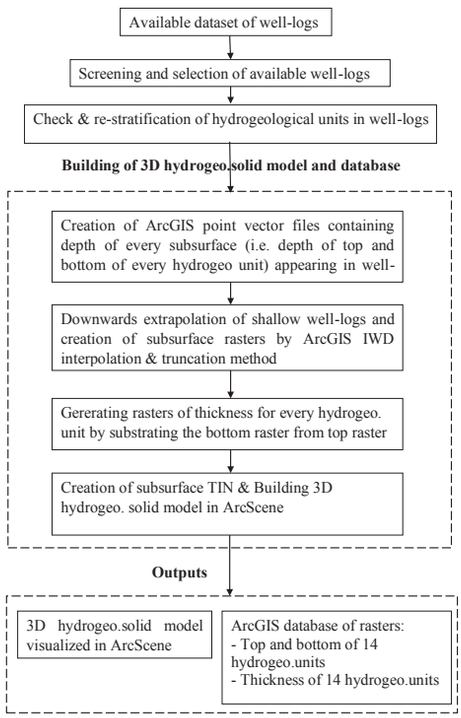

Fig. 4. Flowchart for building the 3D hydrogeological solid model and GIS database.

The modelling was carried out with ArcGIS software and underwent the following steps:

(i) Check and re-stratification (if necessary) of the hydrogeological units defined in the well logs:

In this research work, hydrogeological units are defined on the basis of the following criteria where each hydrogeological unit is composed of one or several consecutive lithological layers falling within one geological age. The unit is considered as an aquifer if (i) the total thickness of coarse-grained layers is ≥60% of the total thickness of that unit and (ii) the minimum thickness of the unit is ≥5 m. Vice versa, an aquitard is assigned if the total thickness of fine-grained layers is ≥60% of the total thickness of that unit and the minimum thickness of the unit is ≥5 m. The unit is given a name in accordance with geological age, i.e., aquitard Q2 and aquifer qh are Holocene age, etc. It is also conceptualized that for each geological age, the aquitard is overlying the aquifer. For instance, aquitard Q_1^3 is located above the aquifer qp3 (Table 1).

Table 1. Averaged thickness and distribution depth of geological and hydrogeological units.

Geological age	Overlying aquitard, average thickness and distribution depth (m)	Underlying aquifer, average thickness and distribution depth (m)
Holocene	Q_2; 20.8; +0.1 ÷ -72.9	qh; 5.1; +1.8 ÷ -72.9
Upper Pleistocene	Q_1^3; 2.9; -0.9 ÷ -104.3	qp3; 19.5; -2.1 ÷ -134.2
Middle-upper Pleistocene	Q_1^{2-3}; 16.4; -6.1 ÷ -161.5	qp23; 33.1; -13.2 ÷ -180.7
Lower Pleistocene	Q_1^1; 17.1; -28.3 ÷ -219.9	qp1; 32.3; -31.2 ÷ -248.4
Middle Pliocene	N_2^2; 15.8; -55.3 ÷ -316.3	n22; 37.9; -61.3 ÷ -413.4
Lower Pliocene	N_2^1; 23.4; -81.1 ÷ -430.3	n21; 22.1; -102.8 ÷ -458.3
Upper Miocene	N_1^3; 21.6; -142.4 ÷ -492.7	n13; 22.3; -161.1 ÷ -558.6

With the definition and criteria described above, a careful check and restratification (if necessary) was carried out for each well log to better define each hydrogeological unit appearance in the selected well logs. If a short drilling interval composed of one or several very thin lithological layers (i.e., the total thickness is less than 5 m) appears in the well logs, which is supposed to be defined as a hydrogeological unit, a cross-check was carried out to see if such unit exists in the nearby well logs. If it does exist there, the thin drilling interval is defined as a hydrogeological unit regardless of the 5-m minimum thickness criteria. This criteria-break is necessary as it mitigates the abrupt disappearance of a hydrogeological unit in some places, and thus allows a modelling of a smooth edged thinning of a unit as it appears in reality.

(ii) Extrapolation for shallow boreholes and creation of unit surfaces:

As mentioned in the above section, not all the selected boreholes were drilled through the 14 hydrogeological units (Table 2). The well logs of shallow boreholes must be extrapolated downwards to capture the elevation of the top and bottom of subsequent lower aquitards/aquifers for 3D modelling. An interpolation was initially used for NAWAPI's well log dataset by applying averaging (or inverse distance weighting - IDW) of the elevation of the top (or bottom) from the known elevation from the surrounding well logs. A detailed check for well logs in Ca Mau province revealed that elevation averaging method does not work well in some situations, especially those where the average bottom elevation for a hydrogeological unit is higher than the known bottom elevation of an overlying hydrogeological unit at the interpolation point. Therefore, a surface truncation method in combination with ArcGIS IDW interpolation was applied to create the top and bottom surfaces of each hydrological unit using known elevations. An in depth discussion on 3D structural geologic modelling can be found in F. Wellmann, et al. (2018) [18], while comparison of the three most common numerical interpretation methods, namely, IDW, triangulation, and kriging, are discussed in Russell, et al. (2015) [19] and MacCormack, et al. (2012) [20]. A pictorial explanation of the surface truncation method is presented in Fig. 7 in Wellmann, et al. (2018) [18], and insight into the ArcGIS IDW interpretation method is given in the following website: https://pro.arcgis.com/en/pro-app/latest/help/analysis/geostatistical-analyst/how-invers e-distance-weighted-interpolation-works.htm.

Table 2. Number of boreholes reaching into each aquifer.

Total number of selected boreholes	Aquifer qh	Aquifer qp3	Aquifer qp2-3	Aquifer qp1	Aquifer n22	Aquifer n21	Aquifer n13	Bedrock
1,214	1,214	1,158	946	816	773	615	472	436

To apply the abovementioned methods for the 3D modelling of the VMD, the surface was created from the top down, i.e., the Q_2 top surface was created first, followed by the Q_2 bottom using ArcGIS IDW, etc. The ArcGIS IDW interpolation was carried out in two steps. The first step was using boreholes that reach the bottommost unit to generate a "tentative" surface, and to assign a surface elevation to a borehole that does not reach the bottom if the drilling depth is shallower than the "tentative" surface elevation (i.e., downwards extrapolation for shallow boreholes). The second step is done with all boreholes, including the extrapolated boreholes, to generate the unit bottom. The thickness of Q_2 was then formed by subtracting the bottom from the top. The cells with negative thickness were considered to be areas where the unit does not exist, i.e., creating a "vertical hydrogeological window", and therefore were assigned zero thickness values. The bottom was then recalculated by subtracting the new thickness from the top, which also became the top of the underlying aquifer (i.e., truncating the bottom where it is higher than the top). This calculation sequence was carried out for every hydrogeological unit from the uppermost to the bottommost to create a set of 200 m resolution raster files representing the top, thickness, and bottom of each aquifer and aquitard.

5. Results

The resulting 3D hydrogeological solid model and GIS database, i.e., the set of rasters for the top, bottom, and thickness of the 14 hydrogeological units, can be visualized in 3D view with AcrScene or 2D view with ArcMap as shown in Figs. 5 and 6 below. Although the 3D model and GIS database are built for ArcGIS software, they can be viewed with any geological-water resource professional software like Rockworks or GMS without any complicated import/export procedure.

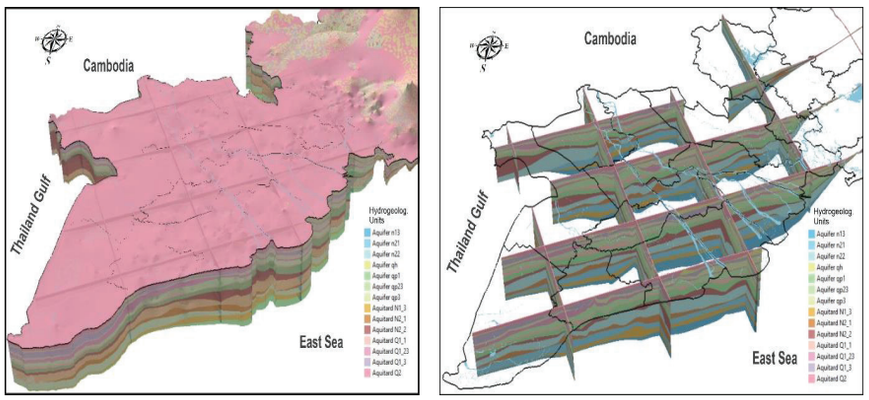

(A) (B)

Fig. 5. A 3D view of (A) the 3D hydrogeological model and (B) cross-sections in the VMD.

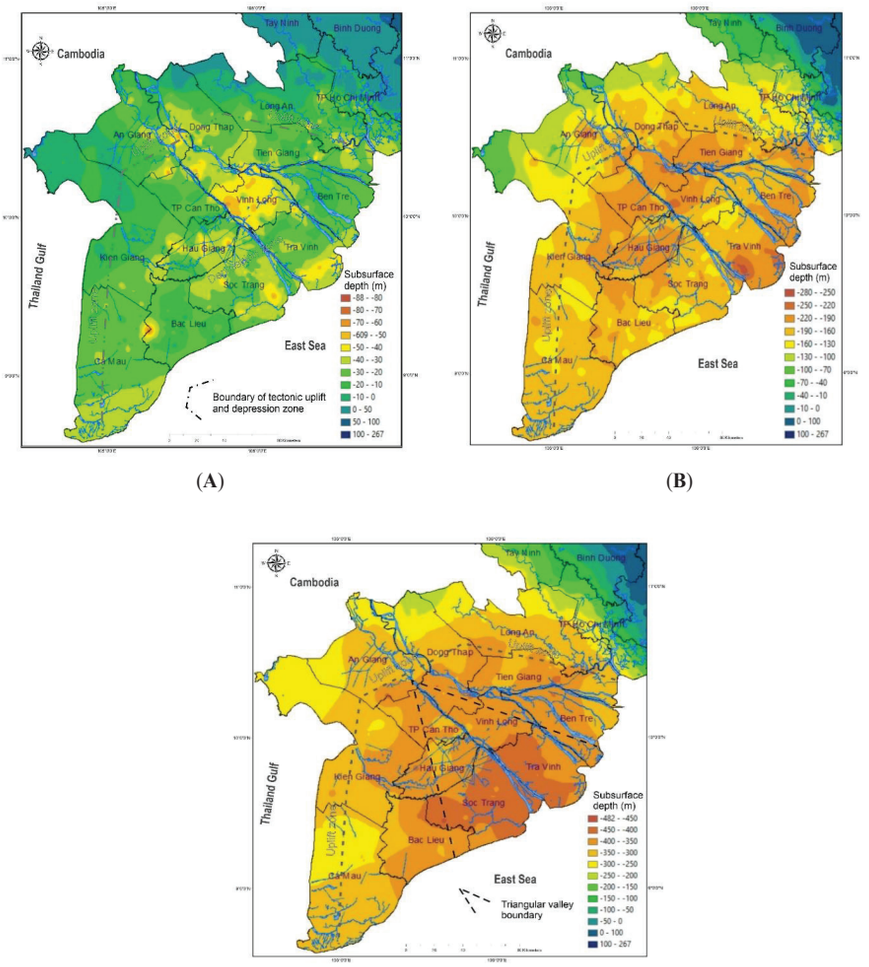

(A) (B)

(C)

Fig. 6. Subsurface depth of the VMD at the beginning of (A) Holocene (8.2-11.7 Ka), (B) Pleistocene (1.8-2.58 Ma), (C) Late Miocene (7.3-11.63 Ma), and boundary of tectonic uplifted zones outlined by Bao, et al. (2001) [21] **and Trang, et al. (2019)** [13].

6. Discussion

The 3D hydrogeological solid model and GIS database constructed in this work can be exploited in various ways for different types of groundwater management. In this research work, we present only two examples of using the 3D model and GIS database for two specific topics related to groundwater use and management in the VMD: land subsidence and vertical intrusion of contaminants and salt water.

6.1. Role of tectonic vertical displacement in current land subsidence

Land subsidence in the VMD is often linked to excessive groundwater exploitation, but it can be also caused by other factors like tectonic vertical displacement. In this research work, we verify this assumption as described below.

A recent publication by W.J. Schmidt, et al. (2017) [22] describes the structural features and deformation history of the Cuu Long basin (offshore of the Mekong delta) in significant detail. In this work, the authors connected the onshore North - Northwest oriented mafic veins with similar offshore faulting systems in the Cuu Long basin. These veins are considered weak zones in the basement prior to rifting and were later reactivated in early Eocene rifting. Besides, this paper describes a major faulting system in the Mekong delta and defines a linkage between the Mae Ping fault in Thailand and Cambodia oriented on the western side of the Kampot Folding system. The change from left-lateral displacement to right-lateral displacement during the transpression period from mid-early Oligocene to mid-late Oligocene (31-25 Ma) (C.R. Morley, et al., 2007 [3-22] and the reactivation since Early Eocene (20-25 Ma) of this fault has been considered to result in vertical neo-tectonic movement in some locations in the Mekong delta [21]. The present delta was formed and shaped in the Holocene [12-13-23]. In this study, a verification and delineation of uplift

and depression zones from the abovementioned publications are made using the 3D solid model and 3D hydrogeological database. As shown in Fig. 6C, in the Late Miocene, the VMD was shaped as a triangular valley of alluvium and a depression zone at depths of -400 to -480 m were observed in the provinces of Soc Trang and Tra Vinh along the Hau river. Surrounding this valley is an uplift zone. The transgression from Late Miocene to Early Pleistocene filled up this valley with marine sediments, but it remained a depression zone at depths ranging between -160 and -280 m in the central provinces of Hau Giang, Can Tho, Vinh Long, and Dong Thap, and the coastal provinces of Tra Vinh and Ben Tre (Fig. 6B). In the Early Holocene, depression zones were much less prevalent in both area and magnitude, although the uplifting continued (Fig. 6A). Therefore, the contribution of tectonic vertical displacement to the current land subsidence at a rate of 1-4 cm/year [4, 5] is not meaningful.

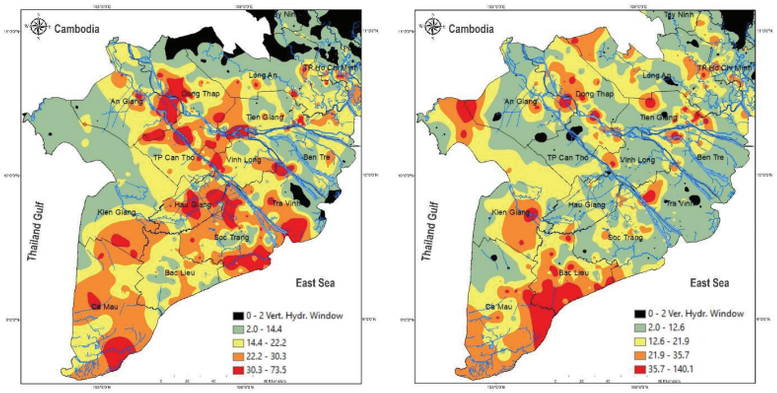

(A) (B)

Fig. 7. Thickness distribution maps of (A) aquitard Q_2 and (B) aquitard Q_1^{2-3} showing "vertical hydrogeological windows" (where aquitard thickness <2 m) and possible seeping zones (where aquitard thickness 2-14 m) between aquifer qh - ground surface and qp23 - qp3.

6.2. Vertical intrusion of contaminant and salt water

Salt water is reported to appear in many areas distributed along the coastal provinces of Ca Mau, Bac Lieu, Soc Trang, and Tra Vinh. Especially in the Ben Tre province, the groundwater is almost salty and therefore the surface water is the main source of water supply for domestic use and agricultural production [8]. In addition, other contaminations in the VMD have been reported in a publication by J. Buschmann, et al. (2008) [24]. From this report, the arsenic concentration ranged from 0.1-1,340 µg/l with 37% of the studied wells exceeding WHO guidelines of 10 µg/l arsenic. Meanwhile, 50% of the studied wells exceeded the manganese WHO guideline of 0.4 mg/l. In this research work, we attempt to obtain a prediction of the pathway of these contaminations with the 3D solid model and the 3D hydrogeological database.

Contaminant transport likely occurs in either direct hydraulic interaction zones through "vertical hydrogeological windows" or in seeping zones of less permeable aquitards. Maps of seven aquitards were created with the 3D hydrogeological database, which show aquitards are 20-140 m thick and are quite well confined from the aquifers around each other. A few zones of direct hydraulic interaction (i.e., thickness ≤2 m) and zones of possible seeping (i.e., thickness 2-14 m) are an exception, and these occur in the topmost aquitard Q_2 and in the aquitard Q_1^{2-3} intercalated between aquifers qp3 and qp23 (Fig. 7). Distributions of these zones in the topmost aquitard show arsenic and manganese contamination in groundwater are not likely exogenetic in origin, at least for the central part of the VMD and the Ca Mau peninsular (Figs. 7A, 7B). Vertical intrusion of contaminants from aquifers qp3 to qp23 is possible through an extensive distribution of seeping zones where aquitard thicknesses range between 2-12.6 m. Contamination seepage from other aquifers likely does not occur because of the thick aquitards confining them. The above facts imply an endogenous origin of these contaminants related to sediment deposition.

7. Conclusions

A 3D hydrogeological solid model and GIS database of the VMD were constructed in this research work. The database and solid model were based on 1,214 carefully selected boreholes scattered across the study region. Because of the high heterogeneity of lithology, and only a small number of well logs reaching the deepest aquifer, inverse distance weighting (IDW) was used to interpolate the elevations of the top and bottom from the known elevations from the surrounding well logs as well as a surface truncation method being applied when the bottom is higher than the top.

The constructed 3D hydrogeological database and 3D stratification solid model are applied to analyze the role of tectonic vertical displacement in current land subsidence and the possible vertical intrusion of contaminants and salt water in the VMD. The result shows that tectonic vertical displacement is negligible in comparison to the current land subsidence rate of 1-4 cm/year, and the contamination is of endogenous origin and likely does not transfer across aquifers.

Apart from the abovementioned application, the 3D hydrogeological solid model and GIS database can also be applied to different types of groundwater management, for

instance, groundwater vulnerability mapping, site selection and design of artificial recharge, underground construction to mitigate saltwater intrusion, rough estimation of transboundary groundwater flow, or site selection of a production well field, etc.

CRedit author statements

Vu Thanh Tam, Nguyen Ngoc Ha, Ho Van Thuy: Conceptualisation, Methodology, Data curation, Formal analysis, Writing - Review & Editing.

ACKNOWLEDGEMENTS

This research work is carried out within the framework of the Vietnam - German research cooperation project "Integrated Solutions for Sustainable Development in the Mekong delta - ViWaT", namely component project ViWAT1 coded DTDL.CN-44/18. Special thanks are given to technical staff of IGPVN (Improvement of Groundwater Protection in Vietnam) and DWRPIS (Division for Water Resources Planning and Investigation for the South) for their enthusiastic collection and pre-processing of well logs available in the Vietnam Mekong delta.

COMPETING INTERESTS

The authors declare that there is no conflict of interest regarding the publication of this article.

REFERENCES

[1] General Statistics Office (2019), *Statistical Yearbook of Vietnam 2019*, 1034pp (in Vietnamese).

[2] X.L. Pichon, M. Fournier, L. Jolivet (1992), "Kinematics, topography, shortening, and extrusion in the India - Eurasia collision", *Tectonics*, **11(6)**, pp.1085-1098, DOI: 10.1029/92TC01566.

[3] C.K. Morley, M. Smith, A. Carter, et al. (2007), "Evolution of deformation styles at a major restraining bend, constraints from cooling histories, Mae Ping fault zone, western Thailand", *Geological Society London Special Publications*, **290(1)**, pp.325-349, DOI: 10.1144/SP290.12.

[4] Copernicus Emergency Management Service - Mapping (2019), *EMSN-062: Assessing Changes in Ground Subsidence Rates, Mekong Delta, Vietnam*, Copernicus EMS, 31pp.

[5] L.E. Erban, S.M. Gorelick, H.A. Zebker (2014), "Groundwater extraction, land subsidence, and sea-level rise in the Mekong delta, Vietnam", *Environ. Res. Lett.*, **9(8)**, DOI: 10.1088/1748-9326/9/8/084010.

[6] P.S.J. Minderhoud, G. Erkens, P.V. Hung, et al. (2017), "Impacts of 25 years of groundwater extraction on subsidence in the Mekong delta, Vietnam", *Environ. Res. Lett.*, **12(6)**, DOI: 10.1088/1748-9326/aa7146.

[7] Division for Water Resources Planning and Investigation for The South of Vietnam (2014), *Synthetic Report of The Project Assessment of Impact of Global Climate Change to The Groundwater Resources in the Mekong Delta, Proposal of Resilient Measures*, 328pp (in Vietnamese).

[8] National Center for Water Resources Planning and Investigation (2018), *Synthetic Report of The Project Groundwater Resources Compilation - Mapping Scaled 1:200.000 for Provinces of Vietnam*, 194pp (in Vietnamese).

[9] P. Vermeulen, N.H. Quan, N.D.G. Nam, et al. (2013), "Groundwater modeling for the Mekong delta using iMOD", *The 20th Int. Congr Model. Simultation*, pp.2499-2505.

[10] C. Zoccarato, P.S.J. Minderhoud, P. Teatini (2018), "The role of sedimentation and natural compaction in a prograding delta: insights from the mega Mekong delta, Vietnam", *Nature Scientific Reports*, **8**, DOI: 10.1038/s41598-018-29734-7.

[11] J.L. Gunnink, H.V. Pham, G.H.O. Essink, et al. (2021), "The three-dimensional groundwater salinity distribution and fresh groundwater volumes in the Mekong delta, Vietnam, inferred from geostatistical analyses", *Earth System Science Data*, **13(7)**, pp.3297-3319, DOI: 10.5194/essd-13-3297-2021.

[12] N.V. Lap, T.T.K. Oanh, M. Tateishi (2000), "Late Holocene depositional environments and coastal evolution of the Mekong delta, southern Vietnam", *Journal of Asian Earth Sciences*, **18(4)**, pp.427-439, DOI: 10.1016/S1367-9120(99)00076-0.

[13] N.T.H. Trang, T. Nghi, D.X. Thanh, et al. (2019), "Late pleistocene - holocene sedimentary evolution of nam no plain and correlation from the Ca Mau peninsula to the Mekong river delta in midle-late holocene", *VNU Journal of Science: Earth and Environmental Sciences*, **35(4)**, pp.97-120, DOI: 10.25073/2588-1094/vnuees.4476 (in Vietnamese).

[14] N.N. Hoa (Chief Editor) (1996), *Geological and Minerals Mapping Scale 1:200,000, Map Sheets C-48-XIV+XV C-48-XVI, C-48- XVI, C-48-XXI+XXII, C-48-XXIII+XXIX, C-48-XXVII+XXVIII - Summary Report and Maps,* Archive of General Department of Geology & Minerals of Vietnam (in Vietnamese).

[15] Ministry of Natural Resources and Environment of Vietnam (2019), *Database of Licensed Production Wells* (in Vietnamese).

[16] Department of Natural Resources and Environment of Ca Mau province (2018), *Report of Water Resources Planning till 2025 with Outlook for 2035 for Ca Mau province*, 320pp (in Vietnamese).

[17] H.Q. Khai, K. Kangjoo, P.N. Long, et al. (2019), "A hydrogeological and geochemical review of groundwater issues in southern Vietnam", *Geosciences Journal*, **23(6)**, pp.1005-1023, DOI: 10.1007/s12303-019-0021-z.

[18] F. Wellmann, G. Caumon (2018), "3-D structural geological models: Concepts, methods, and uncertainties", *Advances in Geophysics*, **59(1)**, DOI: 10.1016/bs.agph.2018.09.001.

[19] H.A.J. Russell, B. Brodaric, G. Keller, et al. (2015), *A Perspective on A Three-Dimensional Framework for Canadian Geology,* AER/AGS Special Report 101, 27pp.

[20] K.E. MacCormack, C.H. Eyles (2012), "Assessing the impact of program selection on the accuracy of 3D models", *Geosphere*, **8(2)**, pp.534-543, DOI: 10.1130/GES00732.1.

[21] N.X. Bao, N.V. Binh, P.H. Long, et al. (2001), *Structure and Metallogeny of Vietnam*, South Vietnam Geological Mapping Division, Ho Chi Minh city (in Vietnamese).

[22] W.J. Schmidt, B.H. Hoang, J.W. Handschy, et al. (2017), "Tectonic evolution and regional setting of the Cuu Long basin, Vietnam", *Tectonophysics*, **757**, pp.36-57, DOI: 10.1016/j.tecto.2019.03.001.

[23] T.T.K. Oanh, N.V. Lap, M. Tateishi, et al. (2002), "Holocene delta evolution and sediment discharge of the Mekong river, Southern Vietnam", *Quaternary Science Reviews*, **21(16-17)**, pp.1807-1819, DOI: 10.1016/S0277-3791(02)00007-0.

[24] J. Buschmann, M. Berg, C. Stengel, et al. (2008), "Contamination of drinking water resources in the Mekong delta floodplains: Arsenic and other trace metals pose serious health risks to population", *Environment International*, **34(6)**, pp.756-764, DOI: 10.1016/j.envint.2007.12.025.

Table of contents in 2021

No	Authors	Title	Issue	Page
PHYSICAL SCIENCES				
1	*Doan Van Hong Thien, Nguyen Thi Bich Thuyen, Tran Thi Bich Quyen, Nguyen Huu Chiem, Van Pham Dan Thuy, Pham Hung Viet*	Microwave-assisted synthesis of nanorod hydroxyapatite from eggshells.	1	3
2	*Quang Minh Do, Ngoc Tri Huynh Nguyen, Thi Hong Hoa Huynh, Hong Lien Pham, Thi Thu Ho, Do Trung Kien Kieu, Ngoc Minh Huynh*	Study on the fluoride-releasing ability of dental GIC materials in deionized water and artificial saliva environments.	1	7
3	*Mai Thi Tuyet Phan, Trang Thu La, Thu Hong Anh Ngo*	Study on extracting hemicellulose, cellulose, and carboxymethyl cellulose from Vietnamese rice straw waste.	1	15
4	*Hoang-Quan Dinh, Thanh-Bang Nguyen*	Composition of ground granulated blast-furnace slag and fly ash-based geopolymer activated by sodium silicate and sodium hydroxide solution: multi-response optimization using Response Surface Methodology.	1	21
5	*Nguyen Cong Nguyen, Hau Thi Nguyen, Shiao-Shing Chen, Xuan Thanh Bui*	Application of an innovative draw solute in forward osmosis (FO) processes.	1	30
6	*Tran Duc Dai, Dao Duc Thien, Nguyen Thanh Tam*	Flavone glycosides from *Uraria crinita*.	2	3
7	*Van Phuc Dinh*	Investigation of the removal of Ni(II) from aqueous solution using pomelo fruit peel.	2	7
8	*Mai Thi Tuyet Phan, Boi Van Luu, Lan Ngoc Pham*	Synthesis and elaboration of modified comb type (maleic anhydride-α-tetradecene) copolymers for cold flow improvers of biodiesel.	2	13
9	*Thi Hien Dinh, Minh Hai Nguyen*	Structure and luminescent property of a Sm^{3+} complex containing benzoyltrifluoroacetone and 1,2-bis[(anthracen-9-ylmethyl)amino]ethane ligands.	2	20
10	*Trung-Kien Hoang, L. Vido, Dinh-Quang Nguyen*	A simple approach for air-gap permeance calculations in double excitation synchronous motor modelling with reluctance network.	2	25
11	*Hai Thanh Le, Hien Thi-Thu Pham*	An effective method for detecting dorsal hand veins utilising near-infrared imaging technology.	2	32
12	*Manh-Hung Ha, Hoang-Anh Pham*	Optimum sizing of members of truss structures using direct design and a self-adaptive mutation differential evolution.	2	39
13	*Thi Kim Chi Nguyen, Duy Hung Nguyen, Tan Vinh Le, Thanh Vu Tran, Chi Nguyen Vo, Thi Kim Trung Pham*	Luminescence properties of Mn^{4+}-doped $CaAl_2O_4$ as a red emitting phosphor for white LEDs.	3	3
14	*Quoc Viet Bui, Thuy Vy Phan, Tien Khoa Le*	Development of new homogeneous photo-Fenton catalytic systems using oxalic acid and ferric ions in very low concentrations.	3	8
15	*Thuy-Duy Thi Nguyen, Anh Vy Truong, Hoang Phuong Tran*	Metal- and solvent-free preparation of benzo[4,5]imidazo[1,2-a]pyrimidine derivatives catalysed by deep eutectic solvents.	3	15
16	*Phan Minh Vuong, Do Huu Duy Khoa, Phan Thanh Thao*	Study on optimization of ternary complex of piroxicam-*β*-cyclodextrin-lysine inclusion in supercritical CO_2.	3	18
17	*Ngoc Lan Pham, Van Boi Luu, Thi Tuyet Mai Phan, Thi Son Nguyen*	Synthesis and characterization of alkyl-methacrylate-maleic anhydride copolymer for use as a biodiesel flow improver.	3	24
18	*Ngoc Xuan Dat Mai, Tan Le-Hoang Doan, Le Nguyen Bao Thu, Bach Thang Phan*	Evaluation of removal efficiency of Fe(III) and Al(III) ions in acid sulfate water using agarose-based magnesium oxide composite.	3	30
19	*Cao-Son Nguyen, Thanh-Hoan Nguyen, Son-Lam Nguyen, Anh-Hoa Bui*	Study on the reducibility of iron ore pellets at high temperature.	4	3
20	*Thi Thuy Dung Phung, Thu Thuy Truong, Thanh Luan Nguyen, Tran Ha Nguyen*	Synthesis of a new furan-bearing triazine dichloride compound.	4	8
21	*Thi Huong Trinh, Quoc Tuan Nguyen, Thi Huyen Trang Nguyen, Dang Giap Do, Trong Tuan Tran*	Induction and evaluation of secondary metabolite and antioxidant activity in adventitious root of *Codonopsis javanica*.	4	11
22	*Thu Huong Nguyen, Thanh Long Ngo, Huu Quang Nguyen*	Physicochemical parameters and mineral components in Vietnam honey as a promising tool for classifying biological origin of honeys.	4	17
23	*Tue Ngoc Nguyen, Khanh Quoc Dang, Duc Trung Nguyen*	Adsorptive removal of methyl orange and methylene blue from aqueous solutions with *Acacia crassicarpa* activated carbon.	4	23
24	*Doan Van Hong Thien, Thao Phuong Nguyen, Mong Linh Nguyen Thi, Ngoc Tuyet Tran, Thanh Nhan Le, Trung Nam Nguyen, Manh Can Le, Chanh-Nghiem Nguyen, Dan-Thuy Van-Pham*	Effects of compressing parameters and $Mg(OH)_2$ content on mechanical properties and flame retardancy of rice straw-fibre reinforced composites.	4	28
LIFE SCIENCES				
25	*Nguyen Quang Thinh*	Influences of seed priming with *Spirulina platensis* extract on seed quality properties in black gram (*Vigna mungo* L.).	1	36
26	*Linh Nguyen Thuy, Trang Tran Thi Thu, Hue Luu Thi Minh, Hang Dao Viet*	Evaluation of clinical characteristics and lower esophageal sphincter pressure on high resolution manometry in achalasia patients after treatment.	1	42
27	*Le Nhat Minh, Vo Trong Nhan, Thi Thao Do, Tran Thu Huong, Le Tri Vien, Phung Thi Kim Hue*	Study on cancer stem cell labeling and inhibition efficiency of LV3 nanocomplex *in vitro*.	1	47
28	*Nguyen Thanh Viet, Nguyen Minh Nam, Nguyen Vu Trung, Do Tuan Anh, Hoang Van Tong*	Meningococcal disease in one soldier patient: case report from Vietnam.	1	54
29	*Hang Thi Nguyet Pham, Hong Nguyen Tran, Xoan Thi Le, Khoi Minh Nguyen, Hiep Tuan Nguyen, Lap Thi Nguyen, Folk R. William*	Effect of *Centella asiatica* on cognitive deficits caused in trimethyltin-induced neurotoxicity model mice.	1	59
30	*Phuong Thi Bich Chu, Hanh Thi Thu Phan, Hoang Duc Nguyen, Trang Thi Phuong Phan*	Development of inducer-free expression plasmids using IPTG-inducible P*spac* promoter for *Bacillus subtilis*.	1	64

31	*Hong Ha Bui, Lan Huong Nguyen, Thanh Tri Nguyen, Phuoc Dan Nguyen*	**Co-digestion of domestic wastewater and organic fraction of food waste using anaerobic membrane bioreactor: a pilot scale study.**	1	71
32	*Nhat Tam Le, Nguyen Que Anh Huynh, Nhu Khue Doan, Thuy Xuan Uyen Phan, Ba Thanh Nguyen, Sao Mai Dam, Thi Van Thi Tran, Le Phuong Lien Nguyen, Van Hai Chu, Huynh Anh Vu Truong*	**The combination of microbiological, biochemical, and quality index methods in quality evaluation of Pacific white shrimps *(Litopenaeus vannamei)* preserved at 0°C.**	2	45
33	*Truong Ngoc Quynh Phuong, Pham Van Hung, Nguyen Thi Lan Phi*	**Extraction of flavonoids in pomelo peels using Box-Behnken response surface design and their biological activities.**	2	52
34	*Tran Thi Hoan, Tu Quang Hien, Mai Anh Khoa, Tu Quang Trung*	**Determination of the appropriate level of manure fertilisation for *Moringa oleifera* grown for animal feed.**	2	58
35	*Nguyen Thi Thanh Loan, Le Thi Xoan, Pham Thi Nguyet Hang, Nguyen Van Tai*	**Contribution of ginsenosides Rg1, Rb1 to the neuroprotective effect of *Panax notoginseng* in mouse organotypic hippocampal slice cultures exposed to oxygen and glucose deprivation.**	2	64
36	*Le Nguyen Thanh, Nguyen Phuong Thao, Nguyen Tu Minh, Trinh Khanh Huyen, Vu Thi Kim Oanh, Dinh Ngoc Thuc, Tran Thi Ngat, Nguyen Thi Phuong Lien*	**Chemical constituents and antimicrobial activity of *Lisotrigona cacciae* propolis collected in Hoa Binh province.**	2	70
37	*The Duc Ngo*	**Herbicide resistant weeds: the case of resistance to glyphosate.**	2	74
38	*Thanh-Tri Do, Bich-Huy Tran-Thi, Binh-Nguyen Ong, Tuan-Loc Le, Thanh-Cong Nguyen, Quoc-Dang Quan, Thuong-Chi Le, Dai-Long Tran, Michael Melkonian, Hoang-Dung Tran*	**Effects of red and blue light emitting diodes on biomass and astaxanthin of *Haematococcus pluvialis* in pilot scale angled twin-layer porous substrate photobioreactors.**	2	81
39	*Dang Giang Chau Nguyen, Thi Lan Anh Tran, Thi Thanh Lam Tran, Thi My Duyen Ngo, Thai Long Hoang, Van Hop Nguyen, Kurt Kalcher*	**Degradation of the insecticides fipronil and cypermethrin in green onions (*Allium fistulosum*) and mustard greens (*Brassica juncea*).**	3	35
40	*Quy Tung Le, Chiti Sritontip*	**Effects of nano-bubbles on seed germination of muskmelon.**	3	42
41	*Thi Lan Anh Luong, Thu Lan Hoang, Minh Ngoc Nguyen, Ngoc Dung Nguyen*	**A procedure to detect 6 basic STSs and 11 extended STSs in the AZF region using multiplex PCR.**	3	48
42	*Xuan Truong Le, Hue Minh Nguyen, Ngoc Quynh Le, Thi Thu Loan Trinh, Van Thanh Tran*	**Formulation of enteric coated microspheres containing pantoprazole.**	3	56
43	*Van Thong Ngo, Huu Hanh Tran, Chi Tao Phan*	**Morphological characteristics and mitochondrial COI gene of the green water dragon in Phu Quoc island, Vietnam.**	3	63
44	*Thanh Khiem Nguyen, Hong Son Trinh, Gia Anh Pham, Ham Hoi Nguyen, Trung Nghia Bui, Manh Thau Cao, Quang Nghia Nguyen, Viet Khai Ninh, Tuan Hiep Luong, Tien Quyet Nguyen*	**Clinical and subclinical characteristics of brain-dead donors for liver transplantation in Viet Duc University Hospital.**	4	36
45	*Thi-My-Linh Lam, Minh-Tuan Le, Manh-Ha Bui*	**Study on α-glucosidase inhibitory activity of 40 kinds of vegetables, tubers, and fruits in An Giang.**	4	42
46	*Thanh Tung Bui, Bao Kim Nguyen, Minh Ngoc Le, The Toan Nguyen, The Hai Pham*	***In silico* screening of drug inhibitors of SARS-CoV-2 RNA-dependent RNA polymerase target.**	4	47
47	*Thu Hien Nguyen, Thi Xoan Le, Van Tai Nguyen, Thi Nguyet Hang Pham, Minh Khoi Nguyen, Matsumoto Kinzo*	**The antidepressant-like effects of an n-butanol fraction of *Ocimum sanctum* Linn. extract in unpredictable chronic mild stress-induced depression in mice.**	4	55
48	*Nguyen Thuan Thien Truong, The Hao Nguyen, Cong Chinh Bui, Thi Thu Hoai Nguyen*	**Effects of different shrimp extracts on *Vibrio parahaemolyticus* growth and virulence.**	4	62
EARTH SCIENCES				
49	*Tan-Phong Ngo, Thuy-Chung Kieu-Le*	**Application of particle image velocimetry (PIV) to measure the displacement of sandy soil in laboratory.**	3	70
ENVIRONMENTAL SCIENCES				
50	*Viet Hung Bui, Ngoc Diep Nguyen*	**Fluctuations in agriculture and sediment in the Mekong delta of Vietnam due to increased upstream water use.**	1	77
51	*Nguyen Thanh Tung, Wilai Chiemchaisri, Chart Chiemchaisri, Samunya Sanguanpak*	**Removal of greenhouse gas in biofilter using organic and inorganic media.**	1	83
52	*Huynh Thi Lan Huong, Pham Ngoc Anh*	**Sustainability assessment of community-based water resource management of irrigation systems for agriculture.**	1	90
53	*Thi Yen Ta, Thi Anh Tuyet Nguyen, Hoang Thi Hong Van*	**Analysis of production, consumption and environmental burden of plastic industry in Vietnam by input-output table.**	2	89
54	*Nguyen Phuong Tan Le, Nguyen Khoi Dao*	**Application of livelihood vulnerability index in evaluating household's livelihood vulnerability to climate change in Can Gio district, Ho Chi Minh city, Vietnam.**	3	78
55	*Thi Thanh Diem Ngo, Minh Tien Tran*	**Removal of heavy metals derived from COD analysis wastewater by electrolysis using graphite electrode.**	3	85
56	*An Trung Nguyen, Thi Cam Ha Nguyen, Tien Thinh Lai, Hoang Giang Nguyen, Ha Vu, Thanh Long Nguyen*	**Developing a database for Cs-137 radioactivity concentration and assessing residual levels in surface soils of Quang Ninh, Hai Phong, and Lang Son provinces.**	3	92
57	*Diep Thi Ngoc Phan, Binh Duc Nguyen, Paul Liew, Ha Thi Thu Pham, Tung Thanh Nguyen, Hieu Trung Nguyen*	**Evaluating the potential of aquaculture in the Hoa Binh reservoir with carrying capacity and water quality indices.**	4	66
58	*Vo Quoc Bao, Tran Thi Van*	**An empirical relationship between $PM_{2.5}$ and aerosol optical depth from MODIS satellite images for spatial simulation over Ho Chi Minh city.**	4	72
59	*Nguyen Thi Kim Oanh*	**Rice straw open burning: emissions, effects and multiple benefits of non-burning alternatives.**	4	79
60	*Vu Thanh Tam, Nguyen Ngoc Ha, Ho Van Thuy*	**Establishing 3D hydrogeological solid model and database for sustainable groundwater management in the Vietnam Mekong delta.**	4	86

Vietnam Journal of Science, Technology and Engineering (VJSTE): Manuscript Template

General Instructions on using this template and submitting a manuscript to VJSTE: Thank you for preparing a manuscript for submission to VJSTE. Using this template, or following the guidelines below, will help us in processing your article.

The structure of different types of articles may vary according to the type of study, and the content of the article.

The following are the detailed main components of the original research and review articles submitted to the journal.

Original research

The original research should have three following parts:

Preliminary section: It includes title, list of all contributing authors with their institutional affiliation, and abstract (160-250 words) with at least 3 keywords.

Title: How to format a science article (replace with your real title)

Author(s): List the author name(s) separated by commas. Use superscript numbers to link affiliations, and symbols *†‡ for author notes. For example, Y. Obsie[1*], S.A. Adem[1, 2]

**Corresponding author(s):* Include the email addresses or telephone numbers of the corresponding author(s). Please use the asterisk (*) symbol for the corresponding author information. This information is at the bottom of the manuscript's first page.

Author's affiliation addresses:

[1]Affiliations should be preceded by superscript numbers corresponding to the author list

[2]For any institutions, please provide the institution name, street, district, city, country

Received ; revised ; accepted

Abstract:
Start your abstract here…
Keywords: **keyword 1, keyword 2, keyword 3…**
Classification number(s): **1.1, 3.4, 5.3, etc.**

Abstract: The abstract should range between 160 and 250 words and be structured in a single paragraph following keywords in a separate line. The abstract should represent the main part of the research manuscript. It should reflect a brief and comprehensive background following the aim of the study (main questions to be addressed), methods used for investigating the problem, a summary of significant findings, main conclusions, and implications of the results.

Keywords: They should come immediately after the abstract and contain 3-7 specific and relevant keywords. They should reflect the research study and the relevant field of research.

Classification numbers: Depend on the Journal's Classification Scheme.

Author(s) are encouraged to write a "Highlights" that summarises the most exciting, interesting points from your manuscript.

Manuscript section: It is the main body of the scientific manuscript including: 1) Introduction; 2) Material(s) and method(s); 3) Results and discussion (separation of these two sections is acceptable); 4) Conclusions; 5) Recommendations/Suggestions/ Implications/Study limitations...(if any). These sections may slightly vary depending on the type of research approach and design used in the research. Each section should be numbered.

All of the Figures, Tables, and Equations should be cited in numerical order.

Figures

Fig. #: (Begin each figure caption with a label, "**Fig. 1.**" for example, as a new paragraph).

Fig. 1. The figure caption should begin with an overall descriptive statement of the figure followed by additional text. They should be immediately after each figure. Figure parts are indicated with capital letters **(A)**. If you prefer, you can place both the actual figures and captions logically through the text near where they are cited rather than at the end of the file (but not both). If a paragraph in the main text begins with the name of a figure, write out "Figure" in full (e.g., <para> "Figure 1 shows...").

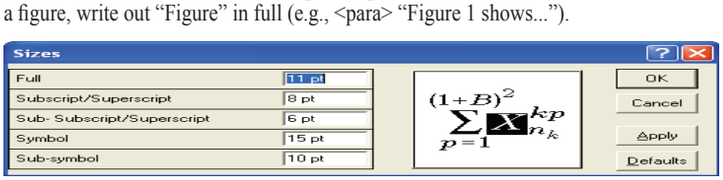

Fig. 1. The figure caption.

Tables

Table #: (Begin each table caption with a label "**Table 1.**", etc. as a new paragraph).

Table 1. Start this caption with a short description of your table. Format tables using the Word Table commands and structures. Do not create tables using spaces or tabs characters.

Table 1. Caption.

a	b	c	d	e
f				
g				
h				

Equations

$$\int_a^b x dx \tag{1}$$

Equations can be included. We do not recommend using the native Word 2007, 2008, 2010 or 2011 equation editor. This can in some cases produce less reliable MathML, the online markup language we use, which may result in display errors. Instead, use the legacy equation editor in Word (Insert menu; select insert object; select word equation) or use MathType (recommended). If you enter equations in simple LaTeX, check that they will convert accurately (Word 2007 and higher can convert simple LaTeX equations).

Closing section: It includes appendices/supplementary materials/data availability statement (if applicable), CRediT author statement (for multiple authors), acknowledgements (if applicable), competing interests, ethics (if any) and a complete list of references corresponding to all the citations given in the text of the manuscript. The appendices/supplementary materials may include data files and other material relevant to the research that should be submitted in separate files if required.

APPENDICES (if any)

The appendices should ideally be under 1000 words (approximately 2 A4 pages) for printing version. With longer appendices, they are only accepted for online publication.

CRediT author statement (for multiple authors)

CRediT offers authors the opportunity to share an accurate and detailed description of their diverse contributions to the published work.

ACKNOWLEDGEMENTS (if applicable)

This section is for the researchers who were funded for the research projects, and it should enclose all sources of financial support.

COMPETING INTERESTS

The author(s) declare(s) that there is no conflict of interest regarding the publication of this article.

REFERENCES

For in-text citation: References should be cited in the bracket with a number [1]. Multiple reference citations are separated by commas [2, 3] or if a series, dashes [4-6]. When citing sources with the author(s) and the year, they should be shortened to the first author's name, followed by et al. (with more than one author) and the year.

For reference list: With less than or equal to three authors, list all the author(s). With more than three authors, the first three should be listed and followed by et al.

References are listed in numerical order, and in the same order in which they are cited in text. The reference list should include all and only those references you have cited in the text. The reference list appears at the end of the article.

The reference consists of: Initial(s) and first/last name of the author(s), author' names separated by commas (Year of publication), "Titles of journal articles or chapter of book", *Title of Journal, Book or Other Publication*, **Volume(Number)** (if any), page numbers (if any), DOI (if any), URL and accessed date (if any) (in its original language if not English).

To cite a website and online/electronic resources, please include the accessed date (day month year).

Example of a reference list:

[1] T. Binzoni, T.S. Leung, D. Boggett, et al. (2003), "Non-invasive laser Doppler perfusion measurements of large tissue volumes and human skeletal muscle blood RMS velocity", *Phys. Med. Biol.*, **48(1)**, pp.2527-2549, DOI: 10.1088/0031-9155-48-15-318.

[2] H.W. Bischoff, H.C. Bold (1963), *Some Soil Algae from Enchanted Rock and Related Algal Species*, University of Texas Publications, 95pp.

[3] R. Busi (2016), "Weedy rice in the Philippines and Vietnam", https://www.aciar.gov.au/publication/technical-publications/weedy-rice-philippines-and-vietnam-final-report, accessed 15 July 2018.

Review articles

They should be different from the original research as they would contain different sections on the literature review. Authors may structure this part as per nature, background, and available literature on the issue argued in the manuscript.

For more detailed instructions, please visit our website: vietnamscience.vn or vietnamscience.vjst.vn

This manuscript template has been used from 2021 onwards.

P-ISSN 2525-2461 • E-ISSN 2615-9937

Vietnam Journal of Science, Technology and Engineering

DECEMBER 2021 • VOLUME 63 NUMBER 4

EDITORIAL OFFICE

113 Tran Duy Hung Str., Cau Giay Dist., Hanoi, Vietnam

Tel: (84.24) 39436793; Fax: (84.24) 39436794

Email: vjste@most.gov.vn

Website: vietnamscience.vn or vietnamscience.vjst.vn

PUBLICATION LICENCE

No. 459/GP-BTTTT 20th July 2021